

ABSTRACT

Title of Thesis: COMPARISON OF INFILTRATION EQUATIONS AND
 THEIR FIELD VALIDATION WITH RAINFALL
 SIMULATION

Degree Candidate: Ellen R. Turner

Degree and Year: Master of Science, 2006

Thesis directed by: Dr. Gary Felton

 Department of Biological Resources Engineering

Infiltration is a complex process with many factors contributing to the rate. Different approximate equations for infiltration differ in the parameters they require and predict different infiltration rate curves.

Five equations including those of Kostiakov, Horton, Holtan, Philip and Green-Ampt were compared to determine which one most accurately predicted measured infiltration rates from rainfall simulation events at two different locations. Parameters were developed from measured infiltration data and laboratory analyses of soil samples.

The Green-Ampt, Holtan and Philip equations with respective root mean squared errors of 0.15, 0.17, and 0.19 cmh^{-1} , provided the first, second and third best estimates of infiltration rates, for observed infiltration data at the University of Maryland's Research and Education Center in Upper Marlboro, Maryland. An atypical infiltration curve was

observed for the Poplar Hill site on the Eastern Shore of Maryland for which infiltration rate was constant and equal to rainfall rate.

Key words: Infiltration rate equation, Rainfall simulation, Parameter calibration, Model validation, Approximate infiltration model.

**COMPARISON OF INFILTRATION EQUATIONS AND THEIR
FIELD VALIDATION BY RAINFALL SIMULATION**

by

Ellen Turner

**Thesis submitted to the Faculty of the Graduate School of the
University of Maryland, College Park in partial fulfillment
of the requirements for the degree of
Master of Science
2006**

Advisory Committee:

**Dr. Gary Felton, Chair
Dr. Hubert Montas
Dr. Adel Shirmohammadi**

©Copyright by
Ellen Turner
2006

ACKNOWLEDGEMENTS

I wish to thank the Department of Biological Resources Engineering, for providing me with a research assistantship for the first two years of my Masters program at the University of Maryland at College Park, and for providing me with the equipment that enabled me to carry out this research. Additionally I would like to thank the Department of Chemistry for providing me with teaching assistantships for the 3rd and 4th year, which provided me with a stipend on which to live while I conducted my research. I would like to thank Dr. Gary Felton, the chairman of my graduate committee, for his guidance, and support. Thank you Dr. Adel Shirmohammadi for your valuable suggestions, insights and encouragement and for serving on my graduate committee. I also want to thank Dr. Hubert Montas for serving on my graduate committee, Dr. Mary Christman for her support with statistics, and Bob Dixon and Gary Seibel for their assistance with repairing and modifying laboratory equipment. Additionally, I am grateful to my mentor and supervisor at the USDA Produce Quality and Safety Laboratory, Dr. Yaguang Luo, for her support over the last 2 years, during which I have learned a great deal about conducting scientific research and writing manuscripts.

I would like to thank the Graduate students in the Department of Biological Resources Engineering. Thank you F. Koh, Dr. A. Lomander, Dr. L. Barker, Dr. D. Blersch, Dr. A. Pouyan Nejadhashemi, and A. Sexton for listening, and for sharing opinions, ideas, and fun times. I thank Kristin Hughes for her help collecting soil

samples and data during rainfall simulations, as well as for her friendship and support. I thank the supporting staff T. Scites, T. Schuler, T. Abe, I. Anderson, and C. Brackens. To the entire BRE faculty, students and staff, thank you for your support.

I would like to thank my father, Dr. Alan Greenberg, and mother, Dr. Linn Turner, for each providing me with love, encouragement and support. Special thanks to my fiancé, Ali Neshati, P.E. who has shown a great capacity for patience and understanding as he has endured the past five years of my graduate studies and research and has provided inexhaustible love, support, and encouragement.

TABLE OF CONTENTS

ACKNOWLEDGEMENTS	ii
TABLE OF CONTENTS	iv
LIST OF TABLES	vi
LIST OF FIGURES	vii
TABLE OF SYMBOLS	xi
CHAPTER I – INTRODUCTION.....	1
Justification / Rationale	1
Research Objectives	6
CHAPTER II - LITERATURE REVIEW AND EQUATIONS.....	7
Factors that contribute to infiltration rate	7
Physical Basis of Equations / Richards Equation	15
Approximate Models	19
Kostiakov Equation.....	20
Horton Equation.....	24
Holtan Equation	27
Philip Equation.....	31
Smith & Parlange Equation	35
Green-Ampt Equation.....	36
Summary of Literature Review	47
CHAPTER III - METHODS AND MATERIALS.....	50
Study Sites	50
Rainfall Simulations	54
Field Measurements	54
Development of Infiltration Curves	55
Sampling Procedure	56
Laboratory Measurements/ Development of Parameters	57
Initial Volumetric Soil Water Content and Bulk Density.....	57
Saturated Hydraulic Conductivity.....	59
Soil Water Retention Curve Determination.....	61
Sensitivity Analysis	67
Kostiakov Equation Sensitivity.....	69
Horton Equation Sensitivity.....	69
Holtan Equation Sensitivity	70
Philip Equation Sensitivity	70
Green-Ampt Equation Sensitivity.....	71
Model Calibration	72
Kostiakov Equation.....	74
Horton Equation.....	75
Holtan Equation	76
Philip Equation.....	78
Green-Ampt Equation.....	79

Model Validation	80
Statistical Methods	81
CHAPTER IV - RESULTS AND DISCUSSION	83
Comparison of Sites	83
Discussion of Infiltration Curves	83
Discussion of Laboratory Results	86
Initial Water Content.....	86
Bulk Density Measurement.....	88
Saturated Hydraulic Conductivity.....	90
Soil Water Retention Curves.....	92
Bubbling Pressure.....	93
Sensitivity Analysis Results	94
Kostiakov Sensitivity Analysis.....	95
Horton Sensitivity Analysis.....	97
Holtan Sensitivity Analysis.....	99
Philip Sensitivity Analysis.....	102
Green-Ampt Sensitivity Analysis.....	104
Evaluation of Equations - Upper Marlboro Site	108
Holtan Equation.....	112
Philip Equation.....	113
Green and Ampt Equation.....	116
Evaluation of Equations - Poplar Hill Site	118
CHAPTER V. – CONCLUSIONS	120
CHAPTER VI. – SUGGESTIONS FOR FUTURE RESEARCH	122
Appendix A - Table of Equations	123
Appendix B - Tables of Parameters Developed From Soil Samples	124
Appendix B-1 - Table of Parameters for Upper Marlboro Site.....	125
Appendix B-1 - Table of Parameters for Upper Marlboro Site (cont.).....	127
Appendix B-2 - Table of Parameters for Poplar Hill Site.....	128
Appendix B-2 - Table of Parameters for Poplar Hill Site (cont.).....	130
Appendix C - Soil Water Retention Curves	131
Appendix C-1 – SWRCs for Upper Marlboro Site for Each of Six Depths.....	132
Appendix C-2 – SWRCs for Poplar Hill Site for Each of Six Depths.....	138
Appendix D - Capillary Pressure Head as a Function of Saturation	144
Appendix D1- Capillary Pressure Head vs. Saturation - Upper Marlboro Site.....	145
Appendix D2 - Capillary Pressure Head vs Saturation - Poplar Hill Site.....	151
Appendix E - Graphs of Log S_e vs. Log h - Bubbling Pressure Determination ..	158
Appendix E-1 - Log S_e vs. Log h for Upper Marlboro Site for Six Depths.....	159
Appendix E-2 - Log S_e vs. Log h for Poplar Hill Site for Six Depths.....	165
Appendix F - Sensitivity Analyses	171
LITERATURE REFERENCES	177

LIST OF TABLES

Table 1. Symbols used in text	xi
Table 2. Estimates by Hydrology Group for the final infiltration	30
Table 3. Estimates of vegetative parameter "a" in the Holtan infiltration equation	30
Table 4. Source of parameters in each equation.	73
Table 5. Base parameter values for each equation.....	95
Table 6. Condition numbers for Kostikov parameters at 1/3 rd and 2/3 rd the duration of rainfall.	96
Table 7. Condition numbers for Horton parameters at 1/3 rd and 2/3 rd the duration of rainfall.	99
Table 8. Condition numbers for Holtan Equation parameters at 1/3 rd and 2/3 rd duration of rainfall	101
Table 9. Condition numbers for Philip Equation parameters at 1/3 rd and 2/3 rd the duration of rainfall.....	103
Table 10. Condition numbers for Green-Ampt parameters at 1/3 rd and 2/3 rd the duration of rainfall.....	107
Table 11. Sensitive infiltration parameters	107
Table 12. Infiltration curves for all five models and observed infiltration.	110
Table 13. Comparison of goodness of fit for five infiltration equations	110
Table 14. Constant and varied parameters for each equation for the Upper Marlboro site.	112
Table 15. Philip infiltration rates using 3 different values for Ca	114
Table 16. Green-Ampt infiltration rates for a series of depths. Predicted infiltration rates greater than rainfall rates are assumed to be equal to rainfall rates.	117
Table 17. Green-Ampt infiltration rates after the start of predicted runoff.	117
Table 18. Equations for infiltration capacity and time of ponding	123
Table 19. Parameters for Upper Marlboro Site.....	125
Table 20. Parameters for Poplar Hill Site	128
Table 21. Kostikov equation sensitivity analysis	172
Table 22. Horton equation sensitivity analysis	173
Table 23. Holtan equation sensitivity analysis	174
Table 24. Philip equation sensitivity analysis.....	175
Table 25. Green-Ampt equation sensitivity analysis	176

LIST OF FIGURES

Figure 1. Horton infiltration rate curve.....	27
Figure 2. Illustration shows uniform water entry assumption, transmission zone, and sharply defined wetting front.....	37
Figure 3. Illustration of Brooks and Corey method for finding bubbling pressure.	42
Figure 4. Map of Maryland Showing the locations of the two study sites.	51
Figure 5. Preparing soil samples at Poplar Hill just before the November Rainfall simulation.....	52
Figure 6. February Rainfall simulation at Upper Marlboro.....	52
Figure 7. Diagram of constant head system for conductivity measurement. After Black et al., (1965).....	59
Figure 8. Tempe cell apparatus. After Black et al. (1965).....	62
Figure 9. Procedure for first estimation of S_r ; rsf determined from the angle formed between the last two points and a vertical line.	65
Figure 10. December 21 st observed infiltration and predicted infiltration rate curves for Kostiakov and Horton models.	73
Figure 11. The Kostiakov parameters α and K_k were determined by graphing $\log(f)$ as a function of $\log(t)$	74
Figure 12. Horton base parameters β and f_0 can be determined from the slope and y-intercept of the plot of $\ln(f_p - f_c)$ as a function of time.	76
Figure 13. Infiltration rate curve, along with rainfall, and runoff rate curves for Upper Marlboro site for February 28th, 2002 rainfall simulation.	84
Figure 14. Initially dry conditions at Poplar Hill site for November 1st, 2001 rainfall simulation. Infiltration approximately equals rainfall.	85
Figure 15. Average initial water content increases with depth for initially dry conditions at Poplar Hill site. No clear trend is seen for initially wet conditions.	87
Figure 16. Average initial water content was greater at the surface due to organic matter and protection from insolation afforded by vegetative cover and plant residues, but otherwise showed a trend of increasing water with increased depth. The higher values at the greater depths also reflect increasing clay content. Error bars show standard errors for the mean of 5 replicates.	88
Figure 17. Poplar Hill bulk density values change little with depth. Upper Marlboro soils are more heterogeneous, with greater variation in densities between layers. Density increases with depth until a plow pan is reached and then decreases due to increasing clay content in the deeper layers. Error bars show standard errors for the mean of 5 replicates.	90
Figure 18. Saturated hydraulic conductivities for Upper Marlboro site decline with depth. For the Poplar Hill site, no such trend is seen. Error bars show standard errors for the mean of five replicates.	91
Figure 19. Upper Marlboro and Poplar Hill soil water retention curves for 0-6 cm depth.	93

Figure 20. Average bubbling pressure of soil samples from Upper Marlboro and Poplar Hill sites as a function of depth. Error bars show standard errors for the mean of 5 replicates.	94
Figure 21. Kostiakov infiltration rate sensitivity to change in α is greatest initially, but decreases to zero at $t = 1$ h, and then gradually increases again.	96
Figure 22. Infiltration rate sensitivity to f_c increases over time.	97
Figure 23. Horton infiltration rate sensitivity decreases with increasing values of β	98
Figure 24. Horton infiltration rate sensitivity to f_0 decreases over time.	98
Figure 25. Holtan infiltration rate sensitivity to f_c increases slightly over time.	99
Figure 26. Holtan infiltration rate sensitivity to G_{la} decreases over time.	100
Figure 27. Holtan infiltration rate sensitivity to initial SA decreases over time.	101
Figure 28. Philip infiltration rate shows low sensitivity to change in C_a	102
Figure 29. Philip infiltration rate shows initially high, but decreasing sensitivity to change in sorptivity over time.	103
Figure 30. Green-Ampt infiltration rate is directly proportional to saturated hydraulic conductivity, however, saturated hydraulic conductivity decreases as the depth of the wetting front proceeds.	105
Figure 31. Green-Ampt infiltration rate shows low sensitivity to changes in moisture deficit which decreases over time.	106
Figure 32. Green-Ampt equation also shows low sensitivity to changes in S_f	106
Figure 33. Comparison of infiltration equations for Upper Marlboro site.	109
Figure 34. Predicted infiltration rates plotted against observed values.	111
Figure 35. Philip infiltration curves for three different values for C_a	115
Figure 36. Philip equation provides a good estimate of measured infiltration whether or not M_i and S_f are averaged over depth.	116
Figure 37. Green-Ampt and Philip both predict infiltration capacities greater than the observed rainfall rate over the entire hour during which runoff was measured.	119
Figure 38. Soil water retention curves for Upper Marlboro site for samples from depth of 0-6 cm.	132
Figure 39. Soil water retention curves for Upper Marlboro site for samples from depth of 10-16 cm.	133
Figure 40. Soil water retention curves for Upper Marlboro site for samples from depth of 20-26 cm.	134
Figure 41. Soil water retention curves for Upper Marlboro site for samples from depth of 30-36 cm.	135
Figure 42. Soil water retention curves for Upper Marlboro site for samples from depth of 40-46 cm.	136
Figure 43. Soil water retention curves for Upper Marlboro site for samples from depth of 50-56 cm.	137
Figure 44. Soil water retention curves for Poplar Hill site for samples from depth of 0-6 cm.	138
Figure 45. Soil water retention curves for Poplar Hill site for samples from depth of 10-16 cm.	139
Figure 46. Soil water retention curves for Poplar Hill site for samples from depth of 20-26 cm.	140

Figure 47. Soil water retention curves for Poplar Hill site for samples from depth of 30-36 cm.....	141
Figure 48. Soil water retention curves for Poplar Hill site for samples from depth of 40-46 cm.....	142
Figure 49. Soil water retention curves for Poplar Hill site for samples from depth of 50-56 cm.....	143
Figure 50. Capillary pressure head as a function of saturation for Upper Marlboro site for soil samples from depth of 0-6 cm.....	145
Figure 51. Capillary pressure head as a function of saturation for Upper Marlboro site for soil samples from depth of 10-16 cm.....	146
Figure 52. Capillary pressure head as a function of saturation for Upper Marlboro site for soil samples from depth of 20-26 cm.....	147
Figure 53. Capillary pressure head as a function of saturation for Upper Marlboro site for soil samples from depth of 30-36 cm.....	148
Figure 54. Capillary pressure head as a function of saturation for Upper Marlboro site for soil samples from depth of 40-46 cm.....	149
Figure 55. Capillary pressure head as a function of saturation for Upper Marlboro site for soil samples from depth of 50-56 cm.....	150
Figure 56. Capillary pressure head as a function of saturation for Poplar Hill site for soil samples from depth of 0-6 cm	151
Figure 57. Capillary pressure head as a function of saturation for Poplar Hill site for soil samples from depth of 10-16 cm	152
Figure 58. Capillary pressure head as a function of saturation for Poplar Hill site for soil samples from depth of 20-26 cm	153
Figure 59. Capillary pressure head as a function of saturation for Poplar Hill site for soil samples from depth of 30-36 cm	154
Figure 60. Capillary pressure head as a function of saturation for Poplar Hill site for soil samples from depth of 40-46 cm	155
Figure 61. Capillary pressure head as a function of saturation for Poplar Hill site for soil samples from depth of 50-56 cm	156
Figure 62. Curves for $\log S_e$ vs. $\log h$ used to determine bubbling pressure for Upper Marlboro site for soil depth 0-6 cm	159
Figure 63. Curves for $\log S_e$ vs. $\log h$ used to determine bubbling pressure for Upper Marlboro site for soil depth 10-16 cm	160
Figure 64. Curves for $\log S_e$ vs. $\log h$ used to determine bubbling pressure for Upper Marlboro site for soil depth 20-26 cm	161
Figure 65. Curves for $\log S_e$ vs. $\log h$ used to determine bubbling pressure for Upper Marlboro site for soil depth 30-36 cm	162
Figure 66. Curves for $\log S_e$ vs. $\log h$ used to determine bubbling pressure for Upper Marlboro site for soil depth 40-46 cm	163
Figure 67. Curves for $\log S_e$ vs. $\log h$ used to determine bubbling pressure for Upper Marlboro site for soil depth 50-56 cm	164
Figure 68. Curves for $\log S_e$ vs. $\log h$ used to determine bubbling pressure for Poplar Hill site for soil depth 0-6 cm	165
Figure 69. Curves for $\log S_e$ vs. $\log h$ used to determine bubbling pressure for Poplar Hill site for soil depth 10-16 cm	166

Figure 70. Curves for $\log S_e$ vs. $\log h$ used to determine bubbling pressure for Poplar Hill site for soil depth 20-26 cm	167
Figure 71. Curves for $\log S_e$ vs. $\log h$ used to determine bubbling pressure for Poplar Hill site for soil depth 30-36 cm	168
Figure 72. Curves for $\log S_e$ vs. $\log h$ used to determine bubbling pressure for Poplar Hill site for soil depth 40-46 cm	169
Figure 73. Curves for $\log S_e$ vs. $\log h$ used to determine bubbling pressure for Poplar Hill site for soil depth 50-56 cm	170

TABLE OF SYMBOLS

Table 1. Symbols used in text

Symbol	Definition	Units
A	Cross sectional Area	L^2
a	i.e. index of surface-connected porosity, and a function of surface conditions and the density of plant roots.	
b	y-intercept	
B	A parameter in the Smith Parlange equation which is a function of the soil water content and is approximately equal to one half the sorptivity squared.	
c	Value of dependent variable	
Δc	Change in value of dependent variable	
C_a	A rate constant that may be approximated by $K_s/3$, f_c , or $2K_s/3$. (Philip)	Lt^{-1}
$C(h)$	water holding capacity = $\partial\theta/\partial h$	L^{-1}
C_v	viscous resistance correction factor (Morel-Seytoux & Khanji,1974)	
CN_k	Condition number	
d	diameter	L
d	depth of a soil layer	L
D	Total depth of combined soil layers	L
$D(\theta)$	diffusivity	L^2t^{-1}
f	Infiltration rate	Lt^{-1}
f_c	final constant infiltration rate as soil approaches saturation	Lt^{-1}
f_o	the infiltration capacity at onset of infiltration	Lt^{-1}
f_p	infiltration capacity	Lt^{-1}
f_{pond}	Infiltration at time of ponding	Lt^{-1}
F	cumulative infiltration	L

Symbol	Definition	Units
F_p	Cumulative infiltration at time of ponding	L
g	acceleration due to gravity	Lt^{-2}
GI	growth index of crop in percent of maturity (Holtan)	
h	Capillary pressure head	L
h_b	bubbling pressure measured in cm of water (Brooks-Corey)	L
h_{ce}	Water entry suction	L
H	Total hydraulic head	L
H_o	Ponded depth	L
k	Average measured value of typical literature value for parameter	
Δk	Change in parameter value	
K_e	Effective saturated hydraulic conductivity	Lt^{-1}
K_i	Saturated hydraulic conductivity for layer i , where $i = 1 \dots 6$	Lt^{-1}
K_{fs}	hydraulic conductivity of the transmission zone (Green – Ampt)	Lt^{-1}
$K(h)$	hydraulic conductivity = $k\rho g/\mu$	Lt^{-1}
K_k	Empirical constant in Kostiakov equation	
K_r	relative hydraulic conductivity = $K(h)/K_s$	
L	Length or dimension of distance	
L_f	distance from the soil surface to the wetting zone. (Green – Ampt)	L
m	slope	
m_s	Mass of soil	M
m_w	Mass of water	M
M	Dimension of mass	
M_i	moisture deficit = $\theta_i - \theta_s$	L^3L^{-3}
n	Number of measurements	
O_i	Observed value	
P	Cumulative rainfall depth	L

Symbol	Definition	Units
P_i	Predicted value	
$P(t)$	application or precipitation rate	Lt^{-1}
q_z	specific flow rate in the z direction	Lt^{-1}
Q	flow rate	L^3t^{-1}
ri	Replication, where $i = 1..5$	
R	rainfall intensity	Lt^{-1}
R_p	rainfall rate at time of ponding (Smith, Parlange)	Lt^{-1}
RO	Cumulative runoff depth	L
RO_t	Average runoff depth for time interval, Δt	L
rsf	Residual saturation factor	
S	sorptivity	$Lt^{-1/2}$
SA	available storage in the surface layer of "A" horizon, in equivalent inches of water = $(\theta_s - \theta_i) d$ (Holtan)	L
S_{av}	average suction head at the wetting front	L
S_e	effective saturation	
S_{eff}	effective sorptivity	$Lt^{-1/2}$
S_f	effective suction at the wetting front	L
S_i	saturation	
S_r	residual saturation	
SS	Surface storage depth	L
t	time	t
Δt	Time interval	t
t_p	time of ponding	t
V	volume	L^3
V_s	Volume of soil	L^3
V_w	Volume of water	L^3

Symbol	Definition	Units
z	vertical coordinate	L
α	Empirical constant in Kostiakov equation	
α_i	Angle formed between last 2 points of capillary pressure vs. saturation curve and a vertical line.	
β	a soil parameter that controls the rate of decrease of infiltration and must depend on initial water content, θ_i and application rate, R. (Horton)	
χ	A unitless empirical constant (Verma and Brutsaert)	
ε	An empirical constant (Verma and Brutsaert)	$(ML^{-1}t^{-2})^\chi$
γ	Specific weight of a fluid	
ϕ	porosity	L^3L^{-3}
η	Exponent to which the ratio of bubbling pressure over the capillary pressure is raised to describe the relative permeability of the wetting phase. $\eta = 2 + 3\lambda$ (Brooks-Corey)	
λ	pore-size distribution index (Brooks-Corey)	
μ	dynamic viscosity	$ML^{-1}t^{-1}$
θ	volumetric water content; dimensionless	L^3L^{-3}
θ_L	Water content for which hydraulic conductivity is equal to rainfall rate	L^3L^{-3}
θ_m	gravimetric water content; dimensionless	MM^{-1}
θ_s	saturated water content; dimensionless	L^3L^{-3}
ρ_b	bulk density of soil	ML^{-3}
ρ_w	density of water	ML^{-3}
ψ	soil water suction ($\psi = -h$).	L
ψ_c	capillary pressure	$ML^{-1}t^{-2}$

CHAPTER I – INTRODUCTION

Justification / Rationale

Infiltration is one of the major components of the hydrologic cycle. Water that falls as precipitation may run over land eventually reaching streams, lakes, rivers and oceans or infiltrate through the soil surface, into the soil profile. Water that runs off over land causes erosion, flooding and degradation of water quality. Infiltration, on the other hand, constitutes the sole source of water to sustain the growth of vegetation, is filtered by the soil which removes many contaminants through physical, chemical and biological processes, and replenishes the ground water supply to wells, springs and streams (Rawls et al.,1993; Oram, 2005). Infiltration is critical because it supports life on land on our planet. The ability to quantify infiltration is of great importance in watershed management. Prediction of flooding, erosion and pollutant transport all depend on the rate of runoff which is directly affected by the rate of infiltration. Quantification of infiltration is also necessary to determine the availability of water for crop growth and to estimate the amount of additional water needed for irrigation. Also, by understanding how infiltration rates are affected by surface conditions, measures can be taken to increase infiltration rates and reduce the erosion and flooding caused by overland flow. In order to develop improved hydrologic models, accurate methods for characterizing infiltration are required (Shirmohammadi, 1984). In spite of its great importance, many water quality models still lack proper quantification of infiltration. The widely used water

quality models including ANSWERS (Areal Non-point Source Watershed Environment Simulation) (Beasley and Huggins, 1980), CREAMS (Knisel, 1980), GLEAMS (Leonard et al., 1987), (Young et al., 1989), EPIC (Sharpley and Williams, 1990), and SWAT (Arnold et al., 1998) all use the SCS Curve Number method, an empirical formula for predicting runoff from daily rainfall (Croley, 2005). Croley and He (2005) note that several researchers have expressed concern that it does not reproduce measured runoff from specific storm rainfall events because the time distribution is not considered (Kawkins, 1978; Wischmeier and Smith, 1978; Beven, 2000; Garen and Moore, 2005). Additional limitations of the Curve Number method include lack of explicit account for the effect of the antecedent moisture conditions in runoff computation, difficulties in separating storm runoff from the total discharge hydrograph, and runoff processes not considered by the empirical formula (Beven, 2000; Garen and Moore, 2005). Consequently, estimates of runoff and infiltration derived from the Curve Number method may not be representative of observed values. Since infiltration and runoff estimates are used to determine sediment, nutrient, and pesticide loadings, use of the Curve Number method may also result in inaccurate estimates of non-point source pollution rates (Croley and He, 2005).

Infiltration modeling approaches are often separated into three categories: physically based, approximate, and empirical models. The physically based approaches require solution of the Richards' equation (Richards, 1931), which describes water flow in soils in terms of the hydraulic conductivity and the soil water pressure as functions of soil water content, for specified boundary conditions. Solving this equation is extremely

difficult for many flow problems requiring detailed data input and use of numerical methods (Rawls et al, 1993).

In 1982, Skaggs and Khaleel stated that although numerical methods that allow the hydrologist to quantify the vertical percolation of water are critical for assessment of groundwater recharge and in the analysis of contaminant movement through soil, numerical solutions are costly, data intensive, and time intensive computational procedures requiring numerous field measurements to be made and therefore are rarely used in practice. Since the above statement was written, improvements in computer technology have greatly facilitated the use of numerical techniques. However, the large quantity and the complexity of the measurements necessary to obtain much of the soil property data required for these numerical solutions impose a more severe limitation that has not diminished with time. Consequently, for many applications, equations that simplify the concepts involved in the infiltration process are advantageous (Rawls et al., 1993).

Simplified approaches include empirical models such as Kostiaikov, Horton, and Holtan, and approximate physically based models like those of Green and Ampt and Philip. Empirical models tend to be less restricted by assumptions of soil surface and soil profile conditions, but more restricted by the conditions for which they were calibrated, since their parameters are determined based on actual field-measured infiltration data (Hillel, 1998; Skaggs and Khaleel, 1982). Equations that are physically based approximations use parameters that can be obtained from soil water properties and do not require measured infiltration data.

It has been noted that different approximate equations for infiltration result in different predictions for infiltration rate, time of ponding and time of runoff even when measurements from the same soil samples are used to derive parameter values. Also, different equations for infiltration require different parameters to be used. There are many factors that contribute to the infiltration rate including time from onset of rain or irrigation, initial water content of the soil, hydraulic conductivity, surface conditions, and profile depth and layering (Hillel, 1998).

All the infiltration equations make use of some of these factors in characterizing infiltration. However the more physically based equations rely more heavily on the soil hydraulic and physical properties occurring within the profile, such as saturated hydraulic conductivity, soil moisture gradient, and suction at the wetting front. Empirical models rely more on parameters that are determined by curve fitting or estimated by other means and thus may better reflect the effect of differences in surface conditions than the physical models, as long as parameters are calibrated separately for those different conditions. Additionally, sometimes approximate physically based models are used as empirical models with parameters determined in a similar manner. The assumptions, form and intent of each equation need to be considered in deciding which equation to use for a particular application.

Data were collected from rainfall simulation events at two different locations and laboratory analyses of soil samples from those locations were conducted to obtain measurements from which different parameters for different infiltration models were developed. These parameters were then used in five infiltration rate equations to determine their prediction accuracy in mimicking the measured infiltration rates. The

equations investigated in this study were those of Kostiakov, Horton, Holtan, Philip, and Green-Ampt (Hillel, 1998; Rawls et al., 1993, Skaggs and Khaleel, 1982; Clemmens, 1983; Hartley, 1992; Horton, 1940; Bevin, 2004; Holtan et al. 1967; Holtan and Lopez, 1970; Philip, 1957a,b,c; Green and Ampt, 1911).

Data collected during an earlier rainfall simulation at one of the sites was used to calibrate the infiltration models. The two rainfall simulation locations allowed an evaluation of the prediction accuracy of the five equations for two different types of coastal plain soil. Additionally, a dry and a wet run were executed at one rainfall simulation site so that the effects of different initial water contents on the ability of the various field equations to predict infiltration could be examined. This research should benefit soil and water conservation engineers by providing a recommendation for the most appropriate infiltration model(s) to use for each of these two Coastal Plain soils and for each antecedent water condition.

It is expected that under particular conditions, one equation will provide better predictions for infiltration than another. However, it has not been spelled out, which infiltration equations work best under which conditions. It is the goal of this study to compare predictions of infiltration rates by five equations with measured values at two different sites and to evaluate the predictive abilities of these equations under the specific conditions. This study is just a small step toward filling in this gap. It would require a great many other studies to complete this task.

Research Objectives

- I. Determine which parameters of each of the five equations are the most sensitive.
- II. Determine the prediction accuracy of each of the five equations for the two rainfall simulation sites by using the root mean squared error to determine goodness of fit for each predicted infiltration rate against measured values.
- III. Make recommendation for the best equation to use for each coastal plain soil type and initial water content.

CHAPTER II - LITERATURE REVIEW AND EQUATIONS

Factors that contribute to infiltration rate

Infiltration is the entrance of water originating from rainfall, snowmelt or irrigation, from the soil surface into the top layer of the soil. Redistribution is the movement of water from point to point within the soil. These two processes cannot be separated because the rate of infiltration is strongly influenced by the rate of water movement within the soil below. After each infiltration event, soil water movement continues to redistribute the water below the surface of the soil (Rawls et al., 1993). Many of the same factors that control infiltration rate also have an important role in the redistribution of water below the soil surface during and after infiltration. Thus, an understanding of infiltration and the factors that affect it is important not only in the determination of surface runoff, but also in understanding subsurface movement and storage of water within a watershed (Skaggs and Khaleel, 1982).

The movement of water is always from higher energy state to lower energy state and the driving force for the movement is the potential difference between energy states. Three important forces affect the movement of water through soil. First the gravitational force, or potential difference, causes water to flow vertically downward. This is because the gravitational potential energy level of water at a given elevation in the soil profile is

higher than that of water at a lower elevation. Also, if there is standing water on the surface, the weight of the ponded water exerts hydrostatic pressure which increases the rate of infiltration, also due to the gravitational force. Second adhesion, or the attraction of the soil matrix for water is responsible for the phenomena of adsorption and capillarity. The matric or capillary potential refers to the energy state of the water molecules adsorbed onto the soil solids which is much reduced compared to that of bulk water (Hillel, 1998). To a lesser extent cohesion, which describes the attraction of water molecules to each other, lowers the energy state. Together adhesive and cohesive forces produce a suction force within soil that reduces the rate of movement of water below the soil surface. The higher the soil water content the weaker the suction force and the lower the matric potential difference. Third, the attraction of ions and other solutes towards water, result in osmotic forces, that tend to reduce the energy level in the soil solution. Osmotic movement of pure water across a semipermeable membrane into a soil solution is evidence of the lower energy state of the soil solution (Bolt and Miller, 1958; Hilhorst et al., 2001).

Factors that control infiltration rate include soil properties that are strongly affected by these three forces, such as hydraulic conductivity, diffusivity and water holding capacity. These soil properties are related to the characteristics of soil texture, structure, composition, and degree of compaction, which influence soil matric forces and pore space. Additionally, antecedent water content, type of vegetative or other ground cover, slope, rainfall intensity and movement and entrapment of soil air are important factors that also affect infiltration rates. The hydraulic conductivity is of critical importance to infiltration rate since it expresses how easily water flows through soil and is a measure of

the soil's resistance to flow. The unsaturated hydraulic conductivity is a function of pressure head (Serrano, 1997) and distribution of water in the soil matrix. The saturated hydraulic conductivity, the hydraulic conductivity at full saturation, is used as a parameter in many of the infiltration equations, since it is easier to determine than either the unsaturated hydraulic conductivity or the diffusivity.

Diffusivity is equal to the hydraulic conductivity divided by the differential water capacity (the rate of change of water content with soil water pressure), or the flux of water per unit gradient of water content in the absence of other force fields (SSSA, 1975). Since diffusivity is directly proportional to hydraulic conductivity, usually only the saturated hydraulic conductivity is used in the approximate infiltration equations.

Water holding capacity is the amount of water a soil can hold due to pore size distribution, texture, structure, percentage of organic matter, chemical composition, and current water content. For saturated conditions, the water holding capacity is zero and the hydraulic head is positive (Skaggs and Khaleel, 1982). While the water holding capacity can be found in the h based Richards equation (2.7), it is not directly used as a parameter in the approximate equations. However, the water holding capacity influences the values of the average suction at the wetting front and sorptivity, as well as some of the empirical parameters. The soil texture which refers to the proportion of sand, silt, and clay that a soil comprises directly affects the hydraulic conductivity, diffusivity and water holding capacity. Soils with higher sand percentages have larger size particles, larger pores, lower water holding capacity and higher hydraulic conductivity, diffusivity and infiltration rates than clay soils which have smaller micropores and bind water molecules more tightly.

Soil structure describes the adhesion and aggregation of soil particles and formation of plates, blocks, columns, lumps, and cracks and is affected by chemical composition of soil particles, amount of organic matter present, soil texture, water content, and activity of organisms such as earthworms, insects, fungi, plant roots and microbes. Soil structure affects the path by which water moves through the soil (Brady and Weil, 1999).

Micropores are generally less than a micrometer in width, and occur typically in clayey soils (Hillel, 1998). Water in these pores is referred to as adsorbed, bound or residual water because it is discontinuous and is affected by such phenomena as cation adsorption, hydration, anion exclusion and salt sieving, and therefore does not participate in normal flow behavior (Hillel, 1998). Capillary pores are the typical pores in a medium textured soil that range in width from several micrometers to a few millimeters. Water in these pores obey the laws of capillarity and Darcian flow (Hillel, 1998). A deep homogeneous soil (containing only capillary pores), such as is assumed in many infiltration equations, is subject to uniform flow in which the infiltration rate decreases as the moisture gradient declines. Macropores are diverse structural pores that are relatively large compared to those in the surrounding soil (Beven and Germann, 1982). They are channels formed by biological activity such as that of plant roots and earthworms, and cracks and fissures caused by physical and chemical weathering processes (Beven and Germann, 1982). When empty of water, macropores constitute barriers to capillary flow, permitting only slow film-creep along their walls. When filled with water however, macropores permit very rapid, often turbulent, downward movement of water to lower layers of the soil profile (Hillel, 1998). This rapid channel drainage that often bypasses much of the soil matrix and can drastically alter infiltration rates is called preferential

flow (Simunek et al. 2003). Even for relatively small earthworm channels, the flow rate in macropores seems to be always higher than the rainfall intensity (Bouma et al., 1982). However, because of the inherent modeling difficulties, most infiltration equations assume uniform flow, ignoring the existence of preferential flow. Correct assessment of the internal hydrological behavior of the soil profile is especially important for the simulation of pollutant transport processes or for assessment of land-use (Weiler, 2005).

Soil compaction results from applying pressure on the soil surface, which reduces pore space, damages soil structure, reduces the air available to plant roots and other soil organisms and reduces infiltration rates. Rainfall on bare soil can cause soil compaction. Often where soils have been plowed repeatedly with heavy equipment there is a hardened and compacted layer below the topsoil called a plowpan, which may impede redistribution. A naturally hardened layer called a fragipan may also obstruct the vertical movement of water (Brady and Weil, 1999).

Antecedent or initial water content affects the moisture gradient of the soil at the wetting front, the available pore space to store water and the hydraulic conductivity of the soil. Initial water content is therefore a critical factor in determining the rate of infiltration and the rate at which the wetting front proceeds through the soil profile. The drier the soil is initially, the steeper the hydraulic gradient and the greater the available storage capacity; both factors that increase infiltration rate (Skaggs and Khaleel, 1982). The wetting front proceeds more slowly in drier soils, because of the greater storage capacity, which fills as the wetting front proceeds (Philip, 1957c).

Vegetation and other ground covers such as mulches and plant residues reduce soil temperature and evaporation from the soil surface, but vegetation also loses moisture

through transpiration. Vegetation increases infiltration rates by loosening soil through root growth and along with natural mulches and plant residues, intercept rain drops, which compact and damage the structure of bare soil and cause surface sealing and crusting. Living and dead plant material also add organic matter to the soil which improves soil structure and water holding capacity and provide habitat for earthworms which further enhance the soil constitution and increase infiltration rates. Soil water content is also affected by seasonal changes in water use by plants, stage of plant growth, spacing of plants, type of vegetation, depth of roots, and extent of canopy coverage.

Slope also affects infiltration rate. A decrease in water infiltration rate was observed with increase in the slope steepness for grass covered slopes (Haggard et al., 2005; Huat et al., 2006). According to Haggard et al. (2005), the slope may have the greatest effect on surface runoff production and infiltration rate when the soil is close to saturation. On the other hand there is evidence that on bare sloping land infiltration rates are higher than on bare flat land (Poesen, 1984). This effect is most likely due to reduced seal development on sloping land, as greater runoff velocities maintain a larger proportion of sediment particles in a suspended state resulting in more open pore structure (Römken et al., 1985).

Rainfall intensity is the instantaneous rainfall rate, and for a uniform storm or rainfall simulation may be obtained by dividing the depth of rainfall by the duration of rainfall. For non-ponded conditions, the maximal rate of infiltration called the infiltration capacity by Horton (1940) or infiltrability by Hillel (1971), equals or exceeds the rainfall intensity and the rainfall intensity provides the upper limit for the infiltration rate. The infiltration rate, therefore equals the rainfall rate until the time of ponding. If the rate of

rainfall is less than the saturated hydraulic conductivity for the soil, infiltration may continue indefinitely at the rainfall rate without the occurrence of ponding. In this case the water content of the soil does not reach saturation, but approaches a limiting value, which depends on the rainfall intensity. For a given rainfall intensity, R , the soil profile approaches a uniform water content θ_L , where θ_L is the water content for which the hydraulic conductivity, K , is equal to the rainfall rate, R ; $K(\theta_L) = R$. Since unsaturated hydraulic conductivity increases with increasing water content, the higher the rainfall intensity, the higher the value of θ_L (Skaggs and Khaleel, 1982).

When the rainfall intensity exceeds the ability of the soil to absorb water, infiltration proceeds at the infiltration capacity. At the time of ponding, the infiltration capacity can no longer keep pace with the rainfall intensity and depression storage fills up and then overflows as runoff. If the rainfall has a higher intensity, depression storage will fill faster and time of runoff will occur sooner, after the time of ponding. The rate of infiltration (f) after time of ponding, however, will not depend on rainfall intensity (R) for f less than R except to the degree that more intense rainfall may cause greater raindrop splash and greater surface sealing. Raindrop splash is the splashing of soil particles (and water) into the air when bombarded by raindrops. This damages the surface soil structure and causes soil detachment and surface sealing which occurs when enough soil particles that splash into the air, land in pore openings, and block them from infiltrating water. Much of the decrease in infiltration rate seen in unprotected soils is attributed to surface sealing (Shirmohammadi, 1984). Vegetation protects the soil from raindrop splash by intercepting and absorbing the energy of the raindrops. Crusting is the drying out and hardening of the surface sealed layer. Crusting may cause immediate ponding with very

low infiltration rate. A long soaking rain will tend to soften the crust so that after a time infiltration rate may increase.

Water moving into a soil profile displaces air, which is forced out ahead of the wetting front. If there is a barrier to the free movement of air, such as a shallow water table, or when a permeable soil is underlain by a relatively impermeable soil, the air becomes confined and the pressure becomes greater than atmospheric. Compressed air ahead of the wetting front and the counter flow of escaping air may drastically reduce infiltration rates (Shirmohammadi,1985). Wangemann et al. (2000) found that for dry soils and for interrupted flow the main retardant to infiltration was entrapped air, while for wet soils, reduced aggregate stability and surface sealing were the main causes for reduced infiltration rates. Le Van Phuc and Morel-Seytoux (1972) showed that for a two phase flow treatment of infiltration, infiltration rate after a certain time was well below the saturated hydraulic conductivity, which was considered to be a lower limit by all the previous authors. Infiltration tends to be increased for deeper water tables, since the impedance of the compressed air on infiltration is reduced and the soil profile tends to be drier compared to shallow water table conditions (Shirmohammadi, 1984).

Physical Basis of Equations / Richards Equation

A French hydraulic engineer, H. Darcy established in 1856, that the specific flow rate through porous media is proportional to the hydraulic gradient (Kirkham and Powers, 1972).

$$q_z = -K(h) \frac{\partial H}{\partial z} \quad \text{Equation 2.1}$$

where

$H = h + z$ = total hydraulic head; [L],

h = pressure head; [L],

z = vertical distance from the datum plane where $H = 0$; [L],

$\frac{\partial H}{\partial z}$ = hydraulic gradient in the z (vertical) direction,

$K(h)$ = hydraulic conductivity which depends on properties of both the fluid and the porous medium; [Lt^{-1}], and

q_z = specific flow rate ($q = \frac{Q}{A}$) in the z (vertical) direction; [Lt^{-1}].

where

Q = volumetric flow rate; [L^3t^{-1}].

A = area of surface subjected to rainfall or ponding; [L^2].

Darcy's equation is the basis for describing the movement of water through soil.

Hydraulic conductivity is a function of the soil water content, and soil water content is a function of pressure head (Kirkham and Powers, 1972).

A variation of the Darcy equation that applies only to horizontal flow is given by Kirkham and Powers (1972).

$$q = -\frac{K}{\rho g} \left(\frac{p_2 - p_1}{L} \right) \quad \text{Equation 2.2}$$

The relationship between soil water content (θ) and capillary pressure head (h) is a soil property called the soil water retention curve ($h(\theta)$). The function $h(\theta)$ is not a unique function and depends not only on the water content, but also on whether the soil is wetting or drying. In other words, the soil water retention curve exhibits hysteresis. For a detailed discussion of hysteresis, see Childs, (1969).

Richards (1931) derived two equations that are considered to be governing equations of infiltration, because they describe the relationships between the soil properties on which infiltration depends, and are based on Darcy's law and conservation of mass. The soil properties that characterize infiltration are hydraulic conductivity $K(h)$ [Lt^{-1}], diffusivity $D(\theta)$ [L^2t^{-1}], and water holding capacity $C(h)$ [L^{-1}]. For layered soils these properties must be known for each layer, and for anisotropic soils the properties must be known as a function of flow direction (Skaggs and Khaleel, 1982). Anisotropic soils have different physical properties along different axes.

The derivation of the Richards' equation from Darcy's law and the law of conservation of mass is instructive in understanding the infiltration process, as well as in understanding many of the other equations used to approximate infiltration.

Darcy's law repeated from Equation 2.1:

$$q_z = -K(h) \frac{\partial H}{\partial z}$$

where

$H = h + z =$ the hydraulic head; [L],

$q_z =$ specific flow rate ($q = \frac{Q}{A}$) in the z direction; [Lt^{-1}],

$\frac{\partial H}{\partial z}$ = the hydraulic gradient in the z direction and

$K(h)$ = the hydraulic conductivity; [Lt^{-1}].

Conservation of mass requires that the change in water content with respect to time is equal to the change in specific flow rate:

$$\frac{\partial \theta}{\partial t} = -\nabla \cdot q \quad \text{Equation 2.3}$$

Assuming change in flow rate is occurring only in the z direction:

$$\frac{\partial \theta}{\partial t} = -\frac{\partial}{\partial z} [q_z] \quad \text{Equation 2.4}$$

Substituting Equation 2.1 into Equation 2.4:

$$\frac{\partial \theta}{\partial t} = \frac{\partial}{\partial z} \left[K(h) \frac{\partial H}{\partial z} \right] \quad \text{Equation 2.5}$$

Substituting for H in terms of h and z:

$$\frac{\partial \theta}{\partial t} = \frac{\partial}{\partial z} \left[K(h) \frac{\partial h}{\partial z} \right] + \frac{\partial K(h)}{\partial z} \frac{\partial z}{\partial z} \quad \text{Equation 2.6}$$

Using the chain rule, one may state:

$$\frac{\partial \theta}{\partial t} = \frac{d\theta}{dh} \frac{\partial h}{\partial t} \quad \text{Equation 2.7}$$

And the water holding capacity, $C(h)$, is equal to $\partial\theta/\partial h$, which is the slope of the soil-water retention curve.

By substitution:

$$C(h) \frac{\partial h}{\partial t} = \frac{\partial}{\partial z} \left[K(h) \frac{\partial h}{\partial z} \right] + \frac{\partial K(h)}{\partial z} \quad \text{Equation 2.8}$$

This is the h -based Richards equation, which may be used for unsaturated or saturated conditions. The θ -based equation,

$$\frac{\partial \theta}{\partial t} = \frac{\partial}{\partial z} \left[D(\theta) \frac{\partial \theta}{\partial z} \right] + \frac{\partial K(\theta)}{\partial z} \quad \text{Equation 2.9}$$

cannot be used to model flow in soils at or near saturation, because $d\theta$ tends to zero and $D(\theta)$ becomes infinite. The θ based equation also fails in cases of layered profiles, since in cases where abrupt transitions occur between layers, θ is not continuous (Hillel, 1998). Equation 2.9 is the same as Equation 2.8, where

$$D(\theta) = K(h) \frac{dh}{d\theta} \quad \text{Equation 2.10}$$

and $\frac{dh}{d\theta}$ approaches infinity, when moisture content approaches saturation such that $d\theta$ approaches zero. For completely unsaturated flow the θ -based equation is advantageous because changes in both θ and $D(\theta)$ are typically an order of magnitude less than corresponding changes in h and C for the h -based equation. As a result, round-off errors in numerical solutions of the θ -based equation are less significant than for the h -based equation (Skaggs and Khaleel, 1982).

The numerical solution of the Richards equation for a given set of initial and boundary conditions, allows the hydrologist to use the physical properties governing movement of water and air through soils to precisely quantify vertical percolation of water subject to a variety of conditions. These predictions are critical for assessment of groundwater recharge and in the analysis of contaminant movement through soil (Skaggs and Khaleel, 1982).

However, the numerical solution of the Richards equation requires numerous measurements to be made to adequately describe variations in soil properties that occur both vertically in the soil profile and from point to point in the field (Skaggs and Khaleel, 1982), and therefore infiltration models with simplified data requirements are desirable for practical use.

The rationale of simultaneous solutions of Darcy's law and the continuity equation would be highly desirable, but the required estimates of unsaturated hydraulic conductivities and diffusivities are difficult to obtain even in the laboratory. Valid estimates for field scale applications are not available and sequential treatment of successive soil horizons is extremely precarious in the anisotropic conditions characteristic of our watersheds (Holtan, 1967).

Approximate Models

Several equations that simplify the concepts involved in the infiltration process have been developed for field applications. Approximate models such as those of Philip and Green and Ampt apply the physical principles governing infiltration for simplified boundary and initial conditions. They imply ponded surface conditions from time zero on (Hillel, 1998), and are based on assumptions of uniform movement of water from the surface down through deep homogenous soil with a well defined wetting front; assumptions that are more valid for sandy soils than for clay soils (Haverkamp et al., 1987). These assumptions reduce the amount of physical soil data needed from that of numerical solutions, but also limits their applicability under changing initial and boundary conditions (Haverkamp et al., 1987). Equations that are physically based

approximations use parameters that can be obtained from soil water properties and do not require measured infiltration data. Thus they should be able to produce estimates at lower cost than empirical equations.

Other equations are partially or entirely empirical and parameters must be obtained from measured infiltration data or roughly estimated by other means. Empirical equations such as those of Kostiakov and Horton are less restrictive as to mode of water application because they do not require the assumptions regarding soil surface and soil profile conditions that the physically based equations require (Hillel, 1998). Where soils are heterogeneous, and factors such as macropore flow and entrapped air complicate the infiltration process, empirical equations may potentially provide more accurate predictions, as long as they are used under similar conditions to those under which they were developed. This is because their initial parameters are determined based on actual field-measured infiltration data (Skaggs and Khaleel, 1982; Rawls et al. 1993). One characteristic of infiltration that all the equations predict is an initially rapid decrease in rate with time for ponded surfaces (Skaggs and Khaleel, 1982).

Kostiakov Equation

Kostiakov (1932) and independently Lewis (1938) proposed a simple empirical infiltration equation based on curve fitting from field data. It relates infiltration to time as a power function:

$$f_p = K_k t^{-\alpha} \quad \text{Equation 2.11}$$

where

f_p = infiltration capacity [Lt^{-1}],

t = time after infiltration starts [t], and

K_k [L] and α [unitless] are constants that depend on the soil and initial conditions.

The parameters, K_k and α must be evaluated from measured infiltration data, since they have no physical interpretation. The equation describes the measured infiltration curve and given the same soil and same initial water condition, allows prediction of an infiltration curve using the same constants developed for those conditions.

Criddle et al. (1956) used the logarithmic form of the equation

$$\log f_p = \log K_k - \alpha \log t \quad \text{Equation 2.12}$$

to determine the parameter values for K_k and α by plotting $\log f_p$ against $\log t$, which results in a straight line if the Kostiakov equation is applicable to the data. The intercept of the equation (infiltration rate at time $t = 1$) is $\log K_k$ and the slope is $-\alpha$. The higher the value of $-\alpha$, the steeper the slope and the greater the rate of decline of infiltration. The greater the value of K_k , the greater the initial infiltration value (Naeth, 1991). The Kostiakov equation is widely used because of its simplicity, ease of determining the two constants from measured infiltration data and reasonable fit to infiltration data for many soils over short time periods (Clemmens, 1983).

The major flaws of this equation are that it predicts that the infiltration capacity is infinite at t equals zero and approaches zero for long times, while actual infiltration rates approach a steady value (Philip, 1957a; Haverkamp et al., 1987; Naeth, 1991). Also, it can not be adjusted for different field conditions known to have profound effects on infiltration, such as soil water content (Philip, 1957a). Mezencev (1948) proposed a modification to Kostiakov's equation by adding a constant to the equation that represents

the final infiltration rate reached when the soil becomes saturated after prolonged infiltration.

$$f_p = K_k t^{-\alpha} + f_c \quad \text{Equation 2.13}$$

Israelson and Hanson (1967) also developed the modified Kostiakov equation and applied it for estimation of irrigation infiltration. Mbagwu (1993) recommended the modified Kostiakov equation for routine modeling of the infiltration process on soils with rapid water intake rates. The Kostiakov and modified Kostiakov equations tend to be the preferred models used for irrigation infiltration, probably because it is less restrictive as to the mode of water application than some other models. The SIRMOD model (Walker, 1998) simulates the hydraulics of surface irrigation (border, basin and furrow) at the field level and employs the modified Kostiakov infiltration equation to represent infiltration characteristics.

Ghosh (1980, 1983) obtained better results with the Kostiakov equation than the Philip model for fields with wide spatial variability in the infiltration data. Clemmens (1983) found that the Kostiakov equation provided significantly better predictions than the theoretical equations of Philip and GA for border irrigation infiltration data. Naeth (1991) found that the Kostiakov equation fit double ring infiltrometer data very well for all three ecosystems that he studied. Naeth (1988) also found that the Kostiakov equation was sensitive to changes in infiltration capacity brought about through different grazing treatments. However, Gifford (1976) found that the Kostiakov equation did not fit infiltrometer data collected from semi-arid rangelands in Australia and the United States. Gifford (1978) determined that the coefficients in the Kostiakov equation were more

closely related to vegetation factors than to soil factors from infiltrometer data run with soils pre-wet to field capacity prior to the infiltration test.

Ghosh (1985) challenged the commonly accepted view that the value of the α term in the Kostiakov equation lies between zero and one, and proved mathematically that the value of α can be greater than unity. Mbagwu (1990) however, found empirically that the value of α was consistently less than one. Fok (1986) showed that the K_k and α terms of the Kostiakov equation do have physical meaning even though several authors have described it as purely empirical. Mbagwu (1994) found that the two soil properties with greatest influence over the K_k term are the effective porosity and bulk density. Bulk density which correlated inversely with the K_k explained 43% of the variability, effective porosity which is exponentially related to K_k explained 78% of the variability in this parameter. Mbagwu (1994) found a critical effective porosity threshold of 15 – 20 %, below which the value for K_k was drastically reduced. He also found the saturated hydraulic conductivity to be linearly correlated with the Kostiakov's K_k ($r = 0.9823$, $p \leq 0.001$). These three relationships to these physical soil properties he found to be the same for the Kostiakov K_k as they are for the Philip's transmissivity term, C_a . Moreover, Mbagwu (1994) related Kostiakov K_k to Philip's C_a by the equation:

$$K_k = 24.22 C_a - 0.83 \qquad \text{Equation 2.14}$$

which has correlation coefficient (r) of 0.9735, $p \leq 0.001$. Thus the very positive relationship between the two parameters and the similarity of the physical properties that exert influence over them, suggest that the time coefficient K_k in Kostiakov's model has the same physical significance as the Philip's C_a . Both parameters depict the ability of soils to transmit water under ponded infiltration (Mbagwu, 1994). Ghosh (1985) proved

mathematically that the Philip's transmissivity term and the Kostikov's K_k represent similar soil physical properties. Mbagwu (1994) did not find the α term in Kostikov's model to be significantly correlated with any measured soil properties and concluded that α appears to be less influenced by physical properties than other parameters.

Horton Equation

The Horton model of infiltration (Horton, 1939, 1940) is one of the best-known models in hydrology. Horton recognized that infiltration capacity (f_p) decreased with time until it approached a minimum constant rate (f_c). He attributed this decrease in infiltration primarily to factors operating at the soil surface rather than to flow processes within the soil (Xu, 2003). Beven (2004) discovered, upon making a study of Horton's archived scientific papers, that Horton's perceptual model of infiltration processes was far more sophisticated and complete than normally presented in hydrological texts. Furthermore, his understanding of the surface controls on infiltration continue to have relevance today (Beven, 2004).

Horton (1940) noted that his equation

“...can be derived from the simple assumption that the processes involved in the reduction of f_p as rain continues are of the nature of exhaustive properties. These processes include packing of the soil surface by rain, in-washing of fine materials into the soil-surface openings, breaking down of the crumb-structure of the soil, and the swelling of colloids thus closing of sun-checks and other surface openings”.

Horton defines an exhaustion process as one in which the rate of work performed is proportional to the work remaining to be performed. He related the infiltration rate to the rate of work performed and the change in infiltration capacity from f_p to f_c as the work

remaining to be performed, with β as the proportionality factor (Horton, 1940). Horton (1939, 1940) derived his equation for infiltration, which describes a pattern of exponential decay of infiltration rate from this basic relationship.

$$\frac{-df_p}{dt} = \beta(f_p - f_c) \quad \text{Equation 2.15}$$

He divided both sides of equation 2.15 by $f_p - f_c$ and multiplied both sides by dt to yield

$$\frac{-df_p}{f_p - f_c} = \beta dt \quad \text{Equation 2.16}$$

Next he integrated equation 2.16 to obtain

$$\ln(f_p - f_c) = -\beta t + \text{const} \quad \text{Equation 2.17}$$

when $t = 0, f_p = f_o$, therefore const must equal $\ln(f_o - f_c)$. Therefore,

$$\ln \frac{f_p - f_c}{f_o - f_c} = -\beta t \quad \text{Equation 2.18}$$

or

$$\frac{f_p - f_c}{f_o - f_c} = e^{-\beta t} \quad \text{Equation 2.19}$$

The final form of the Horton equation is obtained when both sides of equation 2.18 are multiplied by the denominator on the left hand side followed by addition of f_c to both sides.

$$f_p = f_c + (f_o - f_c) e^{-\beta t} \quad \text{Equation 2.20}$$

where

f_p = the infiltration capacity or potential infiltration rate; $[Lt^{-1}]$,

f_c = the final constant infiltration rate; $[Lt^{-1}]$,

f_o = the infiltration capacity at $t = 0$; $[Lt^{-1}]$,

β = a soil parameter [t^{-1}] that controls the rate of decrease of infiltration and must depend on initial water content, θ_i [L^3L^{-3}] and application rate, R ; [Lt^{-1}].
 t = time after start of infiltration.

The parameters, f_c , β , and f_o must be evaluated from measured infiltration data. Subtracting f_c from both sides of equation 2.20 and then taking the natural log of each side gives the following equation for a straight line.

$$\ln(f_p - f_c) = \ln(f_o - f_c) - \beta t \quad \text{Equation 2.21}$$

When experimental value f_c is subtracted from experimental values for f and the natural log of the resulting values are plotted as a function of time, β can be determined from the slope of the line and f_o can be determined from the intercept. Other methods for finding parameters include a least squares method (Blake et.al., 1968).

Horton's equation has advantages over the Kostiaikov equation. First, at t equals 0, the infiltration capacity is not infinite but takes on the finite value f_o . Also, as t approaches infinity, the infiltration capacity approaches a nonzero constant minimum value of f_c (Horton, 1940; Hillel, 1998). Horton's equation has been widely used because it generally provides a good fit to data. Although the Horton equation is empirical in that β , f_c and f_o must be calculated from experimental data, rather than measured in the laboratory, it does reflect the laws and basic equations of soil physics (Chow et al., 1988).

However, the Horton equation is cumbersome in practice since it contains three constants that must be evaluated experimentally (Hillel, 1998). A further limitation is that it is applicable only when rainfall intensity exceeds f_c (Rawls et al., 1993). Horton's approach has also been criticized because he neglects the role of capillary potential gradients in the decline of infiltration capacity over time and attributes control almost

entirely to surface conditions (Bevin, 2004). Another criticism of the Horton model is that it assumes that hydraulic conductivity is independent of the soil water content (Novotny and Olem, 1994). Fig. 1 shows a Horton Infiltration curve with initial value f_0 and final asymptotic value f_c labeled.

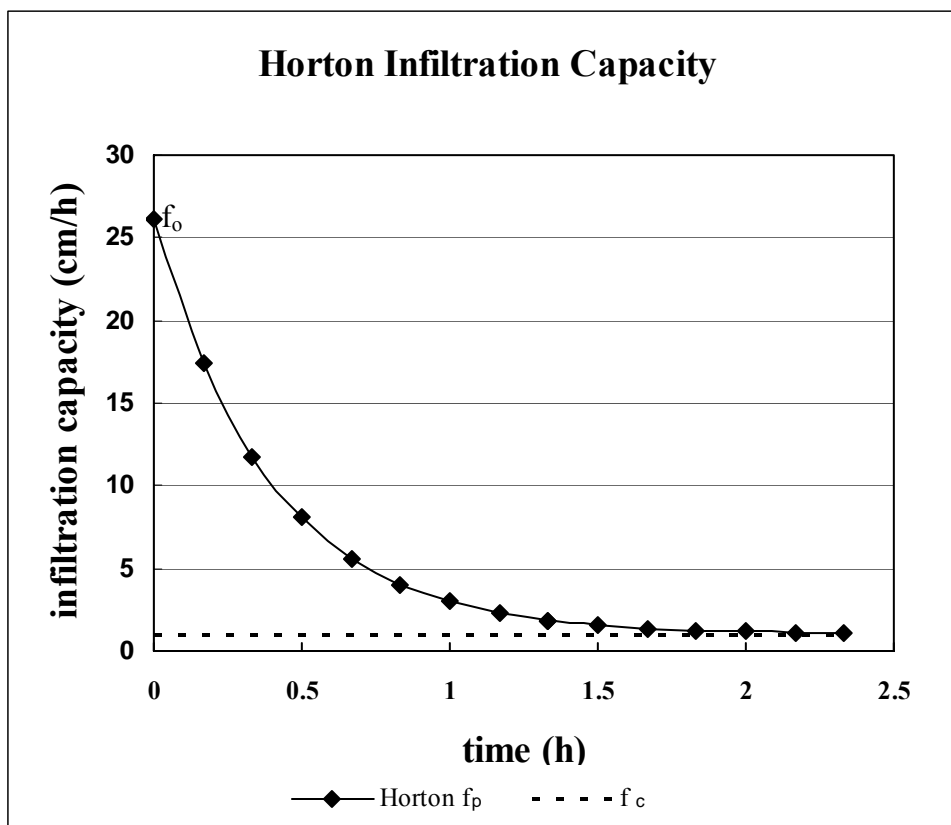


Figure 1. Horton infiltration rate curve

Holtan Equation

Holtan (1961) described an empirical equation based on a storage concept. The equation was developed at the USDA hydrograph laboratory of the Agricultural Research Service in order to provide a means by which infiltration could be estimated using information that was generally available or could be readily obtained for major soils of

the nation (Holtan, 1967). The premise of the equation is that the factors with greatest influence over infiltration rate are soil water storage, surface connected porosity, and the effect of plant root paths (Rawls et al., 1993). After several modifications, the final form of the equation is written as (Holtan and Lopez, 1971):

$$f_p = GIaSA^{1.4} + f_c \quad \text{Equation 2.22}$$

where

f_p = infiltration capacity at given time; [Lt^{-1}],

SA = available storage in the surface layer, "A" horizon at given time; [L],

GI = growth index of crop in percent of maturity

a = an index of surface connected porosity ((in.hr.⁻¹ per (in.)^{1.4} of storage). This is a function of surface conditions and density of plant roots.

f_c = the constant or steady state infiltration rate and in Holtan equation is estimated from the soil hydrologic group; [Lt^{-1}].

SA is computed from:

$$SA = (\theta_s - \theta_i) d \quad \text{Equation 2.23}$$

where

θ_s = saturated water content of the soil; [L^3L^{-3}],

θ_i = actual volumetric water content of the soil; [L^3L^{-3}] and

d = depth of the surface layer; [L].

The Holtan equation is relatively easy to use. The hydrologic soil group can be obtained from the SCS National Engineering Handbook (1964).

Estimates for parameters f_c and a are provided in Table 2 and Table 3. A serious obstacle with the Holtan Equation is the determination of the control depth on which to base SA . Holtan and Creitz (1967) recommended using the depth to the plow layer or to the first impeding layer or depth of A horizon provided in SCS soil survey. However,

Huggins and Monke (1966) found that the effective control depth varied depending on both the surface condition and the farming practices used for seedbed preparation.

Smith (1976) argued that infiltration curves are physically much more closely related to moisture gradients and hydraulic conductivity than to soil porosity and that therefore the Holtan equation could not be expected to adequately describe the infiltration process. However, recent studies have been conducted that show a strong relationship between infiltration rate and soil porosity (Messing et al., 2005; Kozak and Ahuja, 2005). Novotny and Olem, (1994) wrote that although Holtan's model is more complex than Horton's, it appears to be less physically based, since it relates infiltration rate to the total water content in an arbitrarily chosen control layer and to the advancement of the wetting front in the unsaturated soil zone.

Also, since the Holtan equation does not directly reference time, $f(t)$ is difficult to develop. Since infiltration rate is a function of the available water storage, the infiltration equation must be accompanied by a simultaneous solution of the storage equation:

$$SA_t = (SA_{t-1} - F_{t-1} + f_c \Delta t) \quad \text{Equation 2. 24}$$

where

SA_t = available storage at time t; [L],

SA_{t-1} = available storage at time t; [L],

SA_{t-1} = available storage at previous time step; [L],

F_{t-1} = cumulative infiltration at previous time step; [L], and

f_c = final constant infiltration rate (or drainage rate); [Lt^{-1}].

Δt = elapsed time.

Table 2. Estimates by Hydrology Group for the final infiltration rate, f_c in the Holtan Equation (After Musgrave, 1955).

Hydrologic soil group	f_c (in./hr.)
A	0.45 – 0.30
B	0.30 – 0.15
C	0.15 – 0.05
D	0.05 – 0.00

Table 3. Estimates of vegetative parameter "a" in the Holtan infiltration equation (After Frere, et al., 1975).

Land use or cover	Basal area rating*	
	Poor condition	Good condition
Fallow§	0.1	0.3
Row crops	0.1	0.2
Small grains	0.2	0.3
Hay (legumes)	0.2	0.4
Hay (sod)	0.4	0.6
Pasture (Bunch grass)	0.2	0.4
Temporary pasture (sod)	0.2	0.6
Permanent pasture (sod)	0.8	1.0
Woods and forests	0.8	1.0

* Adjustments needed for “weeds” and “grazing”.

§ For fallow land only, poor condition means “after row crop”, and good condition means “after sod”.

Philip Equation

Philip (1957a) developed an infinite-series solution to solve the non-linear partial differential Richards' equation (Richards, 1931), which describes transient fluid flow in a porous medium for both vertical and horizontal infiltration. Philip's rapidly converging series solves the flow equation for a homogeneous deep soil with uniform initial water content under ponded conditions. For cumulative infiltration the general form of the Philip infiltration model is expressed in powers of the square-root of time, t , as

$$F = St^{1/2} + C_{a1}t + C_{a2}t^{3/2} + \dots \quad \text{Equation 2.25}$$

where

F = cumulative infiltration; [L]

S = sorptivity; [$Lt^{-1/2}$], a function of initial and final soil water content, θ_i and θ_n .

C_{a1} , C_{a2} = constants that depend on both soil properties and on θ_i and θ_n .

Philip (1957b) defined sorptivity (S) as the measurable physical quantity that expresses the capacity of a porous medium for capillary uptake and release of a liquid. White and Perroux (1987) referred to sorptivity as an integral property of the soil hydraulic diffusivity. S is constant provided the water content at the inflow end is constant (Jury et al., 1991).

The time derivative of F is the infiltration rate, f ; [Lt^{-1}] which is

$$f = \frac{1}{2}St^{-1/2} + C_{a1} + \frac{3}{2}C_{a2}t^{1/2} + \dots \quad \text{Equation 2.26}$$

For horizontal infiltration (i.e. no gravity driven flow), all terms are zero except for the first term on the right side of equations 2.25 and 2.26 and the equations apply to all times greater than zero (Sullivan et al., 1996). For vertical infiltration, 2.25 and 2.26 apply only

for a short time when the matric-potential gradient is much greater than the gravity-potential gradient (Sullivan et al., 1996). All terms beyond the first two terms on the right-hand side of equations 2.25 and 2.26 are considered to be negligible (Jury et al., 1991).

Philip (1957b) proposed that by truncating his series solution for infiltration from a ponded surface after the first two terms, a concise infiltration rate equation could be obtained which would be useful for small times. The resulting equation is,

$$f = \frac{S}{2} t^{-1/2} + C_a \quad \text{Equation 2.27}$$

where

f = infiltration rate; [Lt^{-1}]

S = sorptivity; [$Lt^{-1/2}$].

t = time after start of infiltration; [t]

C_a = rate constant; [Lt^{-1}]

The form of Philip's truncated equation is very similar to that of Kostiakov. In fact the modified Kostiakov equation with α equal to 0.5 is essentially the same equation. The parameters S and C_a are dependant on the soil and the initial water content and can be evaluated numerically using procedures provided by Philip if the properties of diffusivity and pressure head as a function of soil water content are known. Philip (1957b) and Talsma (1969) showed that the value of the rate constant, C_a , that results from using Philip's method is approximately $K_s/3$. However, the equation predicts values of infiltration rate that are too low for long time periods, because this approximation is not physically consistent; as t approaches infinity, the infiltration rate should approach the

saturated hydraulic conductivity, but C_a does not equal K_s (Philip, 1957b; Youngs, 1968, Skaggs et al., 1969). A comparison of Philip's two-term solution with the GA equation suggested that $C_a = 2/3 K_s$ approximately (Philip, 1957b; Youngs, 1968) with $S = (2M_i K_s S_f)^{1/2}$ where $M_i = (\theta_s - \theta_i)$ is the moisture deficit or air-filled void space, and S_f [L] is the effective suction at the wetting front. Good predictions were obtained for Ballotini glass beads by approximating C_a as $2/3 K_s$, but for slate dust $1/3 K_s$ gave a better fit (Youngs, 1968; Talsma and Parlange, 1972).

A shortcoming of the Philip infiltration model is that the assumptions for which the equation is applicable are rarely found in the field on a large scale. Soil types vary both spatially and with depth, as does vegetation and surface conditions. Although parameter values can be obtained by making point measurements in the field, variability limits the worth of test results for application to larger areas such as watersheds (Sullivan, 1996).

Whisler and Bouwer (1970) found that determining the values of the parameters S and C_a for the Philip equation from physical soil properties was very time consuming and yielded results that were not in agreement with the experimental curve. They were able to obtain close agreement with experimental values when they determined parameter values by curve fitting, but lost the physical significance of the parameters by using this method.

Smiles and Knight (1976) suggested that the appropriateness of infiltration data to the 2-parameter Philip equation can be determined by plotting $Ft^{-1/2}$ as a function of $t^{1/2}$. When equation 2.24 is truncated after the first two terms and both sides are divided through by $t^{1/2}$, an equation for a straight line is obtained

$$Ft^{-1/2} = S + C_a t^{1/2} \quad \text{Equation 2.28}$$

The linearity of this curve for early times indicates that equation 2.26 is appropriate for describing the infiltration process and the values for S and A can be determined from the y-intercept and slope of the line respectively. When used in this manner, the equation is empirical rather than physically based., although it is derived from physical theory.

Philip's model was adapted for constant intensity rainfall by Luce and Cundy (1992) to determine rainfall excess and time of ponding for solution of the kinematic wave overland flow equation. They included depression storage between time of ponding and time of initiation of runoff. The time at which depression storage of depth, h_n is filled is expressed as:

$$h_n = \int_{t_p}^{t_n} R - f(t) dt \quad \text{Equation 2.29}$$

where

R = rainfall intensity

t_p = time of ponding

t_n = time of runoff initiation

and

$$f(t) = S[t - (t_p - t_s)]^{-1/2} + C_a \quad \text{Equation 2.30}$$

where $t_p - t_s$ is a time correction factor, with t_p equaling time of ponding and t_s representing the time when $f(t) = R$ under continuously ponded conditions.

Combining equations 2.29 and 2.30 and integrating gives:

$$h_n = (R - C_a)(t_n - t_p) - 2S(t_n - t_p + t_s)^{1/2} + 2St_s^{1/2} \quad \text{Equation 2.31}$$

The time runoff begins, t_n can be determined by numerically evaluating this equation.

Smith & Parlange Equation

Smith and Parlange (1978) started with Richards' equation and derived an infiltration equation for arbitrary rainfall rates. Ponding time and infiltration capacity after ponding can both be predicted from their model. Only two parameters are used to make predictions by this method, both of which may be calculated from measurable soil properties, or determined from infiltrometer experiments. For soils in which hydraulic conductivity as a function of soil water content varies slowly near saturation, ponding time may be evaluated by:

$$\int_0^{t_p} R dt = \frac{B(\theta_i)}{R_p - K_s} \quad \text{Equation 2.32}$$

$$\approx \frac{S^2/2}{R_p - K_s}$$

where

R = rainfall rate; [Lt^{-1}]

t = time; [t]

R_p = rainfall rate at time of ponding; [Lt^{-1}]

K_s = saturated hydraulic conductivity; [Lt^{-1}]

θ_i = volumetric soil water content; [L^3L^{-3}]

S = sorptivity; [$Lt^{-1/2}$] defined by Philip (1957a,b) and

$$B(\theta_i) \approx (S^2/2)$$

When hydraulic conductivity varies rapidly near saturation, the Smith and Parlange model for time of ponding may be written as,

$$\int_0^{t_p} R dt = \frac{B(\theta_i)}{K_s} \ln \left[\frac{R_p}{R_p - K_s} \right] \quad \text{Equation 2.33}$$

When diffusivity varies slowly near saturation, the value of S^2 may be estimated as,

$$S^2 = 2 \int_{\theta_i}^{\theta_s} (\theta_s - \theta_i) D d\theta \quad \text{Equation 2.34}$$

However, when diffusivity varies rapidly near saturation, the value of S^2 may be estimated as,

$$S^2 = 2 (\theta_s - \theta_i) \int_{\theta_i}^{\theta_s} D d\theta \quad \text{Equation 2.35}$$

Green-Ampt Equation

Green and Ampt (GA) proposed in 1911 an approximate model that directly applies Darcy's law. The original equation was derived for infiltration from a ponded surface into a deep homogeneous soil with uniform initial water content. The GA model has been found to apply best to infiltration into uniform, initially dry, coarse textured soils which exhibit a sharply defined wetting front as depicted in Fig. 2 (Hillel and Gardner, 1970). This pattern is often called a piston displacement profile or plug flow. The transmission zone is a region of nearly constant water content above the wetting front, which lengthens as infiltration proceeds. The wetting front is characterized by a constant matric suction, regardless of time or position and is a plane of separation between the uniformly wetted infiltrated zone and the as-yet totally uninfiltrated zone (Hillel, 1998). These assumptions simplify the flow equation so that it can be solved analytically. Although measured infiltration data are not required to make predictions using the GA

equation, Green and Ampt (1911) recommended that soil physical properties should be measured the field, so that undisturbed field conditions are reflected in the resulting values.

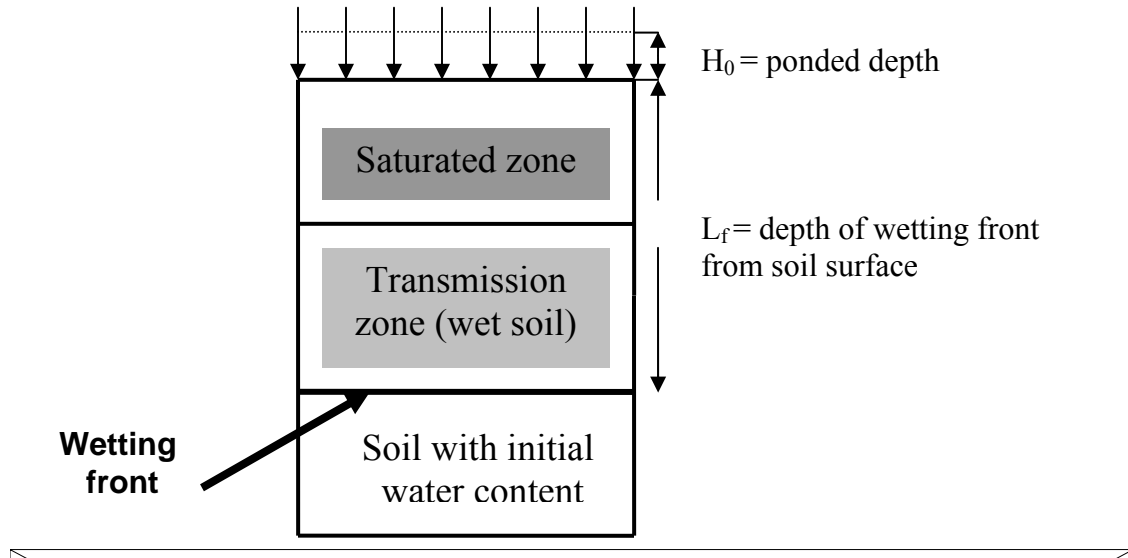


Figure 2. Illustration shows uniform water entry assumption, transmission zone, and sharply defined wetting front.

The following form of the GA equation was derived from direct application of Darcy's Law:

$$f = \frac{K_{fs} (H_0 + S_f + L_f)}{L_f}$$

Equation 2.36

where

f = infiltration rate; [Lt^{-1}],

K_{fs} = hydraulic conductivity of the transmission zone; [Lt^{-1}],

H_0 = the depth of water ponded on the surface; [L],

S_f = the effective suction at the wetting front; [L] and

L_f = the distance from the surface to the wetting front; [L].

Bouwer (1966, 1969) showed that the hydraulic conductivity parameter, as it appears in Equation 2.21, is not the conductivity at full saturated value, because of air entrapped in the soil pores, but is instead the conductivity at residual air saturation. This has also been called ‘resaturated hydraulic conductivity’ (Whisler and Bouwer, 1970). He described measurement of K_{fs} in the field by air-entry permeametry. When field measurements are not feasible, Bouwer (1966) suggested that $K_{fs} = 0.5 K_s$, where K_s is the laboratory value for saturated hydraulic conductivity.

Expressing the cumulative infiltration, F [L] as:

$$F = (\theta_s - \theta_i)L_f = M_i L_f \quad \text{Equation 2.37}$$

and assuming very shallow depth of ponding so that $H_0 \approx 0$, equation 2.36 may be rewritten as,

$$f = K_{fs} + \frac{K_{fs} M_i S_f}{F} \quad \text{Equation 2.38}$$

where M_i is the moisture deficit, or the difference between saturated and initial volumetric water contents. Although Green and Ampt assumed total saturation behind the wetting front, Philip (1954) observed that this was not a necessary requirement. He assumed that θ_s was constant, but not necessarily equal to the total porosity. Similarly, K_{fs} is expected to be slightly less than the saturated hydraulic conductivity. When

$f = \frac{dF}{dt}$ is substituted into Equation 2.38, integration with the condition that $F = 0$ at

$t = 0$, yields:

$$K_{fs} t = F - M_i S_f \ln \left(1 + \frac{F}{M_i S_f} \right)$$

Equation 2.39

This form of the equation relates infiltration volume to time from start of infiltration, which is convenient for some applications.

In spite of the many assumptions under which the GA equation was originally developed, it has been adapted for use under a much wider variety of conditions. The GA equation produced reasonably good predictions for non-uniform soil profiles that become denser with depth (Childs and Bybordi, 1969), for profiles where hydraulic conductivity decreases with depth (Bouwer, 1969) or increases with depth (Bouwer, 1976), and for soils with partially sealed surfaces (Hillel and Gardner, 1970). Bouwer (1969) described a tabular procedure for calculating the GA relationship between cumulative infiltration and time for soils with non-uniform initial water contents and hydraulic conductivities. He showed that the soil profile could be split into layers, each with its own water content, moisture deficit, and hydraulic conductivity from which the GA approach could be used to calculate cumulative infiltration and time intervals (Bouwer, 1969, 1976). Bouwer (1969) calculated an effective hydraulic conductivity for each depth using the harmonic mean of the hydraulic conductivities for the entire profile above that depth.

Morel-Seytoux and Khanji (1974) discovered that the form of Equation 2.23 remains the same when simultaneous movement of water and air is considered. They made slight modifications to the equation using a viscous resistance correction factor, C_v , to account for resistance to air movement and replaced S_f with h , the capillary pressure head, or pressure resulting from soil matric forces. The equation with alterations made by Morel-Seytoux and Khanji (1974) follows:

$$f = \frac{K_s}{C_v} + \frac{K_s M_i h}{C_v F} \quad \text{Equation 2.40}$$

When the air phase is neglected, C_v is 1.0 and Equation 2.40 becomes Equation 2.38. Values for C_v ranged from 1.1 to 1.7 for 5 soils. Infiltration rate (f) was over predicted by Equation 2.25 when K_s was determined by laboratory methods. When K_{fs} was determined in the field and substituted for K_s in Equation 2.40, air resistance was more realistically accounted for and infiltration rate predictions were reliable (Morel-Seytoux and Khanji, 1974).

Shirmohammadi and Skaggs (1985) considered infiltration into soil profiles with shallow water table to be a 3-stage process including an initial stage where pressure builds to a critical value as the air is compressed ahead of the wetting front, an intermediate stage where pressure is maintained at a constant value as air escapes, and a final stage characterized by saturated vertical flow after the wetting front reaches the water table. Their approach used the GA model with modifications to account for the impact of compressed air ahead of the wetting front and the shallow water table.

The effective suction, S_f at the wetting front was obtained by Bouwer (1969) using water entry suction, h_{ce} for S_f . Bouwer suggested that it can also be approximated using one half of the air entry value, also called the bubbling pressure, which like K_{fs} can be measured with an air-entry permeameter.

Wang et al. (1997) derived a set of two-phased flow equations based on the GA model which account for air compression, dynamic change of capillary pressure at the wetting front, and effects of macropores near the soil surface.

Brooks and Corey (1964) described a graphical method for obtaining the bubbling pressure and developed parameters describing pore size distribution and bubbling pressure, which can be used to determine S_f in the Green and Ampt equation (Rawls et al., 1993).

$$S_f = \frac{(2 + 3\lambda)h_b}{2(1 + 3\lambda)} \quad \text{Equation 2.41}$$

where

λ = Brooks-Corey pore-size distribution index, and

h_b = Brooks-Corey bubbling pressure; [L].

In order to determine h_b , it is necessary first to determine S_e :

$$S_{e_i} = \frac{(S_i - S_r)}{(1 - S_r)} \quad \text{Equation 2.42}$$

where

S_e = effective saturation

$S_i = \theta_i/\theta_s$, saturation is the ratio of water content at a given pressure head to saturated water content and

$S_r = \theta_r/\theta_s$ is residual saturation, or the ratio of residual water content at which capillary conductivity is negligible, to water content at saturation.

Brooks and Corey (1964) obtained bubbling pressure (h_b) from the graph of $\log S_e$ versus $\log h$, as shown in Figure 3, by extending a best fit line for the more linear or lower portion of the curve (excluding the wettest portion) through the x-axis. The x-intercept is the log of the bubbling pressure, $\log h_b$. The bubbling pressure is therefore

$$h_b = 10^{\log h_b} .$$

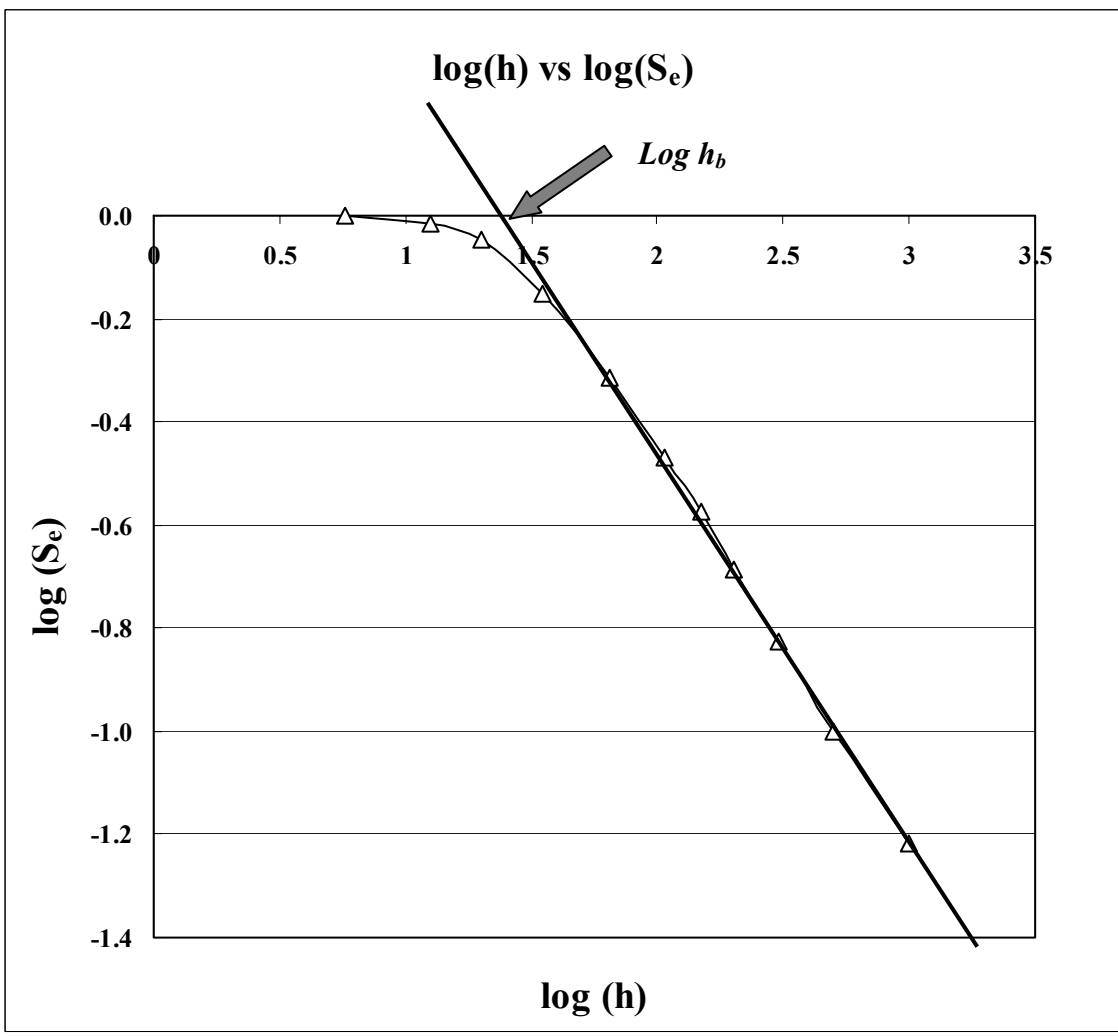


Figure 3. Illustration of Brooks and Corey method for finding bubbling pressure.

The Brooks and Corey model is not accurate for pressure head close to zero, where $x = \log h$ approaches negative infinity, creating a steep asymptote at $h = 0$. A relationship developed by Verma and Brutsaert (1971), provides a smooth transition from very low suction head to the drying curve as shown in Equation 2.43.

$$\theta = nS_i = \frac{n\varepsilon}{(\varepsilon + \psi_c^\lambda)}$$

Equation 2.43

where

θ = soil water content; $[L^3L^{-3}]$,

S_i = degree of saturation; [unitless],

n = porosity; $[L^3L^{-3}]$,

ε = empirical soil parameter that depends mainly on the size of the capillary fringe; $[(ML^{-1}t^{-2})^\gamma]$, and

χ = empirical soil parameter that depends mainly on the pore-size distribution; $[ML^{-1}t^{-2}]$.

ψ_c = capillary pressure; $[ML^{-1}t^{-2}]$.

For the case where capillary pressure, $\psi_c \leq 0$:

$$S_i = 1$$

For the case where capillary pressure, $\psi_c \geq 0$:

$$S_i = \frac{\varepsilon}{(\varepsilon + \psi_c^\chi)}$$

Equation 2.44

The following manipulations of this equation allow the development of the parameters ε and χ . Multiplying both sides of the equation by the denominator on the right side gives:

$$\varepsilon = S_i (\varepsilon + \psi_c^\chi) \quad \text{Equation 2.45}$$

According to the distributive property:

$$\varepsilon - S_i \varepsilon = S_i \psi_c^\chi \quad \text{Equation 2.46}$$

Factoring out ε from the right side gives:

$$\varepsilon(1 - S_i) = S_i \psi_c^\chi \quad \text{Equation 2.47}$$

Dividing both sides of the equation by εS_i gives:

$$\frac{(1 - S_i)}{S_i} = \frac{\psi_c^\chi}{\varepsilon} \quad \text{Equation 2.48}$$

Taking the natural log of each side gives the linear expression:

$$\ln \left[\frac{(1 - S_i)}{S_i} \right] = \chi \ln \psi_c - \ln \varepsilon \quad \text{Equation 2.49}$$

Using soil water retention curve data to determine values for S_i and ψ_c , linear regression can be used with the equation above to determine values for ε , the antilog of the y-intercept, and γ the slope of the regression line.

Mein and Larson (1973) modified the GA equation for use in situations where rainfall intensity is initially less than infiltration capacity. They combined the expression for cumulative infiltration:

$$F = M_i L_f \quad \text{Equation 2.50}$$

with the flow equation where infiltration rate is equal to rainfall intensity, capillary conductivity is assumed to equal K_s , the potential at the surface is zero, and at the wetting front is $(L_f + S_{av})$.

$$R = K_s (S_{av} + L_f) / L_f \quad \text{Equation 2.51}$$

Yielding an expression for cumulative infiltration prior to runoff:

$$F = S_{av} M_i / [(R / K_s) - 1] \quad \text{Equation 2.52}$$

for which $F = 0$ when the soil is saturated and $M_i = 0$ and $F = \infty$ when $R = K_s$ and all rainfall at this low intensity infiltrates.

Although the relationship between infiltration capacity and time depends on rainfall intensity, the relationship between infiltration capacity and cumulative infiltration is essentially independent of rainfall rate. The GA equation is not time based, but Mein and Larson applied the equation to rainfall conditions by determining cumulative infiltration at the time of surface ponding.

$$f = f_{pond} = R = \frac{K_s M_i S_{av}}{F_p} \quad \text{Equation 2.53}$$

where

f_{pond} = infiltration rate at time of ponding; [Lt^{-1}],

R = rainfall rate at time of ponding; [Lt^{-1}] and

F_p = cumulative infiltration at time of ponding; [L].

Since $f = R$ prior to time of ponding, $F_p = R t_p$, then for rainfall at a constant rate infiltration may be expressed as,

$$\begin{aligned} f &= R, & \text{for } t < t_p & \quad \text{Equation 2.54} \\ f &= f_{pond} = R = K_{fs} + \frac{K_{fs} M_i S_{av}}{F_p}, & \text{for } t > t_p & \end{aligned}$$

Mein and Larson (1973) used the unsaturated hydraulic conductivity as a weighting factor and defined the average suction at the wetting front with the equation:

$$S_{av} = \int_0^{\psi_i} \psi dK_r \quad \text{Equation 2.55}$$

where

ψ = soil water suction, $\psi = -h$; [L].

ψ_i = suction; [L] at the initial water content, θ_i and

K_r = relative hydraulic conductivity.

$$K_r = \frac{K(h)}{K_s} \quad \text{Equation 2.56}$$

where

$K(h)$ = unsaturated hydraulic conductivity; [Lt^{-1}] and

K_s = saturated hydraulic conductivity; [Lt^{-1}].

One of the difficulties in obtaining S_{av} by this method is the requirement for the unsaturated hydraulic conductivity, which is not an easy or quick determination to make. Some investigators have used prediction methods to estimate $K(h)$ and then determine S_{av} from equation (2.55). Brakensiek (1977) found that the equation $S_{av} = 0.76 h_b$, where h_b is the desorption bubbling pressure head provided an acceptable estimate for the soils he investigated.

The GA equation is applicable to a wide range of initial, boundary, and soil profile conditions which makes it a popular and widely used method for field applications. The physical significance of parameters and the ability to obtain their values from soil properties makes the model even more attractive. However, as a result of the heterogeneities of field conditions, more reliable predictions are usually made when equation parameters are determined from field measurements. It has been demonstrated that predicted values for infiltration and runoff are most sensitive to errors in moisture deficit, M_i , and saturated hydraulic conductivity, K_s , and less sensitive to errors in S_{av} (Skaggs and Khaleel, 1982).

Summary of Literature Review

Attempts to characterize infiltration for field applications usually involve expression of the infiltration rate or cumulative infiltration algebraically in terms of time and certain soil parameters. The principles governing soil water movement have been applied for simplified boundary and initial conditions in order to develop some of the approximate models, including Green-Ampt, Philip, and Smith-Parlange equations. The parameters for these physical models can be determined from soil water properties when they are available. Other models such as Kostiaikov and Holtan equations are strictly empirical and the parameters must be obtained from measured infiltration data, or from more approximate estimation procedures. Still others including Horton equation are intermediate having some empirical characteristics while still reflecting physical laws of soil water movement. Although attributed to different physical phenomena, all of the approximate models show a rapid decrease in infiltration rate with time during the initial stage of an infiltration event under ponded conditions (Skaggs, 1982). Different equations that describe infiltration produce different predictions for infiltration rates. These equations use different parameters and many were developed for different purposes. Each equation has some shortcomings.

The purely physically based equations, such as GA and Philip equations, are advantageous in not requiring measured infiltration data, but are based on assumptions that can never be entirely valid. Specifically they assume homogeneous soils, uniform initial water content, and piston flow and neglect the effect of entrapped air.

Both of these equations were originally developed for use under ponded conditions and for deep homogenous soils, but the GA equation was subsequently shown to be more versatile, as it can be applied validly under non-ponded conditions and also with a variety of non-homogeneous soil profiles. It has been applied with good results to soil profiles that become denser with depth (Childs and Bybordi, 1969), for profiles where hydraulic conductivity decreases (Bouwer, 1969) or increases with depth (Bouwer, 1976), and for soils with partially sealed surfaces (Hillel and Gardner, 1970). Bouwer (1969) also demonstrated that it could be used with nonuniform initial water contents. Morel-Seytoux and Khanji (1974) discovered that the equation could be used with slight modification when simultaneous movement of water and air is considered. The GA equation, although the earliest proposed, has proven to be the most versatile, and most widely used of all the infiltration equations.

The empirical equations, such as Kostiakov and Horton equations, provide infiltration rates based on measured field data and therefore provide more realistic estimates when measurements can be provided for the same or very similar conditions to the site for which the prediction is to be made. However, the equations have less value as predictive tools when the measured infiltration data on which the parameter values are based, is obtained from a site that differs significantly, from the site of application. Although the parameters depend on initial water content, rainfall application rate, and soil properties, their values cannot be determined by making such measurements, and therefore cannot be easily adjusted to accommodate changes in initial conditions. Actual field measurements of infiltration are required to determine these parameters, making these models much less versatile.

Smith (1976) criticized the Holtan equation for relating infiltration to soil porosity rather than the moisture gradient or hydraulic conductivity, the relationship established by Darcy's law. Holtan attempted to broaden the applicability of his equation by providing tabulated values for various conditions, but these values are very rough estimates. Additionally, determination of the control depth, on which to base available water storage, has proven to be problematic.

CHAPTER III - METHODS AND MATERIALS

Study Sites

Rainfall simulations took place at the University of Maryland's Lower Eastern Shore Research and Education Center (LESREC) Poplar Hill facility on Nanticoke Rd. near Quantico in Wicomico County and at the University of Maryland's Central Maryland Research and Education Center (CMREC) Upper Marlboro facility on Largo Rd in Prince George's County. The site locations are shown on the map in Fig. 4. Soils were coastal plain soils including an Evesboro sandy loam with about 1 percent slope at the Poplar Hill site. The Upper Marlboro soil consisted of a layered Monmouth fine sandy loam to sandy clay soil with clay content increasing with depth below 30 cm and a slope of about 5 percent. The Poplar Hill site had a ground cover of sparse vegetation composed of disturbed grass and weeds. The previous year a soy bean crop was grown at this site. The Upper Marlboro site had a dense weedy ground cover and had been planted in corn the previous year. Rainfall simulations were conducted at the Poplar Hill site on November 1st and 2nd, 2001 for initially dry and initially wet soil conditions, respectively. Fig. 5 shows the preparation of soil samples prior to the November first Rainfall simulation. The plot used in this study is the vacant plot between the plot containing the mound of poultry litter in the foreground and the those containing mounds in the background. Rainfall simulations were conducted on adjacent Upper Marlboro sites on December 21st, 2001 and February 28th, 2002. Fig.

6 is a photograph taken during the February rainfall simulation. Rain gauges are mounted on 3 sawhorses which trisect the plot and runoff is channeled into a flume which is blocked by the shed which houses the recording gauge for runoff.

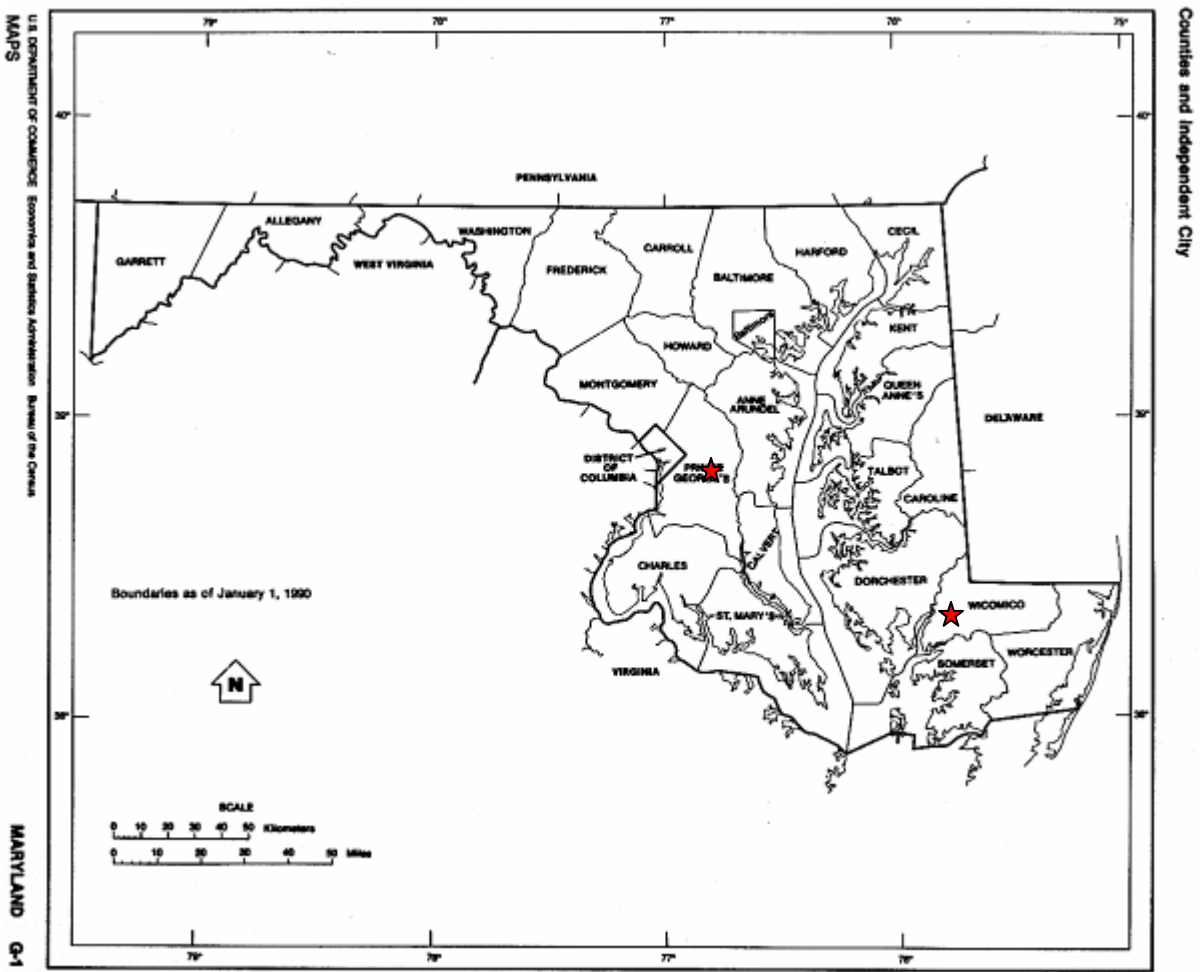


Figure 4. Map of Maryland Showing the locations of the two study sites.



Figure 5. Preparing soil samples at Poplar Hill just before the November Rainfall simulation



Figure 6. February Rainfall simulation at Upper Marlboro

Required Measurements

The five equations that were evaluated are those of Kostiakov, Horton, Holtan, Philip, and GA. These equations require the measurement of the saturated hydraulic conductivity, soil water retention curve, rainfall rate and initial soil water content. Measured infiltration rates from an earlier rainfall simulation were also required to obtain parameter values for Kostiakov and Horton equations. Initial soil water content was determined from samples obtained at the field sites immediately prior to the rainfall simulations. Rainfall rate was measured during each rainfall simulation, and saturated hydraulic conductivity and soil water retention were determined in the lab from samples obtained at the rainfall simulation sites.

Rainfall Simulations

Field Measurements

The simulator produced rainfall at a constant rate, which was determined by volumetric rainfall gauges on site which captured rainfall and from which the depth of rainfall was read. The total rainfall depth divided by the total duration of the rainfall simulation gives the rainfall intensity. H-flumes were used on each site to allow the observation and measurement of runoff. Time of ponding and time of runoff were determined by observation of the soil surface and the runoff flume. A pressure transducer recording gauge was available, which continuously measured and recorded runoff from the H flumes at the Upper Marlboro site in units of feet. This device produced a runoff hydrograph from which the infiltration rate could be established. A runoff hydrograph was determined at the Poplar Hill site by collecting runoff for 30-second periods at 10-minute intervals over the course of one hour (bucket and stopwatch method).

The area of each runoff plot was also measured. The area of the Upper Marlboro plot measured 152 square meters (1638 sq ft) total, including a rectangle 22 meters by 6.7 meters (72ft x 22ft), plus a triangular region, with base 6.7 meters (22ft) and height 1.5 meters (4.9ft), feeding into the runoff flume. The area of the Poplar Hill rainfall plot measured 57 square meters (611sq ft) with rectangle 7.0 meters by 7.3 meters (23ft x 24ft) plus triangular section of base 7.3 meters (24ft), and height 1.5 meters (4.9ft).

Development of Infiltration Curves

Infiltration curves were determined using runoff hydrographs produced from rainfall simulations. Since the recording gage measured runoff in units of feet, a conversion table from USDA Handbook No. 224 was used to convert runoff to units of cubic meters per second (Grant and Dawson, 1978). The average depth of runoff contribution over the entire plot for each time interval was determined by the following equation:

$$RO_t = \Delta t \ Q/A \quad \text{Equation 3.1}$$

where

RO_t = average runoff depth (m) for time interval,

$\Delta t = 30 \text{ sec}$ = length of each time interval during which runoff was collected,

A = area of plot (m^2), and

Q = flow rate of runoff from flume ($\text{m}^3 \text{s}^{-1}$) (from conversion table).

Infiltration was determined by the equation:

$$F = P - RO - SS \quad \text{Equation 3.2}$$

where,

F = Cumulative infiltration (cm),

P = cumulative rainfall (cm),

RO = cumulative runoff (cm), and

SS = surface storage (cm).

Since the Upper Marlboro site showed runoff continuing after the cessation of rainfall, there was evidently a significant time lag for this water to reach the runoff flume

from its points of origination as rainfall. Runoff for the later time intervals at this site necessarily originated during the period of rainfall, and was therefore divided into equal parts and added to the runoff for time periods before cessation of rainfall, starting from time of runoff initiation. Cumulative infiltration depth was then calculated by equation (3.2) using the cumulative runoff values produced by these adjusted runoff values. Infiltration rate was then calculated for each time step by:

$$\frac{dF}{dt} = \frac{F_i - F_{i-1}}{\Delta t}$$

Equation 3.3

where

$$\frac{dF}{dt} = f = \text{infiltration rate (cm h}^{-1}\text{)},$$

F_i = cumulative infiltration at time index, i

F_{i-1} = cumulative infiltration (cm), at time index, i-1 (cm) and

Δt = time interval for one time step (h).

Sampling Procedure

At each site, five soil samples were collected from each of six depths: 0-6 cm (0-2 in), 10-16 cm (4-6in), 20-26 cm (8-10 in), 30-36 cm (12-14 in), 40-46 cm (16-18 in), and 50-56 cm (20-22 in), immediately before each rainfall simulation to be used in determination of initial water content, soil bulk density, and a first run of saturated hydraulic conductivity measurements. Samples were collected in 6-cm long metal cylinders inserted into a sampling tube, which was driven into the soil. In order to avoid making holes in the grass-covered plots before the simulation, soil was sampled from the

area immediately adjacent to the plots. Below each sample, a shovel was used to lower the hole to the next sampling level and a tape measure used to measure the depth until the final depth was obtained. Samples were retained in rings, wrapped in thin perforated plastic or foil, taped with duct tape, labeled, and stored in the shade. Sites were divided into 5 roughly equal segments and samples were obtained from one hole in each segment. An attempt was made to choose ground that appeared to have been undisturbed for some time. A second set of samples had to be obtained at a later date, because the tempe cells that were ordered for use in producing the water retention curves required a different diameter ring from the ones that were available at the time of the rainfall simulations. Larger samples were obtained using a soil auger and sent to the soil lab for texturing.

Laboratory Measurements/ Development of Parameters

Initial Volumetric Soil Water Content and Bulk Density

The **gravimetric method** as described by Gardner (1986) was used to establish initial soil water content for both sites. Wet samples were weighed, dried in force-draft oven at 104°C for 24-48 hours, and then weighed again. Gravimetric soil water content was then determined by the following equation (Gardner, 1986) :

$$\theta_m = \frac{\text{mass wet soil} - \text{mass dry soil}}{\text{mass dry soil}} = \frac{m_w}{m_s} \quad \text{Equation 3.4}$$

To convert to volumetric soil water content, the bulk density of the soil was obtained. The length and diameter of the soil rings were measured and the volume was calculated by:

$$V = \frac{\pi d^2}{4} L$$

Equation 3.5

Bulk density was calculated by:

$$\rho_b = \frac{m_s}{V_s} = \frac{\text{mass of dry soil}}{\text{Volume of soil}}$$

Equation 3.6

Volumetric water content was then calculated by the equation:

$$\frac{V_w}{V_s} = \frac{m_w}{m_s} \frac{m_s}{V_s} \frac{V_w}{m_w}$$

Equation 3.7

where

V_w = volume water (cm³)
 V_s = volume of dry soil (cm³)
 m_w = mass of water (g) and
 m_s = mass of dry soil (g).

$$\theta_i = \theta_m \frac{\rho_b}{\rho_w}$$

or

Equation 3.8

where

$$\theta_i = \frac{V_w}{V_s} = \text{volumetric water content (cm}^3 \text{ cm}^{-3}\text{)}$$

$$\theta_m = \frac{m_w}{m_s} = \text{gravimetric water content (g g}^{-1}\text{),}$$

$$\rho_b = \frac{m_s}{V_s} = \text{bulk density of soil (g cm}^{-3}\text{) and}$$

$$\rho_w = \frac{m_w}{V_w} = \text{density of water (g cm}^{-3}\text{)}.$$

Saturated Hydraulic Conductivity

The **constant-head method** was used to measure saturated hydraulic conductivity. Undisturbed soil samples were retained in metal cylinders covered on one end with a piece of cheese cloth that was held in place with a rubber band. The samples were placed covered end down in a tray of water that was filled to a depth just below the top of the samples. The samples were left to soak until saturated, for at least 16 hours (Black et al., 1965). Figure 7 is a diagram showing the apparatus used for this method.

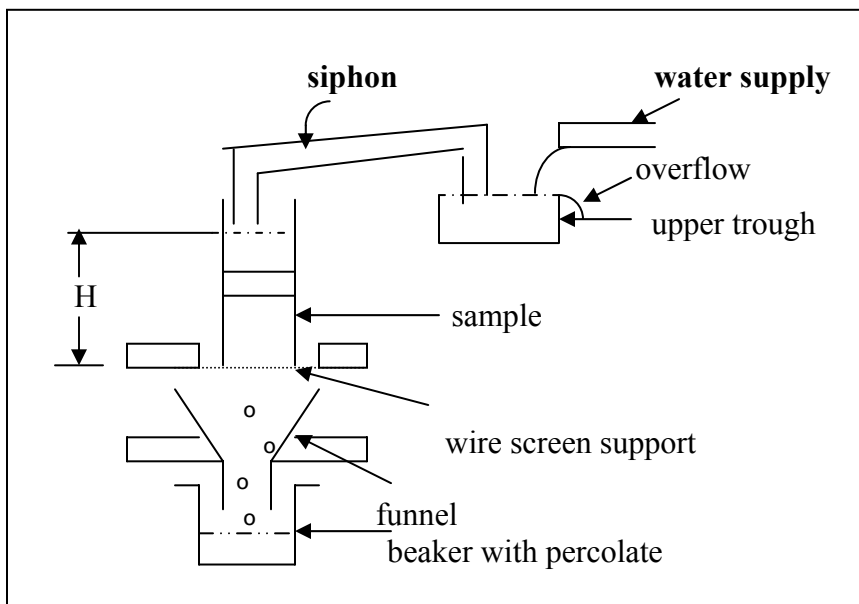


Figure 7. Diagram of constant head system for conductivity measurement. After Black et al., (1965).

When the samples were saturated, the water supply to the upper trough was turned on. Next, an empty soil cylinder was taped securely to the top of each soil-filled cylinder. The lower part of the samples remained immersed in water during these steps. The samples were then transferred to wire screen supports. Glass tubes filled with water with both ends

submerged were positioned to siphon water from the trough to the sample. Water slowly filled the upper cylinders from the trough until they were 2/3 to 3/4 full. The samples were then left with water running in at a constant rate for at least an hour until a constant head of water was maintained above the samples. When the water level above the samples became stable, the percolate was collected in beakers. The volume of water, V that passed through each sample in a timed interval, t was measured, as was the hydraulic head, H , and the water temperature (Black et al., 1965). The volume of percolate was collected for five time periods of 4 to 12 minutes for each sample.

Saturated hydraulic conductivity is calculated by the equation:

$$K_s = \left(\frac{V}{A \Delta t} \right) \left(\frac{L}{H} \right)$$

Equation 3.9

$$\text{or, } K_s = \left(\frac{Q}{A} \right) \left(\frac{L}{H} \right)$$

Equation 3.10

where

A = cross sectional area of sample (cm^2),

L = length of sample (cm),

H = the hydraulic head, or height of water above the bottom of soil sample (cm),

Q = flow rate = V/t (ml min^{-1}),

V = volume of percolate collected (ml), and

Δt = time interval during which percolate was collected (min).

For all but the first batch of samples, a modification was made so that samples were placed in TempeTM cells with a porous foam disk replacing the porous plate, allowing the water to flow through with minimal hindrance, but more effective than cheese cloth at preventing soil particles from passing through.

Since Darcy's law is analogous to Ohm's law for electrical flow and Fourier's law for heat flow, the **effective saturated hydraulic conductivity** for the whole soil profile can be calculated using the average value for each depth in the following formula for flow perpendicular to a series of layers (Schwab et al, 1993):

$$K_e = \frac{D}{\frac{d}{K_1} + \frac{d}{K_2} + \frac{d}{K_3} + \frac{d}{K_4} + \frac{d}{K_5} + \frac{d}{K_6}} \quad \text{Equation 3.11}$$

where

K_e = effective saturated hydraulic conductivity (cm h^{-1}),

D = Total depth of 60 cm,

d = depth of layers 1-6 of 10 cm, and

K_1, \dots, K_6 = average saturated hydraulic conductivities for layers 1-6 (cm h^{-1}).

Soil Water Retention Curve Determination

The soil water retention curve was obtained by making measurements of water content at a series of recorded pressure heads using a Tempe cell apparatus, as shown in Figure 8 below.

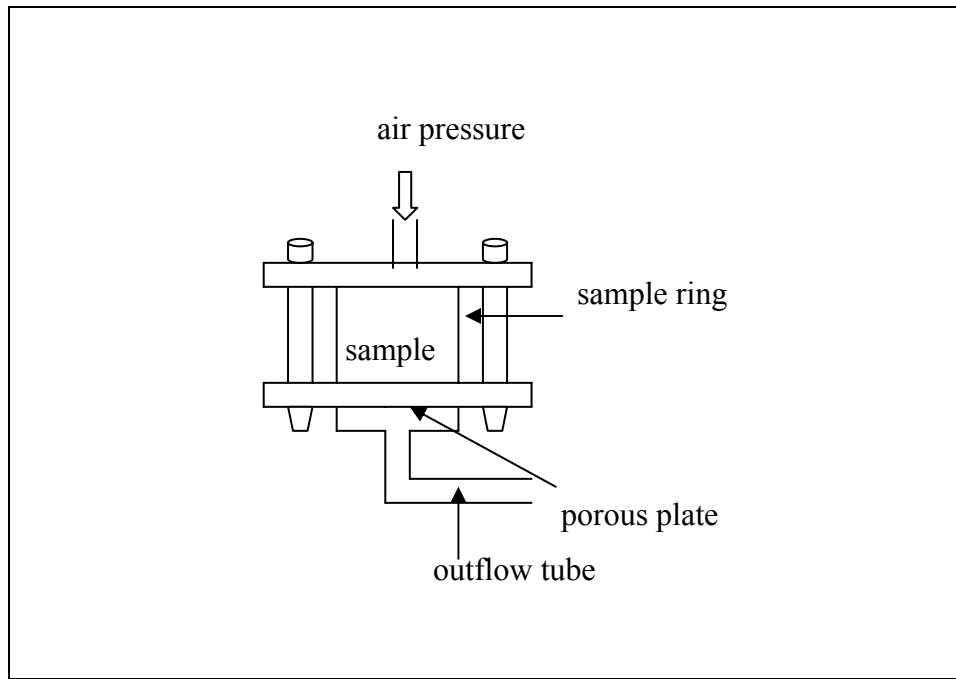


Figure 8. Tempe cell apparatus. After Black et al. (1965).

Two bar porous plates were soaked in water for 24 hours to saturate. Undisturbed samples of soil in retention rings were placed in a tub and the water level was raised gradually to minimize slaking and to force air out slowly as the water level rose. The samples were left to saturate in the water bath for 48 hours. Each sample was placed on a saturated porous plate and clamped in a Tempe cell. The first weight measurement was taken not at saturation but at field saturation, which is approximately $0.8 \theta_s - 0.9 \theta_s$ (Klute, 1986).

Although 4 cm of water was the initial target pressure head for the field saturation measurement, the instability of the initial pressure setting resulted in initial pressure head readings as high as 7.5 cm of water.

The pressure was increased by small increments, creating a hydraulic head on the soil water so that outflow occurred. Since the pressure on the water beneath the plate is atmospheric, the cell pressure is equal to the soil water tension, and the pressure head is the negative of the cell pressure (Black et al., 1965).

For each pressure step, when equilibrium was reached and outflow ceased, the air pressure was shut off and the Tempe cell was removed and weighed and the pressure and weight were recorded. The Tempe cell was then reconnected, air pressure was turned on, and the pressure was then raised to the next designated value and the procedure was repeated until the highest desired pressure of one bar, (or 1000 cm water) was reached. For pressures up to about 90 cm of water, a water manometer was employed, and for greater pressures a mercury manometer was used.

After the final pressure step of one bar, had been reached, the Tempe cell was dismantled and the sample in soil cylinder was weighed, dried in an oven at 104°C and reweighed. The weight of the water retained by the soil sample at one bar was equal to the difference in weight of the sample before and after oven drying. Since the density of water is 1g/cm³, and the mass of the water in grams was equal to the volume of water in cubic centimeters, the water content at one bar could be determined by dividing the volume of water by the total volume of the soil sample. Starting at the last pressure step, the difference in water volume, (weight difference) between each step and the previous step was added to the water volume remaining after that step, and divided by the total sample volume to determine the water content for each pressure step. The water volumes were summed in this backwards, stepwise manner, until the initial water content was determined at field saturation.

Graphs were constructed, plotting θ versus h to determine desorption curves for each sample. Saturation values were determined for each pressure step from the relationship $S_i = \frac{\theta_i}{\theta_s}$.

S_e , or **effective saturation** was determined by:

$$S_{e_i} = \frac{(S_i - S_r)}{(1 - S_r)} \quad \text{Equation 3.12}$$

where

S_r = residual saturation and

S_i = saturation at step i .

Residual saturation (S_r) is an estimated ratio of the residual water content at which the capillary conductivity is negligibly small, to the water content at saturation. S_r was estimated according to the Brooks and Corey method by first selecting a value of S at which the curve of capillary pressure head (h) versus Saturation (S) approached an asymptote (Brooks and Corey, 1964).

In order to further mechanize the process of choosing this first estimate of S_r , the angle that a line through the last two points makes with a vertical line was measured and a residual saturation factor (rsf) was determined according to the size of the angle, as shown in Figure 9. The closer the angle was to zero, the closer the rsf approached one. An angle of one degree was given an rsf of 0.98, meaning that 0.98 multiplied by the last saturation value gave the asymptote value or residual saturation value. An angle of 11.5° , the steepest angle encountered, was assigned an rsf of 0.75. These rsf factors were

chosen so that the asymptotes defined by them visually matched up with the continuation of the curves. Intermediate angles were assigned rsf values by linear interpolation.

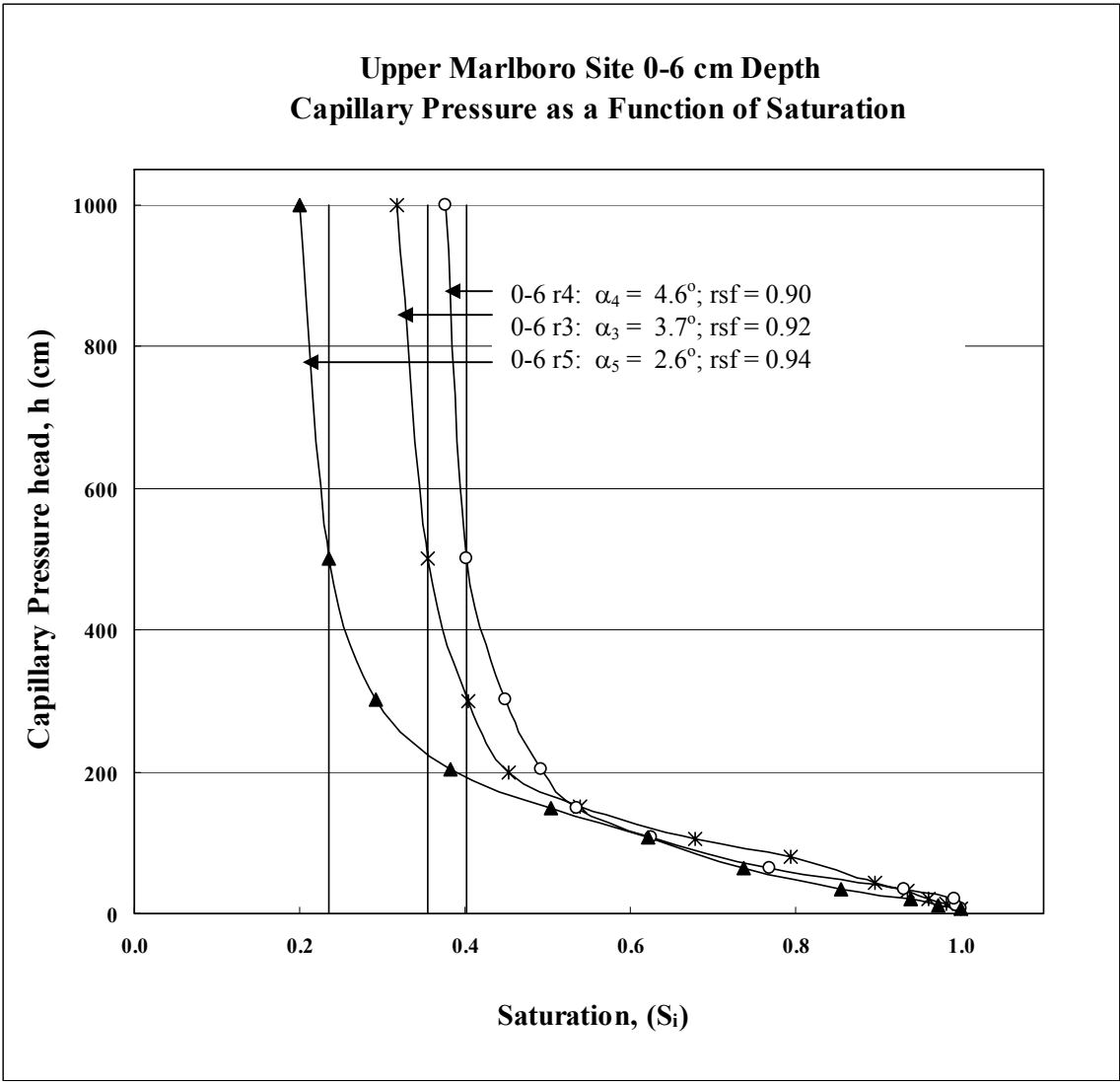


Figure 9. Procedure for first estimation of S_r; rsf determined from the angle formed between the last two points and a vertical line.

Using this estimate for S_r, values of S_e were calculated using Equation 3.12, and then following the Brooks and Corey method, values of log S_e were plotted versus log h. The values in the low capillary range, where the soil is close to saturation, fell on a curve, but the values below this upper region fell approximately on a straight line. According to

the Brooks and Corey method, a second estimate of S_r was obtained by choosing a value of S_e in the high capillary pressure range that did not fall on the straight line and calculating a new value of S_r which caused this value to fall on the straight line, using Equation 3.12, and the value of S at the indicated pressure. The second estimate of S_r was usually sufficient so that when recalculated using the new value of S_r , all the points in the high capillary range lay approximately on a straight line. However if this was not the case the process could be reiterated so that most points fell on a straight line for values of capillary pressure greater than the bubbling pressure (Brooks and Corey, 1964).

Bubbling pressure head, h_b , was determined by plotting $\log S_e$ vs. $\log h$ as shown in Figure 3. The slope, λ , and y-intercept of the linear portion of this curve were determined by regression. The log of the bubbling pressure, which is the x-intercept was determined by rearranging the following equation to the form of an equation for a straight line:

$$S_e = \frac{\theta_i}{\theta_s} = \left(\frac{h_b}{\psi} \right)^\lambda \quad \text{Equation 3.13}$$

$$\log S_e = \lambda \log \left(\frac{h_b}{\psi} \right) \quad \text{Equation 3.14}$$

$$\log S_e = -\lambda \log(\psi) + \lambda \log(h_b) \quad \text{Equation 3.15}$$

where

$$y = \log S_e = \log(\theta/\theta_s),$$

ψ = soil water suction head, $-h$,

$$x = \log(\psi),$$

m = slope = $-\lambda$, and

$$b = \text{y-intercept} = \lambda \log (h_b).$$

At saturation, $S_e = \theta_s/\theta_s = 1$, and $y = \log (\theta_s/\theta_s) = \log 1 = 0$.

The x intercept, $\log (\psi) = \log (h_b)$, therefore, $h_b = 10^{\log (\psi)}$ when $y = 0$.

Since two methods were suggested in the literature for estimating effective suction at the wetting front, S_f , in the Green and Ampt equation, in order to determine which method provides a more reasonable estimate, S_f was approximated by both the water entry suction:

$$h_{ce} = 1/2 h_b \quad \text{Bouwer (1969),} \quad \text{Equation 3.16}$$

and by using the Brooks and Corey parameters as described by Rawls et al. (1993).

$$S_f = h_{ce} \frac{\eta}{(\eta - 1)} \quad \text{Equation 3.17}$$

where

$$\eta = 2 + 3 \lambda \quad \text{Equation 3.18}$$

Sensitivity Analysis

Sensitivity analysis is the process by which the response of a model to systematic changes in the values of explanatory variables is examined (McCuen,1986). This analytical procedure is important in providing assessment of the relative importance of parameters to be considered during model calibration and validation (Shirmohammadi et

al. 2001), and also provides information about how much error can be tolerated in each parameter value.

Parameter perturbation is the method that was used to provide a measure of the sensitivity for each parameter (Chapra, 1997). This procedure allows assessment of the relative impact of changes in a parameter on the response variable by changing the value of a single chosen parameter while holding all other parameters constant. The systematic alteration of the base value by a fixed percentage eliminates the error variation that makes model assessment more cumbersome when solely dealing with measured data (McCuen, 1986). The sensitivity of each parameter is expressed as a condition number. The condition number represents the rate of change of the dependent or predicted variable with respect to the rate of change in the parameter value (independent variable). Condition numbers are calculated according to the following equation:

$$CN_k = \frac{k}{c} \frac{\Delta c}{\Delta k}$$

Equation 3.19

where

CN_k = condition number for the parameter k ,

k = average measured value, or typical literature value for the parameter,

c = dependent variable,

Δc = change in the dependent variable and

Δk = change in the parameter value.

For each parameter/ response variable relationship, a single condition number was calculated, which was then compared to condition numbers for other parameters to determine relative parameter sensitivities. A larger condition number for a particular parameter indicates a more sensitive response variable to changes in that parameter.

For each model, the sensitivity of infiltration rate was evaluated with respect to variation in other parameter values. Each equation was evaluated at two times, 1/3 and 2/3 of the duration of rainfall. Values of each parameter were varied by $\pm 10\%$, $\pm 25\%$, and $\pm 50\%$. The infiltration rate was determined for each value of the parameter of interest while holding all other parameter values constant. The condition numbers for each case were then calculated using equation 3.19.

Kostiakov Equation Sensitivity

For the Kostiakov equation, the base values for the two empirical constants K_k and α are determined by using equation 2.11 and plotting $\log f_p$ against $\log t$ and finding the slope and y-intercept of the resulting straight line (Criddle et al. 1956). The intercept of the equation (infiltration rate at time $t = 1$) is $\log K_k$ and the slope is $-\alpha$. Although empirically determined, K_k and α are related to saturated hydraulic conductivity and moisture deficit, respectively. Infiltration is directly proportional to K_k , but is inversely related to α .

Horton Equation Sensitivity

The parameters adjusted for determination of infiltration sensitivity in the Horton equation included, f_c , the constant infiltration capacity as t approaches infinity, f_o , the infiltration capacity at onset of infiltration, and β , the positive constant based on soil and initial water conditions. The base value for f_c was determined from the infiltration curve

obtained from runoff data from the December 21st Upper Marlboro rainfall simulation by extending the curve to approach an asymptote. According to equation 2.21, the value of f_c was subtracted from the experimental values for f and the natural log of the resulting values were plotted as a function of time as shown in Fig. 8 below. The base values for the parameters β and f_o were determined from the slope and intercept of the line, respectively, where β is equal to the negative of the slope, and the initial infiltration capacity f_o , is equal to the sum of f_c and the exponential of the intercept. Infiltration increases with f_c and f_o , but decreases with increasing β .

Holtan Equation Sensitivity

The parameters in the Holtan equation that were evaluated with respect to infiltration rate sensitivity included the values for a , vegetative parameter, f_c , constant steady infiltration rate estimated from soil hydrologic group and the initial value of available storage, SA . Larger values for the vegetative parameters, a , and, GI indicate conditions of denser plant root growth, and increased connectivity of surface pores, both factors contributing to increased infiltration rates. The final constant rate of infiltration, f_c is also positively related to infiltration rate.

Philip Equation Sensitivity

In the Philip equation, the parameter C_a was estimated to be K_s , $2K_s/3$, $K_s/2$, and $K_s/3$. The infiltration rate sensitivity was evaluated while each of these estimates was

varied about its mean value. Sorptivity, S was also varied about an average value while other parameter values were held constant.

Green-Ampt Equation Sensitivity

In the GA equation, the parameters M_i , S_f , and K_{fs} were varied to determine the sensitivity of infiltration rate with respect to these parameters. Instead of directly including time in this equation, time was indirectly represented by the accumulative infiltration, which was obtained from the estimated depth of the wetting front and corresponding moisture deficit at 1/3 and 2/3 the duration of rainfall. Based on the form of the equation it was apparent that increasing each of the parameters, other than F , would result in an increased infiltration rate. Infiltration rate was expected to be more sensitive to changes in M_i and K_{fs} and less sensitive to changes in S_f , according to a study by Brakensiek and Onstad (1977).

Model Calibration

In order to compare the infiltration equations, parameter values for each equation needed to be determined. The method by which the parameter values were determined for each of the equations is described below. The infiltration curve from a rainfall simulation run in December of 2002 on a plot at the Upper Marlboro site, adjacent to the one used in the February 2002 simulation, was used to calibrate the empirical Kostiakov, and Horton equations. Fig. 10 shows the observed infiltration curve for the December simulation, as well as the Kostiakov and Horton predicted curves. As expected, the predicted curves are a close fit to the curve from which they were calibrated. Infiltration curve parameters for Kostiakov and Horton models were developed from equations 2.11 and 2.21 using logarithmic and semi-log plots of data from the December simulation, respectively. Parameters for the Holtan equation were obtained from measured initial and saturated moisture contents and from tabulated values corresponding to the soil and vegetation characteristics of the site. Parameters for Philip and Green and Ampt equations are developed from soil laboratory measurements including saturated hydraulic conductivity, K_s and soil water retention curves. Table 4 shows the sources for parameters in each of the equations.

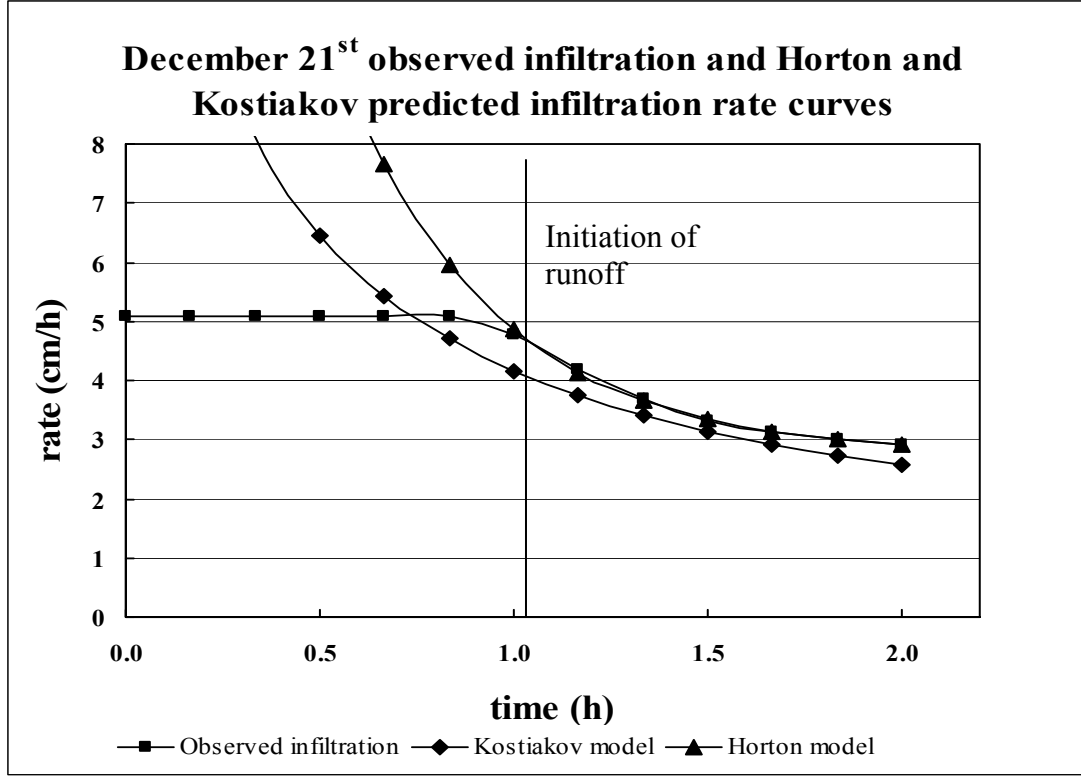


Figure 10. December 21st observed infiltration and predicted infiltration rate curves for Kostiakov and Horton models.

Table 4. Source of parameters in each equation.

Equation name	Equation f	Parameters developed from infiltration curve	Parameters developed from soil laboratory measurements	Parameters obtained from published tables
Kostiakov	$f_p = K_k t_i^{-\alpha}$	α, K_k		
Horton	$f_p = f_c + (f_0 - f_c) e^{-\beta t}$	β, f_c, f_0		
Holtan	$f = GI_a S A^{1.4} + f_c$		SA	GI_a, f_c
Philip	$f = S/2 t^{-1/2} + C_a$		S, C_a	
Green-Ampt	$f = K_s + K_s M_i S_f / F$		K_s, M_i, S_f, F	

Kostiakov Equation

The Kostiakov equation has two empirical constants K_k and α , which were determined using equation 2.11. $\log f$ was plotted against $\log t$ for the December infiltration curve and the slope and y-intercept of the resulting straight line were found (Criddle et al. 1956) as shown in Fig. 11. The intercept of the equation (infiltration rate at time $t = 1$) is $\log K_k$ and the slope is $-\alpha$.

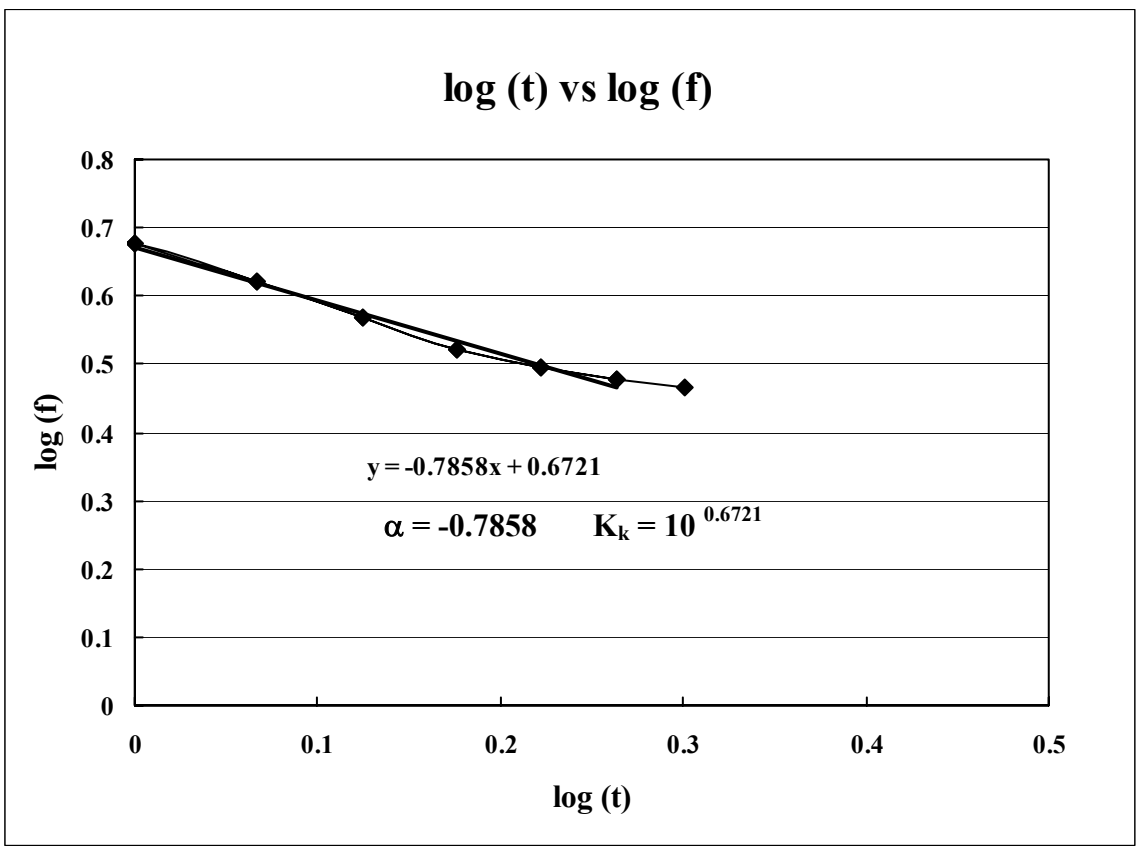


Figure 11. The Kostiakov parameters α and K_k were determined by graphing $\log (f)$ as a function of $\log(t)$.

The calibration curve used to obtain the parameter values for the Kostiakov equation was produced from runoff data from the December 21st rainfall simulation on a plot adjacent to the one used to validate the five equations.

Horton Equation

The parameters in the Horton Equation include, f_c , the constant infiltration capacity as t approaches infinity, f_o , the infiltration capacity at onset of infiltration, and β the positive constant dependent on soil and initial water conditions. The value for f_c was determined from the infiltration curve obtained from runoff data from the December 21st Upper Marlboro rainfall simulation by extending the curve to approach an asymptote.

The value of f_c was subtracted from the experimental values for f and the natural log of the resulting values were plotted as a function of time as shown in Fig. 12 below. β was determined from the slope of the line and f_o from the intercept.

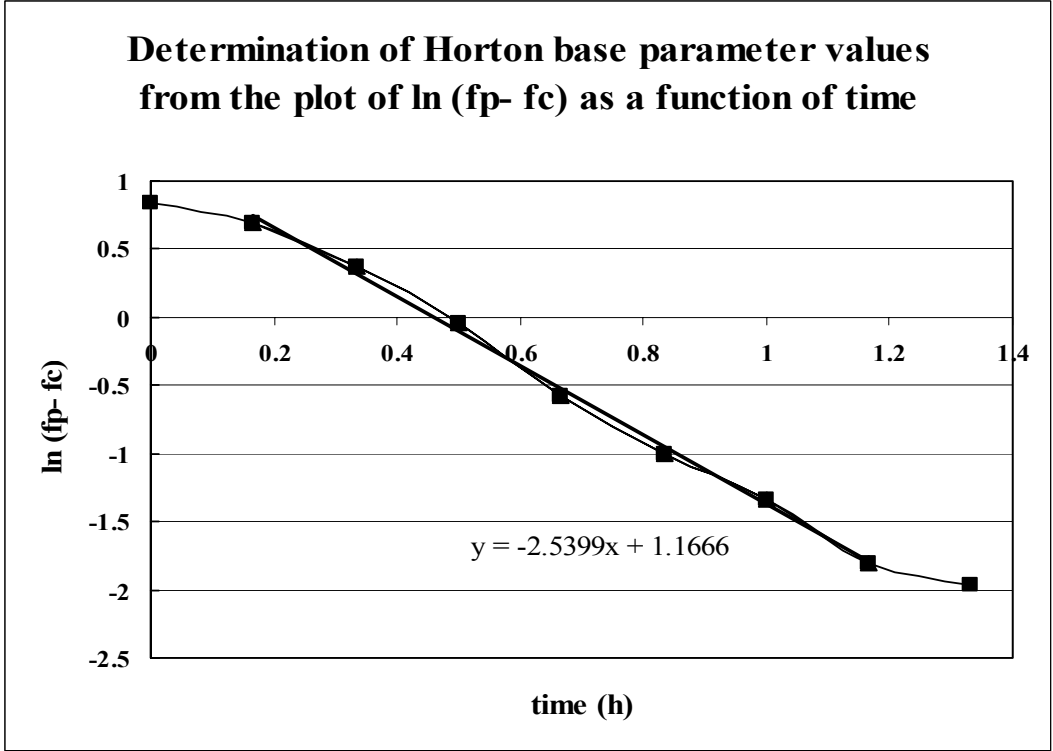


Figure 12. Horton base parameters β and f_o can be determined from the slope and y-intercept of the plot of $\ln (f_p - f_c)$ as a function of time.

The base value for parameter β is equal to the negative slope, and the initial infiltration capacity f_o , was calculated by $f_o - f_c = e^{\text{intercept}}$.

Holtan Equation

The parameters in the Holtan Equation include the values for growth index, GI, vegetative parameter a , and final constant infiltration rate, f_c . For the Upper Marlboro site, the value for a was obtained from Table 3 (Frere, et al., 1975). The value of final constant infiltration, f_c , was estimated from soil hydrologic group based on values provided by Musgrave (1955) shown in Table 2. The value of GI was estimated from a

table based on maturity of ground cover. The starting value for available storage was estimated from the moisture deficit,

$$M_i = \theta_s - \theta_i \quad \text{Equation 3.19}$$

and the depth of the upper soil horizon. The depth of the upper soil horizon was initially estimated based on the position of the clay layer or plow pan. However, this estimate resulted in infiltration starting after only 15 min. The estimate was therefore increased, so that infiltration began at approximately 45 min after the start of rainfall, as actually occurred. The moisture deficit, M_i averaged across the estimated depth of the upper soil horizon, times the estimated depth gives a starting value for available storage. The value of available storage is reduced at each 0.25 hr. time interval according to the equation (Novotny and Olem, 1994):

$$SA_t = SA_{t-1} - f_{t-1}\Delta t + f_c\Delta t \quad \text{Equation 3.20}$$

where

SA_t = available storage at time t (cm),

SA_{t-1} = available storage at previous time step (cm),

f_{t-1} = infiltration rate at previous time step (cm h^{-1}),

f_c = final constant infiltration rate (or drainage rate) (cm h^{-1}) and

Δt = time interval (h).

Since the available storage was evaluated for each time step, the infiltration rate could be determined at each time step, even though the Holtan equation does not directly include time as a parameter (Holtan and Lopez, 1971).

Philip Equation

In the Philip equation, the rate constant, C_a , was estimated by $K_{fs} = 0.5 K_s$, $K_{fs}/3$, and $2K_{fs}/3$.

Sorptivity was determined from the equation:

$$S = (2M_i K_{fs} S_f)^{1/2} \quad \text{Equation 3.21}$$

Where,

S = sorptivity

K_{fs} = effective $K_s/2$, and K_s was calculated from laboratory measurements

S_f = effective suction at the wetting front and

M_i = moisture deficit

S_f and M_i were determined for each depth from laboratory measurements, as shown in equations 3.15 and 3.20 respectively. Since sorptivity was determined for each depth of soil, the sorptivity for each time step was determined from the depth of the wetting front at that time. The depth of penetration of infiltration shown in Table 9 was estimated using the equation:

$$d_t = d_{t-1} + (P - C_a) M_i \quad \text{Equation 3.22}$$

Where

d_t = depth of wetting front at time t ,

P = cumulative rainfall (cm),

C_a = drainage (cm) or final constant infiltration rate (cm h^{-1}) multiplied by time interval (h) and

M_i = moisture deficit (unitless).

Effective sorptivity, S_{eff} was calculated for each depth as the infiltrating water penetrated further into the soil profile according to equation:

$$S_{eff} = \frac{D}{\frac{d_a}{S_a} + \frac{d_b}{S_b} + \frac{d_c}{S_c} + \dots}$$

Equation 3.23

where

$$D = d_a + d_b + d_c + \dots$$

a, b, c represent different soil layers each having depth (d) and sorptivity (S).

When the calculated depth of infiltration penetration was between sampling depths, the effective sorptivities for the two layers were averaged.

Green-Ampt Equation

In the GA equation, parameters which were determined for each of 6 depths include moisture deficit, M_i , determined as shown in Equation 2.22, with θ_i and θ_s measured from soil samples, obtained from the area adjacent to the rainfall plots, immediately prior to each rainfall simulation; effective suction at the wetting front, S_f , obtained from the soil water retention curve data as described previously; and effective saturated hydraulic conductivity, K_e , determined using Equation 3.11, substituting K_{fs} , taken to be $0.5 K_s$, for K_s as suggested by Bouwer (1966). K_s was determined from gravity saturated measurements of soil core samples.

Since parameters were determined for each depth of soil (for a 6 cm sample, for every 10 cm of depth and values for intermediate 4 cm were interpolated), the values for each time step were determined from the depth of soil to which infiltration has

penetrated, in other words the depth of the wetting front. For every six cm increment of the wetting front depth, the cumulative infiltration was determined by multiplying the depth by the average moisture deficit for that layer. Then infiltration rate was determined using Equation 2.23. The time corresponding with each depth of the wetting front was then solved for using Equation 2.24. This method provided an infiltration rate curve with unequal time intervals. Next, infiltration was computed for 0.25 h time intervals by the following method. The last value of infiltration rate greater than the rainfall rate was set equal to rainfall rate, and time was set equal to zero for this step. Cumulative infiltration was then found for each 0.25 h time step by subtracting K_{fs} multiplied by t from both sides of Equation 2.24 and solving for F by finding the value of F that causes the expression to equal zero for each value of t . Finally Equation 2.23 was used again to solve for infiltration rate for each value of cumulative infiltration.

Model Validation

In order to validate the equations, the infiltration curve parameters developed during calibration were used to obtain predicted infiltration rate values for the February 2002 simulation. From each predicted infiltration curve, infiltration rates for each 15 minute time interval after the initiation of runoff were compared with the observed infiltration rate values from the February event and a root mean squared error was calculated to provide a goodness of fit (GOF) term for each model. This GOF was used to evaluate how closely each equation approximated the measured infiltration at each time. The infiltration curves predicted by each of the five equations were graphed along with

the measured infiltration curve to provide a visual comparison of the five models and the measured data.

Statistical Methods

An analysis of variance was conducted to compare the two sites, using the mixed procedure of the Statistical Analysis System (SAS Institute, Cary, NC., USA). Questions to be answered include, whether the sites are significantly different based on the comparison of bulk densities, bubbling pressures and saturated hydraulic conductivities; whether a significant portion of the variability in these three parameters can be attributed to the depth from which the samples were excavated; and whether the Upper Marlboro site shows greater heterogeneity of variance than the Poplar Hill site.

Additionally, goodness of fit of the five equations for infiltration was tested using the Root Mean Squared Error (RMSE) to compare values of infiltration rate evaluated at each time interval, to determine how closely each equation predicts the measured infiltration.

The RMSE provides a measure of the deviation of predicted values from measured data and has frequently been used as a means of evaluating the accuracy of hydrologic models. The RMSE is calculated as follows:

$$RMSE = \sqrt{\frac{\sum_{i=1}^n (P_i - O_i)^2}{n}} \quad \text{Equation 3.24}$$

where

P_i = predicted value

O_i = measured (observed) value, and

n = number of measurements.

Predicted values of infiltration rate were plotted versus observed values and a coefficient of determination (R^2) was calculated for each model according to the equation

$$R^2 = 1 - \frac{SSE}{SST} \quad \text{Equation 3.25}$$

where

$$SSE = \sum (Y_i - \hat{Y}_i)^2 \quad \text{and}$$

$$SST = \left(\sum Y_i^2 \right) - \frac{(\sum Y_i)^2}{n}$$

CHAPTER IV - RESULTS AND DISCUSSION

Comparison of Sites

The soils differ considerably between the Poplar Hill and Upper Marlboro sites. The soil at the Poplar Hill site is a deep, well-drained, sandy soil with relatively high degree of homogeneity both vertically across depths and horizontally from one sample locus to the next. The soil at the Upper Marlboro site is much more stratified as well as more heterogeneous from sample to sample at each depth. The upper 30 cm are sandy loam with high organic matter especially in the surface layer. Below this depth, the clay content increases, with samples in the 40-60 cm depth having greatly reduced permeability.

Discussion of Infiltration Curves

The infiltration curve obtained from the rainfall simulation at the Upper Marlboro site was of a fairly typical shape. The initial infiltration rate was equal to the rainfall rate of about 5 cm h^{-1} , and then decreased in a logarithmic fashion to approach an asymptote representing a final constant infiltration rate of approximately 1.8 cm h^{-1} . Fig. 13 shows the infiltration curve produced for the Upper Marlboro site, along with rainfall, and runoff rate curves for the February 28th, 2002 rainfall simulation.

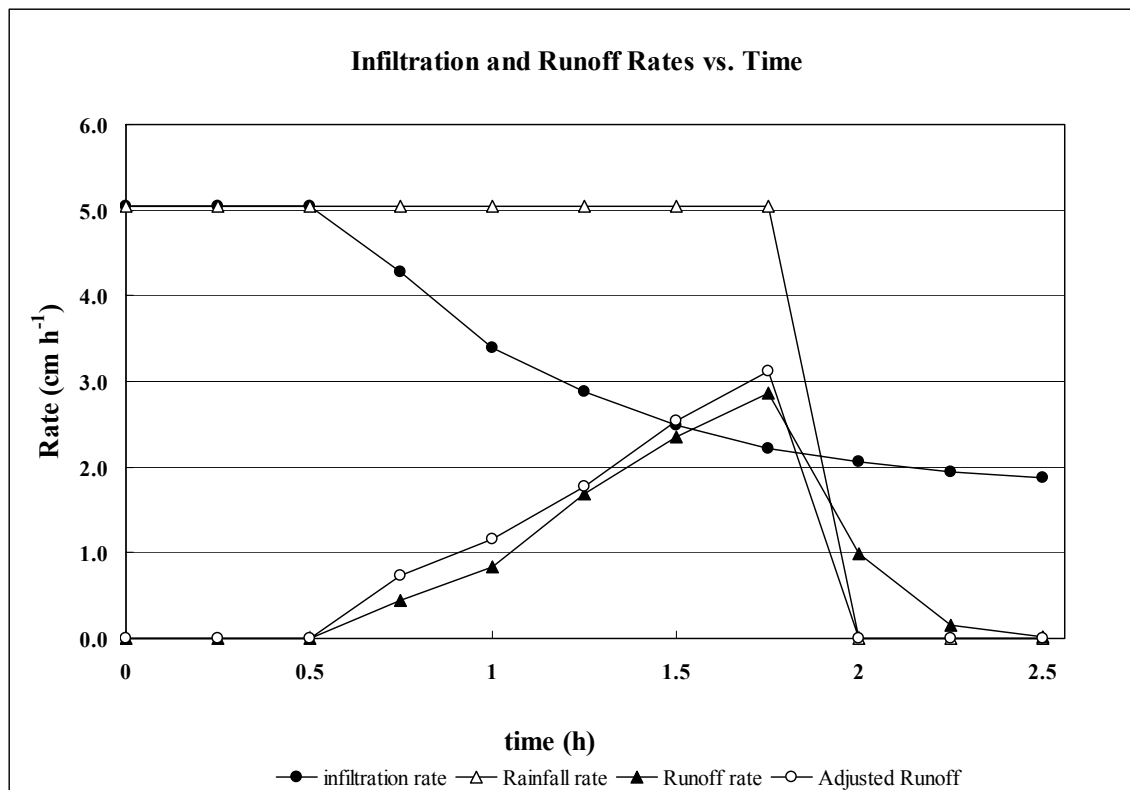


Figure 13. Infiltration rate curve, along with rainfall, and runoff rate curves for Upper Marlboro site for February 28th, 2002 rainfall simulation.

The rainfall simulation at the Poplar Hill site did not provide a typical infiltration rate curve. The infiltration capacity was so high in the sandy soil, that a rate almost constantly equal to the rainfall rate of 5.0 cm h⁻¹ was observed for the wet run, and for the dry run, the infiltration rate initially decreased, but then increased to again match the rainfall rate of about 5.4 cm h⁻¹. Infiltration was very close to the rainfall rate with very little runoff produced for both initially dry and initially wet conditions. The infiltration rate curve for the initially dry run, which produced the greater amount of runoff of the two Poplar Hill rainfall simulations, is shown in Figure 14 below.

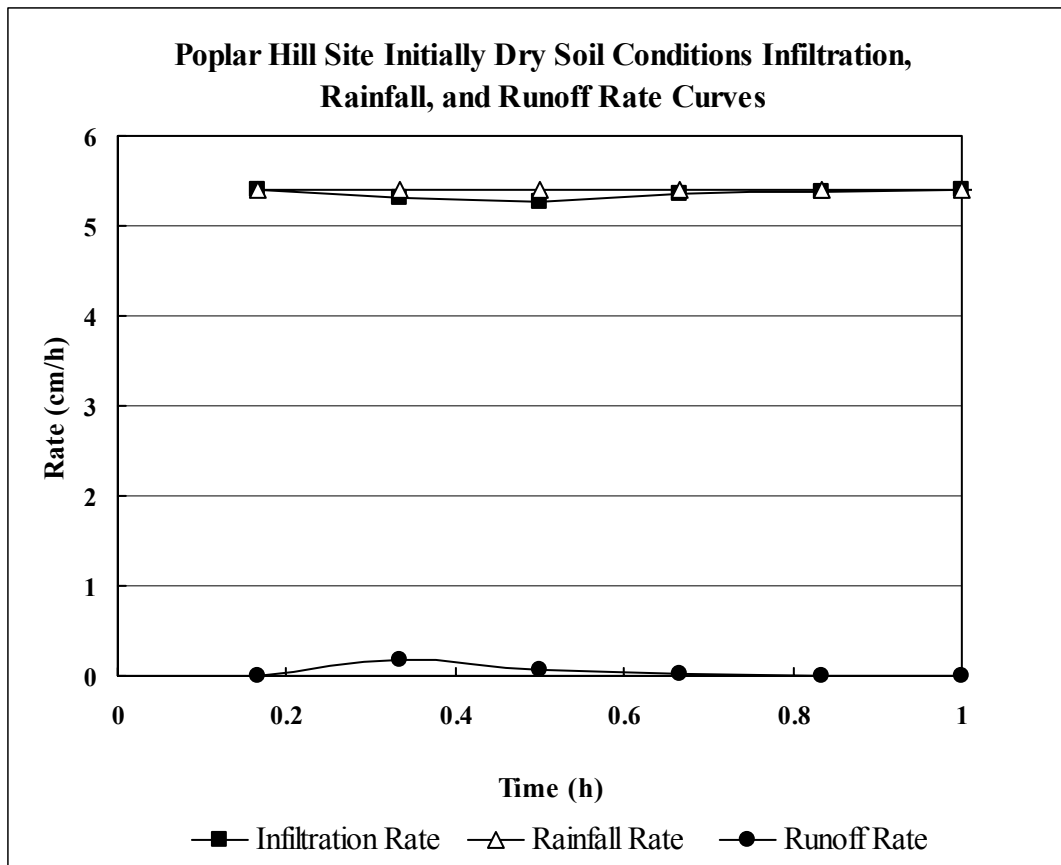


Figure 14. Initially dry conditions at Poplar Hill site for November 1st, 2001 rainfall simulation. Infiltration approximately equals rainfall.

This infiltration behavior may be attributed to an initially slower conductivity due to very dry conditions, which then gradually gave way to increased conductivity as the soil water content increased and pore connectivity increased. Equally likely is the possibility that air counter-flow reduced the infiltration rate initially, but after the air was forced out the rate increased again (Morel-Seytoux and Khanji, 1974). No data exist to postulate further. Unfortunately, the resulting atypical infiltration pattern could not be predicted by any of the existing field equations.

Discussion of Laboratory Results

Initial Water Content

Seasonal and climatic conditions along with soil attributes were seen to have significant impact on initial water content at both rainfall simulation sites. Summer and autumn of 2001 were extraordinarily dry, so that the soil in early November was very hard and dry when the Poplar Hill simulations were run. The surface because of exposure to the sun and wind, with scant vegetation for protection, was the driest layer prior to wetting. Each subsequent depth was moister than the previous layer with the deepest layer having a water content of only 0.11 (cm^3/cm^3). The soil at this site is a well-drained, sandy loam soil that does not hold as much water as would a clay, or clay-loam soil. The average initial water contents at each depth for the Poplar Hill site are shown in Figure 15.

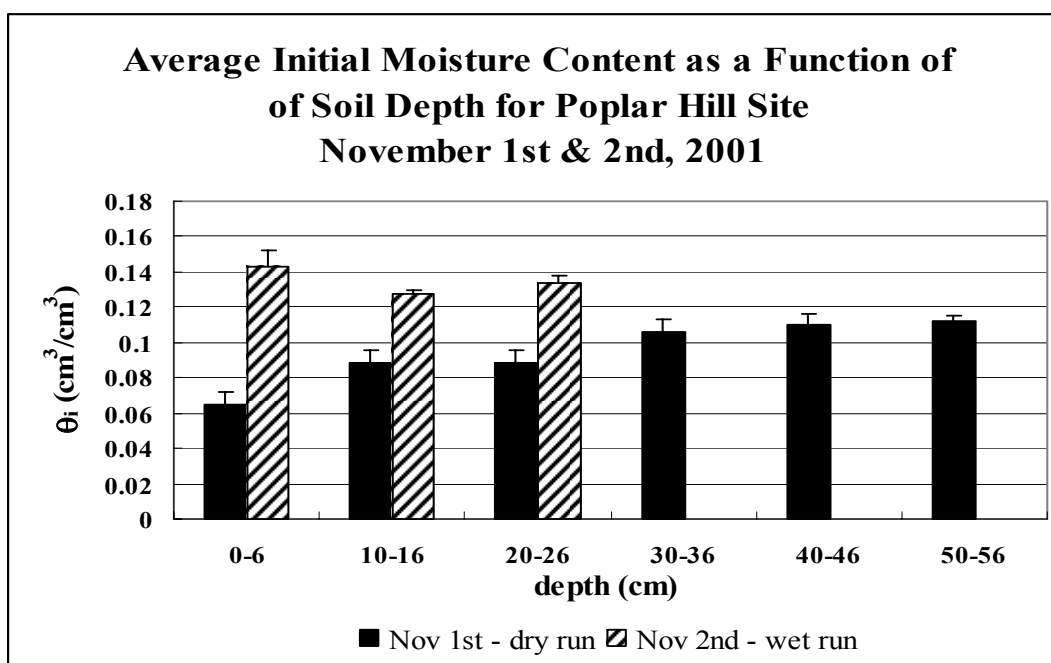


Figure 15. Average initial water content increases with depth for initially dry conditions at Poplar Hill site. No clear trend is seen for initially wet conditions.

The initial water content the morning after the November 1st rainfall simulation, was only 0.143 (cm^3/cm^3) at the surface, which was the wettest depth measured. There was no apparent trend in the water content as a function of depth for the November 2nd samples. No significant differences were observed among water contents at the 3 depths measured.

The Upper Marlboro rainfall simulation took place on February 28th, 2002. After a dry fall, the winter of 2001- 2002 was very mild. As one would expect, the soil was moister in February, ranging from 0.10 to 0.24 $\text{cm}^3 / \text{cm}^3$. The surface layer had higher water content than the next 3 depths, but not as high as the deeper layers. The higher surface water content is probably due to the vegetation and plant residue cover, as well as the greater amount of organic matter in the surface layer. Both of these factors increase water-holding capacity of the surface soil. Clay content increased with depth and consequently, the deeper layers also had greater water-holding capacity. Aside from the damp surface layer, there was a definite trend from lower water at lesser depth to higher water at greater depth as shown in Figure 16.

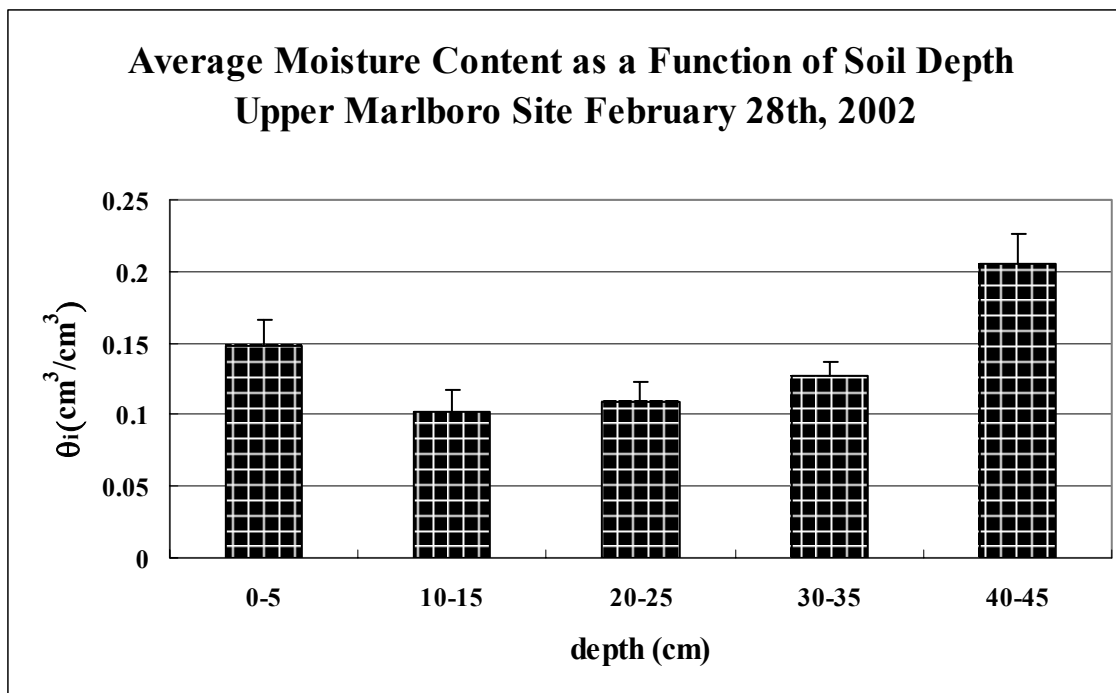


Figure 16. Average initial water content was greater at the surface due to organic matter and protection from insolation afforded by vegetative cover and plant residues, but otherwise showed a trend of increasing water with increased depth. The higher values at the greater depths also reflect increasing clay content. Error bars show standard errors for the mean of 5 replicates.

Bulk Density Measurement

Bulk density was measured after saturated hydraulic conductivity and soil water retention measurements, resulting in slightly lower bulk densities than would have been obtained by measuring bulk density of separate samples, because a small amount of soil was unavoidably lost during these procedures. Poplar Hill bulk density values varied very little with depth (1.56-1.70 g/cm^3), aside from a slightly less dense surface layer, due to plant roots, and other organic matter, and a denser plow pan layer at approximately 20-26 cm. The similarity of bulk density values across depth at this site is not surprising, since the soil is relatively homogeneous with all layers being sandy loam. The values for bulk

density measured from this site correspond to the values for sandy loam (1.7 g/cm^3) and sandy clay loam (1.6 g/cm^3) in a diagram by Williams and Wilkins reproduced in Maidment's Handbook of Hydrology (1993). Recalling that the bulk density measurements were low due to soil loss during other laboratory procedures performed on the soil samples, sandy loam is more plausible at this site. Aside from 30-36 cm depth, the Poplar Hill sandy loam samples had bulk densities higher than those of the Upper Marlboro mixed sandy and clayey loam samples. Upper Marlboro soils show less homogeneity, with the surface layer having considerably lower average bulk density (1.41 g/cm^3) due to more plant roots and worm holes in that layer. Density increases with depth until a plow pan is reached (1.68 g/cm^3) at approximately 30-36 cm depth and then decreases due to high clay content in the deeper layers. Figure 17 shows bulk density as a function of depth for Upper Marlboro and Poplar Hill sites.

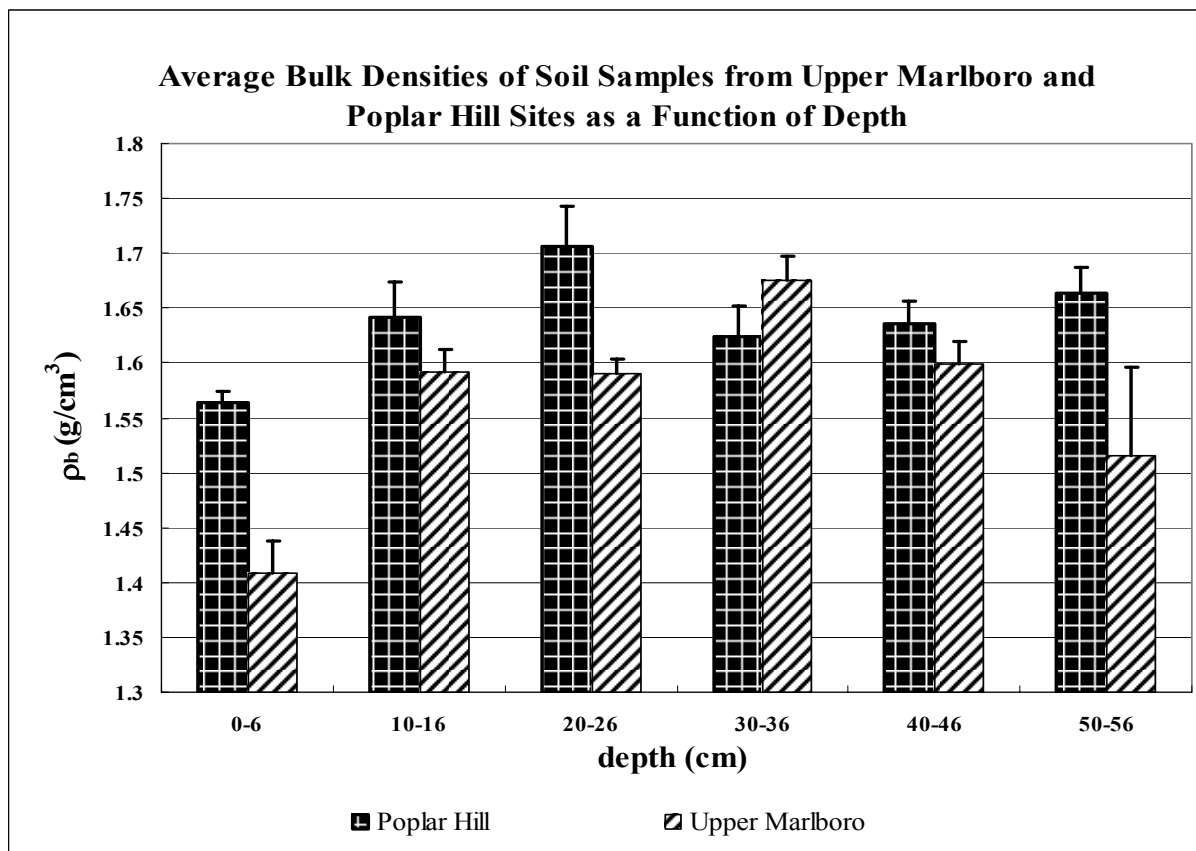


Figure 17. Poplar Hill bulk density values change little with depth. Upper Marlboro soils are more heterogeneous, with greater variation in densities between layers. Density increases with depth until a plow pan is reached and then decreases due to increasing clay content in the deeper layers. Error bars show standard errors for the mean of 5 replicates.

Saturated Hydraulic Conductivity

The upper Marlboro site shows a clear trend of decreasing saturated hydraulic conductivity (K_s) with increasing depth. The surface layer has significantly higher mean K_s (33.08 cm h^{-1}) probably due to the presence of plant roots, worm holes and plant debris which cause increased aeration and looser packing of soil, along with some preferential flow as water finds channels through the soil instead of moving uniformly through the column. With increased depth, higher clay content results in much slower movement of water as very minute pores in clay provide strong resistance to flow

(average $K_s = 1.2 \text{ cm h}^{-1}$ at 50-56 cm depth). There is much less variation in K_s values over depth at the Poplar Hill site ranging from 8.5 to 16.1 cm h^{-1} with generally faster flow rates as a result of the larger pores in sandy soils. The values fluctuate but gradually increase as depth increases. Saturated hydraulic conductivity was strongly affected by depth ($p = 0.0003$), but did not have a significant site effect. There were, however strong site-depth interactions as shown in Figure 18.

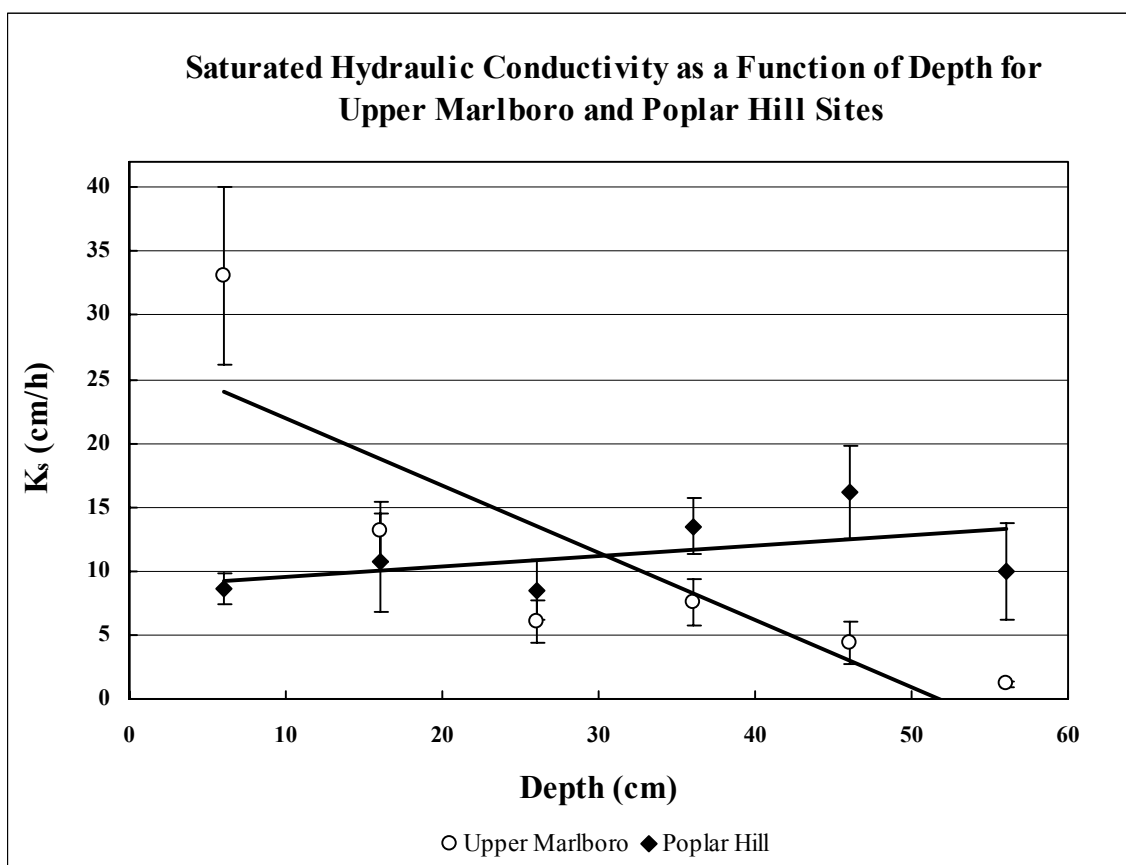


Figure 18. Saturated hydraulic conductivities for Upper Marlboro site decline with depth. For the Poplar Hill site, no such trend is seen. Error bars show standard errors for the mean of five replicates.

The effective saturated hydraulic conductivity (K_e) for the Upper Marlboro and Poplar Hill sites, were calculated to be 3.051 and 10.645 cm h^{-1} , respectively, using Equation 3.11. The values presented here are obtained from laboratory measurements of

soil samples. Field values are generally lower due to the obstruction of flow by trapped air. If the measured values are divided by 2 as suggested by Bouwer (1969), they are in accord with values listed in a table showing average GA parameter values for loamy sand, 5.98, sandy loam 2.18, and loam, 1.32 by Rawls and Brakensiek, reproduced in Maidment (1993).

Soil Water Retention Curves

The Upper Marlboro soil water retention curves generally show higher saturated water content especially in surface and deeper layers and also show a trend of increasing water content with depth for a given pressure. There is much heterogeneity between the Upper Marlboro samples for a given depth, while Poplar Hill samples are much more homogeneous as evidenced by curves for each depth falling very close together. Additionally, Poplar Hill samples show much less variation across depths and water content for a given pressure changes little with depth. Saturated water contents for the Poplar Hill site are considerably lower than for the Upper Marlboro site. Soil water retention curves for 0-6 cm depth at both sites are shown below in Figure 19. Curves for other depths are in Appendix C.

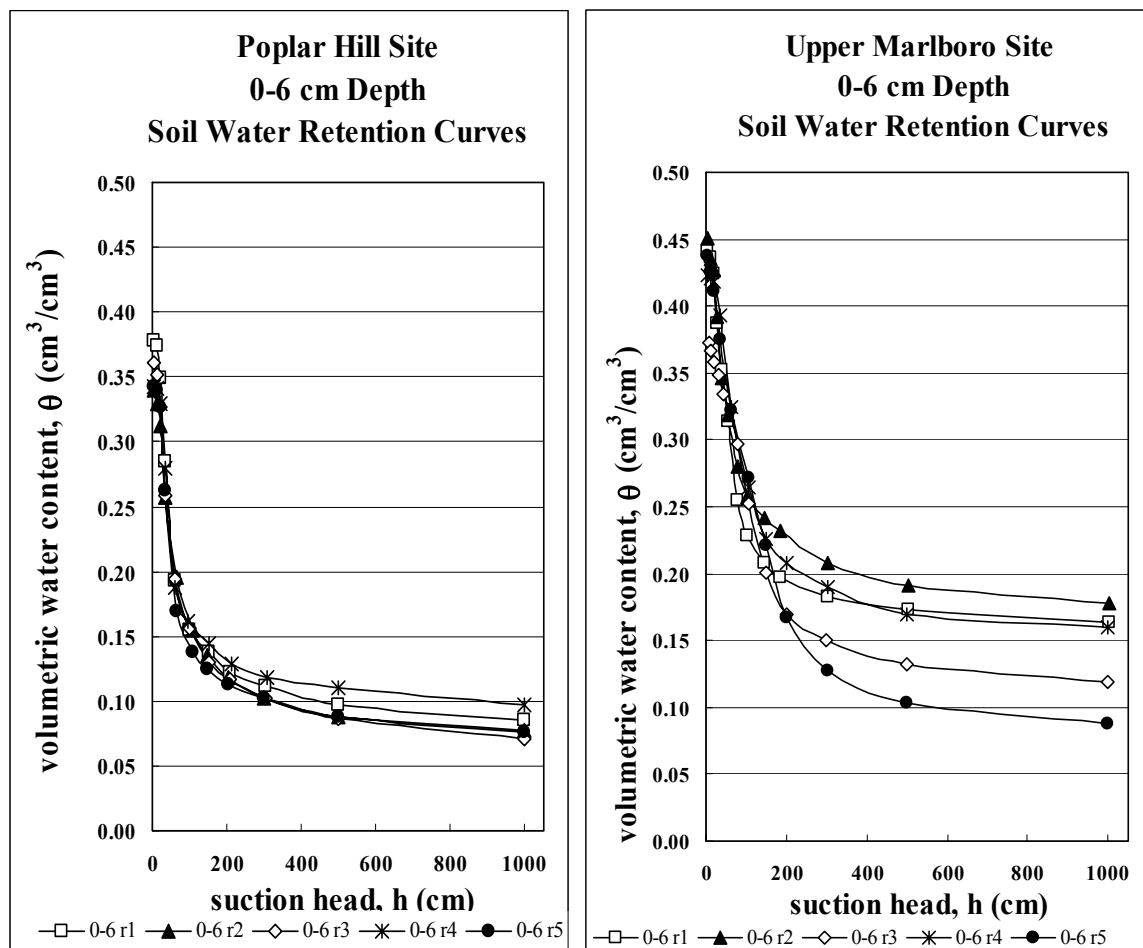


Figure 19. Upper Marlboro and Poplar Hill soil water retention curves for 0-6 cm depth.

Bubbling Pressure

Bubbling pressure head shows a strong site effect as can be seen in Figure 20. Values for Poplar Hill site are all approximately 20 cm, whereas for the Upper Marlboro site, bubbling pressures is depth dependent; average values start around 40 cm at 0-6 cm depth and increase to over 70 cm at 50-56 cm depth. These values although generally slightly higher are within one standard deviation of the average values for the appropriate soil textures listed in a table of water retention properties in Maidment (1993).

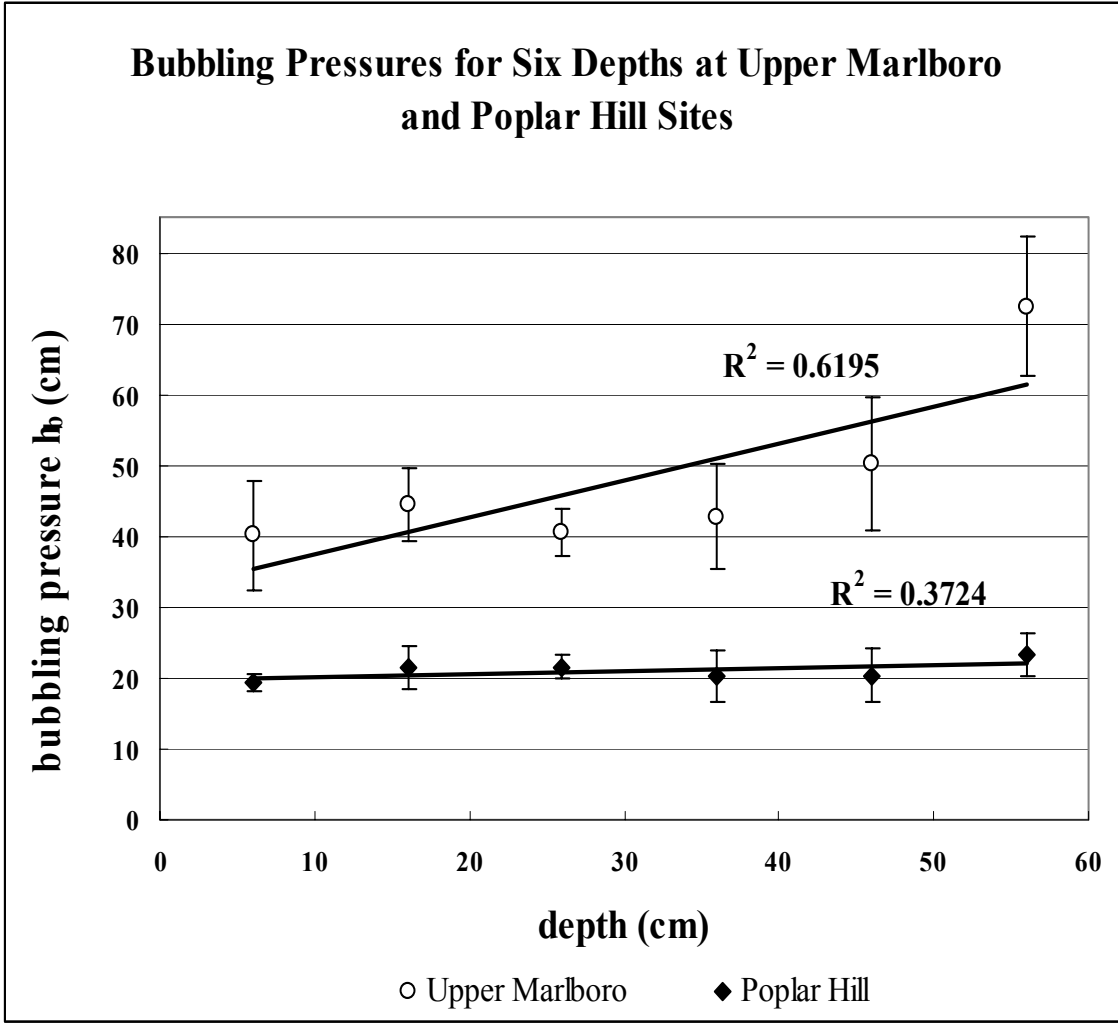


Figure 20. Average bubbling pressure of soil samples from Upper Marlboro and Poplar Hill sites as a function of depth. Error bars show standard errors for the mean of 5 replicates.

Sensitivity Analysis Results

The base values for parameters for each equation are shown in Table 5. Infiltration rates and condition numbers are given in Appendix F. A description of the sensitivities of parameters for each equation and their trends over time follows.

Table 5. Base parameter values for each equation.

Model	Equation (f_p)	Constant or Averaged Parameters	Base Values	Parameters Varied with Time/Depth	Sensitive parameters
Kostiakov	$f_p = K_k t_i^{-\alpha}$	$\alpha,$ K_k	0.789 4.700		K_k
Horton	$f_p = f_c + (f_0 - f_c) e^{-\beta t}$	$\beta,$ $f_0,$ f_c	2.54 5.96 cm h ⁻¹ 2.92 cm h ⁻¹		f_c
Holtan	$f_p = GIaSA^{1.4} + f_c$	GI, a, f_c	1.0 0.3 0.76 cm h ⁻¹	SA	SA GIa
Philip	$f_p = S/2 t^{-1/2} + C_a$	C_a	0.509 cm h ⁻¹	S	S
Green-Ampt	$f_p = K_{fs} + K_{fs} M_i S_f / F$	$M_i(av)$ S_f	0.143 21.7	F, K_{fs} , S_f	K_{fs}

Kostiakov Sensitivity Analysis

The Kostiakov infiltration rate is directly proportional to the parameter K_k and therefore has a condition number equal to 1 for all changes in K_k and at all time steps on the infiltration curve. The infiltration rate has a more complex relationship with the parameter α which is shown in Figure 21. Sensitivity initially decreases with time until reaching zero, and then increases again. The sensitivity of Kostiakov infiltration to α also increases as the value of α increases as can be seen by the increasing condition numbers for this parameter in Table 6. The condition numbers showing the Kostiakov sensitivity for α are quite low over most of the range including the values for 1/3rd and 2/3rd the duration of rainfall.

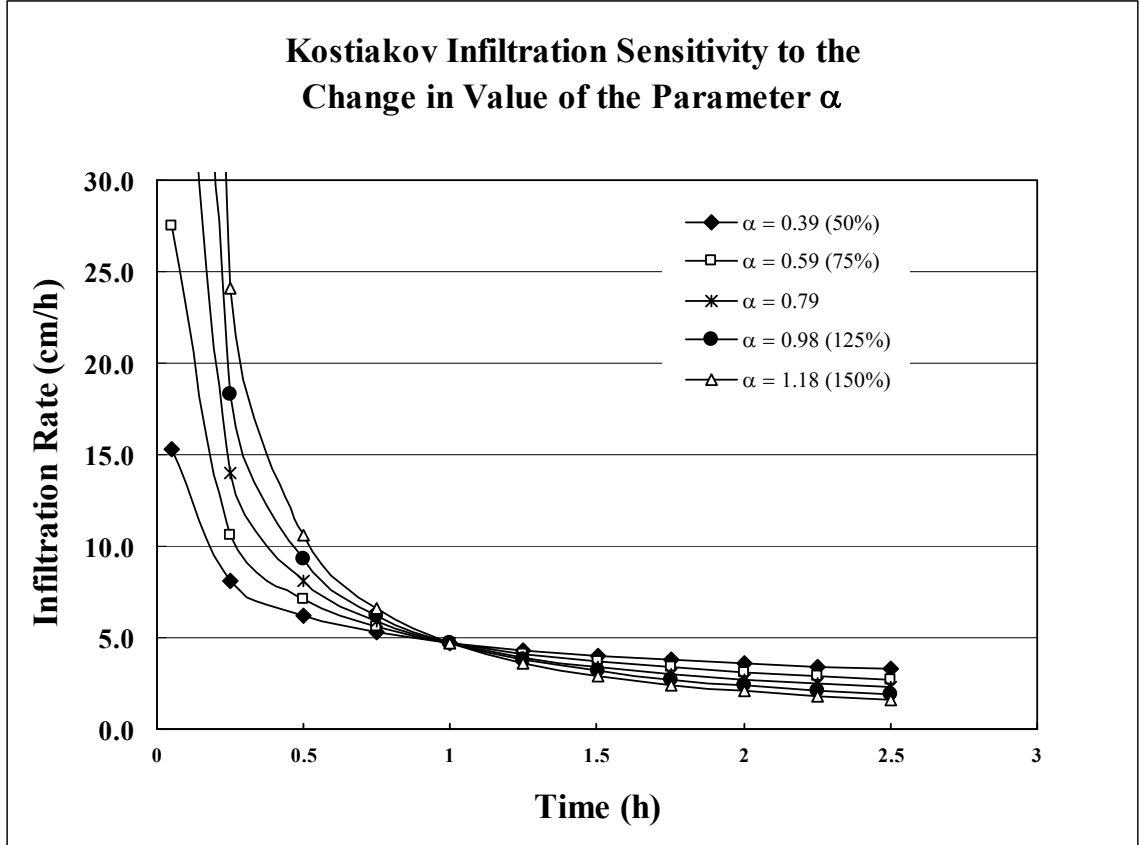


Figure 21. Kostiakov infiltration rate sensitivity to change in α is greatest initially, but decreases to zero at $t = 1$ h, and then gradually increases again.

Table 6. Condition numbers for Kostiakov parameters at 1/3rd and 2/3rd the duration of rainfall.

% change in base parameter values	Condition Numbers for Kostiakov Parameters			
	1/3 duration of rainfall		2/3 duration of rainfall	
	K_k	α	K_k	α
-50	1	0.214	1	-0.345
-25	1	0.220	1	-0.332
-10	1	0.224	1	-0.324
+10	1	0.229	1	-0.313
+25	1	0.233	1	-0.306
+50	1	0.239	1	-0.295

Horton Sensitivity Analysis

The Horton Equation shows greatest sensitivity to the parameter f_c as can be seen in Table 7 by the highest condition numbers for that parameter. Figure 22 shows that the infiltration rate's sensitivity to change in f_c increases over time. The infiltration rate can be seen to decrease along with its sensitivity as the parameter β increases in Figure 23. The Horton infiltration rate's sensitivity to change in f_0 decreases over time, opposite to the trend followed for the parameter f_c (Figure 24). Condition numbers for all three Horton parameters can be seen in 15 for 1/3rd and 2/3rd the duration of rainfall.

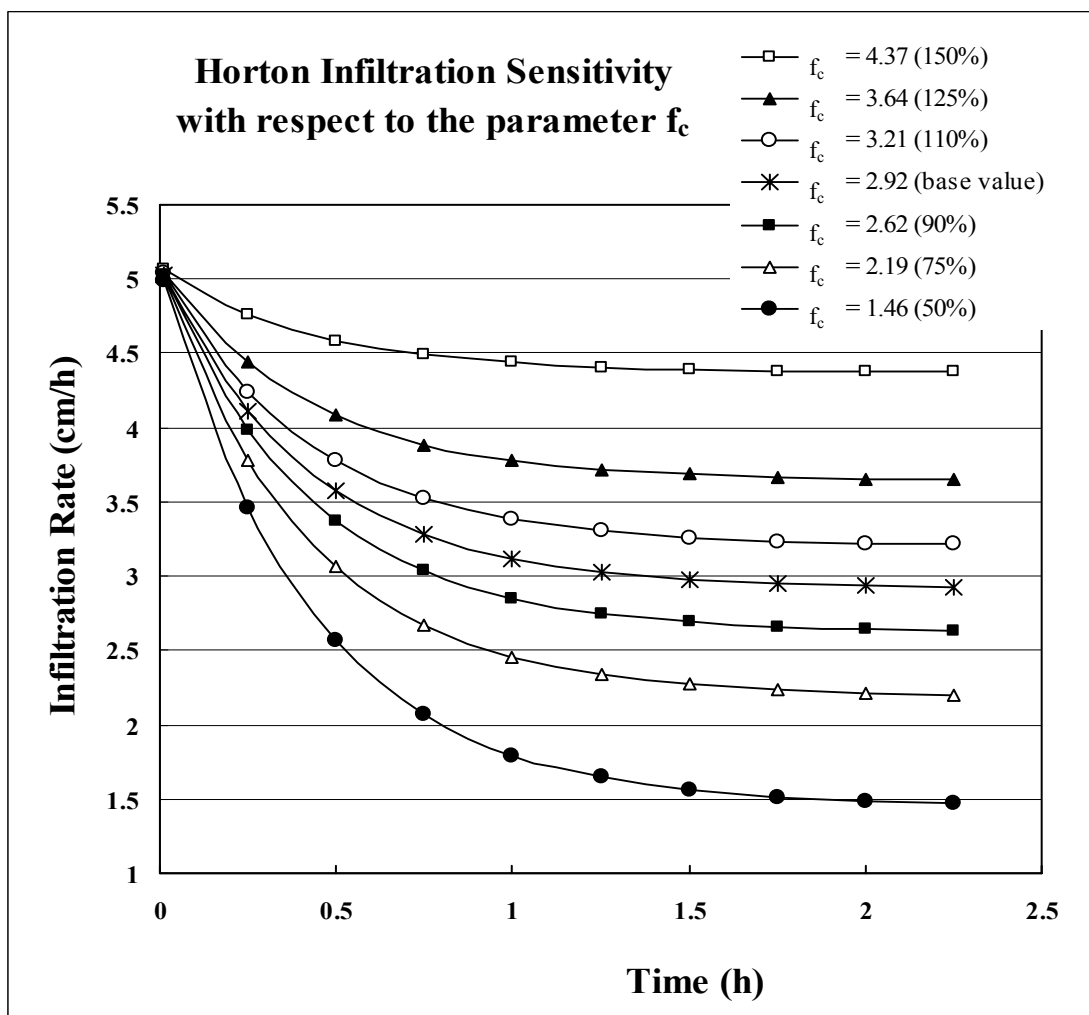


Figure 22. Infiltration rate sensitivity to f_c increases over time.

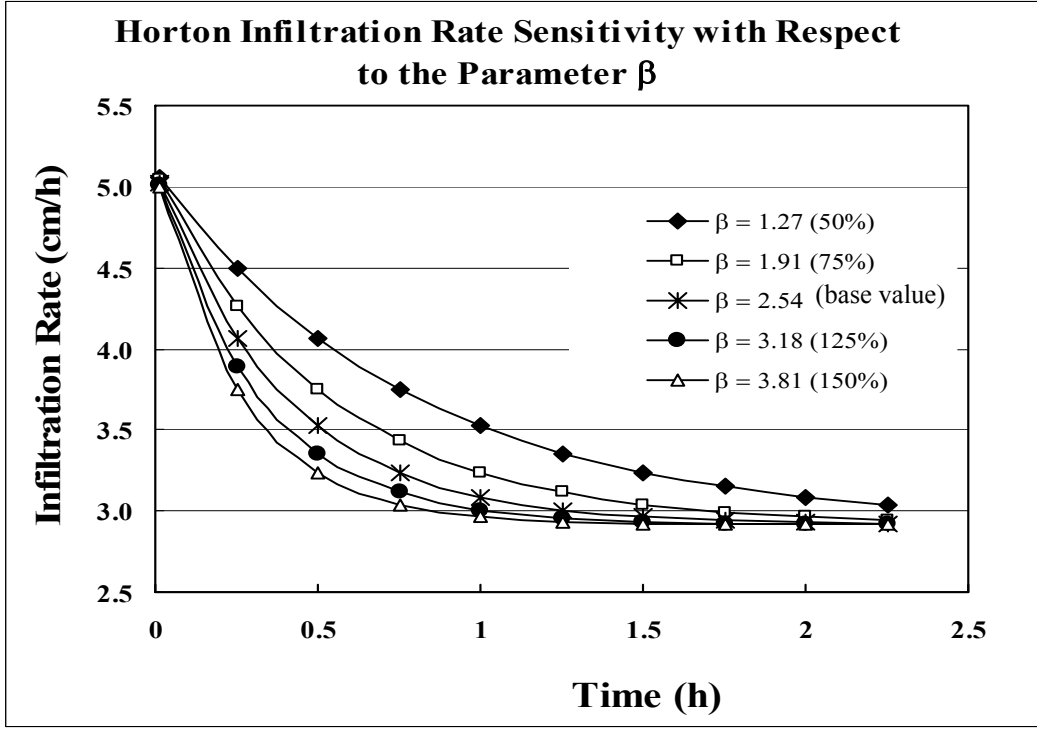


Figure 23. Horton infiltration rate sensitivity decreases with increasing values of β .

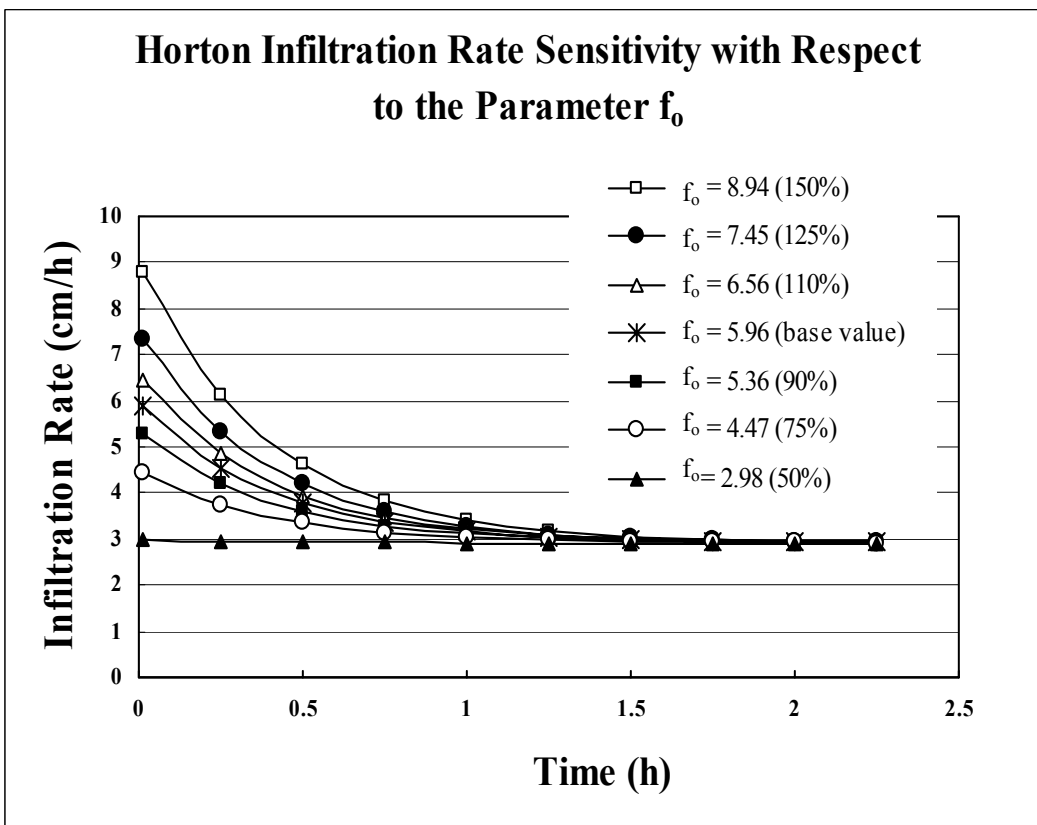


Figure 24. Horton infiltration rate sensitivity to f_0 decreases over time.

Table 7. Condition numbers for Horton parameters at 1/3rd and 2/3rd the duration of rainfall.

% change in base parameter values	Condition Numbers for Horton Parameters					
	1/3 duration of rainfall			2/3 duration of rainfall		
	f_c	f_o	β	f_c	f_o	β
-50	0.74	0.26	-0.43	0.96	0.044	-0.26
-25	0.74	0.26	-0.33	0.96	0.044	-0.14
-10	0.74	0.26	-0.28	0.96	0.044	-0.10
+10	0.74	0.26	-0.23	0.96	0.044	-0.072
+25	0.74	0.26	-0.20	0.96	0.044	-0.056
+50	0.74	0.26	-0.17	0.96	0.044	-0.039

Holtan Sensitivity Analysis

The Holtan equation showed low sensitivity to changes in the parameter value of final constant infiltration f_c with condition numbers equal to 0.19 and 0.35 for 1/3rd and 2/3rd the duration of rainfall respectively. The sensitivity of infiltration rate to this parameter increased gradually over time as shown in Figure 25.

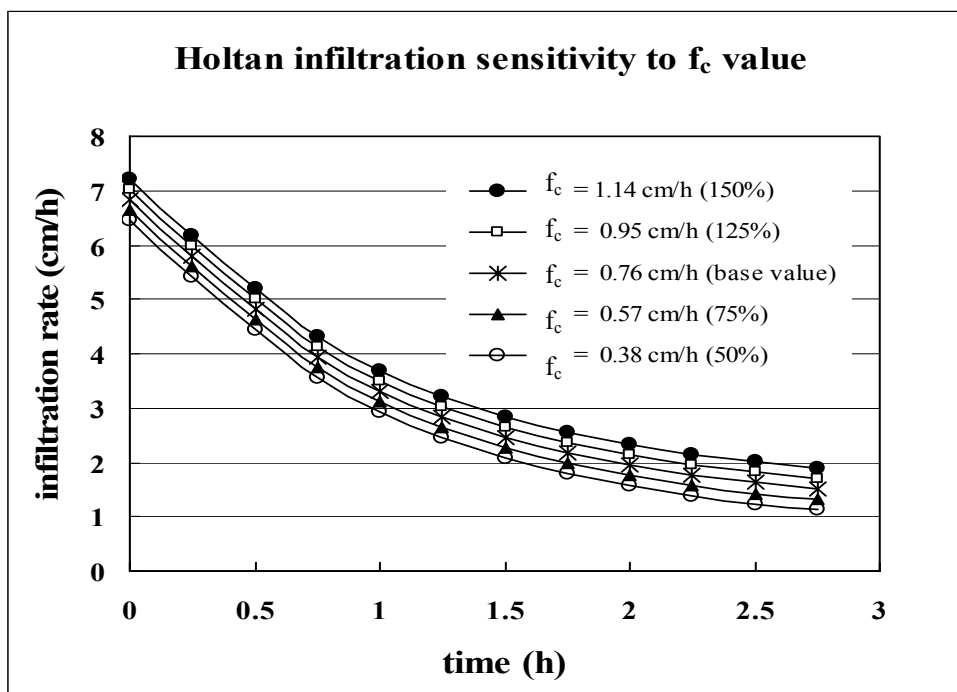


Figure 25. Holtan infiltration rate sensitivity to f_c increases slightly over time.

The Holtan infiltration rates showed much greater sensitivity to the vegetative parameter G_{Ia} and to the initial value of surface storage SA_0 . Figure 26 and Figure 27 show that the sensitivities for these 2 parameters decrease over time. Table 8 shows the condition numbers for all 3 parameters at $1/3^{\text{rd}}$ and $2/3^{\text{rd}}$ the duration of rainfall. Although SA was a sensitive parameter for the Holtan equation, the change in its value affected the time at which infiltration rate became less than rainfall (time of runoff initiation) more than it affected the actual infiltration rates. Therefore, by setting to zero the time immediately prior to runoff initiation, the curves are shifted so they overlap and little difference is seen in runoff rates at the adjusted times.

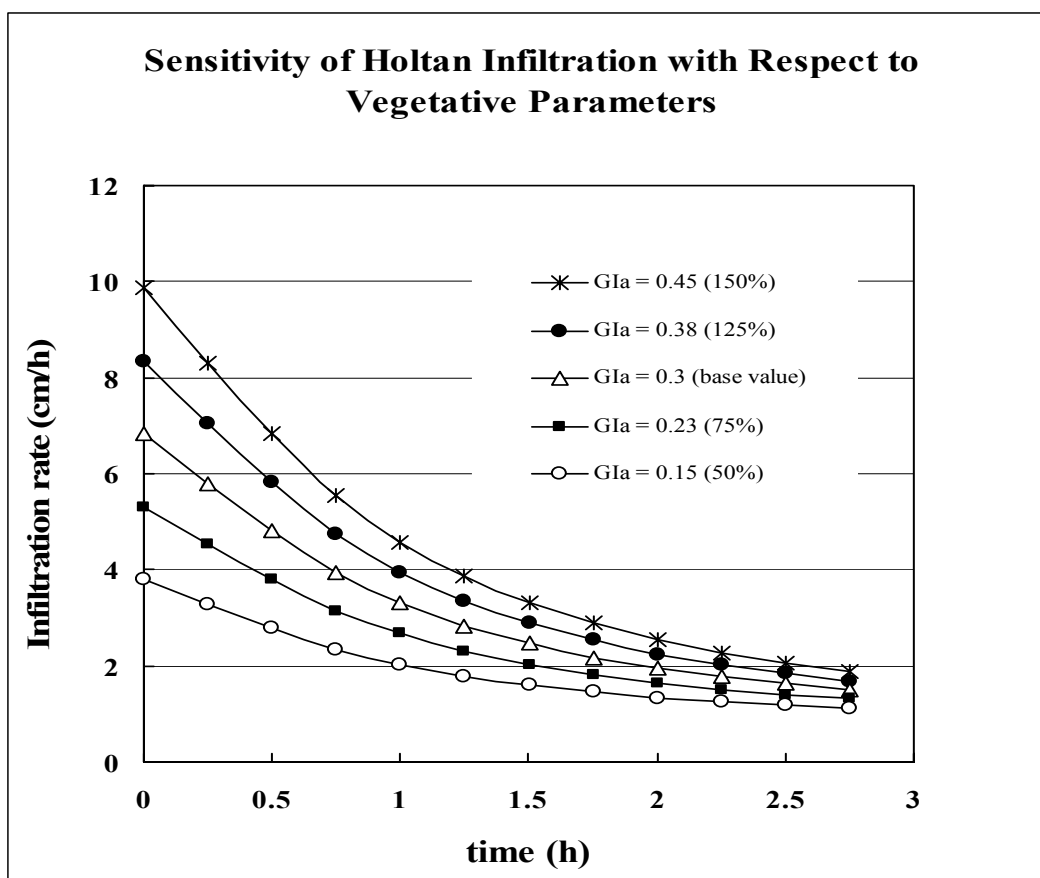


Figure 26. Holtan infiltration rate sensitivity to G_{Ia} decreases over time.

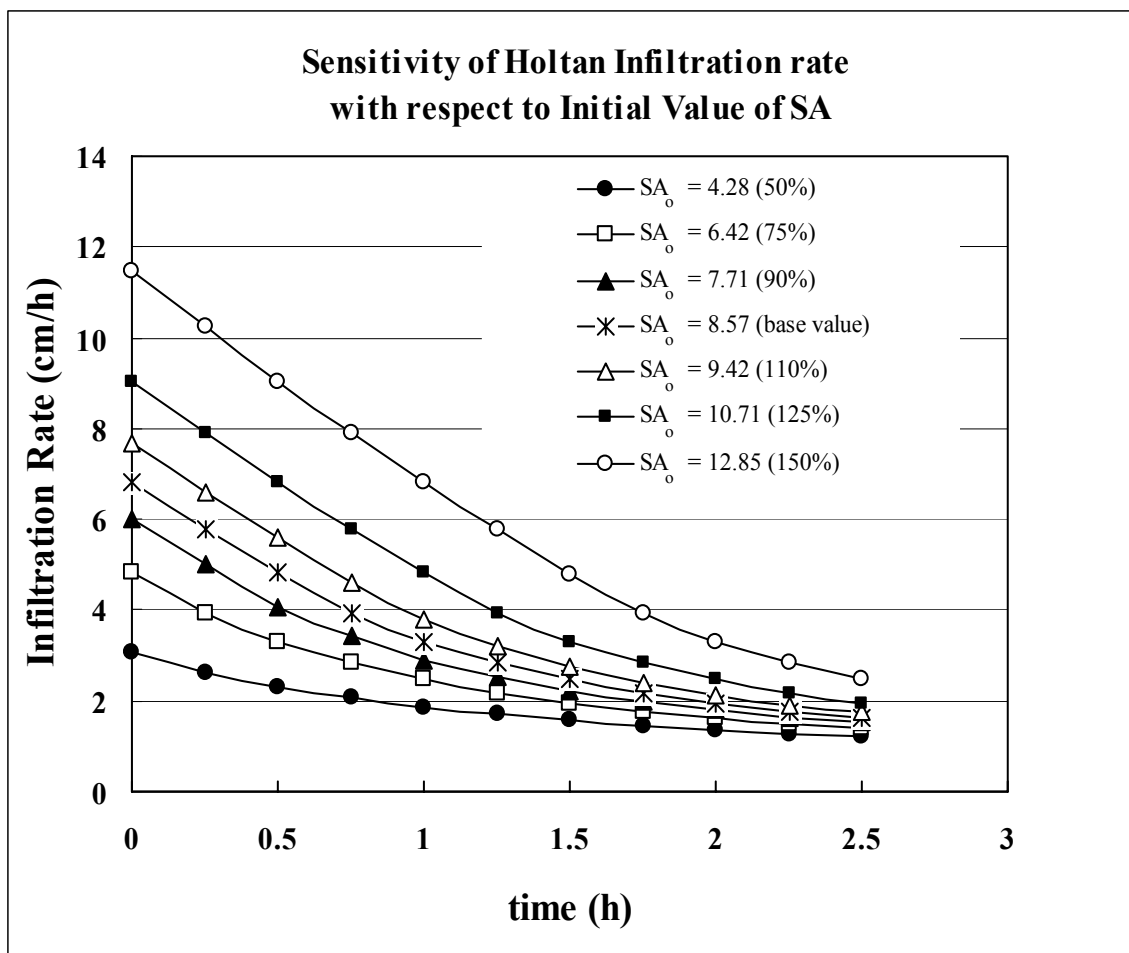


Figure 27. Holtan infiltration rate sensitivity to initial SA decreases over time.

Table 8. Condition numbers for Holtan Equation parameters at 1/3rd and 2/3rd duration of rainfall

% change in base parameter values	Condition numbers for Holtan Parameters					
	1/3 duration of rainfall			2/3 duration of rainfall		
	f_c	Gla	SA _o	f_c	Gla	SA _o
-50	0.19	0.81	0.87	0.35	0.65	0.47
-25	0.19	0.81	1.09	0.35	0.65	0.54
-10	0.19	0.81	1.34	0.35	0.65	0.64
+10	0.19	0.81	1.81	0.35	0.65	0.80
+25	0.19	0.81	2.07	0.35	0.65	0.96
+50	0.19	0.81	2.40	0.35	0.65	1.40

Philip Sensitivity Analysis

The Philip Equation is not very sensitive to changes in the parameter C_a , as can be seen by the close proximity of the curves in

Figure 28 and the low condition numbers in Table 9. Sensitivity of infiltration rate to change in C_a gradually increases over time.

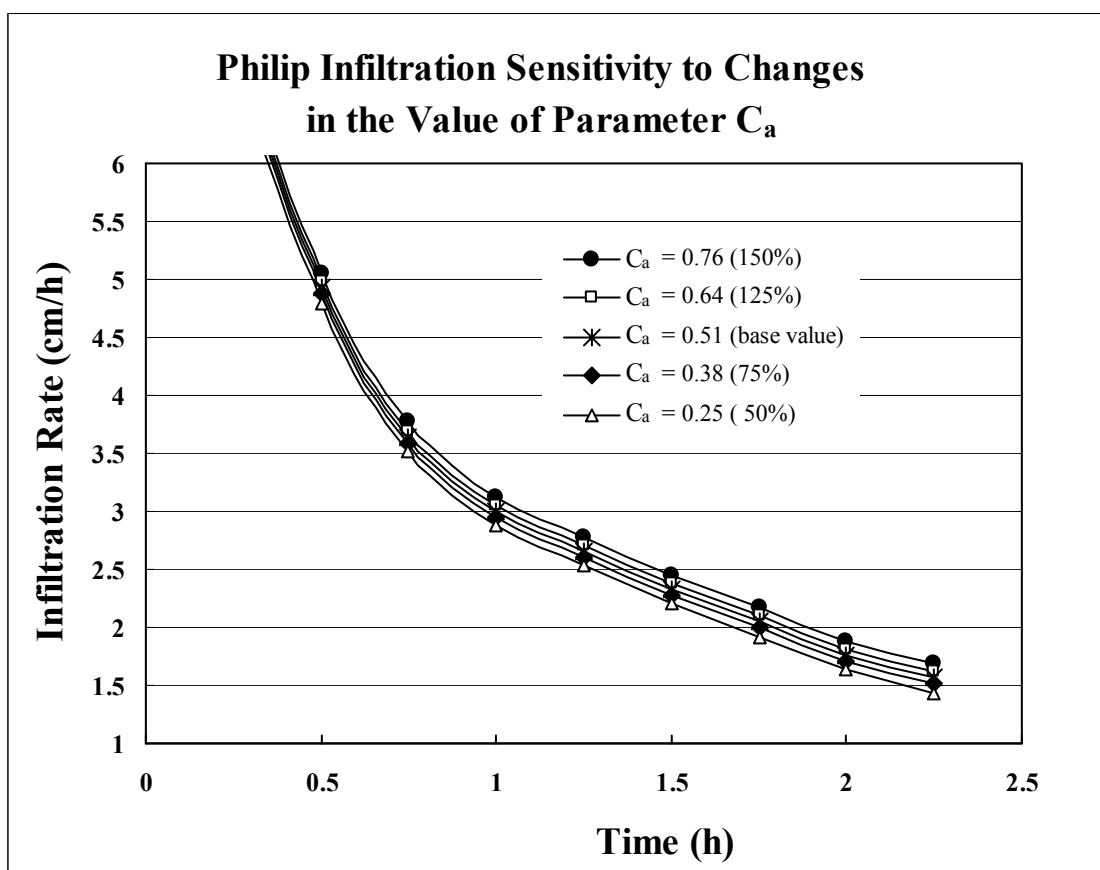


Figure 28. Philip infiltration rate shows low sensitivity to change in C_a .

The Philip equation shows much greater sensitivity to changes in sorptivity as seen in Table 9 by the considerably larger condition numbers for that parameter. Figure 29 shows

an initially high sensitivity of infiltration rate to change in sorptivity that decreases over time.

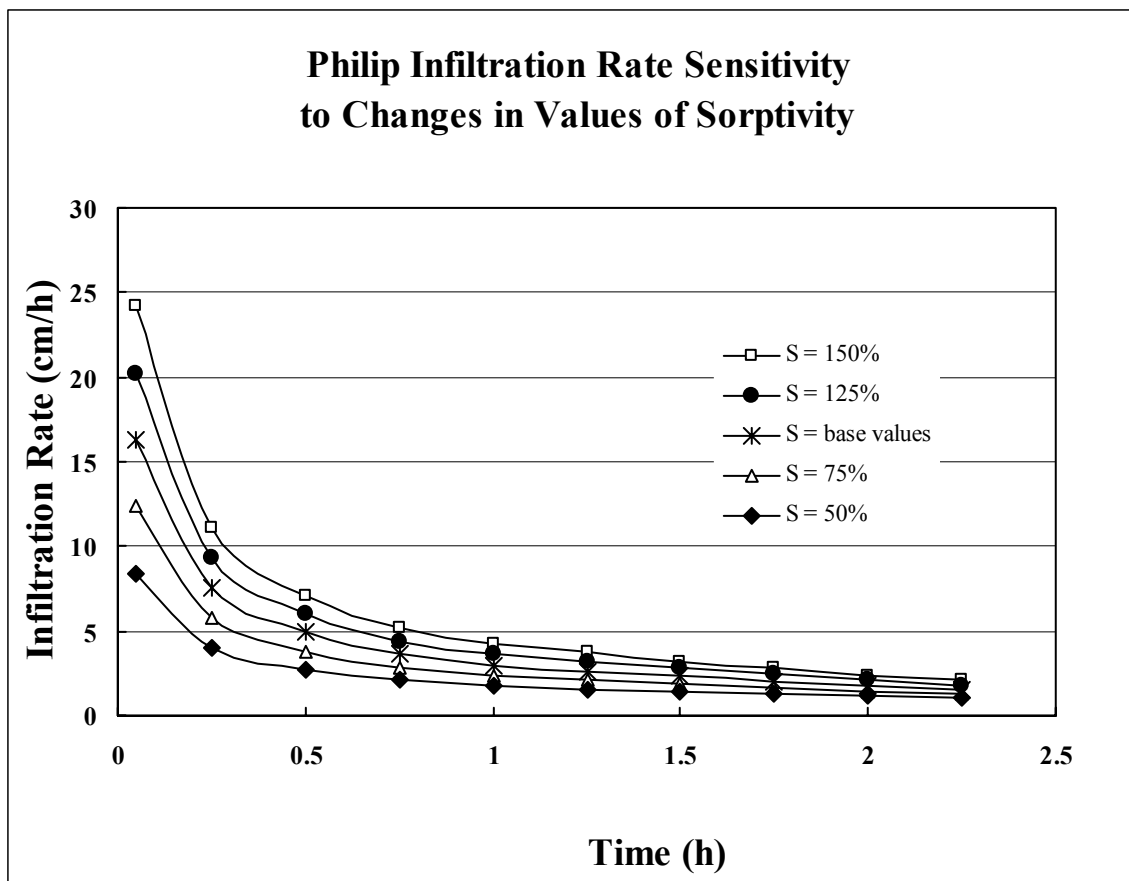


Figure 29. Philip infiltration rate shows initially high, but decreasing sensitivity to change in sorptivity over time.

Table 9. Condition numbers for Philip Equation parameters at 1/3rd and 2/3rd the duration of rainfall.

% change in base parameter values	Condition Numbers for Philip Parameters			
	1/3 duration of rainfall		2/3 duration of rainfall	
	C_a	S	C_a	S
-50	0.099	0.86	0.13	0.78
-25	0.099	0.86	0.13	0.78
-10	0.099	0.86	0.13	0.78
+10	0.099	0.86	0.13	0.78
+25	0.099	0.86	0.13	0.78
+50	0.099	0.86	0.13	0.78

Green-Ampt Sensitivity Analysis

GA equation is much more sensitive to the saturated hydraulic conductivity to which it is directly proportional than it is to moisture deficit or effective suction at the wetting front. Table 10 shows the condition numbers for these parameters. Figure 30, Figure 31 and Figure 32 show how infiltration rate changes with saturated hydraulic conductivity, moisture deficit and effective suction respectively. While the change in infiltration rate remains proportional to the change in saturated hydraulic conductivity, infiltration rate gradually becomes less sensitive to moisture deficit and effective suction over time. In Figure 30, sensitivity to K_{fs} appears to decrease over time, but this is a consequence of using effective K_{fs} that changes as the depth of the wetting front moves rather than an average value for K_{fs} that remains constant over the entire infiltration curve. The lines of the curves representing sensitivity of infiltration rate to changes in K_{fs} would be parallel if the base value for K_{fs} were a constant.

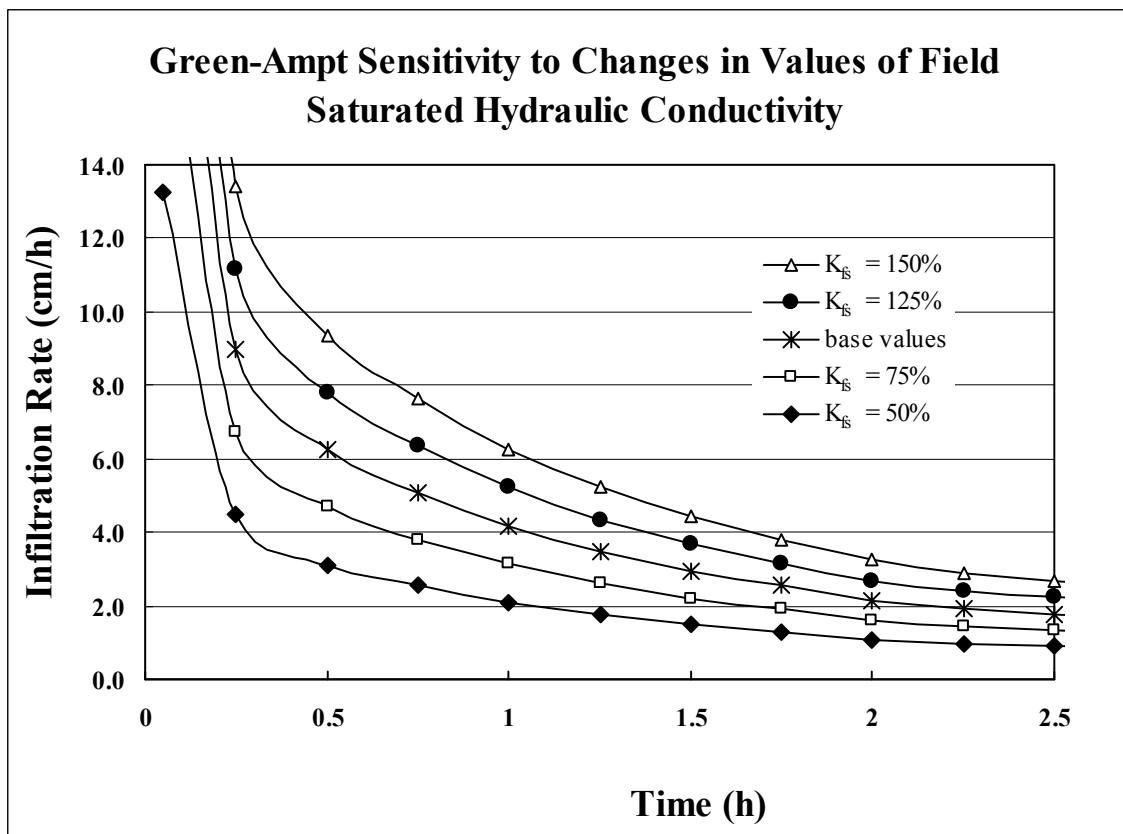


Figure 30. Green-Ampt infiltration rate is directly proportional to saturated hydraulic conductivity, however, saturated hydraulic conductivity decreases as the depth of the wetting front proceeds.

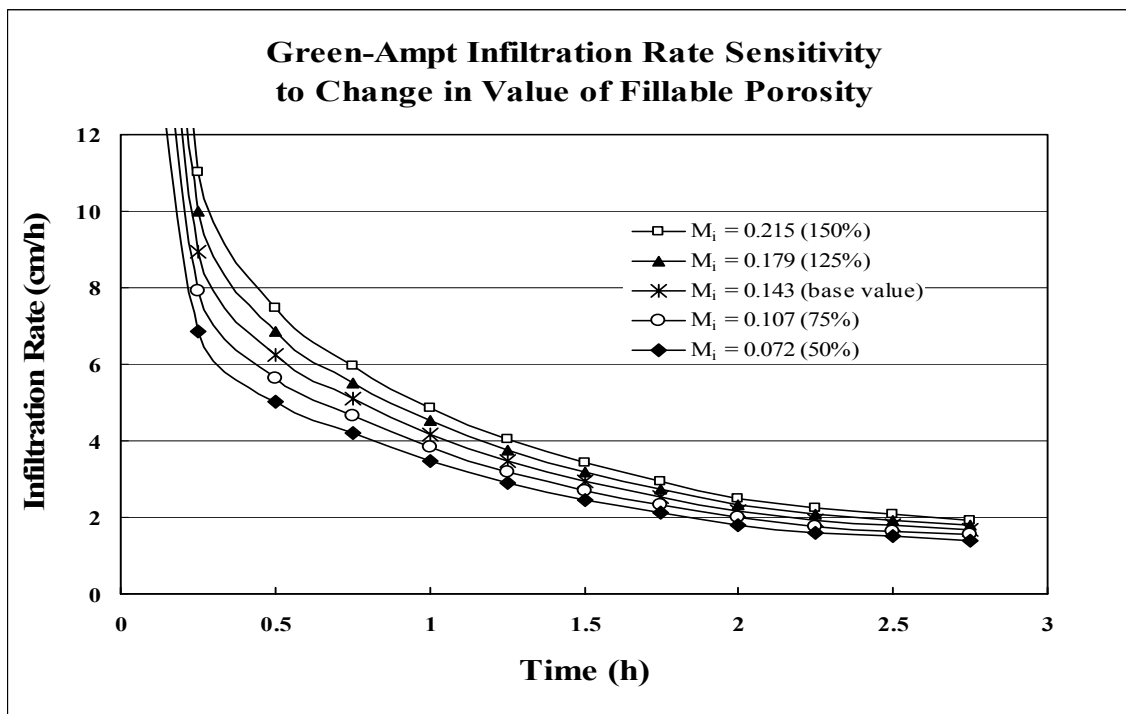


Figure 31. Green-Ampt infiltration rate shows low sensitivity to changes in moisture deficit which decreases over time.

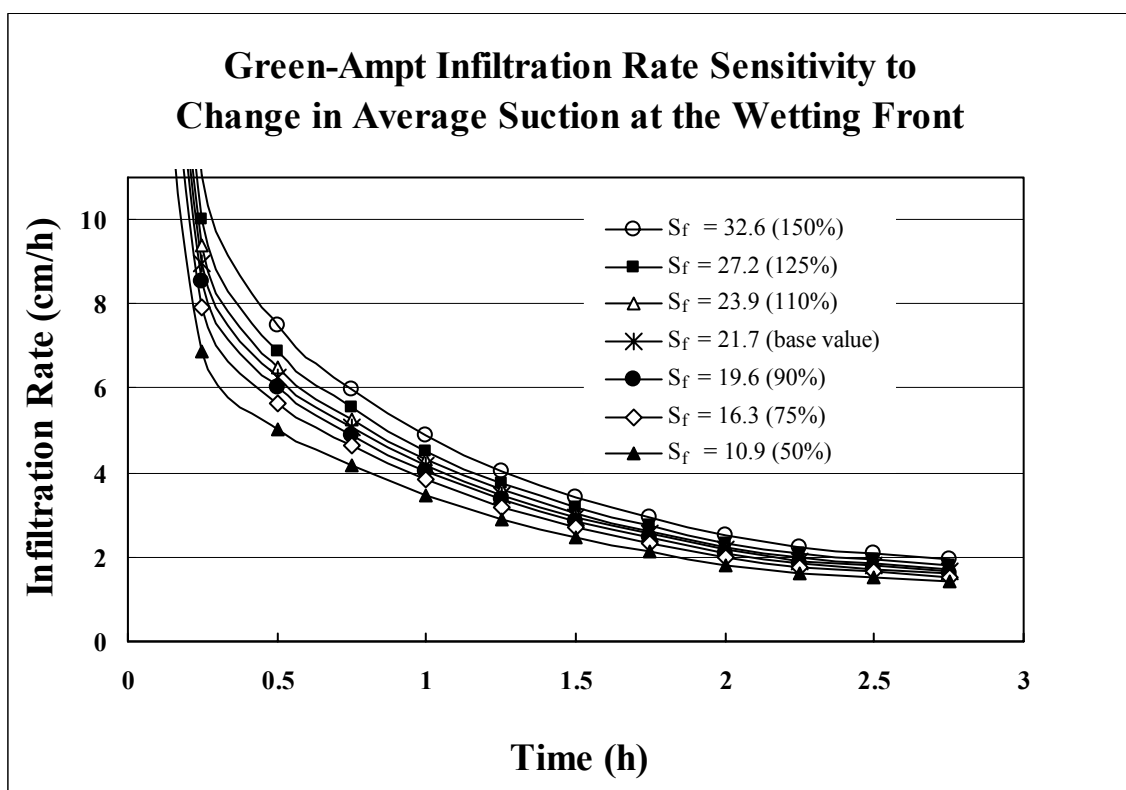


Figure 32. Green-Ampt equation also shows low sensitivity to changes in S_f .

Table 10. Condition numbers for Green-Ampt parameters at 1/3rd and 2/3rd the duration of rainfall.

% change in base parameter values	Condition numbers for Green-Ampt Parameters					
	1/3 duration of rainfall			2/3 duration of rainfall		
	K_{fs}	M_i	S_f	K_{fs}	M_i	S_f
-50	1	0.35	0.35	1	0.32	0.32
-25	1	0.35	0.35	1	0.32	0.32
-10	1	0.35	0.35	1	0.32	0.32
+10	1	0.35	0.35	1	0.32	0.32
+25	1	0.35	0.35	1	0.32	0.32
+50	1	0.35	0.35	1	0.32	0.32

Summary Sensitivity Analysis

The sensitive parameters in the infiltration equations that have a strong effect on the infiltration rate predictions are shown in Table 11.

Table 11. Sensitive infiltration parameters

Infiltration equations	Sensitive parameters	Condition Number
Kostiakov	K_k	1.0
Horton	f_c	0.74-0.96
Holtan	SA and GIA	0.47-2.40, 0.65-0.81
Philip	S	0.76 – 0.82
Green-Ampt	K_{fs}	1.0

The sensitivity of each parameter, as indicated by the condition number, determines how critical that parameter is in calibrating the equation. More sensitive parameters should be calibrated before less sensitive parameters since they have the most impact on the accuracy of the prediction.

Evaluation of Equations - Upper Marlboro Site

The Upper Marlboro site generated a typical infiltration curve with initial rapid decrease in infiltration rate, such as all five of the equations in this study describe. Figure 33 and Table 12 show all 5 models along with calculated infiltration from measured runoff for the Upper Marlboro site. For predicted infiltration rate values greater than the rainfall rate, the rainfall rate is assumed. Time zero is the time step immediately before, or during the start of runoff. Table 13 shows model goodness of fit for all 5 models including RMSE and R^2 values. The GA model with a RMSE of 0.15 cmh^{-1} most closely predicted the measured infiltration, followed by Holtan and Philip models with RMSE values of 0.17 cmh^{-1} and 0.19 cmh^{-1} respectively. Horton and Kostiakov models provided less accurate estimates of the measured infiltration with RMSE values of 0.73 cmh^{-1} and 0.52 cmh^{-1} respectively. The higher final constant infiltration rate for the earlier rainfall simulation that was used to obtain the parameter values for the simulation of interest, resulted in the greater divergence of these models from the values calculated from the observed runoff data. These results demonstrate the lack of flexibility in the Horton and Kostiakov models and hence, the need to be cautious when using one plot to calibrate another, since the plots must be very similar in order for the predictions made from the infiltration data from the first plot to accurately predict infiltration on the second plot. It is preferable to use an earlier simulation on the same plot for calibration if possible. Since GA and Philip model parameters are determined from laboratory measurements of soil samples including saturated hydraulic conductivity, bubbling pressure and soil water contents, and Holtan is estimated from soil type, ground cover characteristics, and moisture deficit, these models are more accurate than the empirical models when the only

available infiltration data is from a calibration plot with soil characteristics that are not a close match to the plot of interest.

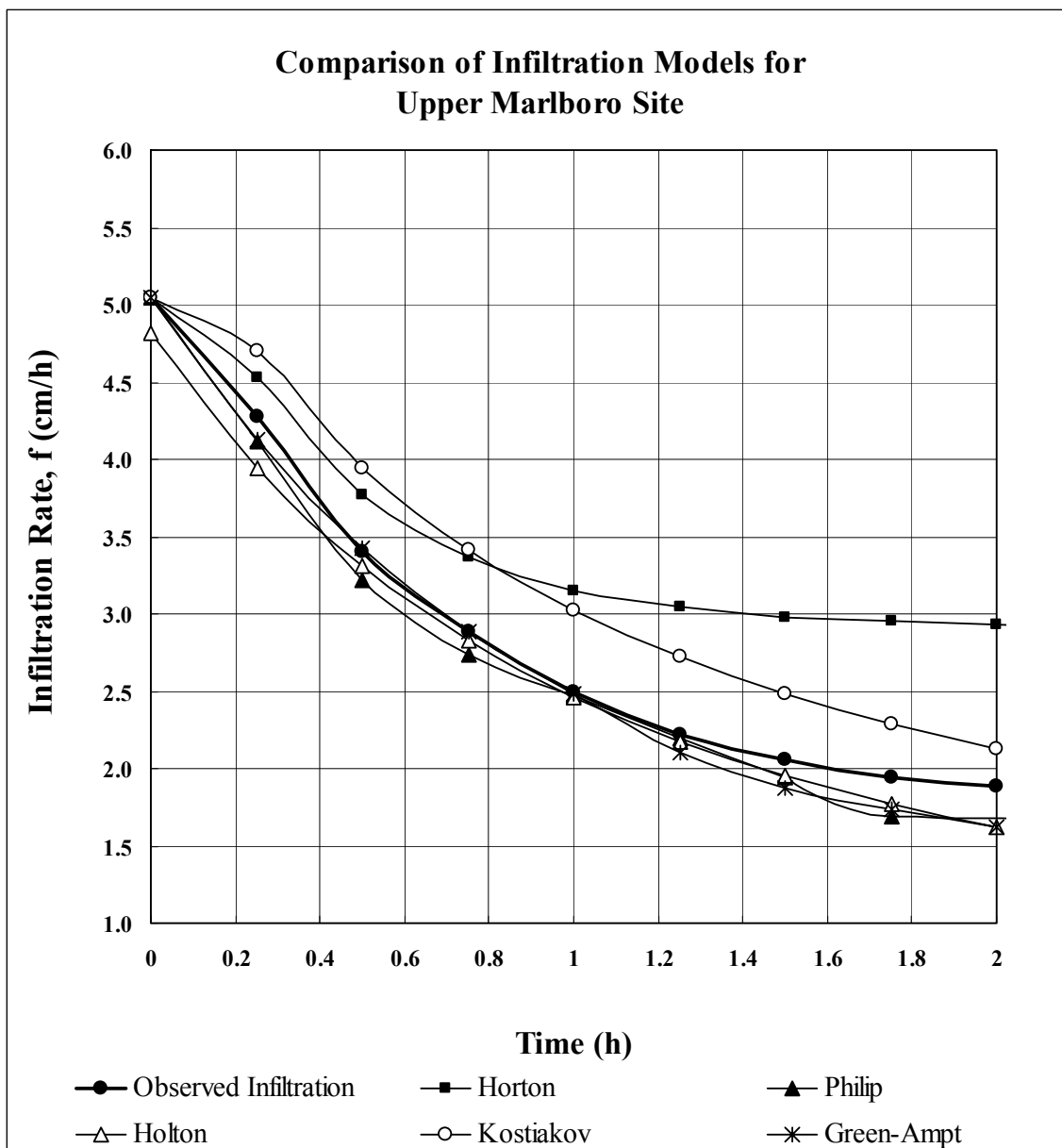


Figure 33. Comparison of infiltration equations for Upper Marlboro site.

Table 12. Infiltration curves for all five models and observed infiltration.

Time (h)	Observed infiltration (cm h ⁻¹)	Horton <i>f</i> (cm h ⁻¹)	Kostiakov <i>f</i> (cm h ⁻¹)	Holtan <i>f</i> (cm h ⁻¹)	Philip <i>f</i> (cm h ⁻¹)	Green-Ampt <i>f</i> (cm h ⁻¹)
0	5.048	5.048	5.048	4.814	5.048	5.048
0.25	4.277	4.529	4.700	3.947	3.966	4.129
0.5	3.400	3.770	3.944	3.310	3.148	3.421
0.75	2.882	3.368	3.418	2.830	2.692	2.887
1.0	2.490	3.155	3.028	2.463	2.436	2.487
1.25	2.217	3.042	2.726	2.177	2.172	2.103
1.5	2.063	2.982	2.485	1.951	1.932	1.872
1.75	1.940	2.951	2.288	1.769	1.676	1.737
2.0	1.880	2.934	2.123	1.623	1.505	1.619

Table 13. Comparison of goodness of fit for five infiltration equations

Model	RMSE (cmh ⁻¹)	R ²
Green-Ampt	0.1504	0.988
Holtan	0.1696	0.978
Philip	0.1917	0.980
Kostiakov	0.4565	0.987
Horton	0.7531	0.974

The R² values indicate the degree to which data variations are explained by each model. RMSE shows the amount of divergence of the model values from the observed values. If the model curve closely parallels the observation curve coefficient of determination (R²) will be close to 1, but the RMSE may not be very low. A model that has a low RMSE will also have a high R², but it may not be as high an R² as a model with a higher RMSE, but that is more parallel, diverging by about the same amount from all observed values. Kostiakov has a high R², but is off, probably because of the value for f_c , the final constant infiltration rate that was obtained from an adjacent site. Horton, although having the highest RMSE still has a high R² as well. Figure 34 shows the model predicted infiltration rates plotted versus the observed infiltration rates to obtain R² values. Table

14 shows the parameters that have constant or averaged values and those that vary with the increasing depth of the wetting front over time for each of the five equations. Kostiakov and Horton over predicted infiltration rates, while Philip, Holtan and Green-Ampt slightly under predicted infiltration rates.

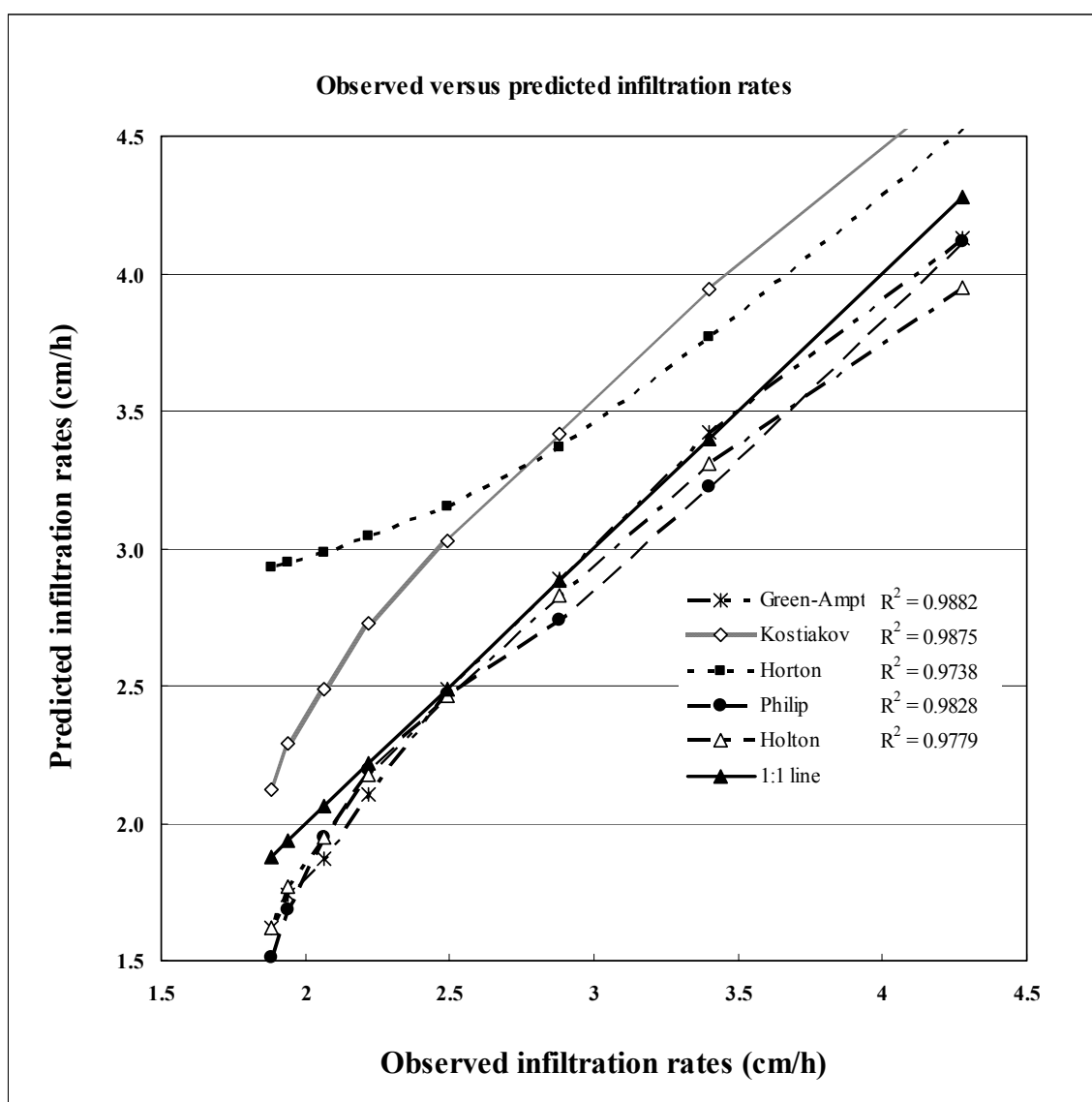


Figure 34. Predicted infiltration rates plotted against observed values.

Table 14. Constant and varied parameters for each equation for the Upper Marlboro site.

Model	Equation (f_p)	Constant or Averaged Parameters	Values	Parameters Varied with Time/Depth
Kostiakov	$f_p = K_k t_i^{-\alpha}$	$\alpha,$ K_k	0.79 4.70	
Horton	$f_p = f_c + (f_o - f_c) e^{-\beta t}$	$\beta,$ $f_o,$ f_c	2.54 5.96 cm/sec 2.92 cm/sec	
Holtan	$f_p = GIaSA^{1.4} + f_c$	$GI,$ $a,$ f_c	1.0 0.3 0.76 cm/sec	SA
Philip	$f_p = S/2 t^{-1/2} + C_a$	C_a	0.509 cm/sec	S
Green-Ampt	$f_p = K_{fs} + K_{fs} M_i S_f / F$	$M_i(av)$	0.143	F, K_{fs} , S_f

Holtan Equation

Initially the depth of the upper soil horizon, which was estimated to be $L = 28$ cm was used, since that is the approximate depth of the A horizon and the depth at which a layer with higher clay content is found. However, this estimate gave values of infiltration that were initially too low and did not correspond with the observed time of ponding and runoff. Therefore, an estimate of $L = 60$ cm was used to obtain a result consistent with the observation that runoff began after about 30 minutes of rainfall. The moisture deficit, $M_i = 0.143$ averaged across the depth, multiplied by the estimated depth gives a starting value of 8.57 cm for available storage. The value of available storage is reduced at each 0.25 hr. time interval according to Equation 3.22. The calculated infiltration rates for

each time step are shown in Table 15 below. While lower estimates for depth of the upper soil horizon reduce the amount of time before runoff begins, they do not have much effect on the shape of the infiltration rate curve.

Table 15. Solution of Holtan's infiltration equation for Upper Marlboro site.

time (h)	SA (cm)	SA ^{1.4}	GIaSA ^{1.4}	f _p (cm h ⁻¹)	f (cm h ⁻¹)	Time from start of runoff (h)
0	8.566	20.224	6.067	6.827	5.048	
0.25	7.494	16.772	5.032	5.792	5.048	
0.5	6.422	13.512	4.054	4.814	4.814	0.000
0.75	5.408	10.624	3.187	3.947	3.947	0.25
1	4.612	8.499	2.550	3.310	3.310	0.5
1.25	3.974	6.901	2.070	2.830	2.830	0.75
1.5	3.456	5.677	1.703	2.463	2.463	1
1.75	3.031	4.723	1.417	2.177	2.177	1.25
2	2.677	3.968	1.191	1.951	1.951	1.5
2.25	2.379	3.365	1.009	1.769	1.769	1.75
2.5	2.127	2.876	0.863	1.623	1.623	2

Philip Equation

Sorptivity (S) calculated for each sampling depth is shown in

Table 16 below. The values for effective sorptivity, (S_{eff}) calculated for each wetting front depth according to Equation 3.25 are shown in Table 17.

Table 16. Calculation of Sorptivity for each depth

depth	av M _i = (θ _s -θ _i)	av K _s (cm h ⁻¹)	av K _{fs} = 1/2K _s	av S _f	S = (2M _i K _{fs} S _f) ^{0.5}
0-6	0.203	22.250	11.125	19.052	9.279
10-16	0.169	10.119	5.060	23.895	6.386
20-26	0.165	4.674	2.337	21.039	4.026
30-36	0.163	5.893	2.947	18.911	4.265
40-46	0.078	2.695	1.347	21.129	2.105
50-56	0.079	0.936	0.468	27.935	1.438

The first three values calculated for infiltration rate, which are greater than rainfall rate, are assumed to be infiltration capacity and to occur prior to runoff initiation. Infiltration rate for these initial time intervals are therefore set equal to rainfall rate. Three different values for C_a are suggested in the literature for the Philip equation. Philip infiltration rate curves are shown in Figure 35. Philip infiltration curves for three different values for C_a . and Table 17 for three different values of C_a : $1/3 K_s$ (Philip,1957b; Talsma ,1969), $2/3 K_s$ (Philip,1957b; Youngs, 1968) and K_s which is the theoretical value that vertical infiltration should approach for long times. Of these three, it was found that the best approximation of the measured infiltration for the Upper Marlboro site was obtained using $C_a = K_{fs} / 3 = 0.5085$, where K_{fs} is the field saturated hydraulic conductivity estimated as $0.5 K_s$, as suggested by Bouwer (1966).

Table 15. Philip infiltration rates using 3 different values for C_a

time (h)	L_f (cm)	S_{eff}	time from start of runoff (h)	f (cm h ⁻¹) $C_a = K_{fs}/3$	f (cm h ⁻¹) $C_a = 2K_{fs}/3$	F (cm h ⁻¹) $C_a = K_{fs}$
0	0			5.048	5.048	5.048
0.25	6.157	6.885		5.048	5.048	5.048
0.50	12.315	6.559	0	5.048	5.048	5.048
0.75	18.472	5.988	0.25	3.966	4.474	4.983
1.0	24.630	5.280	0.5	3.148	3.657	4.165
1.25	30.787	4.882	0.75	2.692	3.200	3.709
1.5	36.944	4.720	1.0	2.436	2.944	3.453
1.75	43.102	4.402	1.25	2.172	2.681	3.189
2.0	49.259	4.026	1.5	1.932	2.440	2.949
2.25	55.417	3.501	1.75	1.676	2.184	2.693
2.5	61.574	3.151	2.0	1.505	2.013	2.522

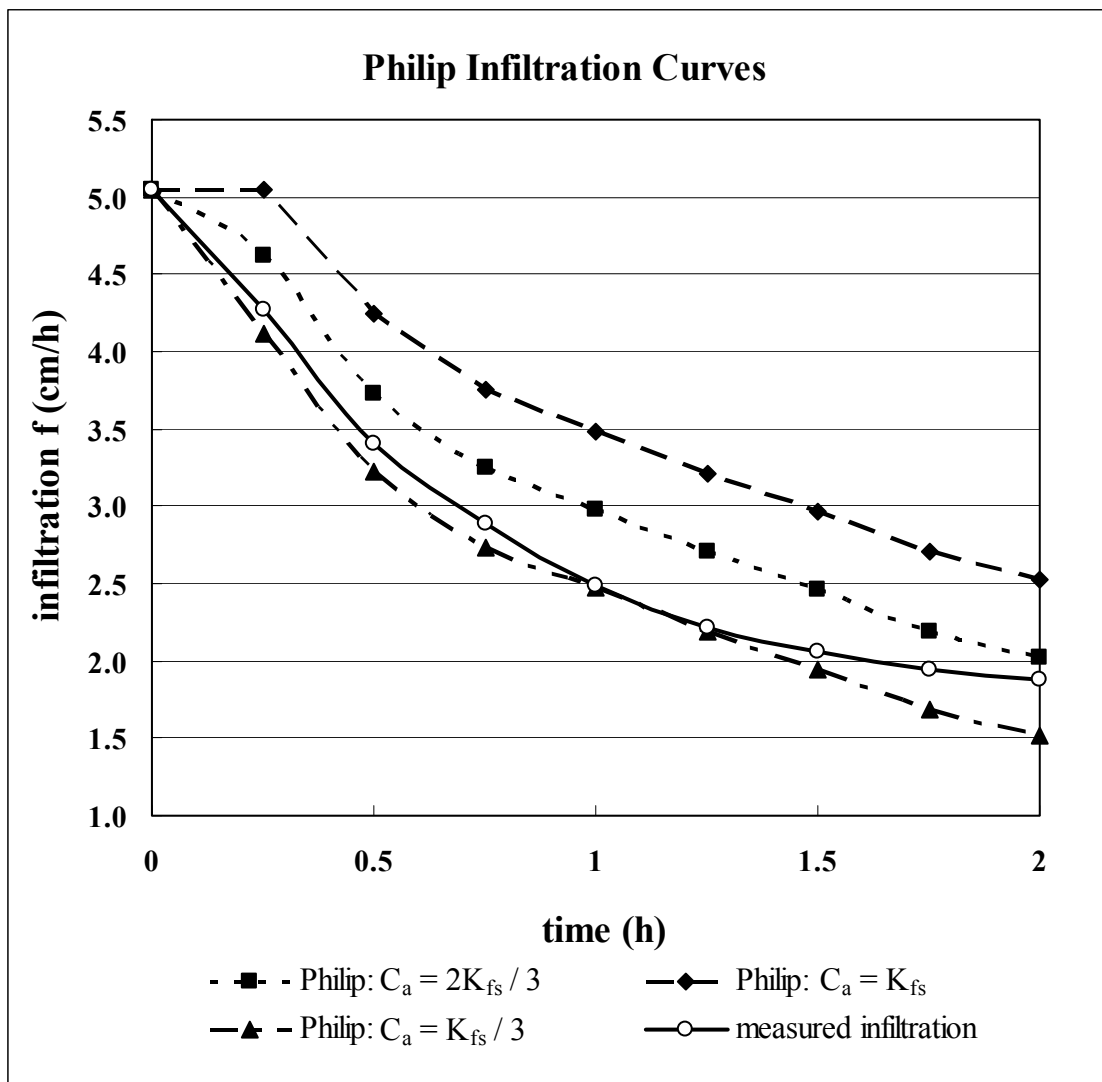


Figure 35. Philip infiltration curves for three different values for C_a .

When S was calculated using values for M_i and S_f that were averaged over depth as opposed to using values for M_i and S_f for each depth, there was little difference in the predicted infiltration rates as shown in Figure 36. Therefore, it should be valid and expedient to use the averaged values in calculations for this model. This produces a smoother curve with simpler computation.

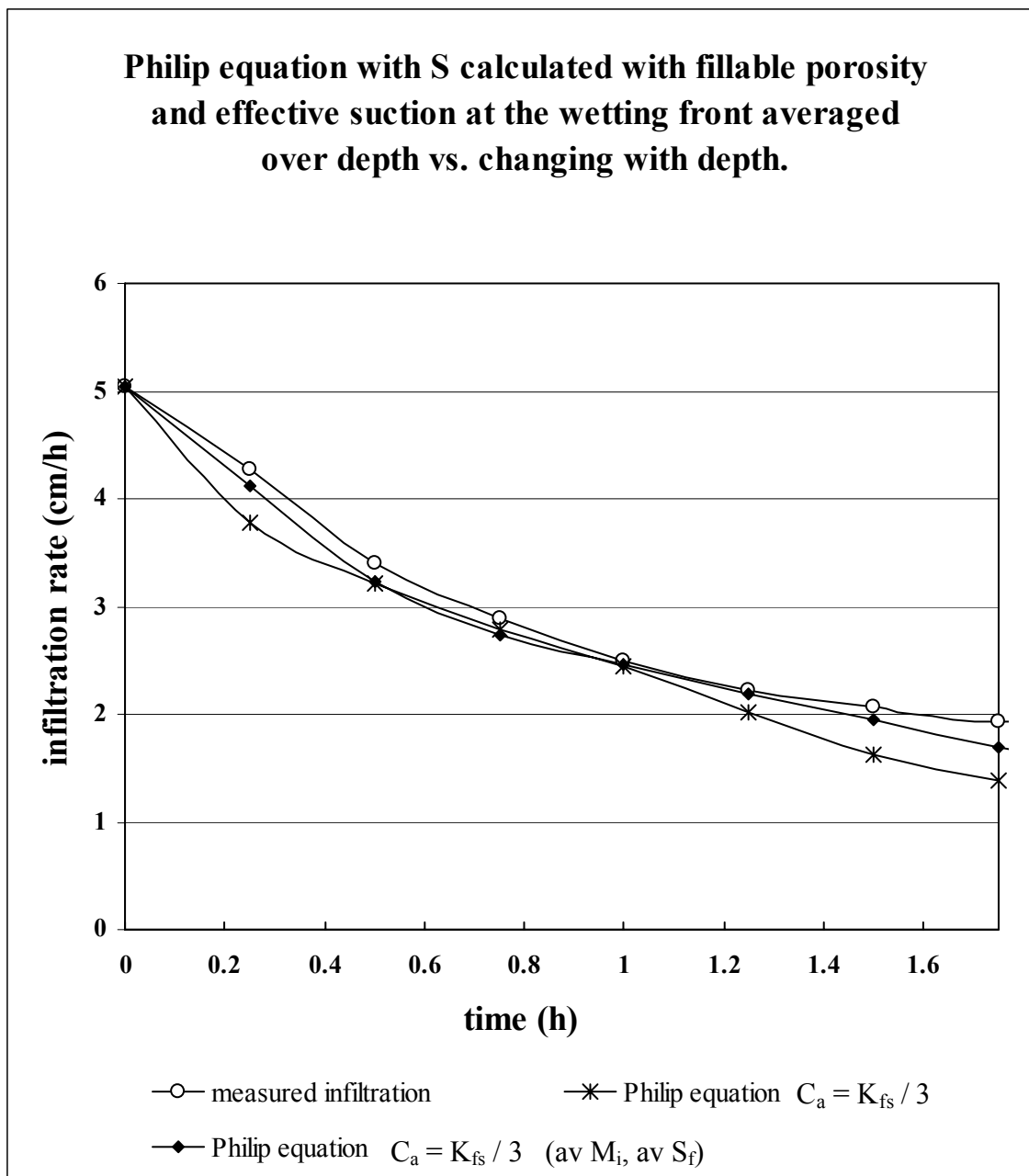


Figure 36. Philip equation provides a good estimate of measured infiltration whether or not M_i and S_f are averaged over depth.

Green and Ampt Equation

The GA equation provided a very good estimate of the observed infiltration, as indicated by the lowest RMSE of 0.15 cmh^{-1} . This result is in agreement with the results of Childs and Bybordi (1969) and Bower (1969), who also found the GA equation to

provide good predictions for layered soils. The model predicted that infiltration would be equal to rainfall for the first 43 minutes of the simulation at which time it would have penetrated to a depth of 36 cm as shown in Table 168. Table 179 shows the infiltration rates after the start of runoff. Infiltration rates for every 0.25 h are obtained by solving numerically for F at each time step.

Table 16. Green-Ampt infiltration rates for a series of depths. Predicted infiltration rates greater than rainfall rates are assumed to be equal to rainfall rates.

Depth, (cm)	$M_i = (\theta_s - \theta_i)$ eff	F (cm)	time (h)	K_{fs} eff	S_f eff	$f_p = K_{fs} + K_{fs}MS_f/F$	$f \leq R$
0		0.000	0.000				
6	0.203	1.218	0.013	11.13	20.89	49.865	5.048
12	0.184	2.211	0.069	6.96	20.14	18.629	5.048
18	0.181	3.252	0.159	5.87	19.95	12.378	5.048
24	0.177	4.255	0.307	4.79	19.77	8.726	5.048
30	0.174	5.207	0.534	3.79	20.01	6.321	5.048
36	0.156	5.631	0.727	3.29	20.34	5.145	5.048
42	0.139	5.850	0.955	2.78	20.68	4.153	4.153
48	0.131	6.309	1.392	2.15	21.44	3.116	3.116
54	0.124	6.674	2.157	1.53	22.19	2.153	2.153
60	0.114	6.863	2.998	1.15	23.42	1.604	1.604

Table 17. Green-Ampt infiltration rates after the start of predicted runoff.

F (cm)	time (h)	Time from start of runoff (h)	$f = K_{fs} + (K_{fs}M_iS_f)/F$ (cm h ⁻¹)	K_{fs} (cm h ⁻¹)	S_f	M_i
5.631	0.727	0	5.145	3.29	20.34	0.156
5.939	0.977	0.25	4.129	2.78	20.68	0.139
6.141	1.227	0.5	3.421	2.34	21.06	0.135
6.218	1.477	0.75	2.887	1.99	21.44	0.131
6.246	1.727	1	2.487	1.72	21.81	0.128
6.047	1.977	1.25	2.103	1.45	21.81	0.124
6.076	2.227	1.5	1.872	1.29	22.19	0.124
6.235	2.477	1.75	1.737	1.21	22.80	0.119
6.369	2.727	2	1.619	1.14	23.42	0.114

Kostiakov and Horton equations did not predict the measured infiltration as well as the other 3 models and therefore, further discussion of these models beyond that on page 108 is not included.

Evaluation of Equations - Poplar Hill Site

The Poplar Hill site generated an almost constant infiltration rate equal to the rainfall rate. Since the measured data did not describe a typical infiltration curve at the Poplar Hill rainfall simulations it did not make sense to attempt to use the Kostiakov or Horton equations. However, since the Holtan, Philip and Green-Amp equations do not require measured infiltration data, they were applied to demonstrate what the predicted curves look like for this site. The estimated final infiltration capacity for the Holtan equation based on soil type from Table 2 is too low an estimate for this site, resulting in under prediction of the infiltration capacity. Also, at the Poplar Hill site, C_a had to be estimated as $2/3 K_{sf}$ in order for predicted infiltration capacity to be greater than rainfall at all times. When C_a was estimated as $1/3 K_{sf}$ infiltration capacity was underestimated, dipping below the rainfall rate for the latter portion of the curve. The GA equation and Philip equation with C_a greater than or equal to $2/3 K_{sf}$ both predict infiltration capacity greater than the observed rainfall rate over the entire hour during which runoff was measured and therefore that infiltration rate equals rainfall rate. One cannot say that one equation is better than the other, since the rainfall rate did not satisfy the infiltration capacity of the Poplar Hill soil and they consequently both predict the same constant rate of infiltration. Figure 37 shows GA equation, Philip equation with C_a greater than or

equal to $2/3 K_{sf}$ and Holtan equation along with the infiltration rates calculated from measured runoff data at the Poplar Hill site.

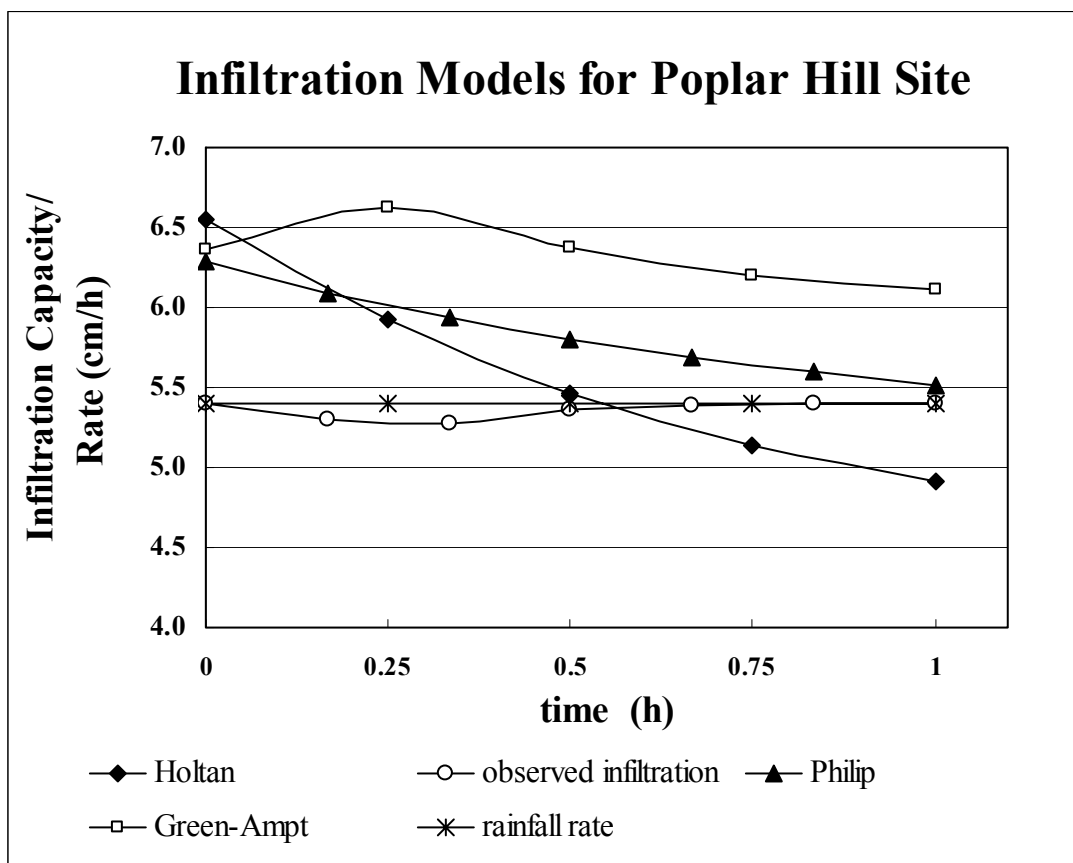


Figure 37. Green-Ampt and Philip both predict infiltration capacities greater than the observed rainfall rate over the entire hour during which runoff was measured.

CHAPTER V. – CONCLUSIONS

This study investigated the parameter sensitivity and prediction accuracy of five infiltration rate equations. The most sensitive parameters were Kostiakov's K_k and GA's K_{fs} with CN of 1.0, followed by Holtan's SA with CN ranging from 0.47 to 2.40, Philip's S (CN of 0.78 to 0.86), Holtan's GIa (CN of 0.65 to 0.81), and Horton's f_c (CN of 0.74).

For the Upper Marlboro site, GA, Holtan and Philip equations provided the first, second and third best estimates of infiltration rates, respectively, in comparison to observed infiltration data. The Kostiakov and Horton equations, which both depended on infiltration data from an earlier simulation, performed on an adjacent plot for parameter calibration, provided the least accurate estimates for infiltration at the Upper Marlboro site. This is due to the lack of flexibility in these models, as seen in their inability to adapt to slightly different field conditions, such as a different final infiltration rate on the calibration plot from that observed on the adjacent plot used for model validation.

For the Upper Marlboro site, GA provided the best result. However, the Holtan equation was a close second and required the least effort to obtain that result, since the only measured data required to use that equation is the moisture deficit. Estimation of the depth of the upper soil horizon is the most difficult aspect of the Holtan equation. When the depth of the A horizon, as given by the SCS handbook was used in the calculation of initial surface storage in the Holtan equation, time of runoff was predicted to occur much earlier than observed. Although the depth of the upper soil horizon used in the initial surface storage computation is important for the prediction of time of runoff, it did not greatly affect the infiltration rates for any time steps, provided that time zero was set as the time step immediately prior to runoff initiation.

As a result of dry soil conditions, and sandy soils with high saturated hydraulic conductivity values, an atypical infiltration curve was observed for the Poplar Hill site for which infiltration rate was constant and equal to rainfall rate. This infiltration pattern was predicted by GA and Philip equations, which predicted infiltration capacity greater than rainfall rate for the entire duration. A higher rate of rainfall would have been necessary at this site in order to observe a traditional infiltration curve for which a valid comparison of all infiltration models could be made. The Kostiakov and Horton equations were not applicable to predict infiltration at this site. The Holtan equation also predicted too low an estimate for final infiltration to be useful at this site. The GA and Philip equations are the more versatile equations, since they were applicable both in situations where rainfall rate was insufficient and sufficient and they do not rely earlier infiltration data which may have been obtained under different field conditions.

CHAPTER VI. – SUGGESTIONS FOR FUTURE RESEARCH

This research was based on data collected from rainfall simulations on two test sites on two different Maryland coastal plain soils. It is necessary to obtain a much broader base of data in order to make inferences about the applicability of the different equations for different types of soils. For example, when using the Philip equation, the lower estimate for C_a was preferable at the Upper Marlboro site, but the higher estimate provided a better result at the Poplar Hill site. It is possible that when Philip equation is used for deep sandy soils the higher estimate is preferable. However, with data from only the two sites, this generalization can not be made. It would be valuable to have data from many different sites, in order to make a stronger assessment of the different infiltration models. Also, it would be beneficial to pre-test the K_s values to determine the necessary rainfall rate before conducting the rainfall simulation.

Appendix A - Table of Equations

Table 18. Equations for infiltration capacity and time of ponding

	Equation (f_p)	Equation (t_p)	$(\theta_s - \theta_i)$	K_s	S_f	R
Kostiakov	$f_p = K_k t_i^{-\alpha}$		α	K_k		
Horton	$f_p = f_c + (f_o - f_c) e^{-\beta t}$		β	f_c		β
Holtan	$f_p = GIaSA^{1.4} + f_c$		SA	*		
Philip	$f_p = S/2 t^{1/2} + C_a$		S	Ca	S	R
Green-Ampt	$f_p = K_s + K_s M_i S_f / F$	$t_p = F_p - M_i S_f \ln (1 + F_p / M_i S_f) / K_s$	M_i	K_s	S_f	
Mein-Larson	$f_{pond} = R = K_s + K_s M_i S_{av} / F_p$	$t_p = K_s M_i S_{av} / R (R - K_s)$	M_i	K_s	S_{av}	R
Smith-Parlange		t_p $\int_0^{t_p} R dt = (S^2/2) / (R_p - K_s)$ $\int_0^{t_p} R dt = (S^2/2) / K_s \ln [R_p / (R_p - K_s)]$	S	K_s	S	R

* empirical estimate of f_c based on soil group

Appendix B - Tables of Parameters Developed From Soil Samples

Table 19. Parameters for Upper Marlboro Site

Appendix B-1 - Table of Parameters for Upper Marlboro Site					Brooks-Corey S_r = effective suction at the wetting front approximated by the water entry suction, h_{ce} or by S_{av} , the average suction at the wetting front.						
					Residual saturation		bubbling pressure head		porosity index		Average suction at the wetting front
depth (cm)	rep	K_s (cm h ⁻¹)	(cm ³ /cm ³)		1st estimate	2 nd estimate	h_b (cm)	$h_{ce} = 1/2h_b$	$\lambda = -\text{slope}$	$\eta = 2+3\lambda$	$S_{av} = h_{ce}\eta/(\eta-1)$
			θ_s	θ_r	S_r	adj S_r	h_b (cm)	$h_{ce} = 1/2h_b$	$\lambda = -\text{slope}$	$\eta = 2+3\lambda$	$S_{av} = h_{ce}\eta/(\eta-1)$
0-6	1	37.69	0.44	0.16	0.35	0.34	24.22	12.11	0.88	4.63	15.44
0-6	2	42.35	0.45	0.17	0.38	0.36	22.69	11.35	0.72	4.15	14.95
0-6	3	14.71	0.37	0.11	0.30	0.29	61.78	30.89	1.22	5.65	37.53
0-6	4	51.58	0.42	0.14	0.32	0.34	36.60	18.30	0.89	4.66	23.29
0-6	5	19.08	0.44	0.09	0.20	0.21	63.64	31.82	1.39	6.16	37.98
10-16	1	18.32	0.31	0.08	0.27	0.27	38.58	19.29	1.04	5.13	23.96
10-16	2	19.12	0.34	0.08	0.27	0.25	34.35	17.18	0.74	4.21	22.52
10-16	3	10.84	0.36	0.12	0.33	0.34	34.76	17.38	0.95	4.86	21.88
10-16	4	8.01	0.34	0.12	0.34	0.36	37.56	18.78	0.89	4.68	23.89
10-16	5	9.17	0.27	0.10	0.38	0.39	49.13	24.57	1.08	5.23	30.38
20-26	1	1.80	0.30	0.09	0.29	0.30	38.22	19.11	1.13	5.40	23.46
20-26	2	2.61	0.32	0.12	0.38	0.38	45.19	22.60	0.81	4.42	29.19
20-26	3	8.91	0.35	0.08	0.25	0.23	29.72	14.86	0.71	4.14	19.59
20-26	4	6.51	0.34	0.08	0.25	0.28	50.78	25.39	0.93	4.79	32.08
20-26	5	10.41	0.34	0.08	0.28	0.25	27.98	13.99	0.63	3.88	18.85
30-36	1	13.12	0.34	0.14	0.41	0.43	53.87	26.94	0.84	4.53	34.56
30-36	2	8.50	0.39	0.17	0.42	0.43	35.92	17.96	0.88	4.64	22.89
30-36	3	8.71	0.35	0.16	0.50	0.45	23.36	11.68	0.35	3.05	17.37
30-36	4	4.60	0.35	0.14	0.40	0.40	65.19	32.60	1.32	5.97	39.16
30-36	5	2.89	0.34	0.09	0.29	0.27	29.41	14.71	0.67	4.02	19.58
40-46	1	3.66	0.38	0.23	0.60	0.61	29.55	14.78	0.54	3.62	20.42
40-46	2	10.20	0.43	0.28	0.72	0.65	77.69	38.85	0.39	3.18	56.65
40-46	3	0.47	0.40	0.29	0.73	0.74	56.62	28.31	0.46	3.37	40.28
40-46	4	2.25	0.36	0.19	0.54	0.56	39.72	19.86	0.58	3.74	27.11
40-46	5	5.07	0.36	0.20	0.56	0.56	35.30	17.65	0.66	3.97	23.59
50-56	1	0.97	0.38	0.27	0.70	0.71	57.32	28.66	0.51	3.53	39.99
50-56	2	1.29	0.37	0.15	0.39	0.49	74.71	37.35	0.31	2.93	56.70
50-56	3	1.42	0.40	0.30	0.75	0.73	77.03	38.51	0.71	4.12	50.88
50-56	4	0.47	0.40	0.19	0.47	0.45	104.96	52.48	0.84	4.52	67.41
50-56	5	1.84	0.42	0.27	0.66	0.74	35.82	17.91	0.29	2.88	27.44

Appendix B-1 - Table of Parameters for Upper Marlboro Site (cont.)

depth (cm)	rep	ρ_b (g/cm³)	ϵ	χ
0-6	1	1.378	36.02	1.272
0-6	2	1.324	20.32	1.006
0-6	3	1.414	49.48	1.192
0-6	4	1.498	110.70	1.407
0-6	5	1.432	29.22	1.171
10-16	1	1.535	177.26	1.826
10-16	2	1.576	27.61	1.064
10-16	3	1.600	138.41	1.512
10-16	4	1.660	27.26	1.001
10-16	5	1.589	121.43	1.117
20-26	1	1.584	44.80	1.456
20-26	2	1.618	124.90	1.494
20-26	3	1.617	103.06	1.501
20-26	4	1.547	55.13	1.268
20-26	5	1.588	28.04	1.061
30-36	1	1.642	123.25	1.332
30-36	2	1.715	40.91	1.051
30-36	3	1.677	33.65	1.208
30-36	4	1.731	88.41	1.266
30-36	5	1.615	38.30	1.147
40-46	1	1.627	252.20	1.536
40-46	2	1.528	207.99	1.383
40-46	3	1.600	233.58	1.056
40-46	4	1.649	21.64	0.657
40-46	5	1.590	21.98	0.687
50-56	1	1.669	250.03	1.133
50-56	2	1.205	121.43	1.117
50-56	3	1.560	222.34	1.031
50-56	4	1.538	150.09	1.232
50-56	5	1.605	44.08	0.602

Appendix B-1 - Table of Parameters for Upper Marlboro Site (cont.)

depth (cm)	av θ_i (cm ³ /cm ³)	av θ_s (cm ³ /cm ³)	av S_{av} (cm)	av S_f	$M_i = (\theta_s - \theta_i)$	av K_s (cm h ⁻¹)
0-6	0.222	0.425	25.841	20.893	0.203	22.250
10-16	0.154	0.322	24.525	19.438	0.169	10.119
20-26	0.164	0.329	24.634	19.189	0.165	4.674
30-36	0.191	0.354	26.713	20.775	0.163	5.893
40-46	0.309	0.387	33.607	23.887	0.078	2.695
50-56	0.315	0.394	48.482	34.983	0.079	0.936
Average	0.226	0.368	30.634	23.194	0.143	* 3.051

* Effective saturated hydraulic conductivity for whole soil column

Depth (cm)	av ρ_b (g/cm ³)	av ρ_s (g/cm ³)	sorptivity (cm h ^{-0.5})		$S^2/2$
			$S = (2MK_s S_{av})^{1/2}$	$S = (2MK_s S_f)^{1/2}$	
0-6	* 1.409	** 1.599	15.283	13.742	94.421
10-16	* 1.592	** 1.751	9.149	8.145	33.174
20-26	* 1.591	** 1.786	6.161	5.437	14.781
30-36	* 1.676	** 1.786	7.169	6.323	19.987
40-46	* 1.599	** 1.727	3.755	3.165	5.010
50-56	* 1.515	** 1.559	2.679	2.276	2.590
Average	1.564	1.730	7.366	6.515	21.221

* ρ_b measurement made after conducting K_s and soil water retention curves.

** ρ_b measurement made without first conducting K_s and soil water retention curves.

Table 20. Parameters for Poplar Hill Site

Appendix B-2 - Table of Parameters for Poplar Hill Site					Brooks-Corey S_r = effective suction at the wetting front approximated by the water suction, h_{ce} or by S_{av} , the average suction at the wetting front.						
			Residual saturation				h_b = bubbling pressure head		λ = porosity index		Average suction at the wetting front
			(cm^3/cm^3)		1st estimate	2 nd estimate					
depth (cm)	rep	$K_s(cmh^{-1})$	θ_s	θ_r	S_r	adj S_r	h_b (cm)	$h_{ce} = 1/2h_b$	$\lambda = -slope$	$\eta = 2+3\lambda$	$S_{av} = h_{ce}\eta/(\eta-1)$
0-6	1	9.128	0.377	17.6	8.78	0.708	4.123	11.596	0.00254	9.128	0.377
0-6	2	12.064	0.340	23.8	11.91	0.746	4.239	15.590	0.00335	12.065	0.340
0-6	3	8.521	0.362	16.8	8.41	0.841	4.524	10.791	0.00237	8.521	0.362
0-6	4	4.300	0.342	19.3	9.63	0.655	3.965	12.880	0.00119	4.300	0.342
0-6	5	8.903	0.343	19.4	9.68	0.727	4.182	12.727	0.00247	8.903	0.343
10-16	1	10.921	0.354	31.3	15.64	0.571	3.714	21.401	0.00303	10.920	0.354
10-16	2	2.862	0.309	18.4	9.21	0.709	4.128	12.154	0.00080	2.862	0.309
10-16	3	6.679	0.330	20.0	10.02	0.640	3.921	13.449	0.00186	6.679	0.330
10-16	4	7.730	0.334	24.0	12.01	0.958	4.874	15.115	0.00215	7.730	0.334
10-16	5	25.119	0.366	13.4	6.70	0.608	3.825	9.071	0.00698	25.119	0.366
20-26	1	7.243	0.311	23.3	11.64	0.777	4.331	15.138	0.00201	7.243	0.311
20-26	2	4.367	0.303	25.9	12.94	0.707	4.122	17.089	0.00121	4.367	0.303
20-26	3	17.314	0.333	16.1	8.07	0.678	4.033	10.729	0.00481	17.314	0.333
20-26	4	8.532	0.312	20.4	10.20	0.734	4.202	13.385	0.00237	8.532	0.312
20-26	5	5.066	0.310	22.2	11.12	0.715	4.146	14.652	0.00141	5.066	0.310
30-36	1	18.004	0.300	18.3	9.13	0.811	4.432	11.790	0.00500	18.004	0.300
30-36	2	9.801	0.344	32.5	16.27	1.078	5.234	20.109	0.00272	9.801	0.344
30-36	3	19.658	0.361	18.3	9.13	0.640	3.921	12.257	0.00546	19.658	0.361
30-36	4	10.453	0.337	22.6	11.29	0.729	4.186	14.833	0.00290	10.453	0.337
30-36	5	9.669	0.318	10.3	5.17	0.581	3.744	7.054	0.00269	9.669	0.318
40-46	1	27.063	0.327	19.5	9.74	0.832	4.496	12.529	0.00752	27.063	0.327
40-46	2	6.373	0.319	13.0	6.49	0.528	3.584	9.000	0.00177	6.373	0.319
40-46	3	15.986	0.315	14.6	7.32	0.708	4.124	9.665	0.00444	15.986	0.315
40-46	4	10.854	0.340	21.3	10.63	0.836	4.507	13.665	0.00301	10.854	0.340
40-46	5	20.351	0.336	33.7	16.85	0.995	4.985	21.080	0.00565	20.351	0.336
50-56	1	9.543	0.322	19.1	9.52	0.711	4.134	12.562	0.00265	9.543	0.322
50-56	2	22.786	0.369	33.9	16.93	0.809	4.426	21.878	0.00633	22.786	0.369
50-56	3	12.329	0.294	19.5	9.75	0.726	4.179	12.817	0.00342	12.329	0.294
50-56	4	5.053	0.300	17.7	8.84	0.684	4.053	11.739	0.00140	5.053	0.300
50-56	5	0.412	0.309	26.5	13.26	0.675	4.024	17.649	0.00011	0.412	0.309

Appendix B-2 - Table of Parameters for Poplar Hill Site (cont)

depth (cm)	rep	ρ_b (g/cm³)	ϵ	χ
0-6	1	1.556	28.12	1.23
0-6	2	1.532	16.88	1.05
0-6	3	1.570	18.31	1.39
0-6	4	1.600	64.24	1.40
0-6	5	1.560	31.20	1.27
10-16	1	1.710	23.69	1.19
10-16	2	1.686	49.13	1.40
10-16	3	1.655	44.89	1.30
10-16	4	1.630	62.00	1.49
10-16	5	1.524	10.78	0.89
20-26	1	1.787	12.97	0.96
20-26	2	1.699	57.43	1.35
20-26	3	1.569	7.00	0.80
20-26	4	1.735	87.03	1.52
20-26	5	1.737	104.98	1.57
30-36	1	1.583	23.07	1.37
30-36	2	1.713	23.93	1.19
30-36	3	1.548	8.35	0.77
30-36	4	1.632	24.74	1.20
30-36	5	1.644	16.90	1.07
40-46	1	1.585	11.68	0.98
40-46	2	1.667	29.20	1.16
40-46	3	1.686	48.60	1.40
40-46	4	1.585	25.30	1.23
40-46	5	1.654	35.66	1.27
50-56	1	1.607	26.43	1.19
50-56	2	1.611	48.47	1.30
50-56	3	1.670	44.22	1.36
50-56	4	1.706	43.77	1.29
50-56	5	1.724	81.79	1.41

Appendix B-2 - Table of Parameters for Poplar Hill Site (cont.)

depth (cm)	dry av θ_i (cm ³ /cm ³)	wet av θ_i (cm ³ /cm ³)	av θ_s (cm ³ /cm ³)	av S_{av} (cm)	av S_f	$M_i = (\theta_s - \theta_i)$
0-6	0.065	0.143	0.353	12.717	9.683	0.288
10-16	0.089	0.127	0.339	14.238	10.716	0.250
20-26	0.089	0.133	0.314	14.199	10.795	0.225
30-36	0.106	----	0.332	13.208	10.197	0.226
40-46	0.110	----	0.327	13.188	10.208	0.217
50-56	----	----	0.353	15.329	11.663	0.288
Average	0.092	0.134	0.339	12.717	9.683	0.250

depth (cm)	av ρ_b (g/cm ³)	av ρ_b (g/cm ³)	av K_s (cm h ⁻¹)	Sorptivity (cm h ^{-0.5})		$S^2/2$
				$S = (2MK_s S_{av})^{1/2}$	$S = (2MK_s S_f)^{1/2}$	
0-6	• 1.564	** 1.645	8.584	7.926	6.916	23.91 7
10-16	• 1.641	** 1.676	10.662	8.708	3.084	4.756
20-26	• 1.706	** 1.727	8.504	7.371	2.624	3.442
30-36	• 1.624	** 1.756	13.517	8.983	3.222	5.192
40-46	• 1.635	** 1.700	16.125	9.615	3.453	5.962
50-56	• 1.664	----	10.024			
Average	1.639	1.672	* 10.645	8.520	3.860	8.654

- ρ_b measurement made after conducting K_s and soil water retention curves.
- * Effective saturated hydraulic conductivity for whole soil column
- ** ρ_b measurement made without first conducting K_s and soil water retention curves.

Appendix C - Soil Water Retention Curves

Appendix C-1 – SWRCs for Upper Marlboro Site for Each of Six Depths

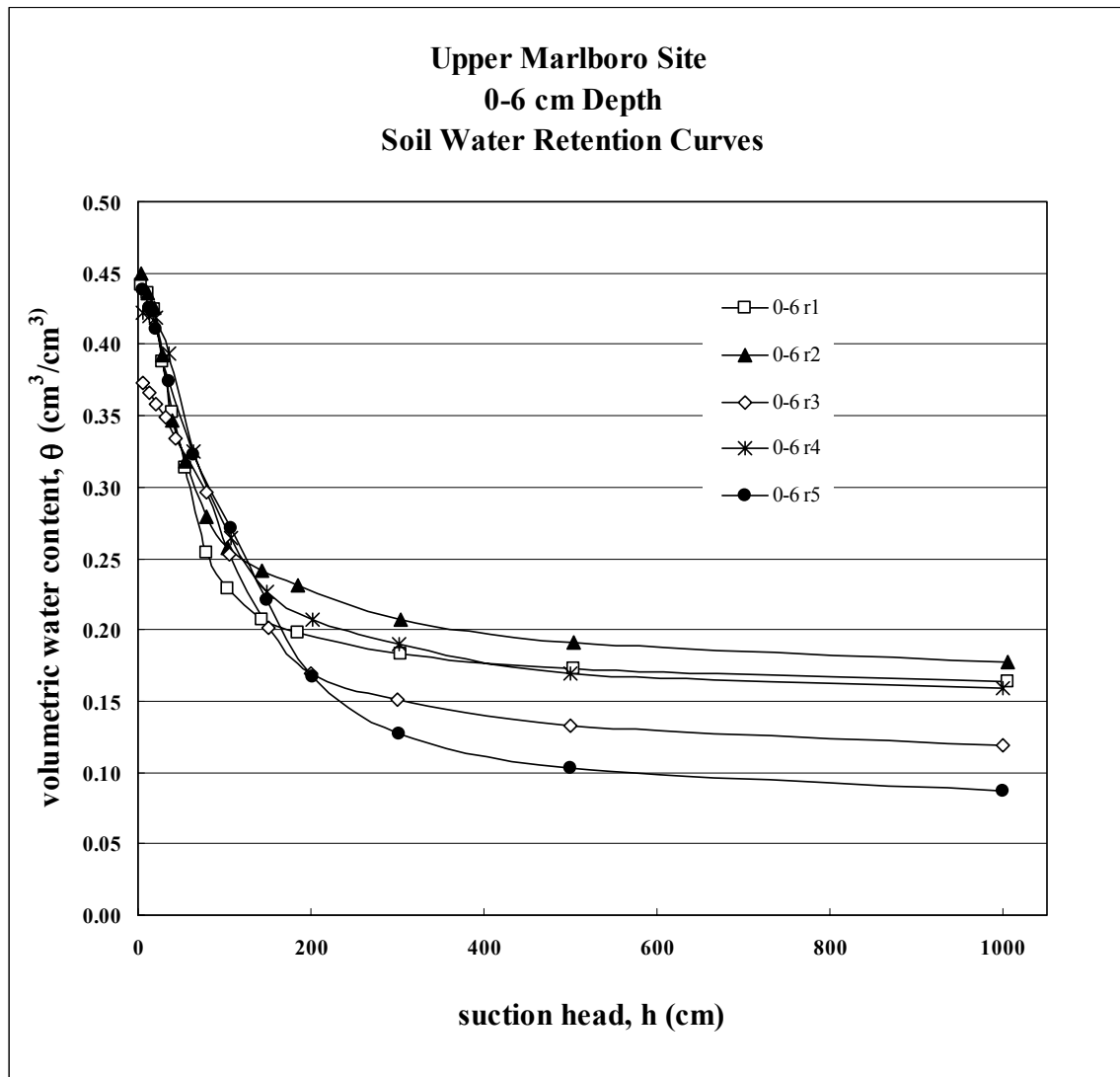


Figure 38. Soil water retention curves for Upper Marlboro site for samples from depth of 0-6 cm

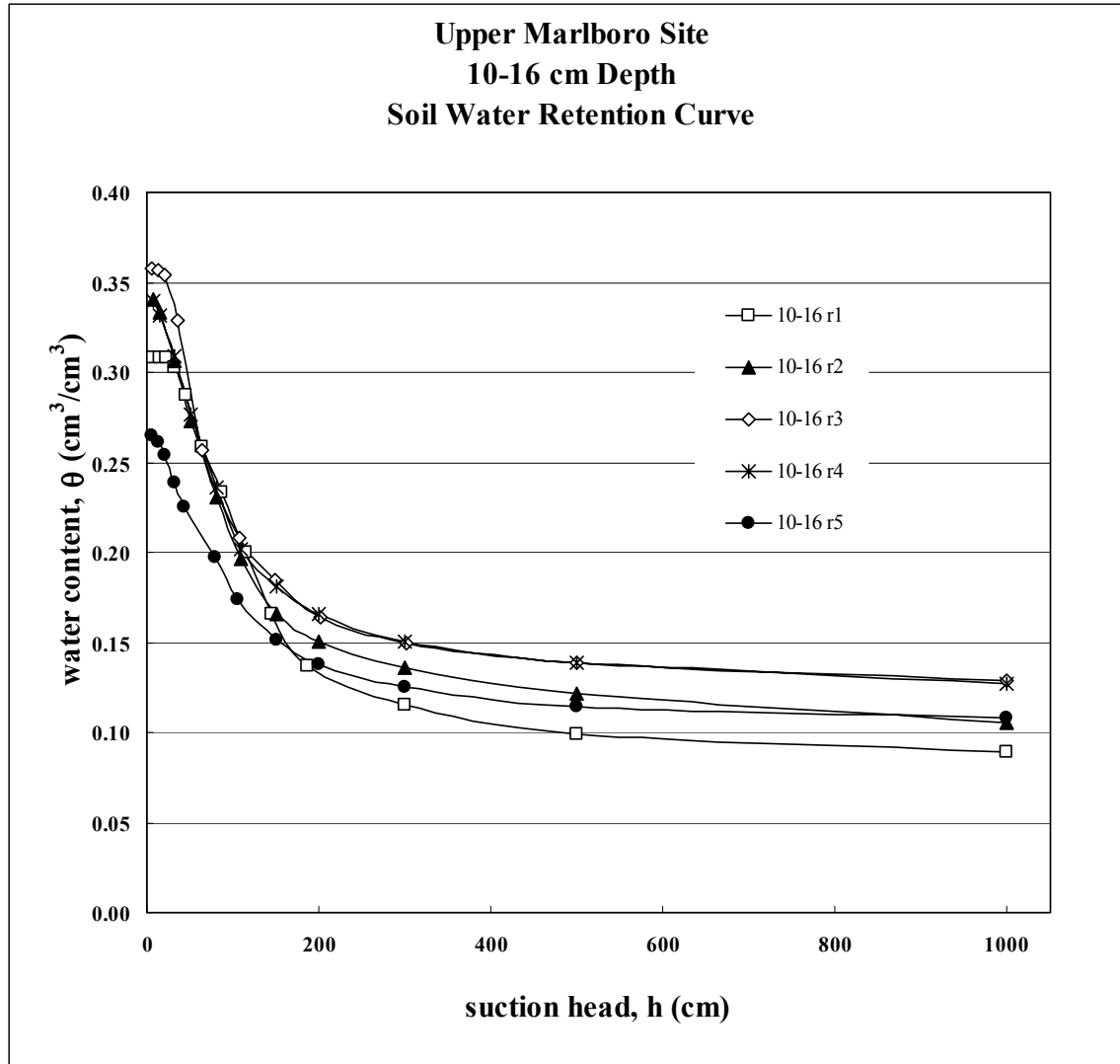


Figure 39. Soil water retention curves for Upper Marlboro site for samples from depth of 10-16 cm

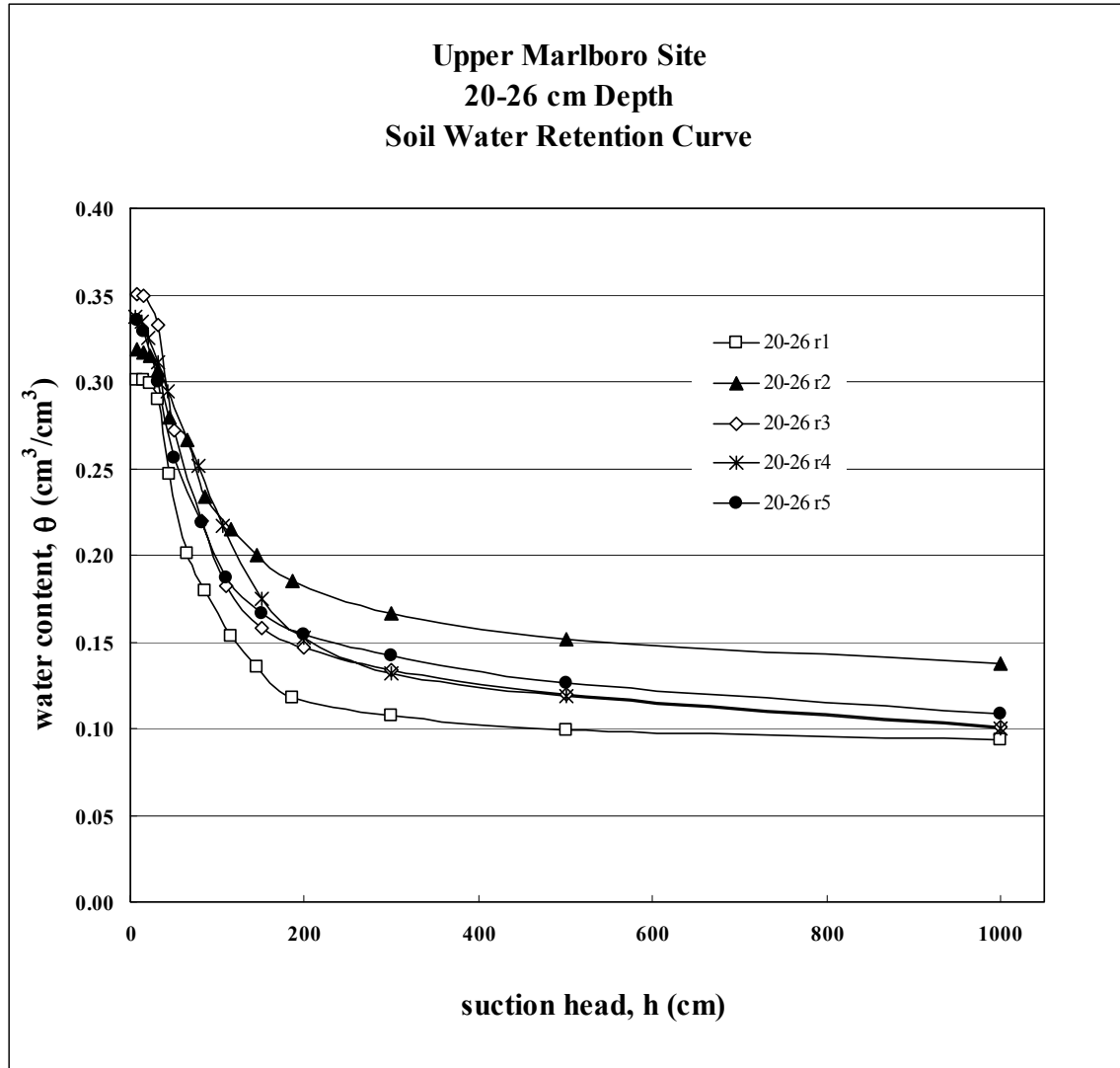


Figure 40. Soil water retention curves for Upper Marlboro site for samples from depth of 20-26 cm

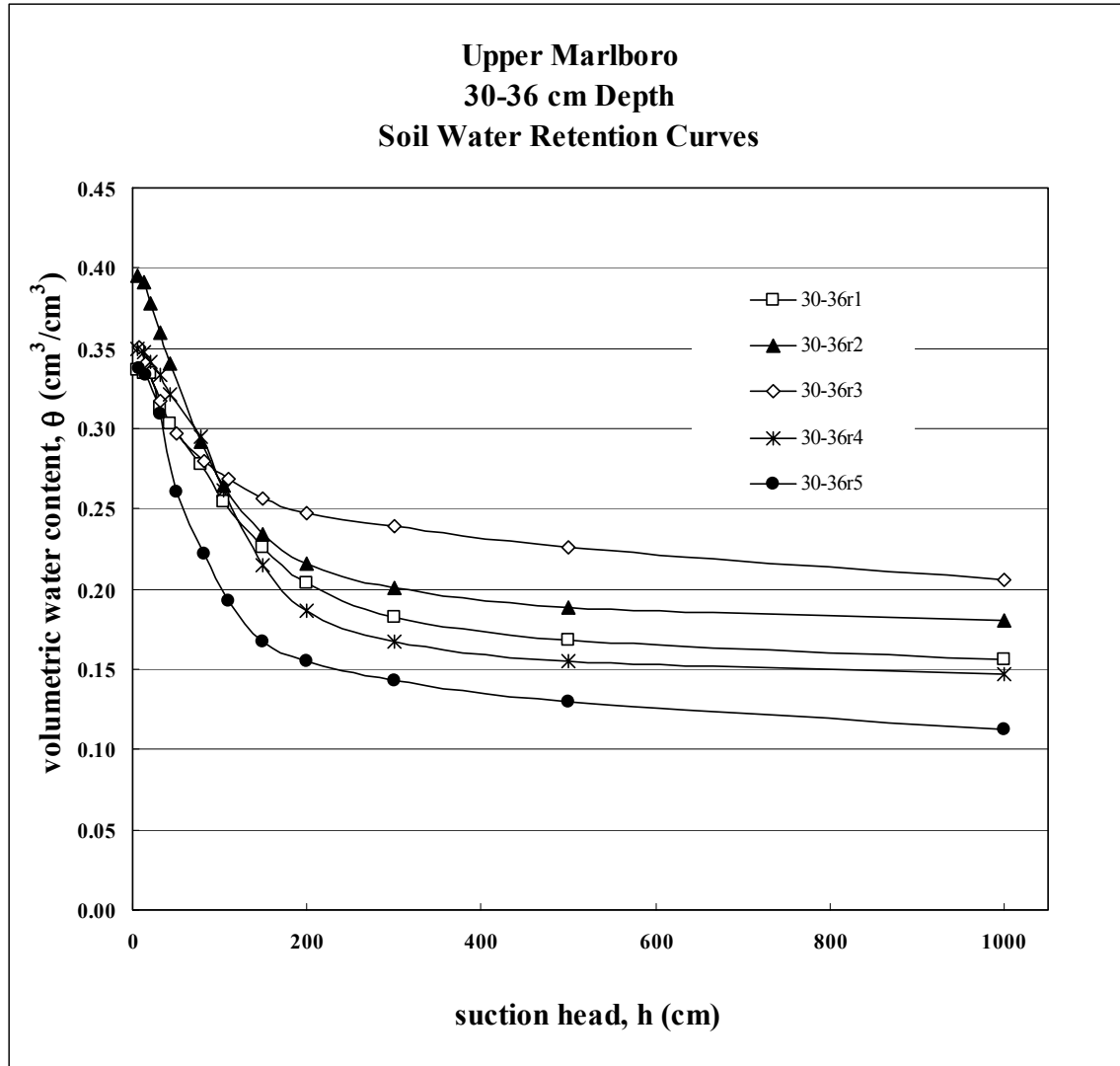


Figure 41. Soil water retention curves for Upper Marlboro site for samples from depth of 30-36 cm

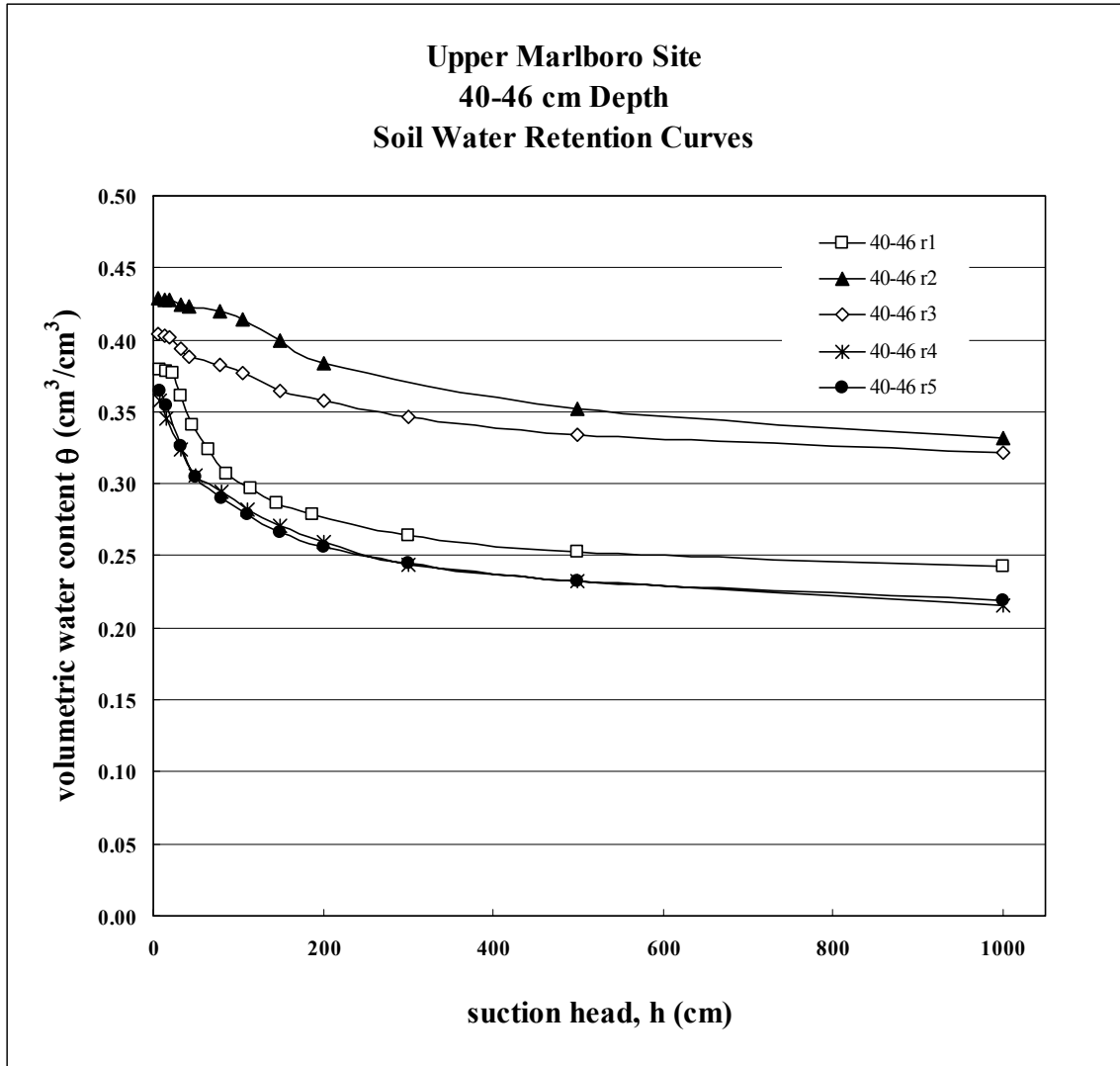


Figure 42. Soil water retention curves for Upper Marlboro site for samples from depth of 40-46 cm

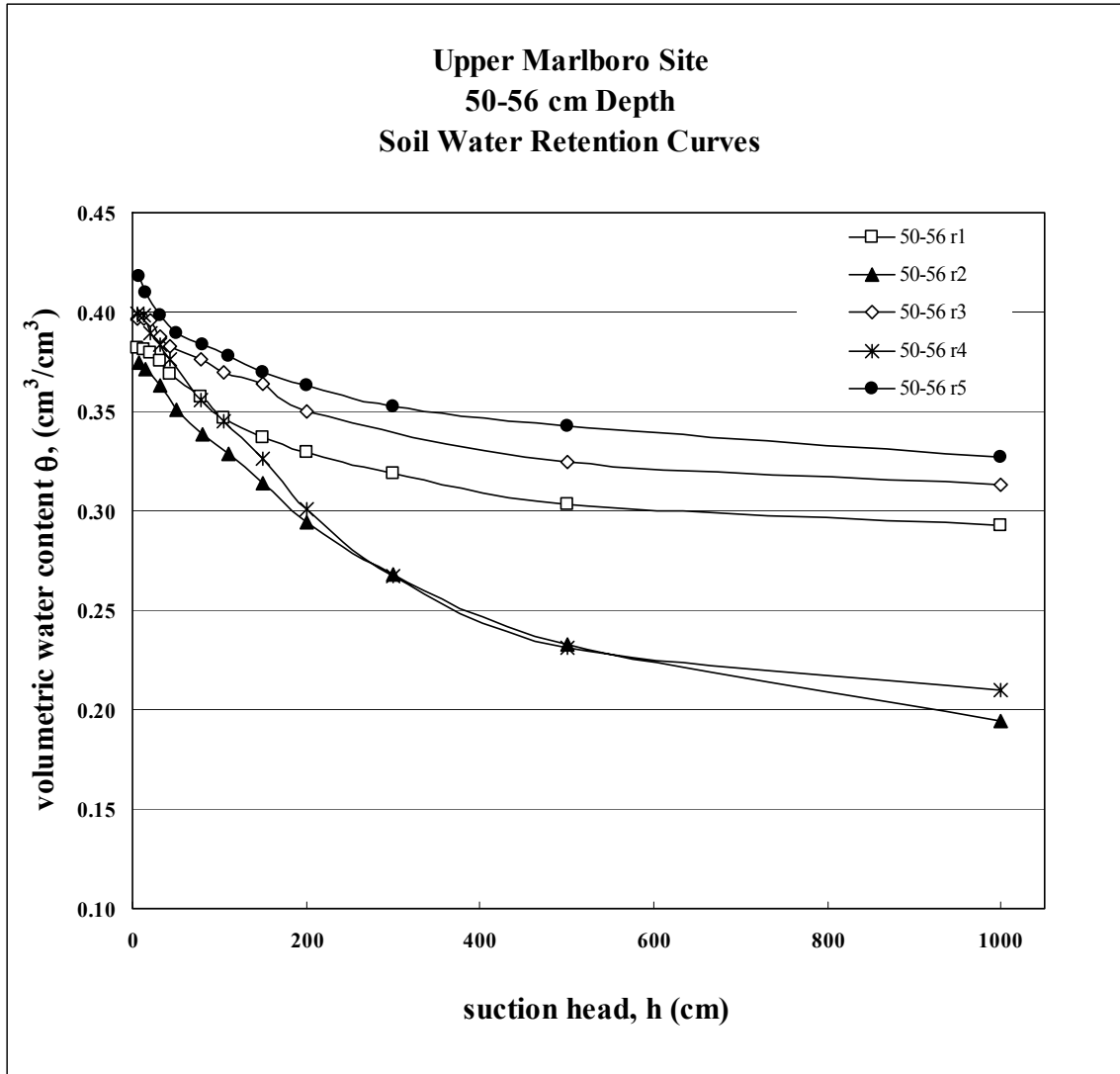


Figure 43. Soil water retention curves for Upper Marlboro site for samples from depth of 50-56 cm

Appendix C-2 – SWRCs for Poplar Hill Site for Each of Six Depths

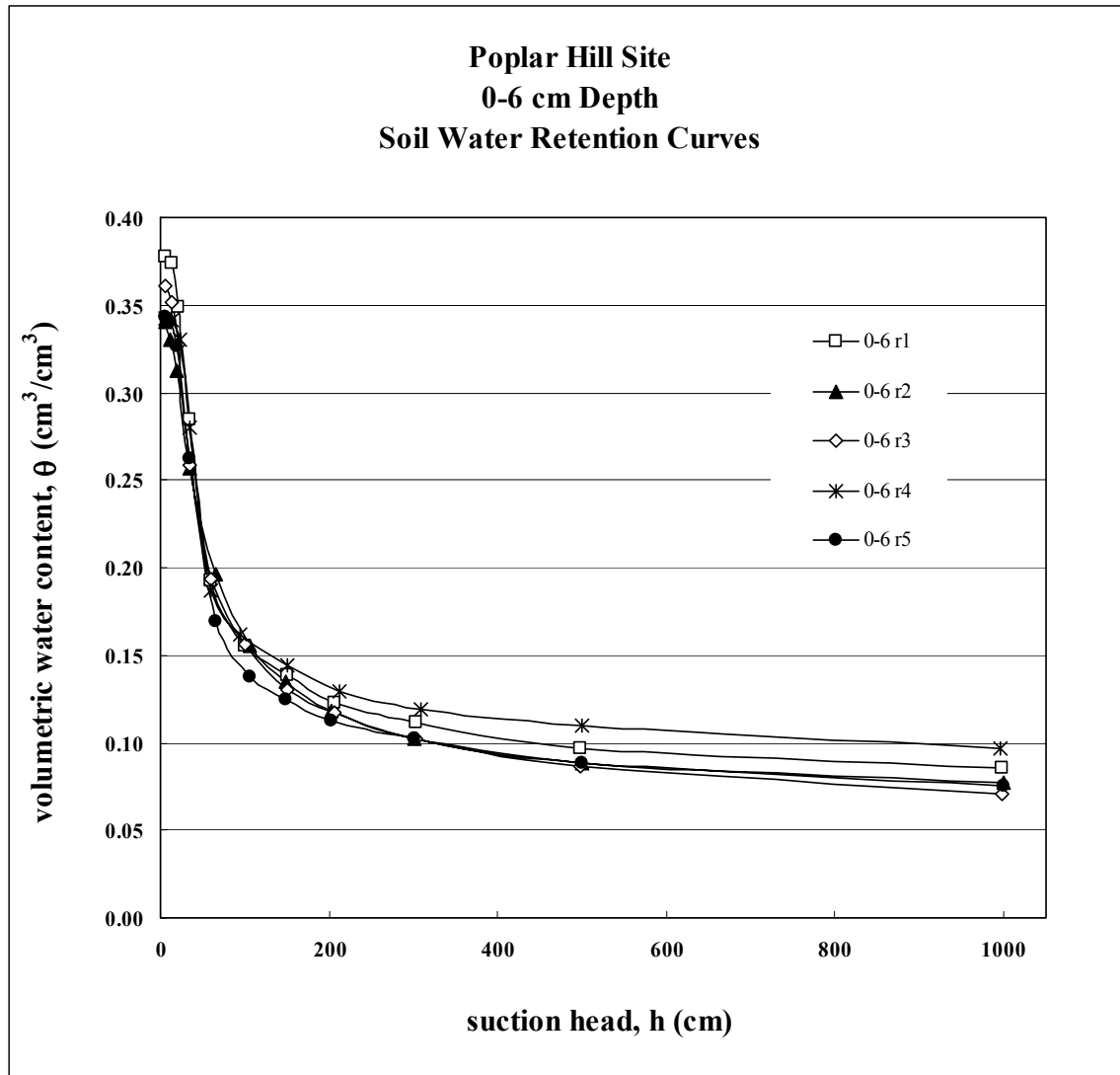


Figure 44. Soil water retention curves for Poplar Hill site for samples from depth of 0-6 cm

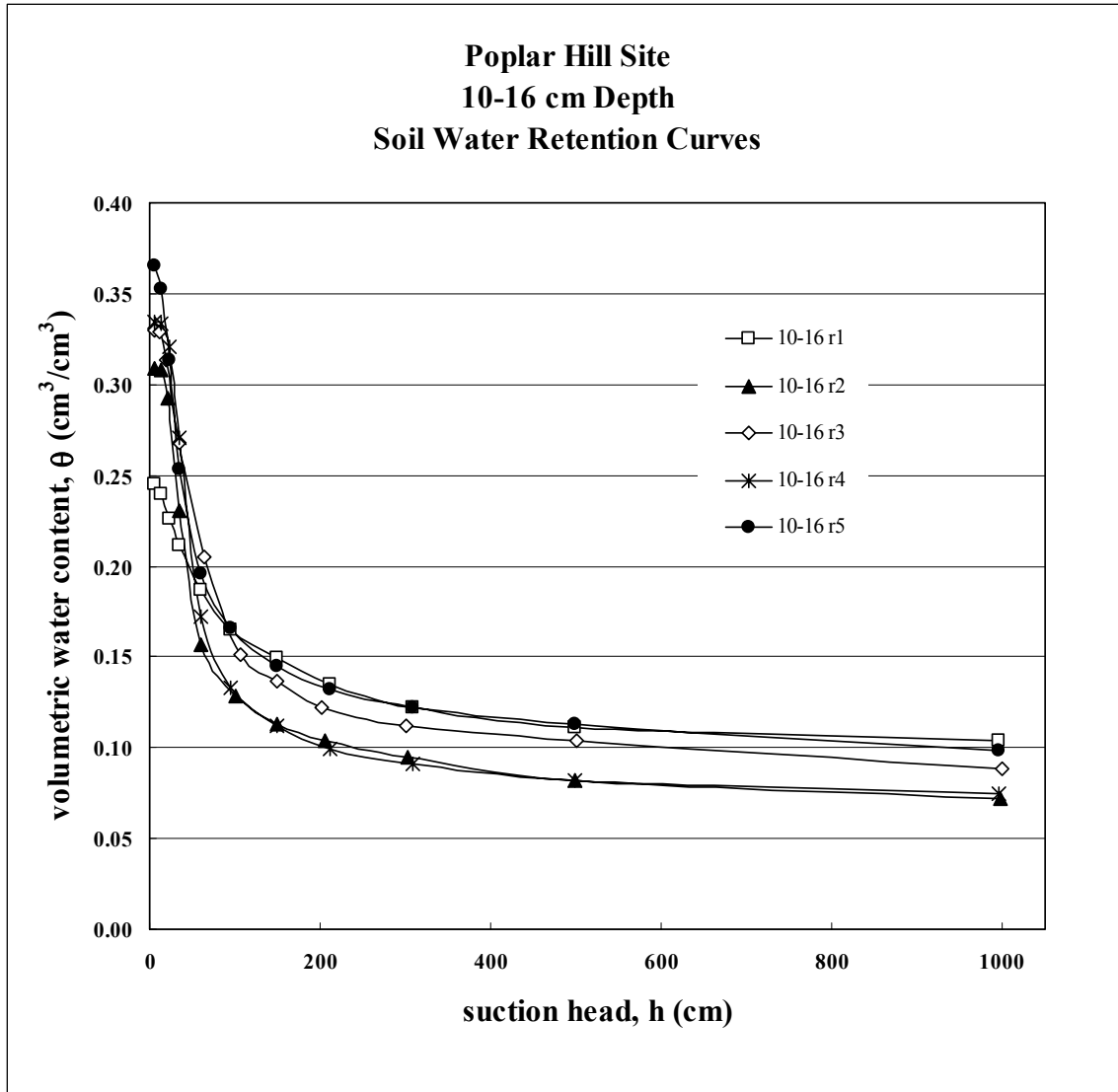


Figure 45. Soil water retention curves for Poplar Hill site for samples from depth of 10-16 cm

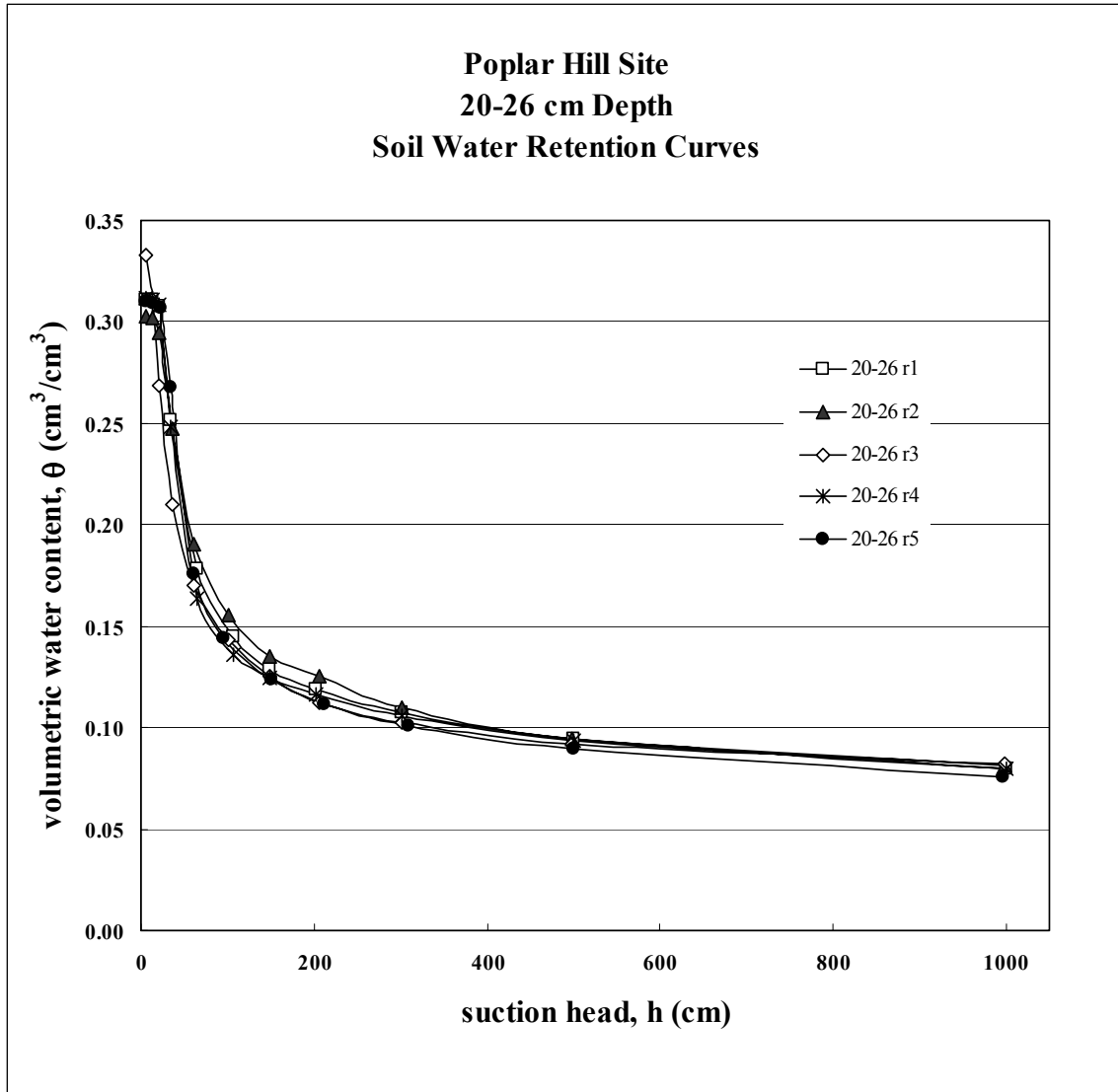


Figure 46. Soil water retention curves for Poplar Hill site for samples from depth of 20-26 cm

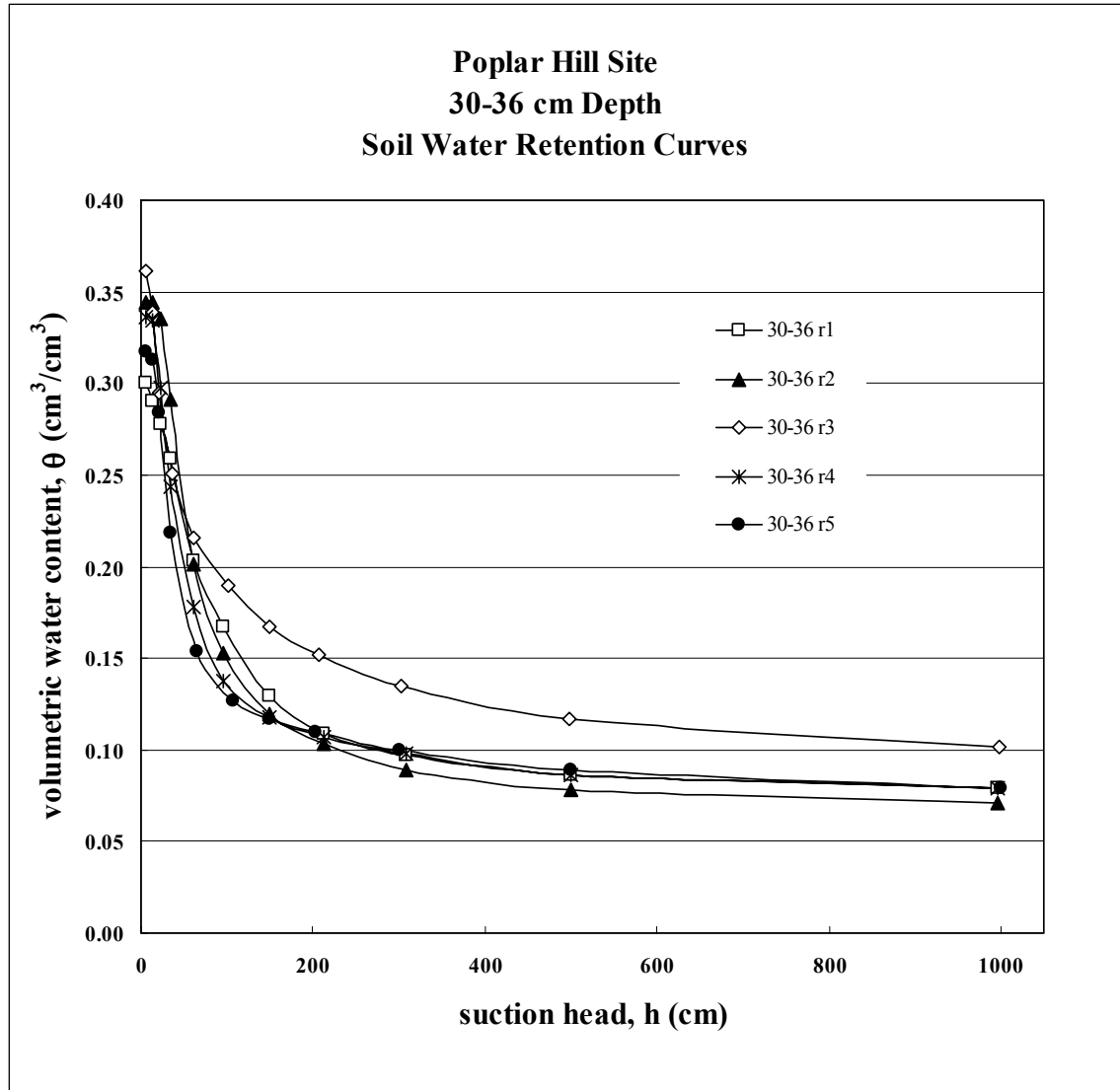


Figure 47. Soil water retention curves for Poplar Hill site for samples from depth of 30-36 cm

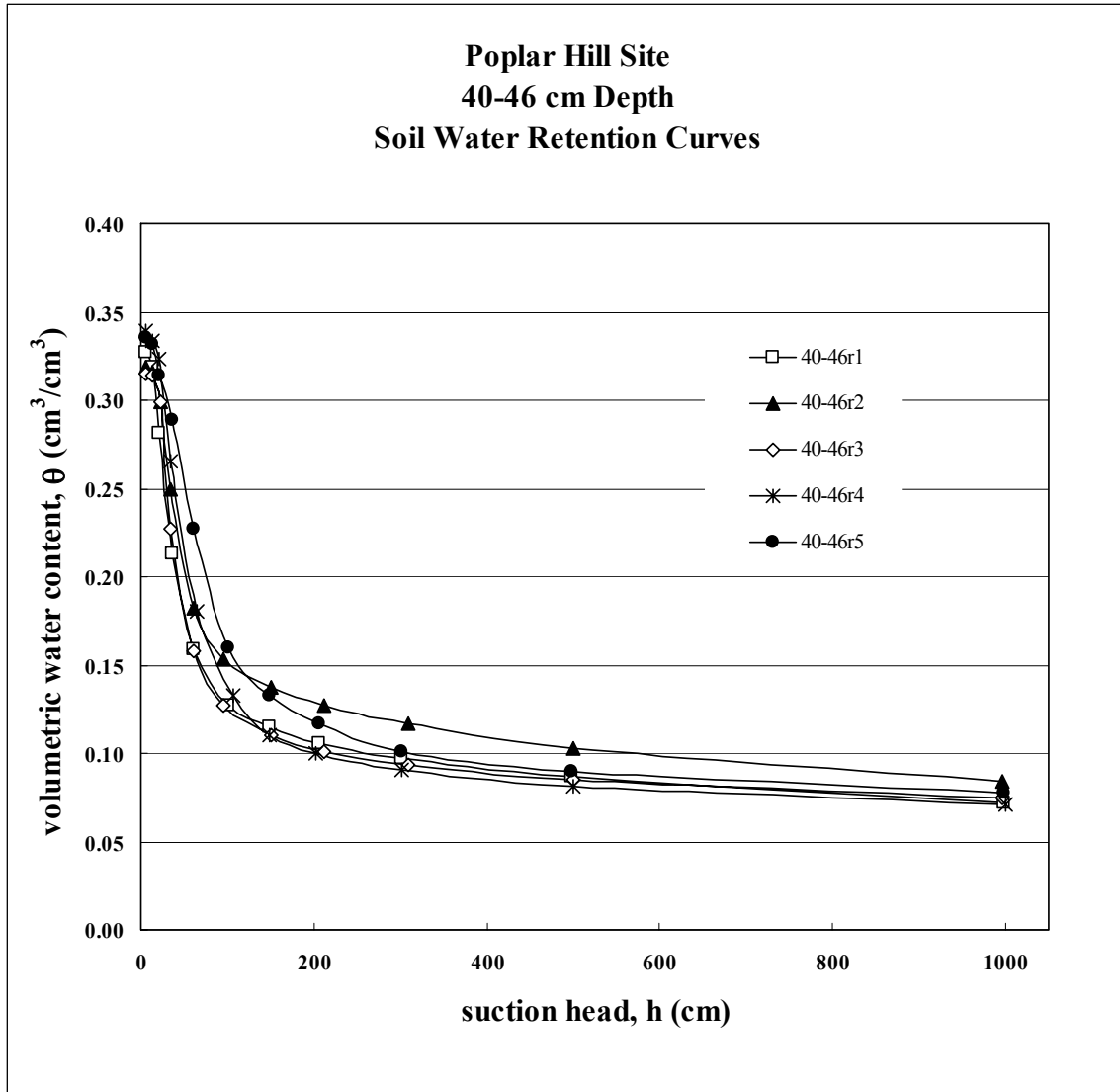


Figure 48. Soil water retention curves for Poplar Hill site for samples from depth of 40-46 cm

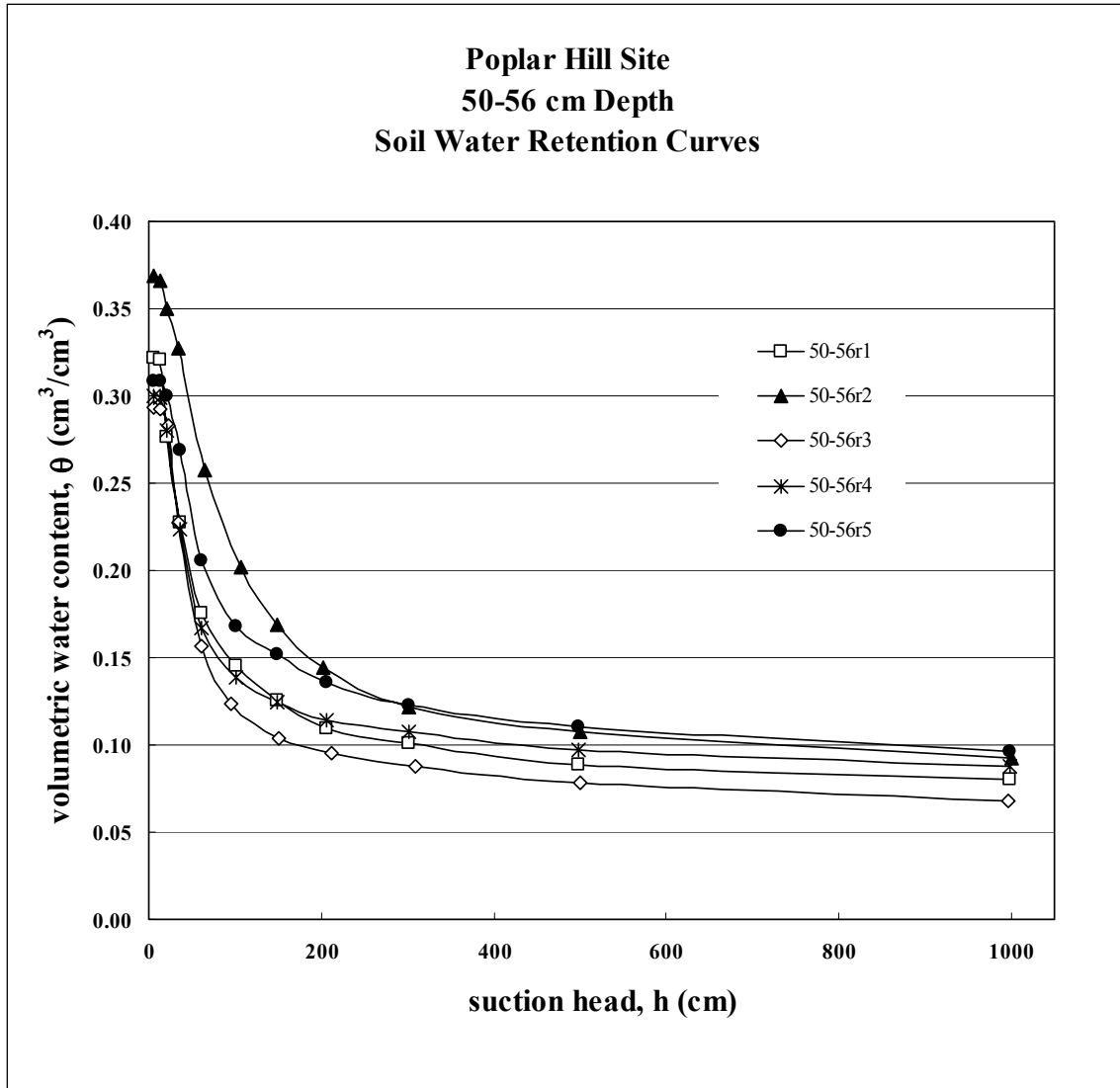


Figure 49. Soil water retention curves for Poplar Hill site for samples from depth of 50-56 cm

Appendix D - Capillary Pressure Head as a Function of Saturation

Appendix D1- Capillary Pressure Head vs. Saturation - Upper Marlboro Site

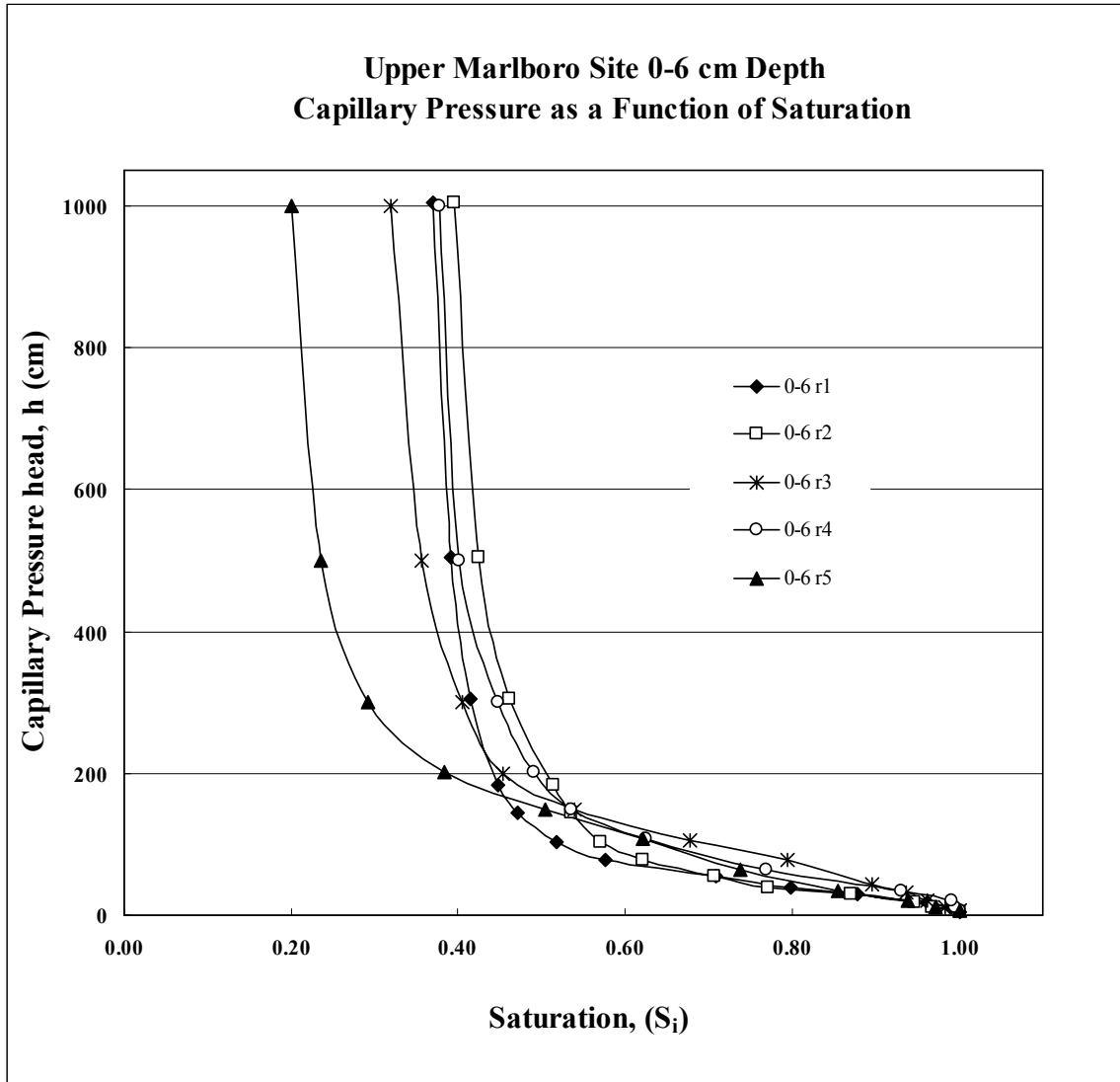


Figure 50. Capillary pressure head as a function of saturation for Upper Marlboro site for soil samples from depth of 0-6 cm

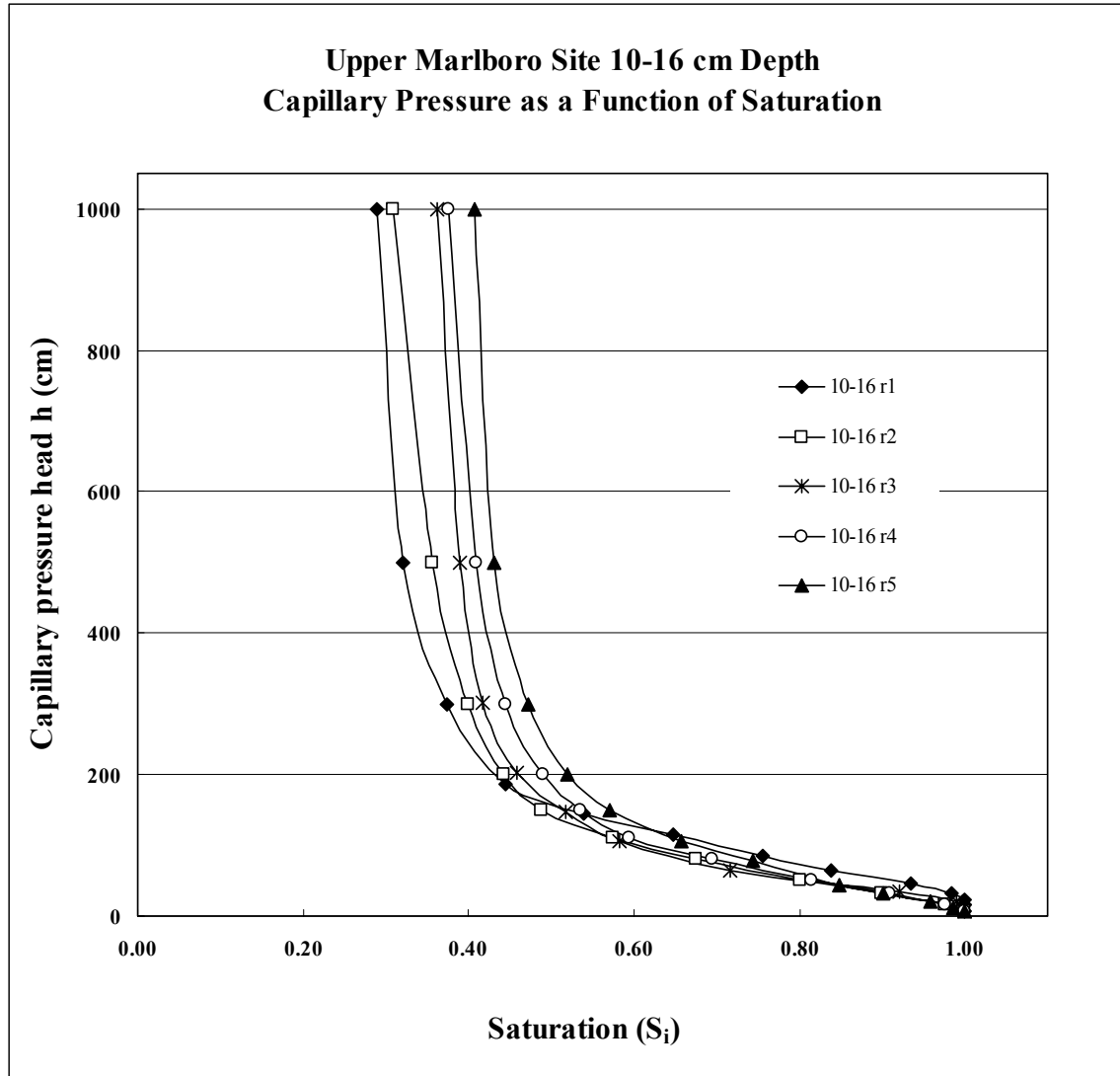


Figure 51. Capillary pressure head as a function of saturation for Upper Marlboro site for soil samples from depth of 10-16 cm

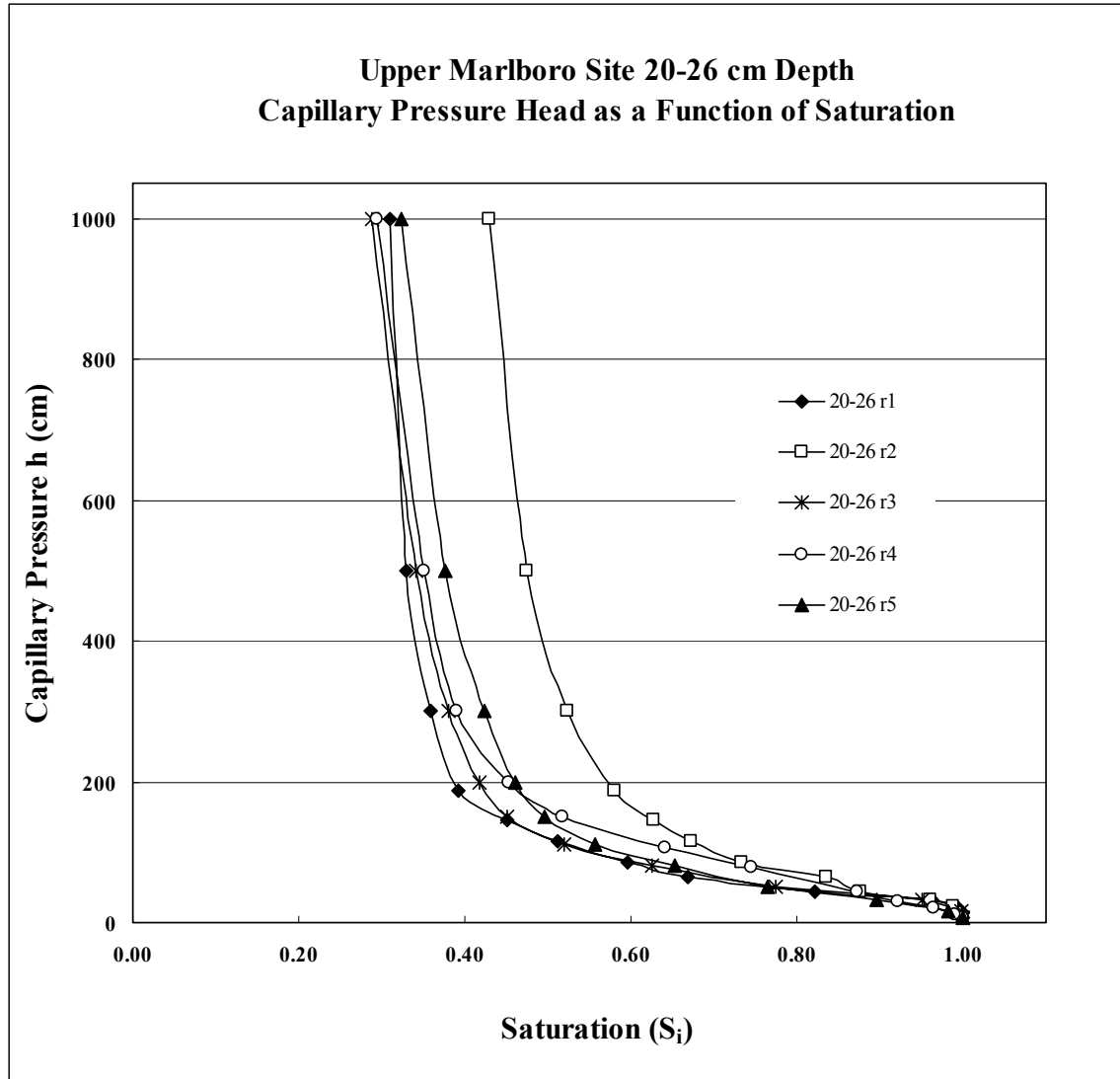


Figure 52. Capillary pressure head as a function of saturation for Upper Marlboro site for soil samples from depth of 20-26 cm

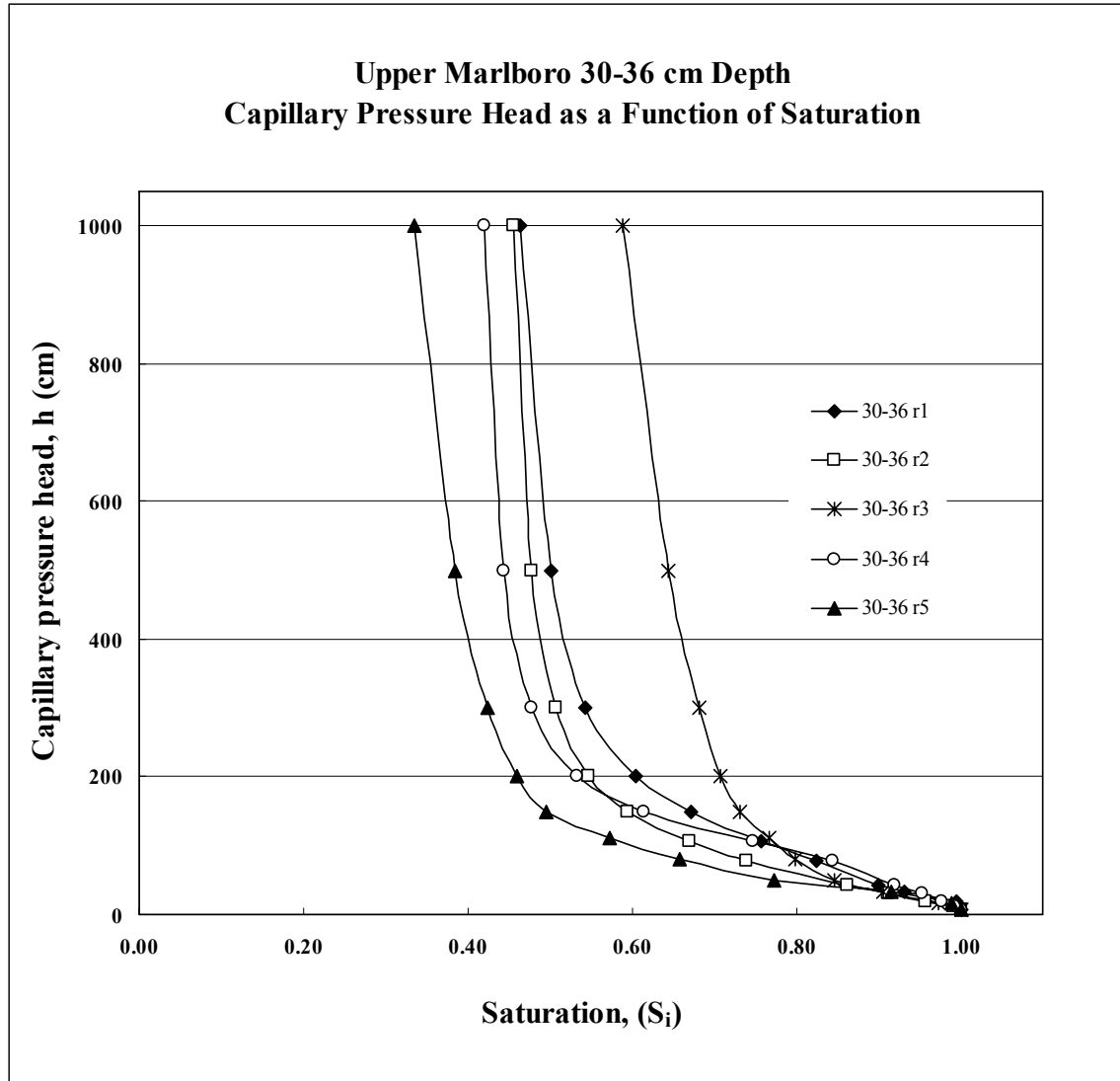


Figure 53. Capillary pressure head as a function of saturation for Upper Marlboro site for soil samples from depth of 30-36 cm

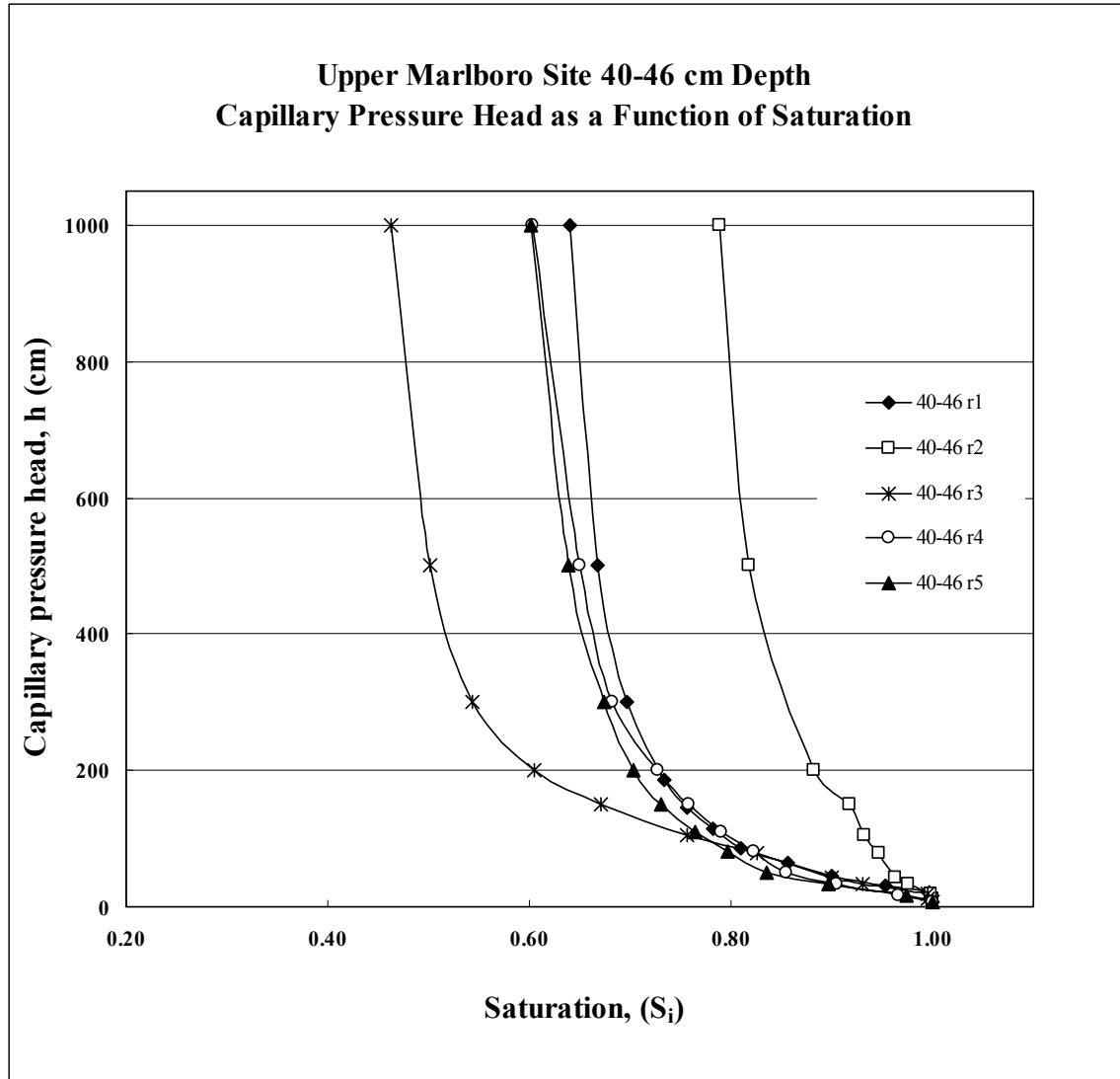


Figure 54. Capillary pressure head as a function of saturation for Upper Marlboro site for soil samples from depth of 40-46 cm

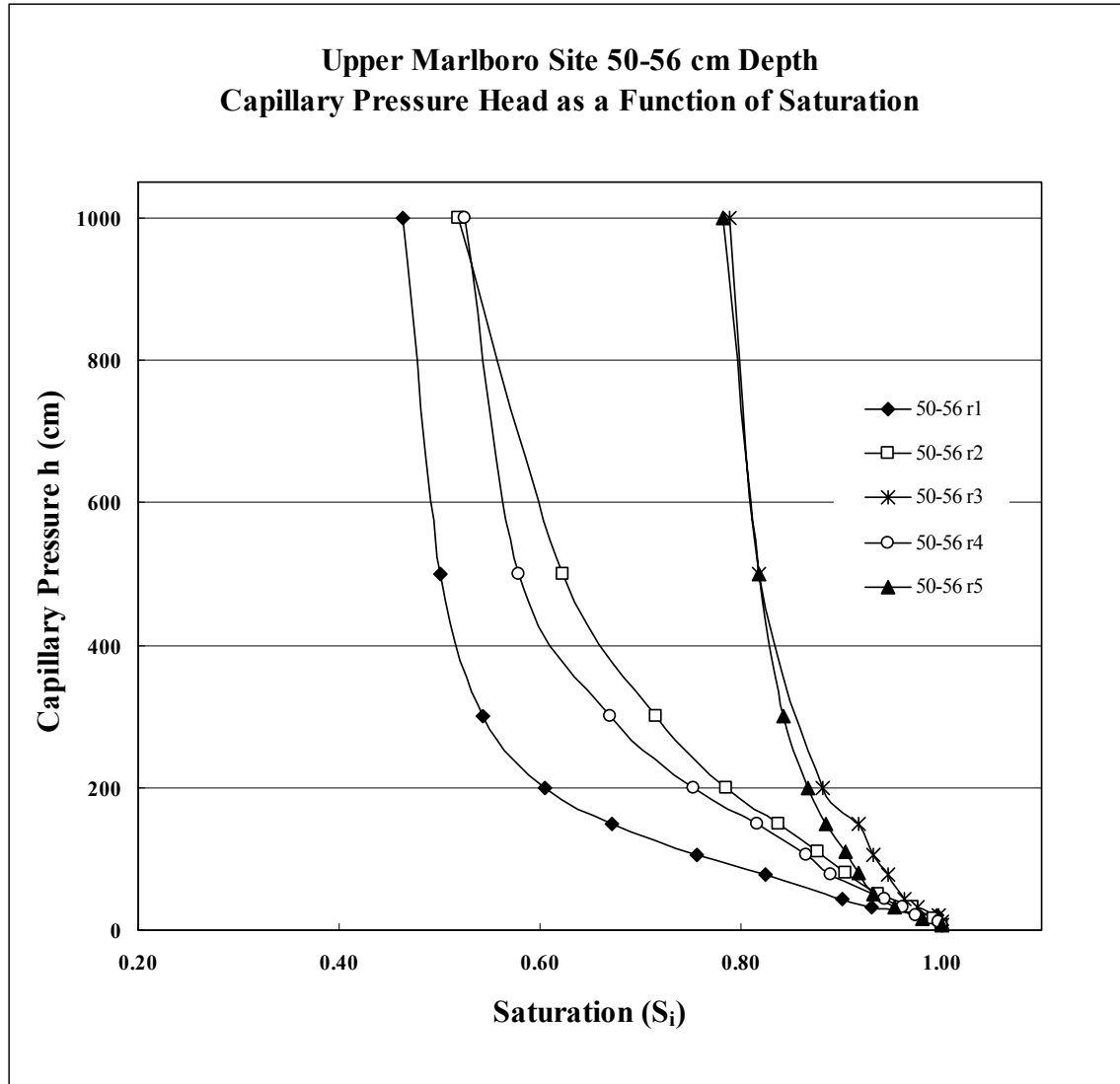


Figure 55. Capillary pressure head as a function of saturation for Upper Marlboro site for soil samples from depth of 50-56 cm

Appendix D2 - Capillary Pressure Head vs Saturation - Poplar Hill Site

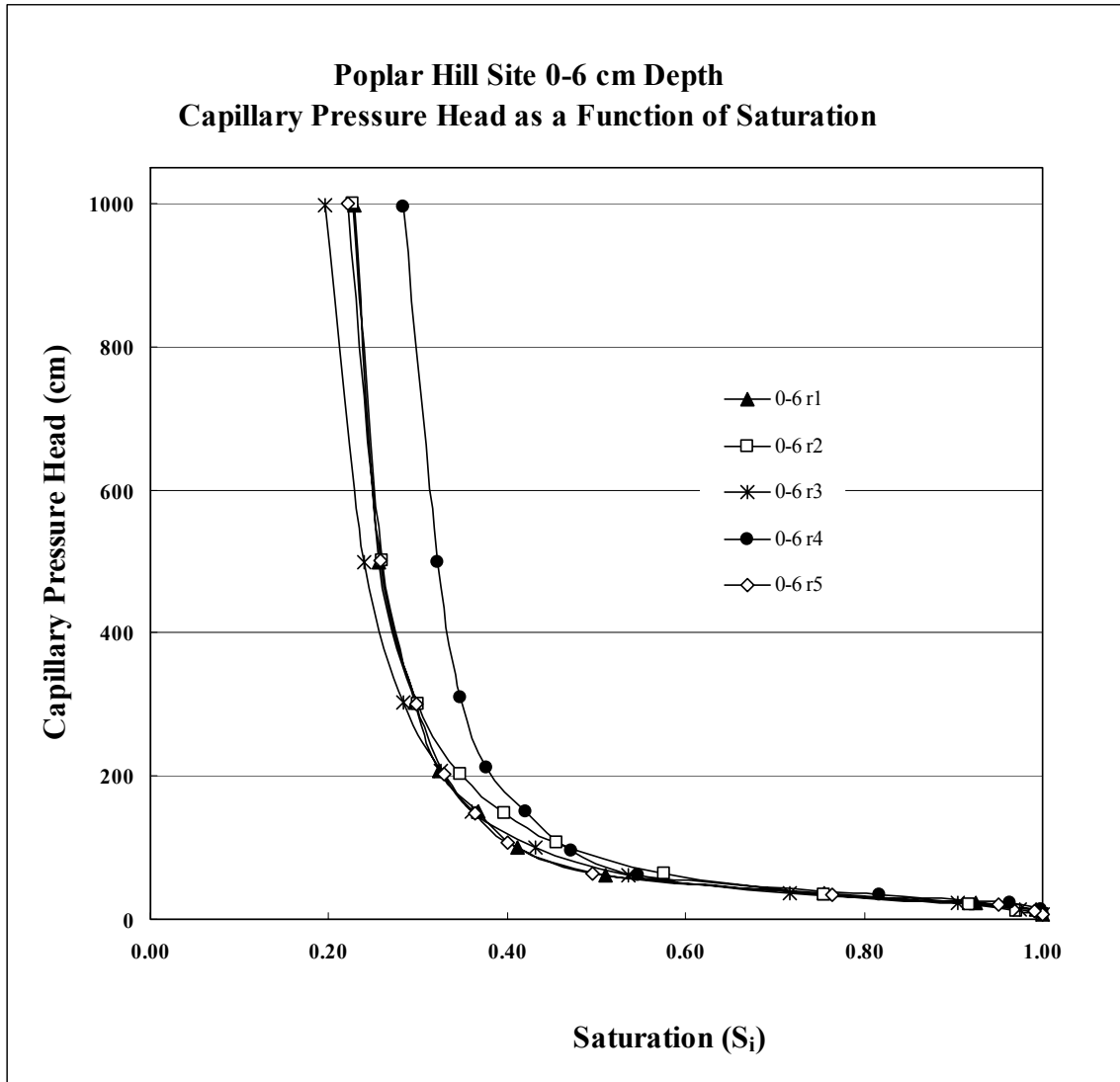


Figure 56. Capillary pressure head as a function of saturation for Poplar Hill site for soil samples from depth of 0-6 cm

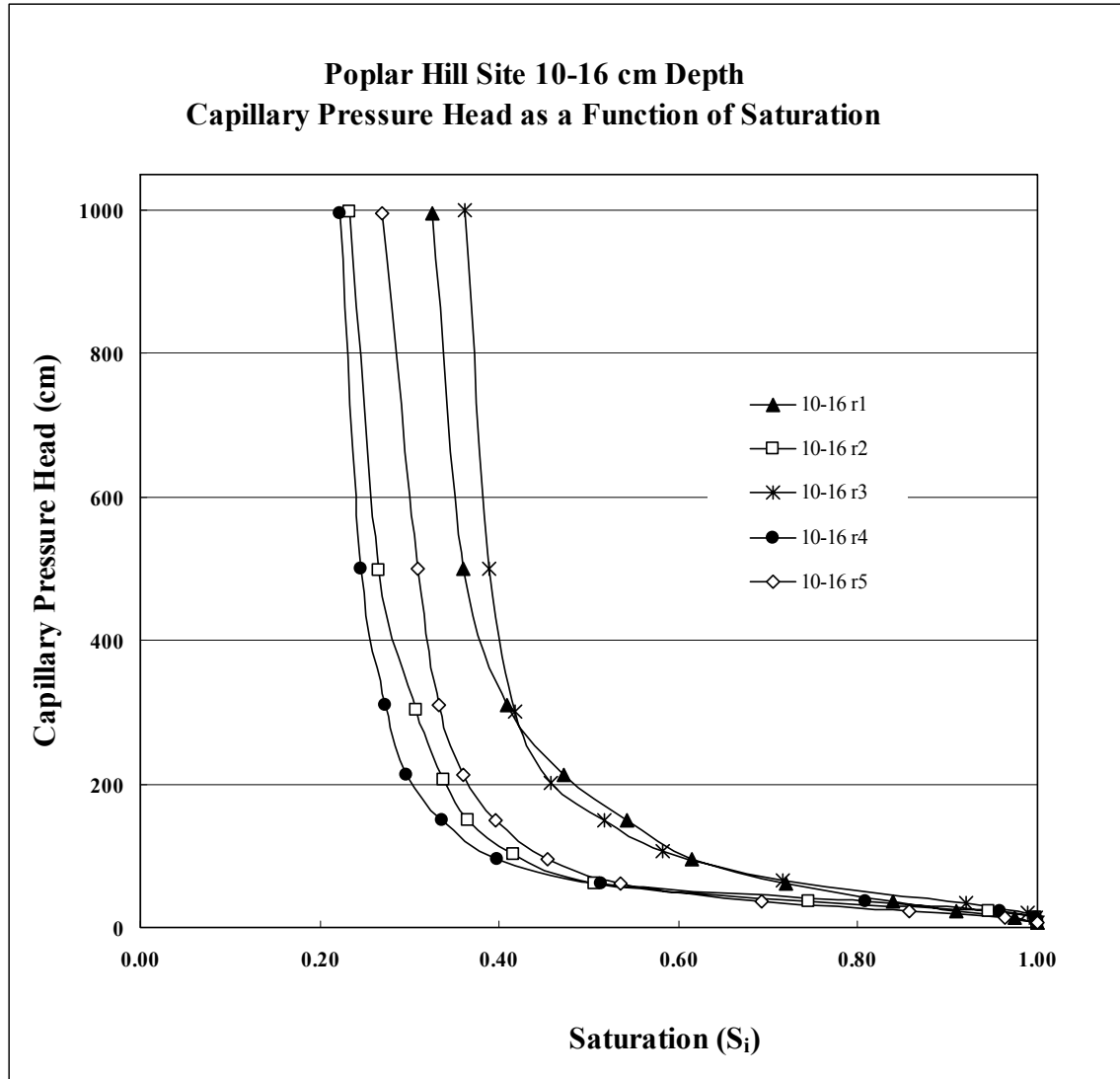


Figure 57. Capillary pressure head as a function of saturation for Poplar Hill site for soil samples from depth of 10-16 cm

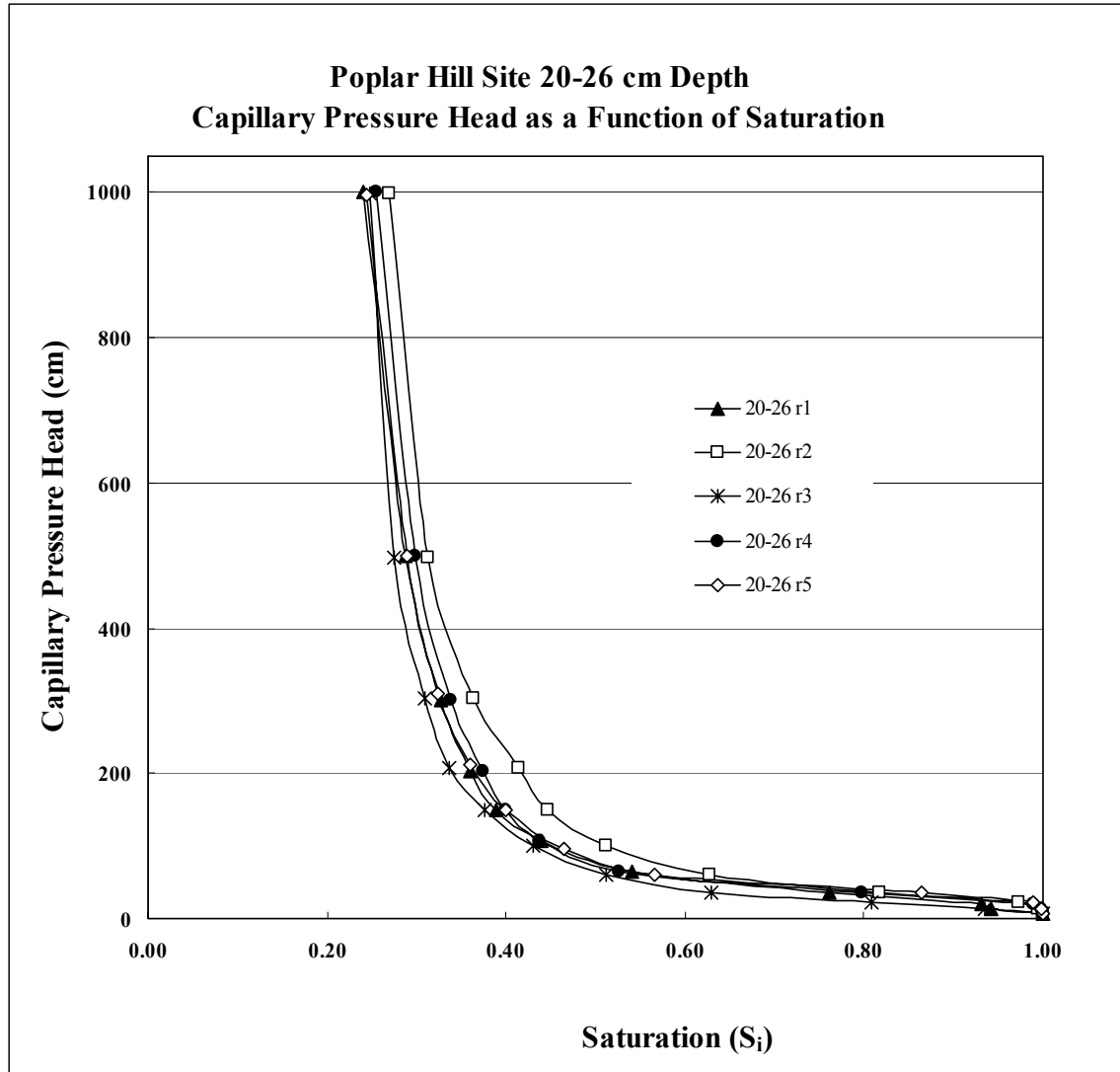


Figure 58. Capillary pressure head as a function of saturation for Poplar Hill site for soil samples from depth of 20-26 cm

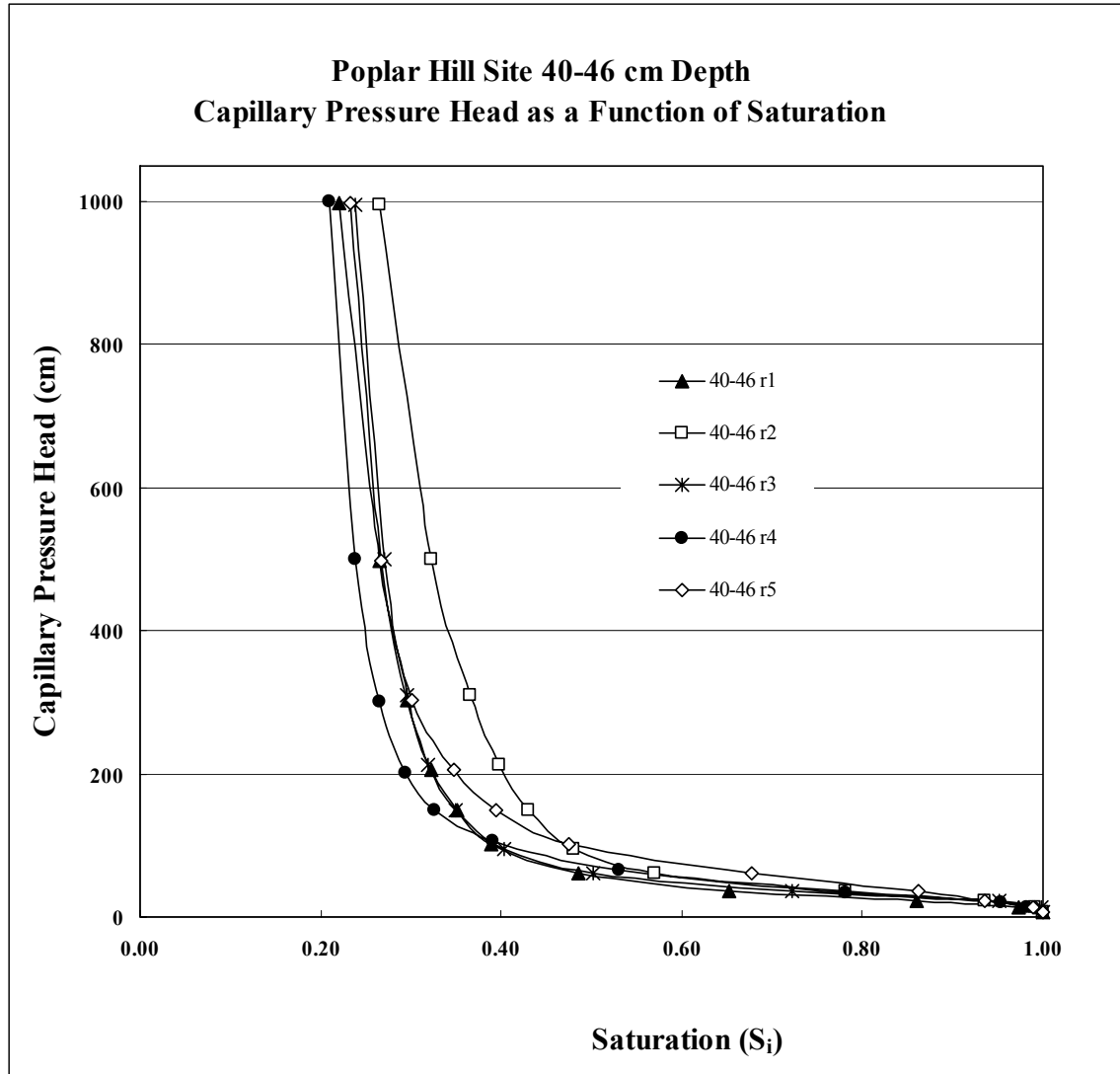


Figure 59. Capillary pressure head as a function of saturation for Poplar Hill site for soil samples from depth of 30-36 cm

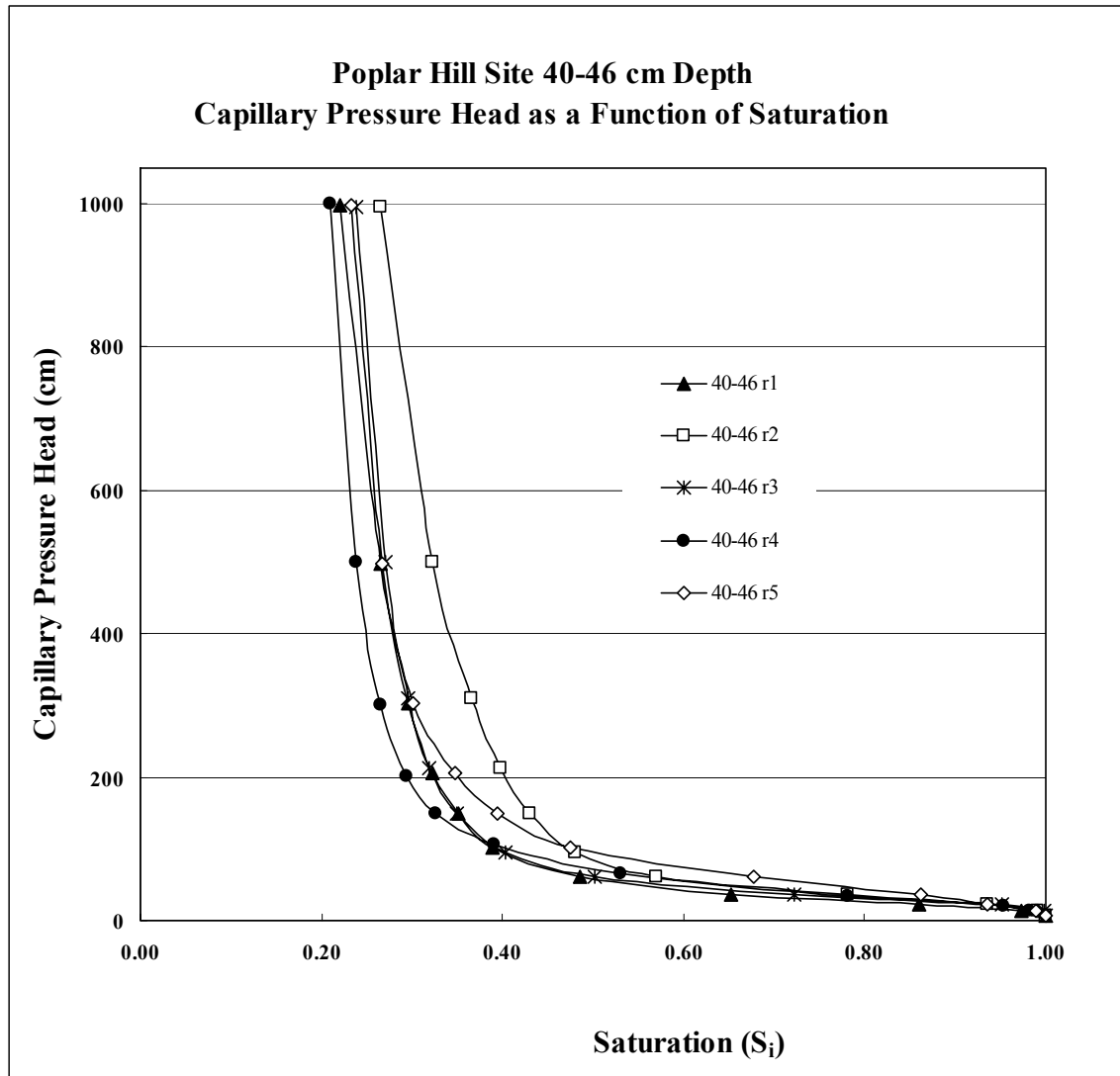


Figure 60. Capillary pressure head as a function of saturation for Poplar Hill site for soil samples from depth of 40-46 cm

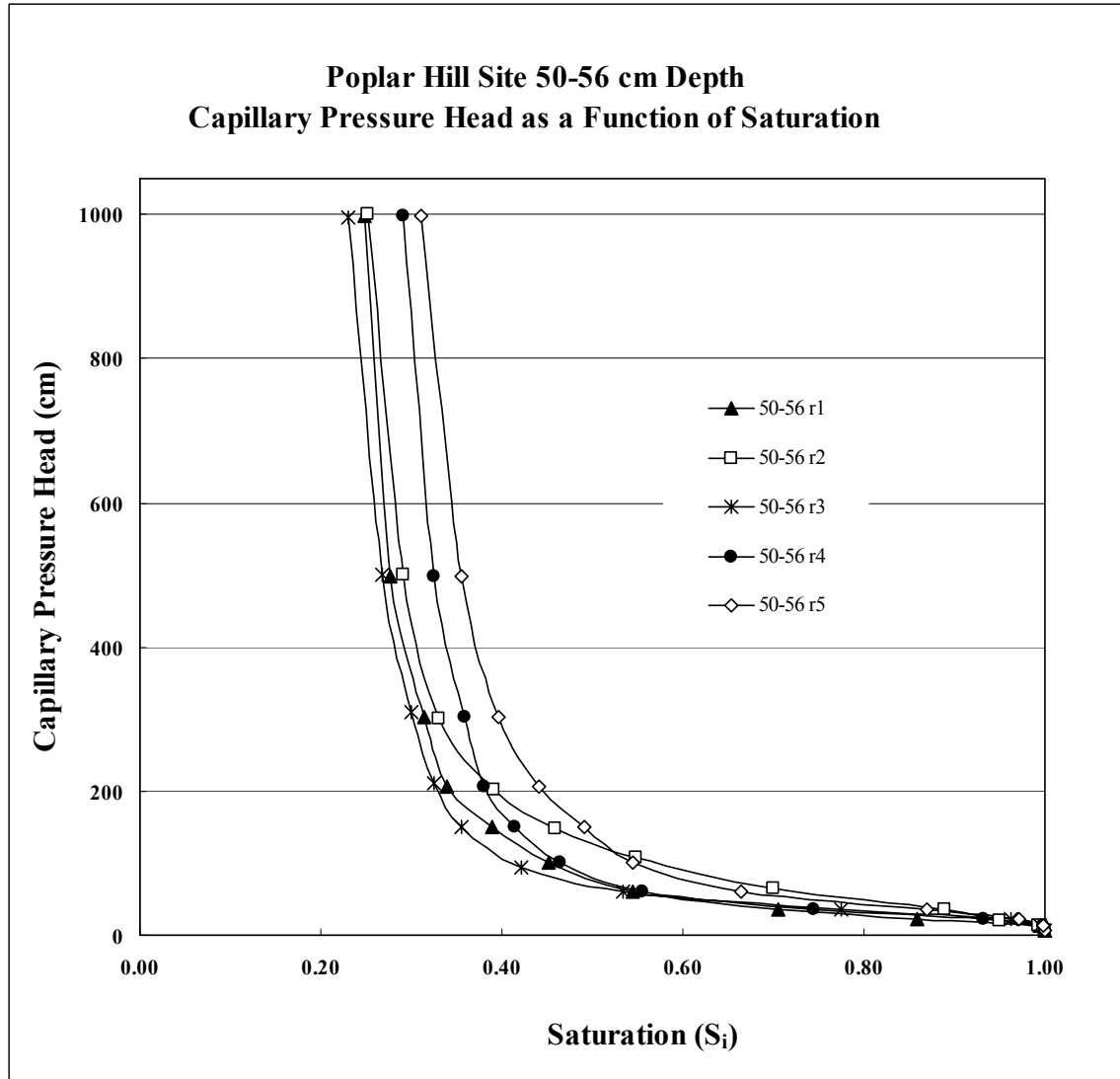


Figure 61. Capillary pressure head as a function of saturation for Poplar Hill site for soil samples from depth of 50-56 cm

Appendix E - Graphs of Log S_e vs. Log h - Bubbling Pressure Determination

Appendix E-1 - Log S_e vs. Log h for Upper Marlboro Site for Six Depths

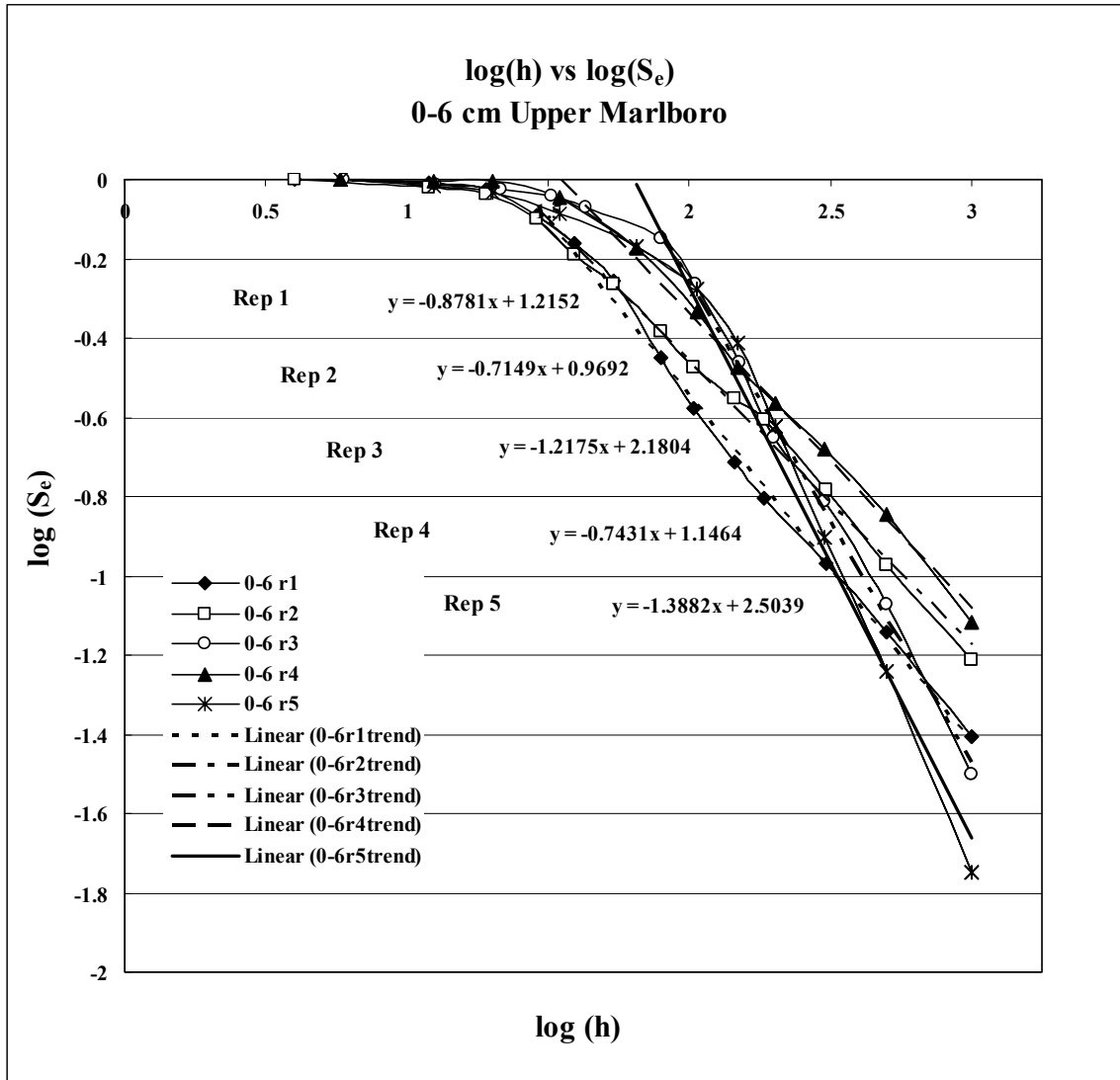


Figure 62. Curves for log S_e vs. log h used to determine bubbling pressure for Upper Marlboro site for soil depth 0-6 cm

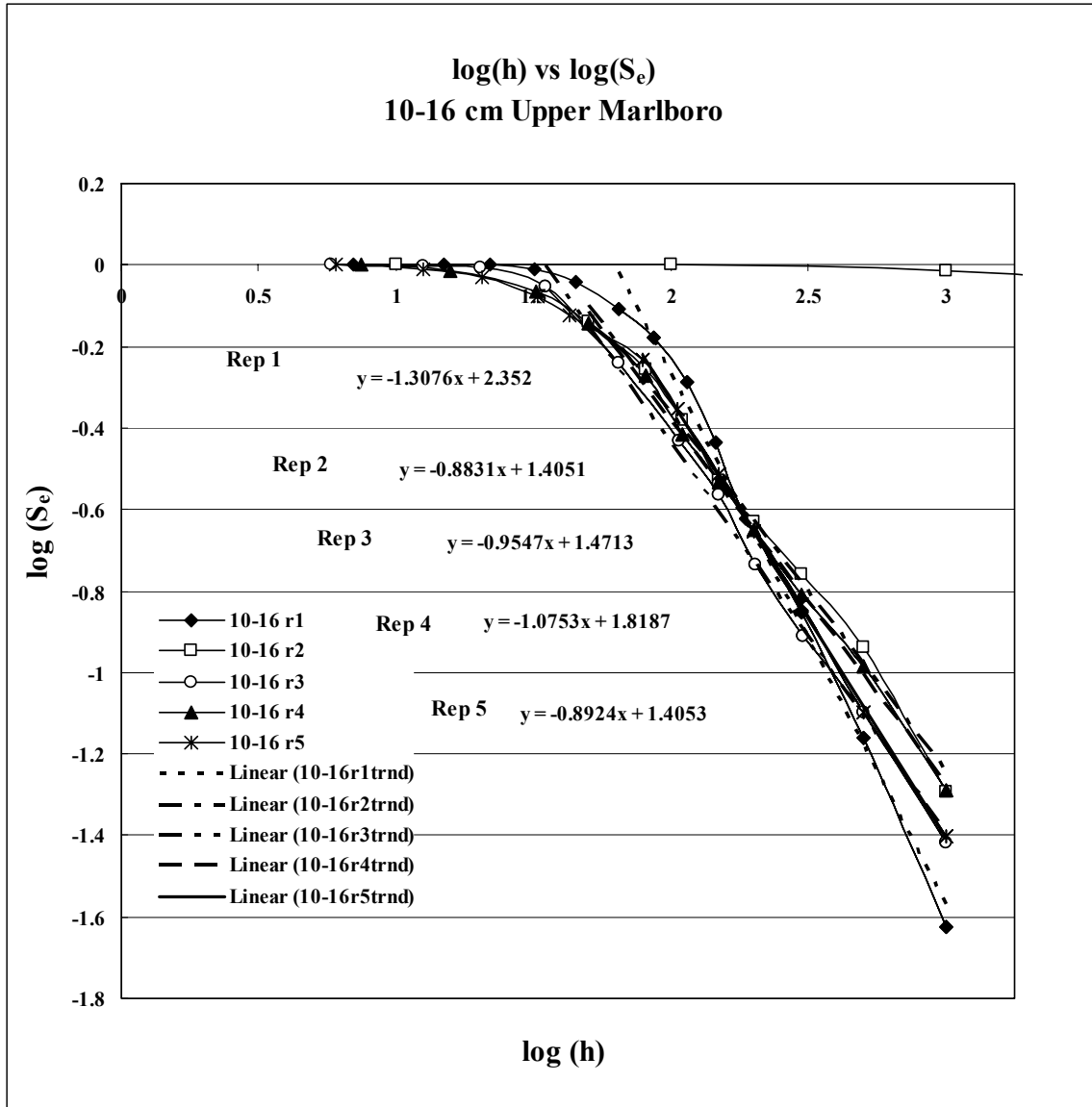


Figure 63. Curves for log S_e vs. log h used to determine bubbling pressure for Upper Marlboro site for soil depth 10-16 cm

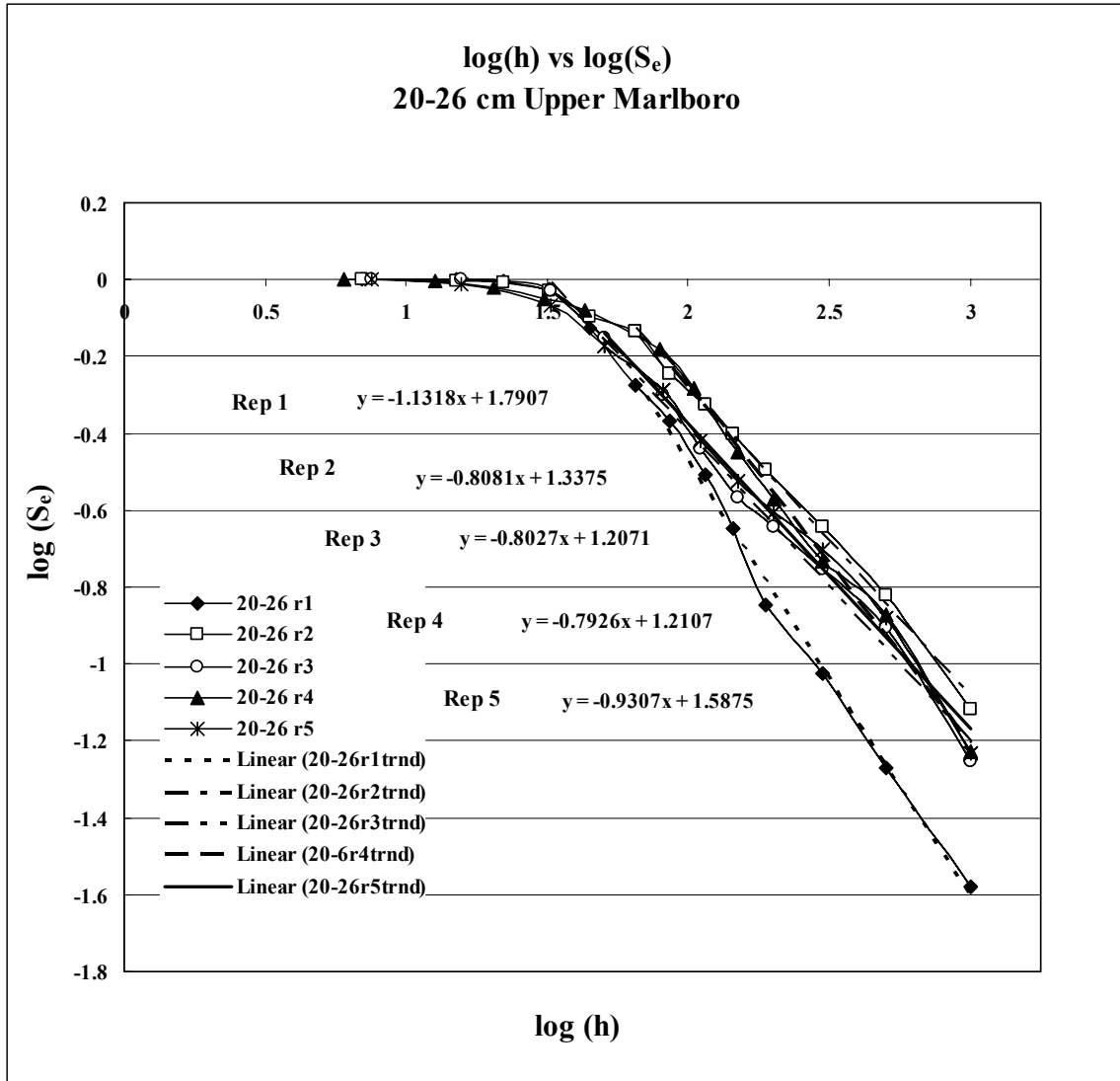


Figure 64. Curves for log S_e vs. log h used to determine bubbling pressure for Upper Marlboro site for soil depth 20-26 cm

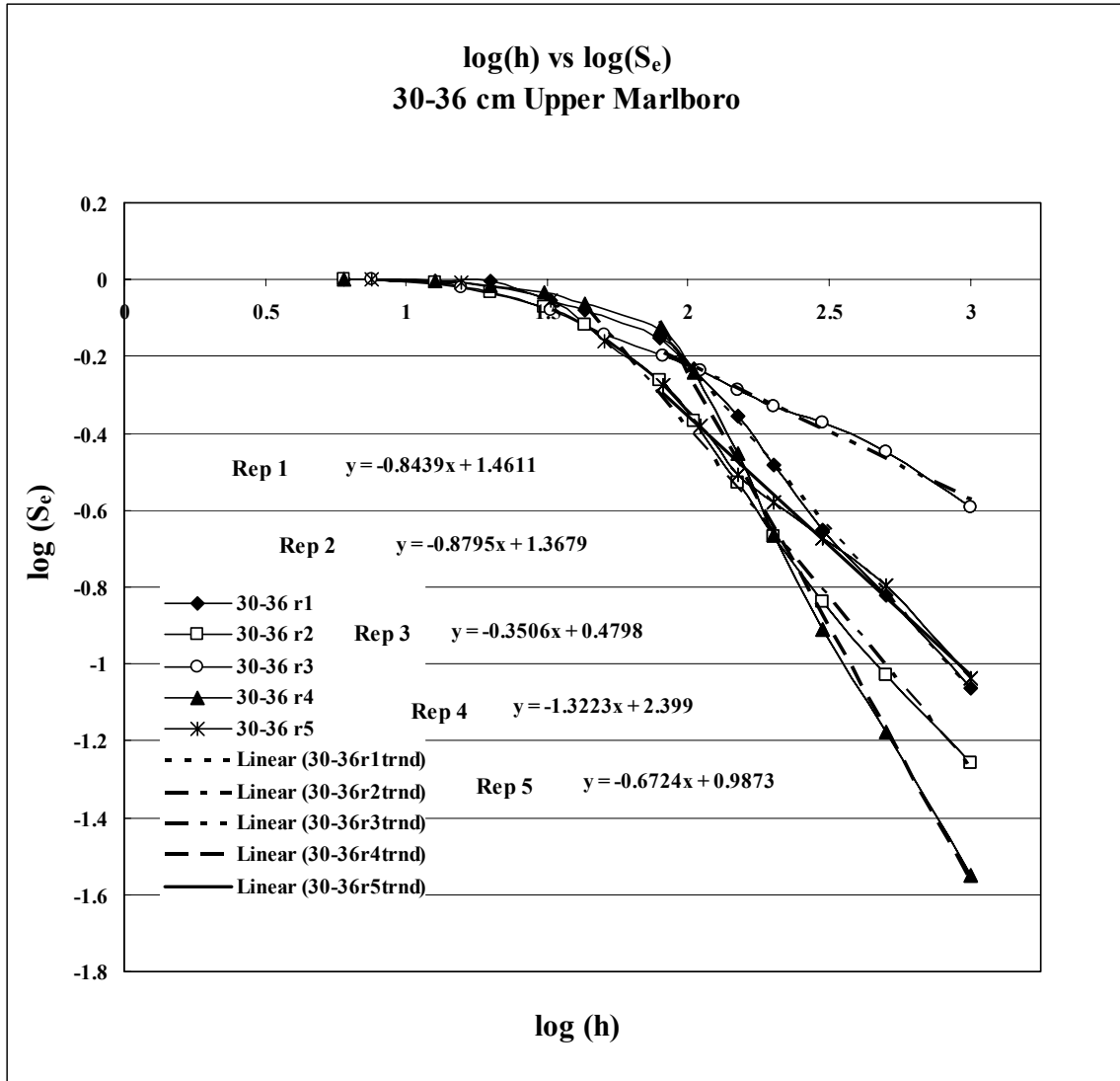


Figure 65. Curves for log S_e vs. log h used to determine bubbling pressure for Upper Marlboro site for soil depth 30-36 cm

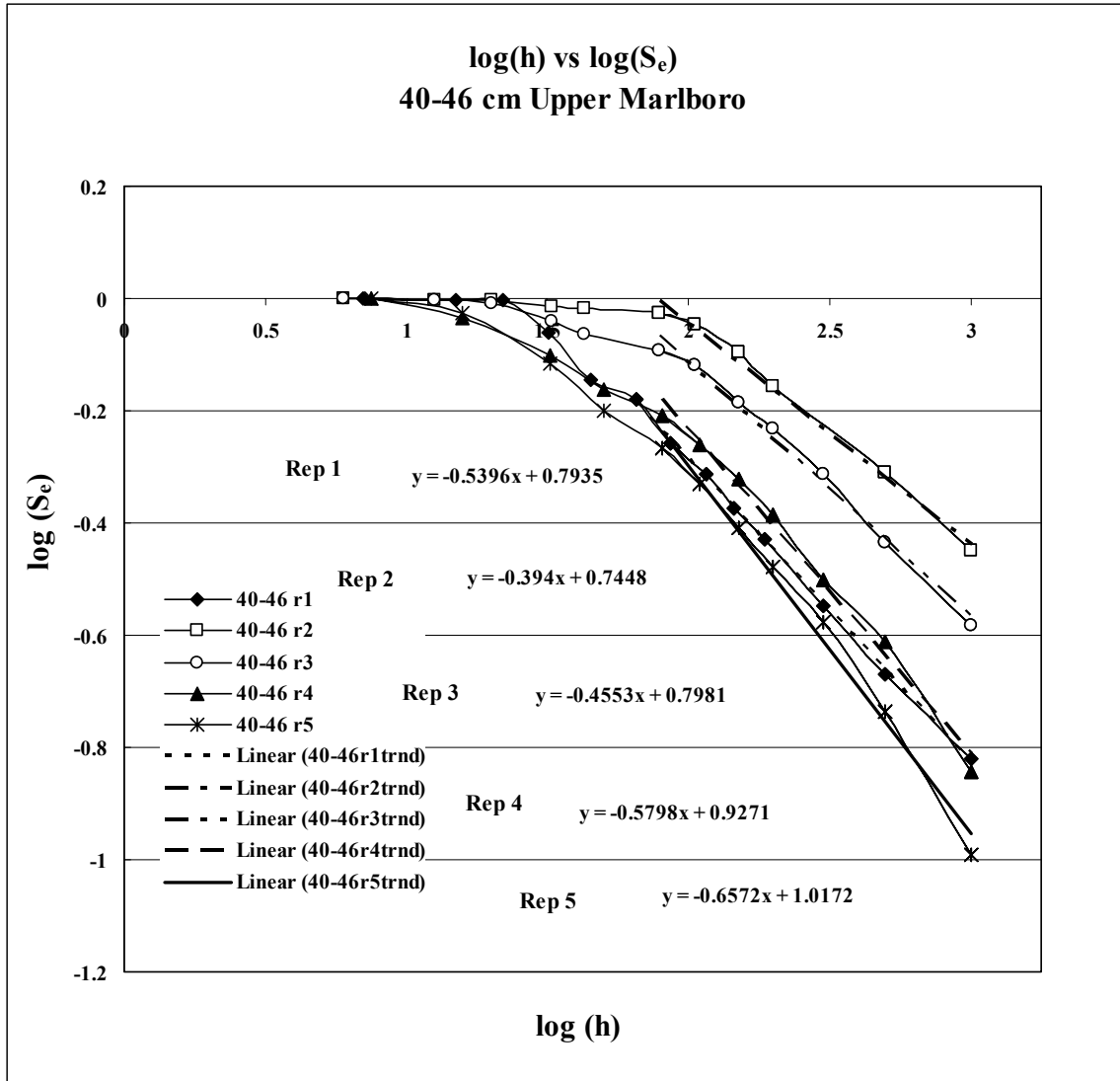


Figure 66. Curves for log S_e vs. log h used to determine bubbling pressure for Upper Marlboro site for soil depth 40-46 cm

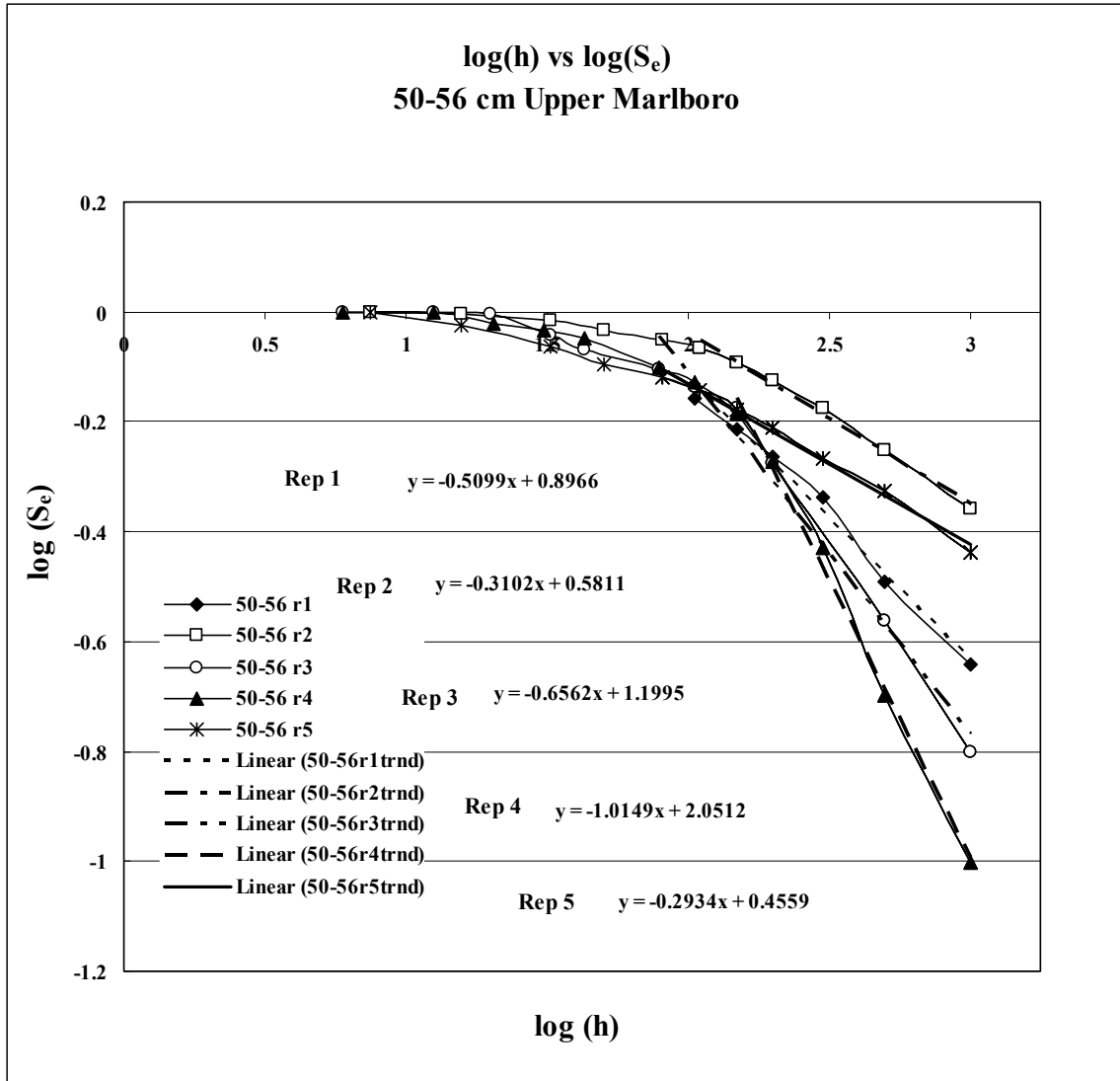


Figure 67. Curves for log S_e vs. log h used to determine bubbling pressure for Upper Marlboro site for soil depth 50-56 cm

Appendix E-2 - Log S_e vs. Log h for Poplar Hill Site for Six Depths

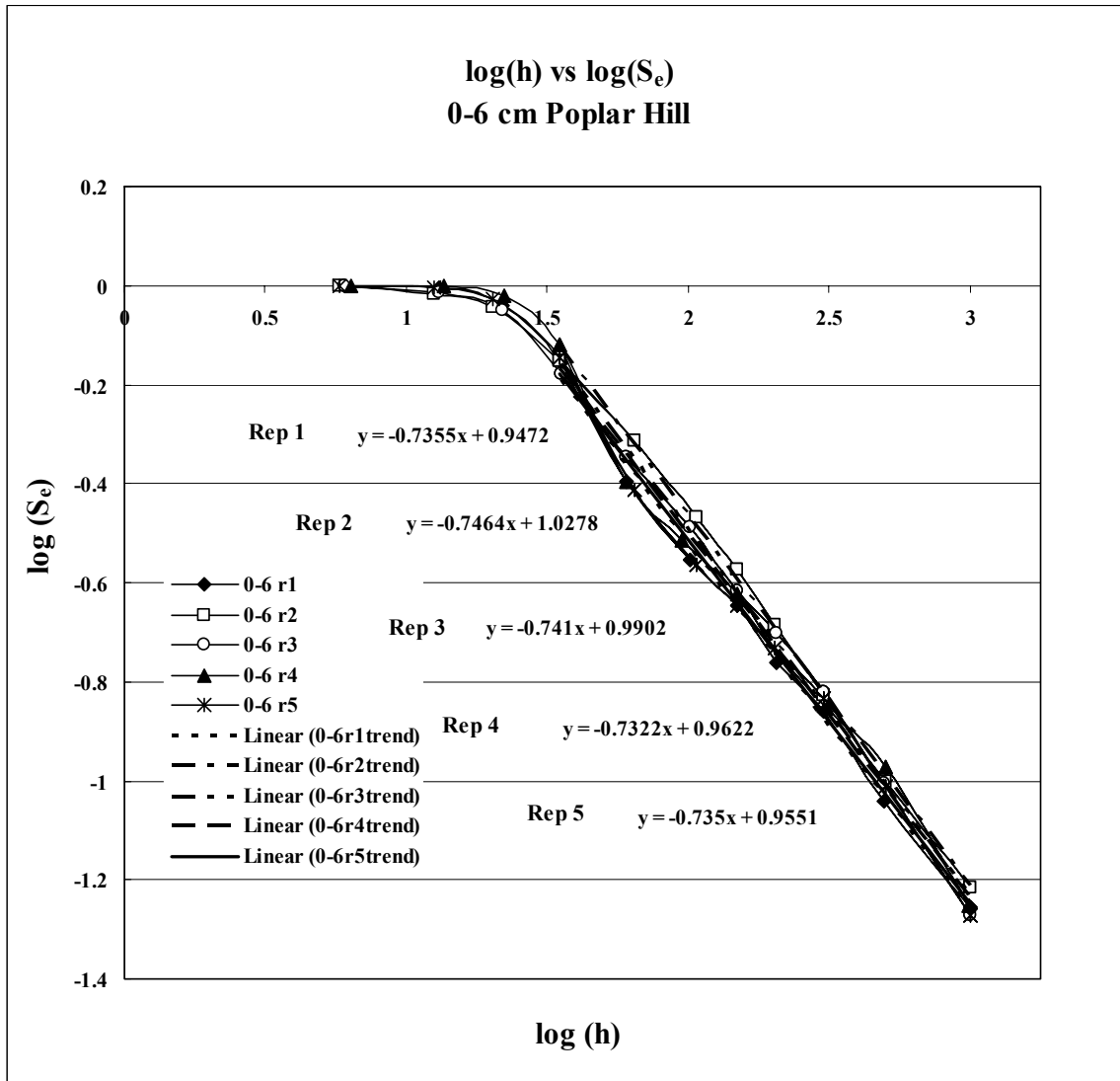


Figure 68. Curves for log S_e vs. log h used to determine bubbling pressure for Poplar Hill site for soil depth 0-6 cm

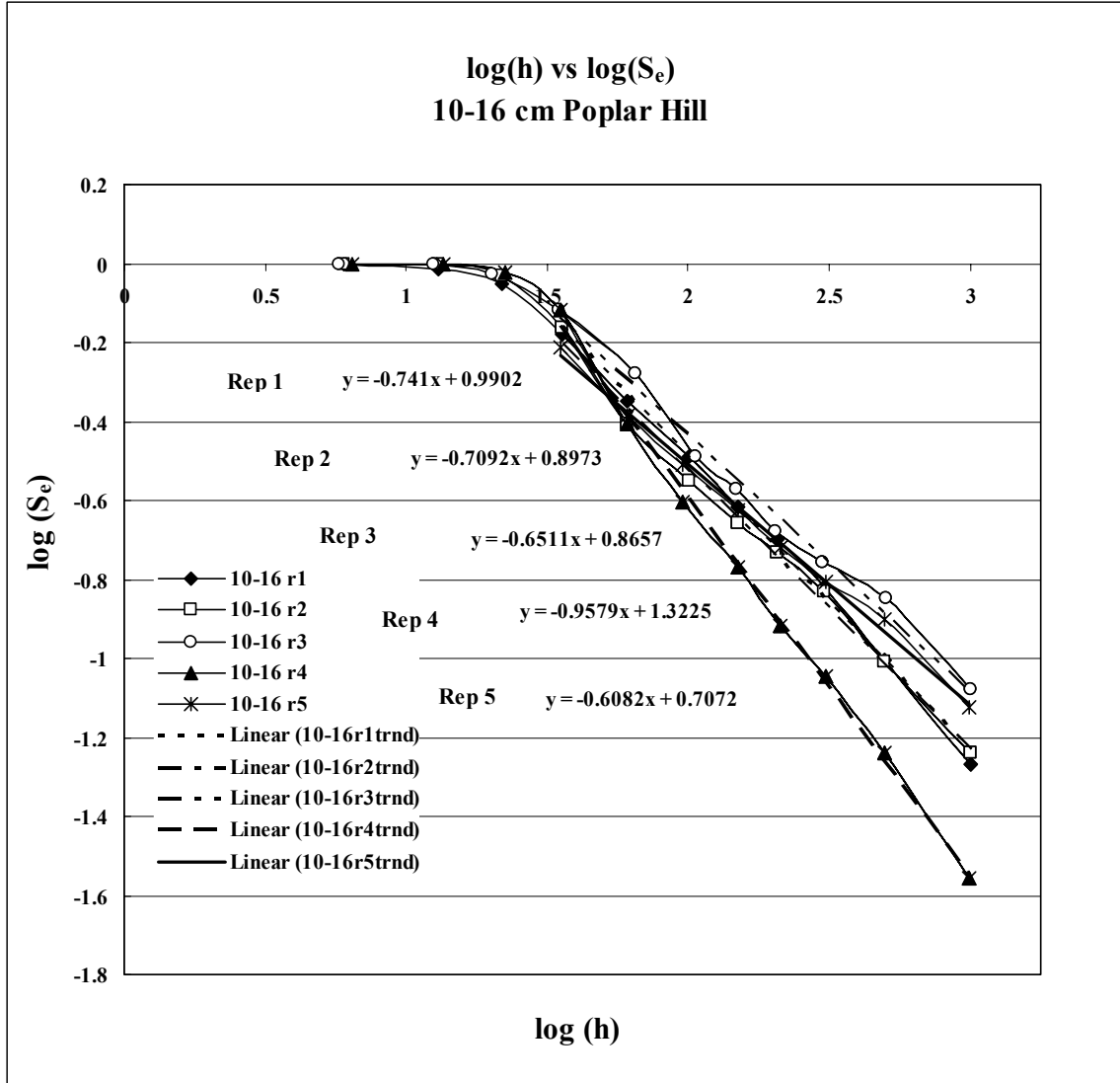


Figure 69. Curves for log S_e vs. log h used to determine bubbling pressure for Poplar Hill site for soil depth 10-16 cm

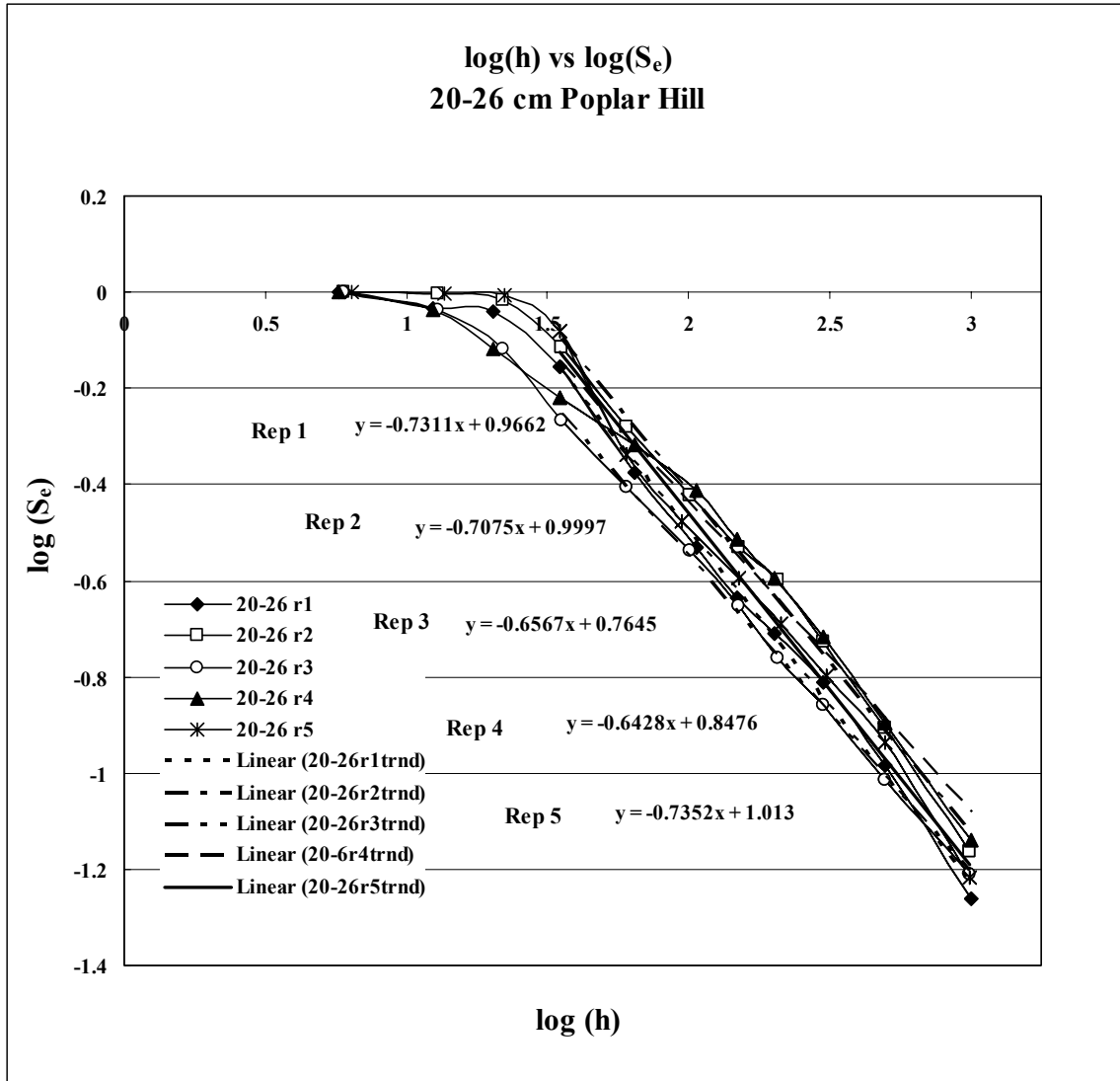


Figure 70. Curves for log S_e vs. log h used to determine bubbling pressure for Poplar Hill site for soil depth 20-26 cm

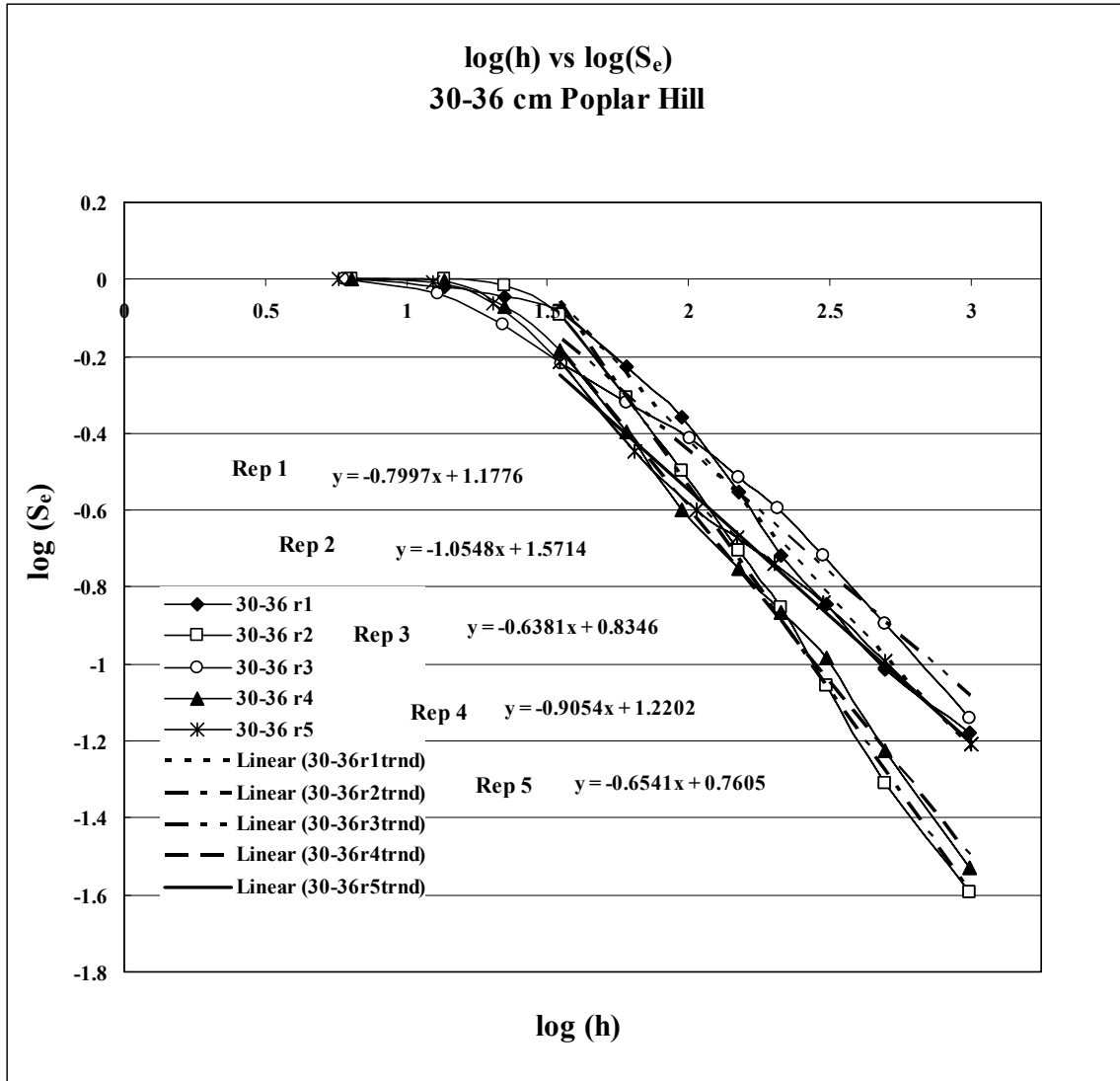


Figure 71. Curves for log S_e vs. log h used to determine bubbling pressure for Poplar Hill site for soil depth 30-36 cm

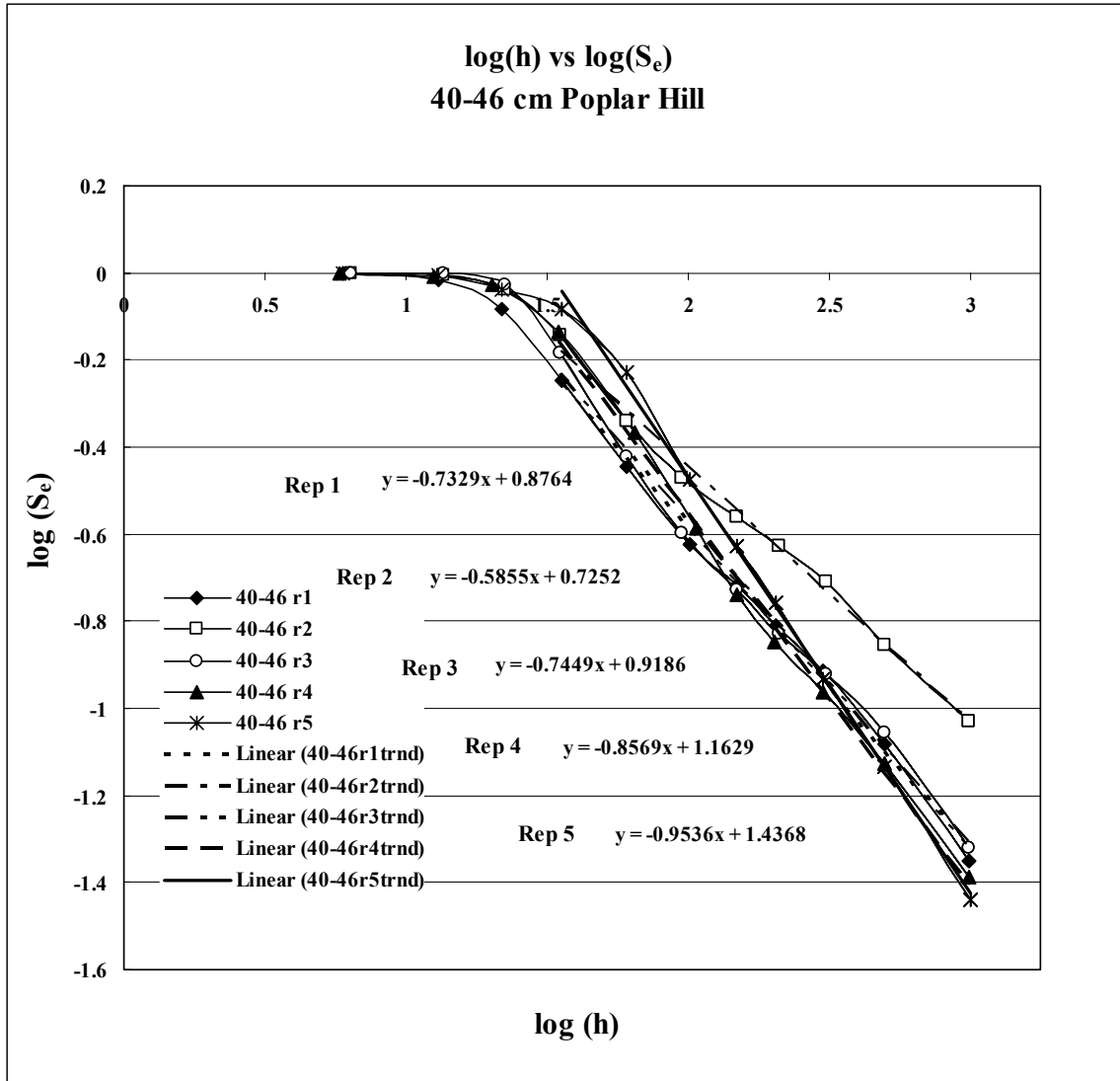


Figure 72. Curves for log S_e vs. log h used to determine bubbling pressure for Poplar Hill site for soil depth 40-46 cm

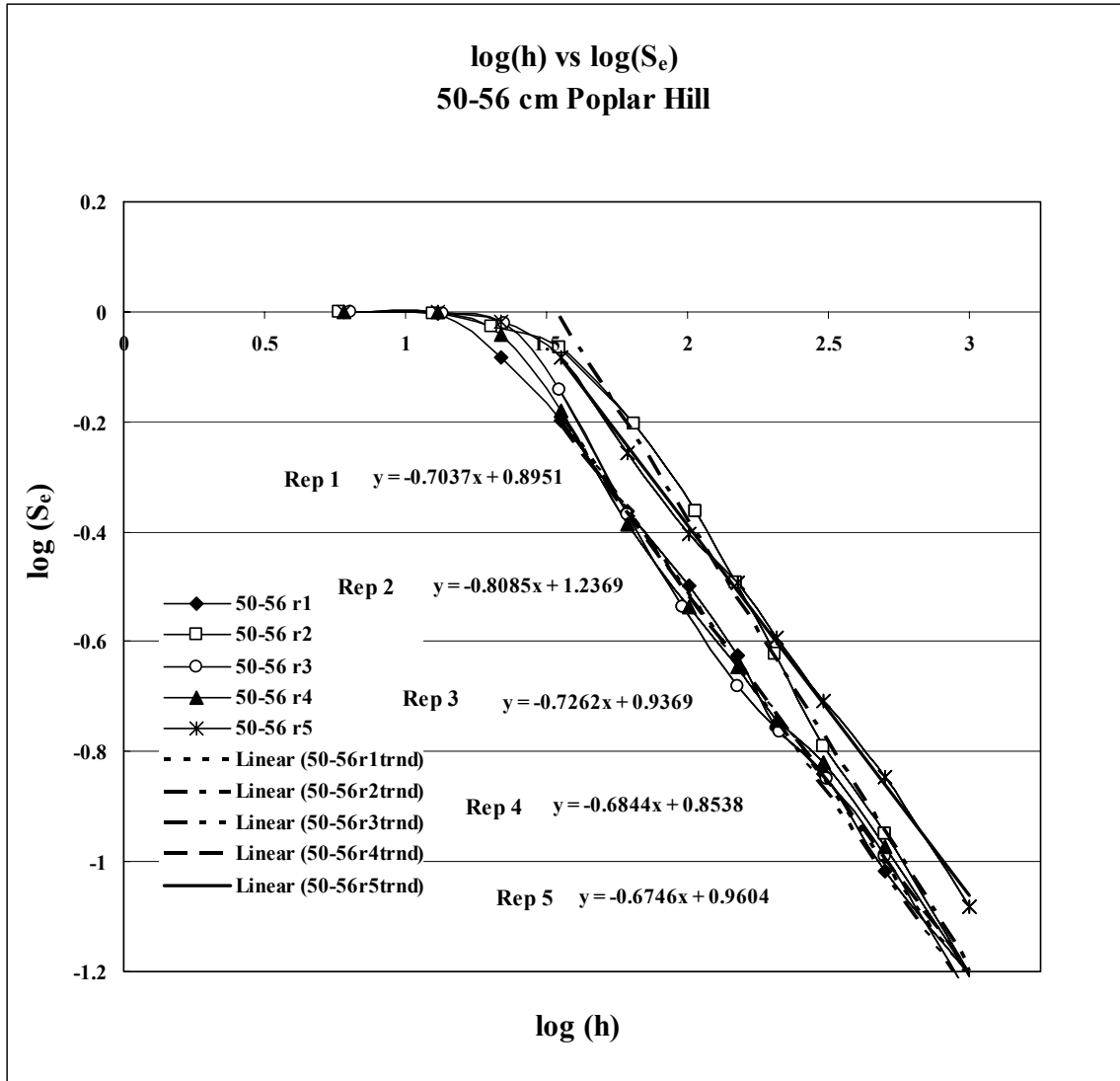


Figure 73. Curves for log S_e vs. log h used to determine bubbling pressure for Poplar Hill site for soil depth 50-56 cm

Appendix F - Sensitivity Analyses

Table 21. Kostiakov equation sensitivity analysis

Kostiakov Equation		$f_p = K_k t^{-\alpha}$			
Parameter	α	K_k	t_1 (hr)	t_2 (hr)	
base values	0.7858	4.700	0.667	1.333	
Dev from base value	K_k	f_1	f_2	CN₁	CN₂
50%	2.350	2.946	1.709	1	1
75%	3.525	4.419	2.563	1	1
90%	4.230	5.303	3.076	1	1
base	4.700	5.892	3.418		
110%	5.170	6.481	3.759	1	1
125%	5.875	7.365	4.272	1	1
150%	7.050	8.838	5.126	1	1
Dev from base value	α	f_1	f_2	CN₁	CN₂
50%	0.393	5.262	4.008	0.21	-0.35
75%	0.589	5.568	3.701	0.22	-0.33
90%	0.707	5.760	3.528	0.22	-0.32
base	0.786	5.892	3.418		
110%	0.864	6.027	3.310	0.23	-0.31
125%	0.982	6.235	3.156	0.23	-0.31
150%	1.179	6.597	2.914	0.24	-0.29

Table 22. Horton equation sensitivity analysis

Horton Equation			$f_p = f_c + (f_o - f_c) e^{-\beta t}$		
Parameter	β	f_c (cm h ⁻¹)	f_o (cm h ⁻¹)	t_1 (h)	t_2 (h)
base values	2.540	2.915	5.96	0.667	1.333
Dev from base value	β	f_1 (cm h⁻¹)	f_2 (cm h⁻¹)	CN₁	CN₂
50%	1.270	4.090	3.368	-0.428	-0.259
75%	1.905	3.645	3.090	-0.328	-0.144
90%	2.286	3.463	3.014	-0.282	-0.105
base	2.540	3.368	2.982		
110%	2.794	3.290	2.961	-0.233	-0.072
125%	3.175	3.196	2.941	-0.204	-0.056
150%	3.810	3.090	2.925	-0.165	-0.039
Dev from base value	f_o (cm h⁻¹)	f_1 (cm h⁻¹)	f_2 (cm h⁻¹)	CN₁	CN₂
50%	2.980	2.925	2.916	0.263	0.044
75%	4.470	3.146	2.949	0.263	0.044
90%	5.364	3.279	2.969	0.263	0.044
base	5.960	3.368	2.982		
110%	6.556	3.457	2.996	0.263	0.044
125%	7.450	3.590	3.015	0.263	0.044
150%	8.940	3.812	3.048	0.263	0.044
Dev from base value	f_c (cm h⁻¹)	f_1 (cm h⁻¹)	f_2 (cm h⁻¹)	CN₁	CN₂
50%	1.458	2.068	1.560	0.74	0.95
75%	2.186	2.674	2.268	0.74	0.95
90%	2.624	3.038	2.693	0.74	0.95
base	2.915	3.280	2.977		
110%	3.207	3.522	3.260	0.74	0.95
125%	3.644	3.886	3.685	0.74	0.95
150%	4.373	4.492	4.393	0.74	0.95

Table 23. Holtan equation sensitivity analysis

Holtan Equation		$f_p = GIaSA^{1.4} + f_c$			
Parameter base values	GIa	f_c (cm h ⁻¹)	SA ₁	SA ₂	
	0.3	0.76	5.408	3.031	
Dev from base value	GIa	f_1 (cm h ⁻¹)	f_2 (cm h ⁻¹)	CN ₁	CN ₂
50%	0.150	2.354	1.468	0.81	0.65
75%	0.225	3.150	1.823	0.81	0.65
90%	0.270	3.629	2.035	0.81	0.65
base	0.300	3.947	2.177		
110%	0.330	4.266	2.318	0.81	0.65
125%	0.375	4.744	2.531	0.81	0.65
150%	0.450	5.541	2.885	0.81	0.65
Dev from base value	f_c (cm h ⁻¹)	f_1 (cm h ⁻¹)	f_2 (cm h ⁻¹)	CN ₁	CN ₂
50%	0.38	3.567	1.797	0.19	0.35
75%	0.57	3.757	1.987	0.19	0.35
90%	0.684	3.871	2.101	0.19	0.35
base	0.76	3.947	2.177		
110%	0.836	4.023	2.253	0.19	0.35
125%	0.95	4.137	2.367	0.19	0.35
150%	1.14	4.327	2.557	0.19	0.35
Time (h)	SA	f_p (cm h ⁻¹)			
0	8.566	5.048			
0.25	7.494	5.048			
0.5	6.422	4.814			
0.667	5.408	3.947			
0.75	4.612	3.310			
1	3.974	2.830			
1.25	3.456	2.463			
1.333	3.031	2.177			
1.5	2.677	1.951			
1.75	2.379	1.769			
2	2.127	1.623			

Table 24. Philip equation sensitivity analysis

Philip Equation		$f = 1/2St^{1/2} + C_a$				
Parameter	$S = (2MK_sS_f)^{1/2}$	$K_f/3$	$2K_f/3$	K_f	t_1 (h)	t_2 (h)
base values	8.047	0.509	1.017	1.526	0.75	1.5
Dev from base value	$C_a = K_s/3$ (cm h ⁻¹)	f_1 (cm h ⁻¹)	f_2 (cm h ⁻¹)	CN_1	CN_2	
50%	0.254	4.900	3.539	0.099	0.134	
75%	0.381	5.027	3.666	0.099	0.134	
90%	0.458	5.104	3.743	0.099	0.134	
base	0.509	5.154	3.794			
110%	0.559	5.205	3.844	0.099	0.134	
125%	0.636	5.281	3.921	0.099	0.134	
150%	0.763	5.409	4.048	0.099	0.134	
Dev from base value	S	f_1 (cm h ⁻¹)	f_2 (cm h ⁻¹)	CN_1	CN_2	
50%	4.023	2.831	2.151	0.82	0.76	
75%	6.035	3.993	2.972	0.82	0.76	
90%	7.242	4.690	3.465	0.82	0.76	
base	8.047	5.154	3.794			
110%	8.852	5.619	4.122	0.82	0.76	
125%	10.059	6.316	4.615	0.82	0.76	
150%	12.070	7.477	5.436	0.82	0.76	

Table 25. Green-Ampt equation sensitivity analysis

Green-Ampt Equation			$f = K_s + (K_s MS_f) / F$		
Parameter base values	S_f 21.73	M_i 0.143	av K_{fs} (cm h⁻¹) 2.640	F₁ (cm) 5.70	F₂ (cm) 6.48
Dev from base value	av K_{fs} (cm h⁻¹)	f₁ (cm h⁻¹)	f₂ (cm h⁻¹)	CN₁	CN₂
50%	1.320	2.040	1.953	1	1
75%	1.980	3.059	2.929	1	1
90%	2.376	3.671	3.515	1	1
base	2.640	4.079	3.906		
110%	2.904	4.487	4.297	1	1
125%	3.300	5.099	4.882	1	1
150%	3.960	6.119	5.859	1	1
Dev from base value	M_i	f₁ (cm h⁻¹)	f₂ (cm h⁻¹)	CN₁	CN₂
50%	0.072	3.360	3.273	0.35	0.32
75%	0.107	3.719	3.589	0.35	0.32
90%	0.129	3.935	3.779	0.35	0.32
base	0.143	4.079	3.906		
110%	0.157	4.223	4.033	0.35	0.32
125%	0.179	4.439	4.222	0.35	0.32
150%	0.215	4.799	4.539	0.35	0.32
Dev from base value	S_f	f₁ (cm h⁻¹)	f₂ (cm h⁻¹)	CN₁	CN₂
50%	10.87	3.360	3.273	0.35	0.32
75%	16.30	3.719	3.589	0.35	0.32
90%	19.56	3.935	3.779	0.35	0.32
base	21.73	4.079	3.906		
110%	23.90	4.223	4.033	0.35	0.32
125%	27.16	4.439	4.222	0.35	0.32
150%	32.60	4.799	4.539	0.35	0.32

LITERATURE REFERENCES

- Arnold, J.G., R. Srinivasin, R.S. Muttiah, and J. R. Williams. 1998. Large Area Hydrologic Modeling and Assessment: Part I. Model Development. *Journal of American Water Research Association* 34(1): 73-89.
- Beasley, D.B. and L.F. Huggins, 1980. ANSWERS (Areal Nonpoint Source Watershed Environment Simulation) - User's Manual. Department of Agricultural Engineering, Purdue University, West Lafayette, Indiana
- Beven, K. J. and P. F. Germann, 1982. Macropores and water flow in soils. *Water Resources Research* 18(5): 1311-1325.
- Beven, K.J. 2000. *Rainfall-Runoff Modeling: The Primer*, John Wiley & Sons, Ltd., New York, New York.
- Bevin, K. J., 2004. Robert E. Horton's perceptual model of infiltration processes. *Hydrological Processes* 18: 3447-3460.
- Black, C. A., D. D. Evans, J. L. White, L. E. Ensminger and F. E. Clark. 1965. *Methods of Soil Analysis*. American Society of Agronomy.
- Blake, G. J., 1968. Infiltration at the Puketurua experimental basin. *Journal of Hydrology* 7(1): 38-46.
- Bolt, G.H., and R.D. Miller. 1958. Calculation of total and component potentials of water in soil. *Transactions, American Geophysical Union* 39:917-928.
- Bouwer, H. 1966. Rapid field measurement of air-entry value and hydraulic conductivity of soil as significant parameters in flow system analysis. *Water Resources Research* 2: 729-738.
- Bouwer, H.. 1969. Infiltration of water into nonuniform soil. *Journal of Irrigation and Drainage Division, ASCE* 95(IR4): 451-462.
- Bouwer, H.. 1976. Infiltration into increasingly permeable soils. *Journal of Irrigation and Drainage Division, ASCE* 102(IR1): 127-136.
- Bouma, J., C. F. M Belmans and L.W. Dekker. 1982. Water infiltration and redistribution in a silt loam subsoil with vertical worm channels. *Soil Science Society of America Journal*. 46: 917-921
- Brady, N. C. and R. R. Weil. 1999. *The Nature and Properties of Soils*. Upper Saddle River, NJ.: Prentice Hall, Inc.

- Brakensiek, D. L. 1977. Estimating the effective capillary pressure in the Green and Ampt infiltration equation. *Water Resources Research* 13(3): 680-682.
- Brakensiek, D. L., and C. A. Onstad. 1977. Parameter estimation of the Green and Ampt infiltration equation. *Water Resources Research* 13(6): 1009-1012.
- Brooks, R. H. and A. T. Corey. 1964. Hydraulic properties of porous media. Hydrology Paper No. 3. Fort Collins, CO.: Colorado State University,.
- Chapra, S. 1997. *Surface Water-quality Modeling*. New York, NY.: McGraw-Hill.
- Childs, E. C. 1969. *An Introduction to the Physical Basis of Soil Water Phenomenon*. New York, NY.: John Wiley and Sons.
- Childs, E. C. and M. Bybordi. 1969. The vertical movement of water in stratified porous material. 1. Infiltration. *Water Resources Research*, 5(2), 446-459.
- Chow, V. T., D. R. Maidment, and L. W. Mays. 1988. *Applied Hydrology*. New York, NY.: McGraw-Hill.
- Clemmens, A. J. 1983. Infiltration equations for border irrigation models. P266-274. In: *Advances in infiltration. Proc. Nat. Conf. on Advances in Infiltration*. Dec. 12-13, 1983. Chicago, Ill. ASAE Pub. 11-83. St. Joseph, Mo.
- Criddle, D. W., S. Davis, C. H. Pair and D. G. Shockley. 1956. Methods for evaluating irrigation systems. USDA Soil Conservation Service. U. S. Government Printing Office.
- Croley, T. E. II., and C. He. 2005. Great Lakes spatially distributed watershed model of water and materials runoff. Proceedings, International Conference on Poyang Lake Wetland Ecological Environment. Advanced Workshop on Watershed Modeling and Water Resources Management, Jiangxi Normal University, Nanchang, Jiangxi, P.R. China, June 27, 2005. 12 pp.
- Fok, Y. S. 1986. "Derivation of Lewis-Kostiakov intake equation", *Journal of Irrigation and Drainage Engineering*. 112: 164-171.
- Frere, M. H., C. A. Onstad and H. N. Holtan. 1975. ACTMO, an agricultural chemical transport model. ARS-H-3, USDA-ARS.
- Gardner, W. 1986. Water Content p. 493-544. In A. Klute (ed.) *Methods of Soil Analysis. Part 1*, 2nd ed. Soil Science Society of America, Madison, WI.
- Garen, D.C. and D. S. Moore. 2005. Curve number hydrology in water quality modeling: uses, abuses, and future directions, *Journal of the American Water Resources Association*, vol. 41, pp. 377-388.

- Gifford, G. F. 1976. Applicability of some infiltration formulae to rangeland infiltrometer data. *J. Hydrol.* 28: 1-11.
- Gifford, G. F. 1978. Use of infiltration coefficients as an aid in defining hydrologic impacts of range management schemes. *J. Range Manage.* 31: 115-117.
- Ghosh, R. K. 1980. Modeling infiltration. *Soil Science* 130: 297-302.
- Ghosh, R. K. 1983. A note on the infiltration equation. *Soil Science* 136: 333-338.
- Ghosh, R. K. 1985. A note on Lewis-Kostiakov's infiltration equation. *Soil Science* 139: 193-196.
- Grant, D. M., and B. D. Dawson. 1997. *ISCO Open Channel Flow Measurement Handbook*. 5th ed. Lincoln, NE.: ISCO, Inc.
- Green, W. H. and G. Ampt. 1911. Studies of Soil Physics, Part 1. The flow of air and water through soils. *Journal of Agricultural Science* 4: 1-24.
- Haggard, B.E., P.A. Moore Jr. and K.R. Brye. 2005. Effect of Slope on Runoff from a Small Variable-Slope Box. *Journal of Environmental Hydrology*. 13: paper 25.
Available: [HTTP://HYDROWEB.COM](http://HYDROWEB.COM).
- Hartley, D. M. 1992. Interpretation of Kostiakov infiltration parameters for borders. *Journal of Irrigation and Drainage Engineering* 118(1): 156-165.
- Haverkamp, R., L. Rendon and G. Vachaud. 1987. Infiltration equations and their applicability for predictive use. P. 142-152. In Yu- SI Fok (ed.) *Infiltration Development and Application*. Honolulu, Hawaii.
- Hilhorst, M. A., C. Dirksen, F. W. H. Kampers and R. A. Feddes. 2001. Dielectric relaxation of bound water versus soil matric pressure. *Soil Science Society of America Journal*. 65: 311-314
- Hillel, D. 1998. *Environmental Soil Physics*. Academic Press. San Diego, CA.
- Hillel, D. 1971. *Soil and Water: Physical Principles and Processes*. Academic Press, New York, NY.
- Hillel, D. and W. R. Gardner. 1969. Steady infiltration into crust topped profiles. *Soil Science* 108: 137-142.
- Hillel, D. and W. R. Gardner. 1970. Transient infiltration into crust topped profiles. *Soil Science* 109: 69-76.

Holtan, 1961. A concept for infiltration estimates in watershed engineering. USDA, Agricultural Research Service Publication 41-51.

Holtan, H. N. and N. R. Creitz. 1967. Influence of soils, vegetation and geomorphology on elements of the flood hydrograph. Symposium on floods and their computation, Leningrad, Russia.

Holtan, H. N., C. B. England and V. O. Shanholtz. 1967. Concepts in Hydrologic Soil Grouping. *Transactions of the ASAE*. Paper No. 65-739: 407- 410.

Holtan, H. N., and N. C. Lopez. 1971. USDAHL-70 model of watershed hydrology. *USDA-ARS Tech. Bull. No. 1435*, Agricultural Research Station, Beltsville, Md..

Horton, R. E. 1939. Analysis of runoff plot experiments with varying infiltration capacity. *Transactions of the American Geophysicists. Union, Part IV*: 693-694.

Horton, R. E. 1940. An approach towards a physical interpretation of infiltration capacity. *Soil Science Society of America* 5: 399-417.

Huat, B. B. K., F. H. J. Ali and T. H. Low. 2006 Water infiltration characteristics of unsaturated soil slope and its effect on suction and stability *Geotechnical and Geological Engineering* 24: 1293–1306.

Huggins, L. F. and E. J. Monke. 1966. The mathematical simulation of the hydrology of small watersheds. Lafayette, Indiana: TR1 Perdue Water Resources Research Center

Israelson, O. W. and V. E. Hansen. 1967. *Irrigation Principles and Practices* pp. 198 – 200 .John Wiley, New Delhi.

Jury, W. A., W. R. Gardener and W. H. Gardener. 1991. *Soil Physics*, 5th edn. Wiley, New York, NY.

Kawkins, R.H. 1978. Runoff curve number relationships with varying site moisture. *Journal of the Irrigation and Drainage Division*, vol. 104, pp. 389-398.

Kirby, R. M., E.D. Matthews and M. A. Bailey. 1967. Soil Survey of Prince Georges County, Maryland. USDA Soil Conservation Service in cooperation with Maryland Agricultural Experiment Station.

Kirkham D. and Powers W. L. 1972. *Advanced Soil Physics*. Wiley, New York, NY.

Klute, A. 1986. Water retention: Laboratory methods. In: Klute, A, ed., *Methods of Soil Analysis* , Part 1: Physical and Mineralogical Methods. Monograph No. 9. American Society of Agronomy, Madison, WI.

Knisel, W.G. 1980. CREAMS: A fieldscale model for Chemical, Runoff, and Erosion from Agricultural Management Systems. USDA, Science and Education Administration, Conservation Report No. 26, Washington, D.C.

Kostiakov, A. N. 1932. On the dynamics of the coefficient of water-percolation in soils and on the necessity for studying it from a dynamic point of view for purposes of amelioration. *Transactions Congress International Society for Soil Science*, 6th, Moscow, Part A: 17-21.

Kozak, J. A. and L. R. Ahuja. 2005. Scaling of infiltration and redistribution of water across soil textural classes. *Soil Science Society of America Journal* 69: 816-827.

Leonard, R.A., W. G. Knisel and D. A. Still. 1987. GLEAMS: Groundwater Loading Effects of Agricultural Management Systems. *Transactions of ASAE*, vol. 30, pp. 1403-1418.

Le Van Phuc and H. J. Morel-Seytoux. 1972. Effect of soil air movement and compressibility on infiltration rates. *Soil Science Society of America Proceedings* 36: 237-241.

Lewis, M. R. 1937. The rate of infiltration of water in irrigation practice. *Transactions of the American Geophysical Union* 18: 361-368.

Maidment, D.R. 1993. *Handbook of Hydrology*. New York, N.Y.: McGraw-Hill Professional.

Mbagwu, J. S. C. 1990. Mulch and tillage effects on water transmission characteristics of an Ultisol and maize grain yield in SE. Nigeria. *Pedologie* 40: 155-168.

Mbagwu, J. S. C. 1993. Testing the goodness of fit of selected infiltration models on soils with different land use histories. International Centre for Theoretical Physics. Trieste, Italy.

Mbagwu, J.S.C. 1994. Soil physical properties influencing the fitting parameters in Philip and Kostiakov infiltration models. International Centre for Theoretical Physics. Trieste, Italy.

McCuen, R. H. 1986. *Hydrologic Modeling; Statistical Methods and Applications*. Englewood Cliffs, N.J.: Prentice-Hall.

Mein, R. G. and C. L. Larson. 1973. Modeling infiltration during a steady rain. *Water Resources Research* 9(2): 384-394.

Messing, I., J. Iwald, D. Lindgren, K. Lindgren, L. Nguyen and T. S. Hai. 2005. Using pore sizes as described in soil profile descriptions to estimate infiltration rate and saturated hydraulic conductivity. *Soil Use and Management* 21: 376-277.

- Mezencev, V. J. 1948. Theory of formation of the surface runoff. *Meteorologiae Hidrologia* 3:33-40.
- Morel-Seytoux, H. J. and J. Khanji. 1974. Derivation of an equation for infiltration. *Water Resources Research* 10(4): 795-800.
- Musgrave, G.W. 1955. How much of the rain enters the soil? In *USDA Water Yearbook of Agriculture*. Washington, D.C., 151-159.
- Naeth, M. A. 1988. *The impact of grazing on litter and hydrology in mixed prairie and fescue grassland ecosystems of Alberta*. Ph.D. Thesis. University of Alberta, Edmonton, Canada.
- Naeth, M.A., D.S. Chanasyk and A.W. Bailey. 1991. Applicability of the Kostiaikov equation to mixed prairie and fescue grasslands of Alberta. *Journal of Range Management* 44 (1): 18-21.
- Novotny, V., and H. Olem. 1994. *Water Quality; Prevention, Identification, and Management of Diffuse Pollution*. New York, NY.: Van Nostrand Reinhold.
- Oram, B. 2005. Hydrological Cycle. Watershed Assessment, Education, Training, Monitoring Resources in Northeastern Pennsylvania. Wilkes University. Environmental Engineering and Earth Sciences Department. Wilkes-Barre, PA <http://www.water-research.net/watershed/hydrologicalcycle.htm> accessed 8/29/06.
- Philip, J. R. 1954. An infiltration equation with physical significance. *Soil Science* 77: 153-157.
- Philip, J. R. 1957a. The theory of infiltration: 1. The infiltration equation and its solution. *Soil Sci.* 83, 345–357.
- Philip, J. R. 1957b. The theory of infiltration: 4. Sorptivity and algebraic infiltration equations. *Soil Science* 84: 257-264.
- Philip, J. R. 1957c. The theory of infiltration: 5. The influence of initial water content. *Soil Science* 84: 329-339.
- Poesen, J. W. A. 1984. The influence of slope angle on infiltration rate and Hortonian overland flow. *Geomorphology* 2(49): 117-131.
- Rawls, W. J., L. R. Ahuja, D. L. Brakensiek, A. Shirmohammadi. 1993. Infiltration and soil water movement. In *Handbook of Hydrology*. McGraw-Hill, Inc.
- Richards, L. A. 1931. Capillary conduction through porous mediums. *Physics* 1: 313-318.

Römken, M. J. M., R.L. Baumhardt, J. Y. Parlange, F. D. Whisler, and S. N. Prasad. 1985. Effect of rainfall characteristics on seal hydraulic conductance. In Callebaut et al. (eds), *Proceedings of the Symposium on the assessment of Soil Surface Sealing and Crusting*. State University of Ghent, Belgium.

Römken, M. J. M., S. N. Prasad and F. D. Whisler. 1990. In Process Studies in Hillslope Hydrology Anderson, M. G. and T. P. Burt, eds. Wiley, New York, NY.

Schwab, G. O., D. D. Fangmeir, J. E. Elliot, and R. K. Frevert. 1993. *Soil and Water Conservation Engineering*. 4th ed. Wiley, New York, N.Y.

Serrano, S. E. 1997. *Hydrology for Engineers, Geologists and Environmental Professionals*. Hydrosience, Inc.

Sharpley, A. N., and J. R. Williams. 1990. EPIC-Erosion Productivity Impact Calculator USDA, Agricultural Research Service, Technical Bulletin No. 1768, Washington, D.C., pp. 235 pp.

Shirmohammadi, A. and R. W. Skaggs. 1984. Effect of soil surface conditions on infiltration for shallow water table soils. *Transactions of the ASAE* 27(6): 1780-1787.

Shirmohammadi, A. and R. W. Skaggs. 1985. Predicting infiltration for shallow water table conditions. *Transactions of the ASAE* 28(6): 1829-1837.

Shirmohammadi, A., T. W. Chu, H. Montas, and T. Sohrabi. 2001. SWAT model and its applicability to watershed nonpoint-source pollution assessment. ASAE Paper No. 012005. St. Joseph, Mich.: ASAE

Simunek, J., N. J. Jarvis, M. T. van Genuchten. 2003. Review and comparison of models for describing non-equilibrium and preferential flow and transport in the vadose zone. *Journal of Hydrology* 272: 14-35

Skaggs, R. W., L. E. Huggins, E. J. Monke and G. R. Foster. 1969. Experimental Evaluation of Infiltration Equations. *Transactions of the ASAE*. Paper No. 3425 : 822-828.

Skaggs, R. W., and R. Khaleel. 1982. Chapter 4: Infiltration. In *Hydrology of Small Watersheds*. St Joseph, Mich.: ASAE.

Smiles, D. E. and J. H. Knight. 1976. A note on the use of the Philip infiltration equation. *Australian Journal of Soil Research* 14: 103-108.

Smith, R. E. 1976. Approximations for vertical infiltration patterns. *Transactions of the ASCE* 19(3): 505-509.

Smith, R. E. and J. Y. Parlange. 1978. A parameter-efficient hydrologic infiltration model. *Water Resources Research* 14(3): 533-538.

Soil Conservation Service, USDA. 1964. Chapter 7 Hydrology Part I: Watershed Planning. In *National Engineering Handbook*.

Soil Science Society of America, 1975, Glossary of soil science terms: Madison, Wisconsin, Soil Science Society of America.

Sullivan, M., J. J. Warwick and S. W. Tyler. 1996. Quantifying and delineating spatial variations of surface infiltration in a small watershed.

Talsma, T. 1969. *In situ* measurement of sorptivity. *Australian Journal of Soil Research* 7: 269-276

Talsma, T. and J. Y. Parlange, 1972. One-dimensional vertical infiltration. *Australian Journal of Soil Research* 10: 143-150.

Verma, R.D. and W. Brutsaert. 1971. Similitude criteria for flow from unconfined aquifers, ASCE, *Journal of Hydraulic Division* 97(HY9), 1493-1509.

Wang, Z., J. Feyen, D. R. Nielsen and M. T. van Genuchten. 1997. Two-phase flow infiltration equations accounting for air entrapment effects.

Walker, W. 1998. SIRMOD - Surface Irrigation Modeling Software. Utah State University.

Wangeman, S. G., R. A. Kohl and P. A. Molumeli. 2000. Infiltration and percolation influenced by antecedent soil water content and air entrapment. *American Society of Agricultural Engineers* 43(6): 1517-1523.

Weiler, M. 2005. An infiltration model based on flow variability in macropores: development, sensitivity analysis and applications. *Journal of Hydrology* 310: 294-315.

Whisler, F.D., and H. Bouwer. 1970. Comparison of methods for calculating vertical drainage and infiltration for soils. *Journal of Hydrology* 10(1): 1-19.

White, I. and K. M. Perroux. 1987. Use of sorptivity to determine field hydraulic properties. *Soil Science Society of America Journal* 51: 1093-1101.

Wischmeier, W. H. and D. D. Smith. 1978. Predicting Rainfall Erosion Losses. *Agricultural Handbook No. 537*, U.S. Department of Agriculture, Washington, D.C

Xu, C. Y. 2003. Approximate infiltration models. Section 5.3 In *Hydrologic Models*. Uppsala University Department of Earth, Air and Water Sciences. Uppsala, Sweden.

Young, R. A., C. A. Onstad, D. D. Bosch and W. P. Anderson. 1989. AGNPS: A Non-Point-Source Pollution Model for Evaluating Agricultural Watersheds, *Journal of Soil and Water Conservation*, vol. 44, pp. 168:173.

Youngs, E. G. 1968. An estimation of sorptivity for infiltration studies from water movement considerations. *Soil Science* 106: 157-163.